TECHNISCHE UNIVERSITÄT DRESDEN

Paleoclimate reconstruction using biomarker and stable isotope analyses of lake sediments in the Bale Mountains, Ethiopia.

DISSERTATION

zur Erlangung des

Doktorgrades der Naturwissenschaften (Dr. rer. nat.)

der Fakultät Umweltwissenschaften,

Technische Universität Dresden

vorgelegt von

Lucas Bittner

1. Gutachter: Prof. Dr. Michael Zech, Institut für Geographie, Technische Universität Dresden
2. Gutachter: Prof. Dr. Torsten Haberzettl, Institut für Geographie und Geologie, Universität Greifswald
3. Gutachterin: Dr. Ana Moreno Caballud, Department of Quaternary Paleoenvironments and Global Change, Pyrenean Institute of Ecology

Dresden, 25.08.2022

Übereinstimmungserklärung

Die Übereinstimmung dieses Exemplars mit dem Original der Dissertation zum Thema: „Paleoclimate reconstruction using biomarker and stable isotope analyses of lake sediments in the Bale Mountains, Ethiopia.“ wird hiermit bestätigt.

Dresden, 24.04.2023

……

Ort, Datum

……

Unterschrift (Name, Vorname)

“The world is made of sugar and dirt.”

Bruno Alfred Döblin

Table of Content

List of abbreviations

AHP	**A**frican **H**umid **P**eriod
brGDGTs	**br**anched **G**lycerol **D**ialkyl **G**lycerol **T**etraethers
CAB	**C**ongo **A**ir **B**oundary
CBT	**C**yclisation of **B**ranched **T**etraethers
cal ka BP	**cal**ibrated **k**ilo **a**nno **B**efore **P**resent
EAL	**E**ast **A**frican **L**akes
EAM	**E**ast **A**frican **M**onsoon
DC	**D**egree of **C**yclisation
DCM	**D**i**c**hloro**m**ethane
DFG	**D**eutsche **F**orschungs**G**emeinschaft (German Research Council)
IPCC	**I**ntergovernmental **P**anel for **C**limate **C**hange
ISM	**I**ndian **S**ummer **M**onsoon
ITCZ	**I**nter**T**ropical **C**onvergence **Z**one
MAT	**M**ean **A**nnual (Air) **T**emperature
MBT	**M**ethylation of **B**ranched **T**etraethers
MSR	**M**ean **S**edimentation **R**ate
OM	**O**rganic **M**atter
PCA	**P**rincipal **C**omponent **A**nalyses
P/E	**P**recipitation to **E**vaporation ratio
SCP	**S**pheroidal **c**arbonaceous **p**article
TC	**T**otal **C**arbon
TLE	**T**otal **L**ipid **E**xtract
TOC	**T**otal **O**rganic **C**arbon
VSMOW	**V**ienna **S**tandard **M**ean **O**cean **W**ater
WAM	**W**est **A**frican **M**onsoon
YD	**Y**ounger **D**ryas
Ara, fuc, xyl	**Ara**binose, **Fuc**ose, **Xyl**ose

List of tables

List of figures

List of papers

This cumulative dissertation is based on three scientific articles:

1. **Bittner, L.**, Bliedtner, M., Grady, D., Gil-Romera, G., Martin-Jones, C., Lemma, B., Mekonnen, B., Lamb, H.F., Yang, H., Glaser, B., Szidat, S., Salazar, G., Rose, N.L., Opgenoorth, L., Miehe, G., Zech, W., Zech, M., 2020. Revisiting afro-alpine Lake Garba Guracha in the Bale Mountains of Ethiopia: rationale, chronology, geochemistry, and paleoenvironmental implications. Journal of Paleolimnology. https://doi.org/10.1007/s10933-020-00138-w

2. **Bittner, L.,** Gil-Romera, G., Grady, D., Lamb, H.F., Lorenz, E., Weiner, M., Meyer, H., Bromm, T., Glaser, B., Zech, M., 2022. The Holocene lake-evaporation history of the afro-alpine Lake Garba Guracha in the Bale Mountains, Ethiopia, based on $\delta^{18}O$ records of sugar biomarker and diatoms. Quaternary Research 1–14. https://doi.org/10.1017/qua.2021.26

3. **Bittner, L.**, De Jonge, C., Gil-Romera, G., Lamb, H.F., Russell, J.M., Zech, M., 2022. A Holocene temperature (brGDGT) record from Garba Guracha, a high-altitude lake in Ethiopia. Biogeosciences Discuss. 2022, 1–33. https://doi.org/10.5194/bg-2022-95_(in revision)

Abstract

While climate change and global warming are affecting eastern Africa today, the understanding of past climatic changes is limited. Especially during the last 15.000 years, eastern Africa has experienced spatially complex climatic changes. Although several paleoclimatic studies have been conducted in eastern Africa, reconstructing temperature changes and the hydrological history of lake archives, the driving mechanisms and teleconnections are yet not fully understood. A deeper understanding is precluded by (i) the lack of long, high-quality records of environmental change, especially in the Horn of Africa region, (ii) the lack of high altitude records, and (iii) insufficiently studied regions like eastern Ethiopia and Somalia. One of the region's most understudied high-altitude areas are the Bale Mountains, even though they encompass the continent's largest area above 4000 m a. s. l. This dissertation aims to further reduce the current lack of paleoclimatic reconstructions in high altitudes in the understudied Horn of Africa region.

High-altitude perennial lakes, especially cirque lakes, are valuable archives for paleoclimate and environmental reconstructions, yielding continuous sedimentation undisturbed by human activity. The only perennial lake in the Bale Mountains, the Garba Guracha, lies in the afro-alpine zone at 3950 m a. s. l. Previous paleolimnological research revealed that Garba Guracha comprises a continuous paleoclimatic and environmental sedimentary record since the last deglaciation. In order to enhance the paleoclimatic knowledge of the Bale Mountains and hence of eastern Africa, new innovative proxies, e.g. brGDGTs, $\delta^{18}O_{fucose}$, $\delta^{18}O_{diatom}$, and $\delta^{2}H_{n\text{-alkane}}$ were applied to newly retrieved sediment cores of Garba Guracha. The application of these analyses and the interpretation of the results imply a deeper understanding of the retrieved sediment cores, concerning mainly sedimentology, chronology and organic matter source identification.

The high-resolution chronology of Garba Guracha, established using different dating methods and compounds (^{210}Pb dating, radiocarbon dating of bulk sedimentary OM, compound class-specific *n*-alkanes, and charcoal), yields a basal age of ~ 16 cal ka BP. The geochemical correlation of tephra layers in the Garba Guracha sediments to dated tephra layers of the region provides an external age control, further supporting the robustness of the new Garba Guracha chronology and the non-existence of systematic age offsets. Similar ages obtained for *n*-alkanes and bulk sediments suggest no pre-aging of the biomarker in the very small afro-alpine catchment indicating short residence times or/and high aquatic productivity. Predominant autochthonous production of organic matter in the relative large lake compared to the catchment size has been proven by relatively low TOC/N ratios and relatively positive $\delta^{13}C$ values. The aquatic origin of the sugar biomarker fucose is further supported by a methodological comparison of $\delta^{18}O_{fucose}$ to a pure aquatic $\delta^{18}O_{diatom}$ record. The good correlation and similar ranges of $\delta^{18}O_{diatom}$ and $\delta^{18}O_{fucose}$ (7.9 ‰ and 7.1 ‰, respectively) not only highlight the potential of $\delta^{18}O_{sugar}$ analyses in paleoclimatic studies but also lead to the conclusion that the Garba Guracha $\delta^{18}O_{fucose}$ record reflects $\delta^{18}O_{lake\ water}$. Therefore, without completely excluding the influence of the 'amount-effect' and the 'source-effect', we interpret the record to reflect primarily the precipitation-to-evaporation ratio (P/E).

The hydrological history of Garba Guracha is influenced by regional and northern hemisphere climatic changes. Precipitation increased at the onset of the Holocene, resulting in an overflowing lake between ~ 10 and ~ 7 cal ka BP (noted by the most negative $\delta^{18}O$ values in the record). This humid phase corresponds to the African Humid Period (AHP), a spatially complex humid phase across equatorial and northern Africa, driven by enhanced West African Monsoon (WAM) and, in the case of the easterly-situated Bale Mountains, East African Monsoon (EAM) activity. While hydrological changes during the AHP in eastern Africa seem to be driven by meridional climatic processes, the high-altitude Garba Guracha archive shows additional similarities to reconstructed monsoonal changes in Oman. A continuous transition towards more positive $\delta^{18}O$ values begins at 7 cal ka BP and indicates a gradual shift from humid to drier climate.

The reconstructed temperature history is strongly linked to supraregional climatic changes associated with insolation forcing and the AHP, as well as with local anomalies associated with catchment deglaciation and hydrology. Cold temperatures prevailed in the high-altitude Garba Guracha until significant warming (3.0 °C in less than 600 years) occurred shortly after the Holocene onset. A thermal maximum prevailed between 9 and 6 cal ka BP, coinciding with humid conditions, followed by a temperature decrease until 1.4 cal ka BP. The temperatures at the Garba Guracha were reconstructed using a modified MBT'_{5ME} calibration by adding 6-methyl brGDGT IIIa' (resulting in the MBT'_{5ME}-Bale Mountain index, $r^2 = 0.93$, $p < 0.05$) due to an uncommon variation in 6-methyl brGDGTs in the modern lake surface sediment samples.

The results of this dissertation reveal regional and global driving mechanisms of climatic changes in the Bale Mountains, further expanding paleoclimatic knowledge about the Horn of Africa. The innovative methodological approach of this thesis highlights the potential of $\delta^{18}O_{sugar}$ analyses and *n*-alkane dating. Moreover, the results underline the need for intensified basic research like local brGDGT calibration studies to advance and specify existing scientific concepts.

Zusammenfassung

Während der Klimawandel und die globale Erwärmung das östliche Afrika schon heutzutage beeinflussen, ist das Wissen über die klimatischen Veränderungen der Vergangenheit begrenzt. Vor allem in den letzten 15.000 Jahren hat das östliche Afrika räumlich komplexe klimatische Veränderungen erlebt. Obwohl in Ostafrika mehrere paläoklimatische Studien durchgeführt wurden, welche die Temperaturänderungen und die hydrologische Vergangenheit von Seearchiven rekonstruierten, sind die treibenden Mechanismen und Telekonnektionen noch nicht vollständig verstanden. Ein tieferes Verständnis wird verhindert durch (i) das Fehlen von zeitlich weit zurückreichenden, qualitativ hochwertigen wissenschaftlichen Daten bezüglich Umweltveränderungen, insbesondere in der Region des Horns von Afrika, (ii) das Fehlen solcher Daten aus großen Höhen und (iii) unzureichend untersuchte Regionen wie der östliche Teil Äthiopiens und Somalia. Eines der am wenigsten untersuchten Hochgebirgsgebiete der Region sind die Bale Mountains, obwohl sie das größte Gebiet des Kontinents oberhalb von 4000 m ü. NN umfassen. Diese Dissertation zielt darauf ab, den derzeitigen Mangel an paläoklimatischen Rekonstruktionen in Hochgebirgen in der untersuchten Region am Horn von Afrika weiter zu verringern.

Hochgelegene perennierende Seen, insbesondere Karseen, sind wertvolle Archive für paläoklimatische und ökologische Rekonstruktionen, da sie kontinuierliche Sedimente liefern, die durch menschliche Aktivitäten nicht gestört wurden. Der einzige ganzjährige See in den Bale Mountains, der Garba Guracha, liegt in der afro-alpinen Zone auf 3950 m ü. NN. Frühere paläolimnologische Untersuchungen ergaben, dass die kontinuierlichen Sedimente des Garba Guracha paläoklimatische und ökologische Informationen seit der letzten Vergletscherung beinhalten. Um das paläoklimatische Wissen über die Bale Mountains und damit über das östliche Afrika zu erweitern, wurden neue innovative Proxies, z. B. brGDGTs, $\delta^{18}O_{fucose}$, $\delta^{18}O_{diatom}$ und $\delta^{2}H_{n\text{-alkane}}$, auf neu geborgene Sedimentkerne des Garba Guracha angewendet. Die Interpretation der Ergebnisse dieser Analysen ermöglichen ein tieferes Verständnis des Sedimentkerns, vor allem in Bezug auf die Sedimentologie, die Chronologie und die Quellen abgelagerten organischen Materials.

Die hochauflösende Chronologie des Garba Guracha, die unter Verwendung verschiedener Datierungsmethoden und -komponenten (^{210}Pb-Datierung, Radiokohlenstoffdatierung an der Gesamtsedimentfraktion, an Holzkohle und komponentenklassenspezifisch an *n*-Alkanen) erstellt wurde, ergibt ein basales Alter von ~ 16 cal ka BP. Die geochemische Korrelation der Tephra-Schichten in den Garba-Guracha-Sedimenten mit datierten Tephra-Schichten aus anderen Seen der Region liefert eine externe Alterskontrolle, die die Robustheit der neuen Garba-Guracha-Chronologie und die Abwesenheit von systematischen Altersverschiebungen weiter untermauert. Ähnliche Altersangaben für *n*-Alkane und der Gesamtsedimentfraktion deuten darauf hin, dass die Biomarker in dem sehr kleinen afro-alpinen Einzugsgebiet kein Pre-aging vorweisen, was auf eine kurze Verweildauer oder/und eine hohe aquatische Produktivität schließen lässt. Die vorherrschende autochthone Produktion von organischem Material in dem im Vergleich zur Größe des Einzugsgebiets relativ großen See wurde durch relativ niedrige TOC/N Verhältnisse,

relativ positive $\delta^{13}C$ Werte und niedrige Werte der Zucker-Biomarker-Verhältnisse nachgewiesen. Der aquatische Ursprung von Fucose wird außerdem durch einen methodischen Vergleich von $\delta^{18}O_{fucose}$ mit dem rein aquatischen $\delta^{18}O_{diatom}$ Rekord unterstützt. Die gute Korrelation und ähnliche Amplitude von $\delta^{18}O_{diatom}$ und $\delta^{18}O_{fucose}$ (7,9 ‰ bzw. 7,1 ‰) unterstreichen nicht nur das Potenzial von $\delta^{18}O$-Zucker-Analysen in paläoklimatischen Studien, sondern lassen auch den Schluss zu, dass $\delta^{18}O_{fucose}$ im Garba Guracha $\delta^{18}O_{Seewasser}$ widerspiegelt. Ohne den Einfluss des "Amount effects" und des "Source effects" völlig auszuschließen, interpretieren wir den $\delta^{18}O$-Datensatz des Garba Guracha daher als das Verhältnis von Niederschlag zu Verdunstung.

Die hydrologische Vergangenheit des Garba Guracha wird von regionalen und nordhemisphärischen klimatischen Veränderungen beeinflusst. Zu Beginn des Holozäns nahmen die Niederschläge zu, was zu einem überlaufenden See zwischen ~ 10 und ~ 7 cal ka BP führte (erkennbar an den negativsten $\delta^{18}O$-Werten im gesamten Kern). Diese Phase entspricht der African Humid Period, einer räumlich unterschiedlich ausgeprägten feuchten Phase im äquatorialen und nördlichen Afrika, die durch eine verstärkte Aktivität des Westafrikanischen Monsuns und, im Fall der östlich gelegenen Bale Mountains, des Ostafrikanischen Monsuns bedingt wurde. Während die hydrologischen Veränderungen der AHP in Ostafrika durch meridionale Klimaprozesse angetrieben zu werden scheinen, zeigt das hochgelegene Garba Guracha Archiv zusätzliche Ähnlichkeiten mit rekonstruierten Monsunveränderungen in Oman. Eine kontinuierliche Verschiebung hin zu positiveren $\delta^{18}O$-Werten beginnt um 7 cal ka BP und deutet auf einen allmählichen Übergang von feuchtem zu trockenem Klima hin.

Die Temperaturen am Garba Guracha wurden mit Hilfe einer modifizierten MBT'_{5ME}-Kalibrierung durch Hinzunahme von 6-Methyl-brGDGT IIIa' rekonstruiert (MBT'_{5ME}-Bale-Mountain-Index - $r^2 = 0,93$, $p < 0,05$). Eine Anpassung der Kalibration war nötig, da die 6-Methyl-brGDGTs in den modernen Seesedimenten der Bale Mountains in bislang unbekannten Mengen auftreten und die Temperatur-Kalibrierung beeinflussen. Die rekonstruierten Temperaturänderungen sind stark von überregionalen klimatischen Einflüssen, wie Insolationsveränderungen und der AHP beeinflusst. Zusätzliche lokale Einflüsse, wie noch nicht abgeschmolzene Eismassen im Einzugsgebiet oder die Veränderungen der Hydrologie sind nicht auszuschließen. Im hochgelegenen Garba Guracha herrschten kalte Temperaturen, bis es kurz nach Beginn des Holozäns zu einer deutlichen Erwärmung (3,0 °C in weniger als 600 Jahren) kam. Zwischen 9 und 6 cal ka BP herrschte ein thermisches Maximum, das mit feuchten Bedingungen zusammenfiel und gefolgt war von einem Temperaturrückgang der bis 1.4 cal ka BP andauerte.

Die Ergebnisse dieser Dissertation zeigen regionale und globale Antriebsmechanismen für klimatische Veränderungen in den Bale Mountains auf und erweitern damit das paläoklimatische Wissen über das Horn von Afrika. Der innovative methodische Ansatz dieser Arbeit hebt das Potenzial von $\delta^{18}O$-Zuckeranalysen und *n*-Alkan-Datierungen hervor. Darüber hinaus unterstreichen die Ergebnisse die Notwendigkeit einer verstärkten Grundlagenforschung, wie z. B. lokaler brGDGT-Kalibrierungsstudien, um die bestehenden wissenschaftlichen Konzepte voranzutreiben und zu präzisieren.

Acknowledgements

This dissertation would not have been possible without the support of several people. My special thanks to Prof. Dr. Michael Zech for guiding me and supervising my doctoral studies. I am grateful for all the challenges you have given me, for the encouragement in difficult times and for the constant support.

Furthermore, I gratefully thank Prof. Dr. Arno Kleber for his support and tireless efforts during the last years. I want to thank Dr. Ana Moreno Caballud for the third review of this thesis.

Special thanks to Graciela Gil-Romera, who always helped with lectures, optimism, and vast experience.

I would also like to thank Prof. Dr. Bruno Glaser (MLU Halle), Prof. Dr. Henry F. Lamb, Dr. Hanno Meyer (AWI Potsdam), Dr. Cindy De Jonge (ETH Zürich) and Prof. Dr. James M. Russell (Brown University). Science is not a one-person job, so I would like to thank all my co-authors, students and colleagues who have helped me along the way.

Furthermore, I would like to thank my colleagues from the University of Halle (MLU Halle) Bety Mekonnen, Bruk Lemma, Marianne Zech, and Heike Maennike for their support and help during the last years.

I want to thank the Bale Mountain Exile Hypothesis team for their outstanding work organising the field trips, meetings, and all the other work in the background. I am grateful for the work of the project speakers Lars Opgenoorth, Thomas Nauss, and Georg Miehe. Nothing would have been possible without the coordinators Katinka Thielsen and Mekbib Fekadu.

During the last years, I was blessed to visit the wonderful country of Ethiopia and to meet and spend time with Terefe, Shanku, Elias and Eremias. Thank you for your help.

I would like to thank my friends and colleagues Tobias Bromm, Steven Polifka, Julian Struck, and Marcel Bliedtner for your friendship, all your support, your time, “geteiltes Leid ist halbes Leid”, an open ear, and lots of fun.

Furthermore, I would like to thank Alexander Groos, Paul Strobel, Miguel Sevillia-Callejo, David Grady, Christopher Roettig, Lisa Zwanzig, Lutz Maerker, Roland Zech, Wolfgang Zech, Marcel Lerch, Ulrike Thieme, Jana Löhrlein, and Doreen Degenhardt, for your support and help.

Most importantly, I have to thank my family, my wife and my kids for all the support, the indulgence, and all the love that kept me going.

Chapter 1

Introduction

1.1 Motivation

Humanity is facing one of its most significant challenges in modern times. Climate change and global warming in particular, will alter the world in many ways. Higher average temperatures and changes in atmospheric and oceanic circulations will lead to consequences humanity cannot yet predict. Rising sea levels and climate extremes like more extended periods of drought and more severe flooding are natural consequences of global warming. These consequences affect humanity and lead to socio-economic problems of global dimensions. The severity of climate change and its global implications have been widely discussed in science, and the main results are summarised in the last report from the Intergovernmental Panel for Climate Change (IPCC) (IPCC, 2021).

The IPCC predicts the strongest effects for semi-arid and arid zones. According to the "State of the climate in Africa 2020" report (WORLD METEOROLOGICAL ORGANIZATION (WMO), 2021), the variability of precipitation has already increased. Wet conditions have increased, for example, in the Sahel, the central Nile catchment and northeastern Africa. On the contrary, precipitation decreased in northwestern Africa and southeastern Africa. Glaciers in the African mountains retreat faster than in any other region on earth. The same holds true for the rates of sea-level rise along the coastlines, except for the Mediterranean (WORLD METEOROLOGICAL ORGANIZATION (WMO), 2021). This can be attributed to the annual mean temperature, which is projected to increase faster than in any other part of the world (NIANG ET AL., 2014). The report's findings support this, with the highest annual mean temperatures recorded in 2020, especially in the northwestern and equatorial western part of the continent and the Horn of Africa region (WORLD METEOROLOGICAL ORGANIZATION (WMO), 2021).

In Ethiopia, located in the Horn of Africa, the mean annual temperature increased by 1.3 °C over the last 60 years. With a rate of 0.32 °C per decade, the increase in temperature was highest in July, August and September (BEZU, 2020). As reported for the African continent, the variation in annual rainfall has increased (ZEGEYE, 2018). Modell studies projected a slight increase in mean rainfall amounts with high regional variability in Ethiopia. Moreover, changes in seasonal rainfall have been recorded since 1981, with increasing precipitation from June to August and October to November and declining rainfall between February and April. The predicted increase in temperature and precipitation will likely result in increased climatic extremes such as heavy rain events (ACCRA 2011).

The increase in temperature and precipitation variation in the last decades has been linked to human influences with only a minor impact of natural forcing (IPCC, 2021). The latest IPCC report highlights the need by the scientific community to use palaeoclimate research as a tool to reconstruct climate baseline conditions when human activities had a lesser impact on climate (NEUKOM ET AL., 2019). Although palaeoclimatology has emerged as a central discipline for understanding present-day climate variability (THOMPSON, 2004), certain areas of the planet remain understudied. An incomplete understanding of global climate complexity leads to a distorted perception of climatic systems (HUGHES ET AL., 2021), which is particularly true for the African continent in general and eastern Africa in particular.

Eastern Africa is not only an understudied region regarding climate research, its climate history is also one of the most complex and globally interconnected (OTTO-BLIESNER ET AL., 2014; TIERNEY & RUSSELL, 2007; TIERNEY ET AL., 2013). In the past, northern and eastern Africa experienced severe climatic fluctuations (LOOMIS ET AL., 2015; TIERNEY & DEMENOCAL, 2013; TIERNEY ET AL., 2008,2017,2011b,2011a; WAGNER ET AL., 2018). The deglaciation of the last glacial maximum is followed by abrupt warming and the increase of precipitation at the African Humid Period onset (AHP) (DEMENOCAL ET AL., 2000), leading to a prolonged humid phase with the greening of the Saharan Desert (BLOM ET AL., 2009). The termination of the AHP concurs with a drying period at the beginning of the Meghalayan (4.2 cal ka BP) (BINI ET AL., 2019). Even though these climatic events prevailed across northern and eastern Africa, their intensity and timing varied regionally (CASTAÑEDA ET AL., 2016). While the understanding of the spatial and temporal differences is still incomplete, the climatic events were connected across the northern hemisphere (BAHAGA ET AL., 2015; DIRO ET AL., 2011; ENDRIS ET AL., 2016; INDEJE ET AL., 2000; OGALLO, 1988; ROPELEWSKI & HALPERT, 1987; TIERNEY & RUSSELL, 2007; TIERNEY ET AL., 2013). Several paleoclimate studies have been conducted in eastern Africa reconstructing precipitation changes (COSTA ET AL., 2014; JAESCHKE ET AL., 2020; JUNGINGER ET AL., 2014; MORRISSEY & SCHOLZ, 2014; TIERNEY ET AL., 2011b; TRAUTH ET AL., 2018; WAGNER ET AL., 2018), and fewer studies have reconstructed the regional temperature history of northeastern Africa (BERKE ET AL., 2012b; CASTAÑEDA ET AL., 2016; GARELICK ET AL., 2022; LOOMIS ET AL., 2015,2017,2012; MORRISSEY ET AL., 2018). However, the hydrological and temperature history of eastern Africa has been reconstructed mainly from low-elevation sites. High-altitude archives, especially lakes, are excellent sensors of environmental change (CATALAN ET AL., 2006,2013) due to the lack of significant anthropogenic disturbance or desiccation (ARNAUD ET AL., 2016). Such high-altitude records are lacking in eastern Africa, especially in the understudied Horn of Africa region.

This thesis focuses on the high-altitude lake Garba Guracha, a cirque lake situated 3950 m a. s. l. in the Bale Mountains southeast of the Rift Valley in Ethiopia. The research is embedded into the interdisciplinary research unit (no. 2358) entitled “The Mountain Exile Hypothesis”, funded by the German Research Foundation (DFG), focusing on the high-altitude ecosystem of the Bale Mountains. The main objectives of the seven subprojects were to reconstruct the environmental and archaeological history of the Bale Mountains. The working hypothesis of the research group is that mountain archipelagos in eastern Africa served as a refuge for humans and animals during periods of climatic stress since the Pleistocene, e.g. during the Last Glacial Maximum. Mountain areas could have been attractive for humans due to the higher availability of water and other resources than the surrounding lowlands. The thesis is embedded into the subproject “P5 - Paleoclimate”, aiming to reconstruct the climate history of the Bale Mountains recorded in the Garba Guracha sediment archive.

The main aim of this thesis is to reconstruct the timing and intensity of (i) changes in the lake hydrology based on biomarker analyses of *n*-alkanes, hemicellulose-derived sugars and diatoms and (ii) changes in air temperature based on branched glycerol dialkyl glycerol tetraethers (brGDGTs). To achieve these main aims, an understanding of the timing and intensity of catchment changes and processes is essential, especially for the interpretation of the isotopic composition of biomarkers. Therefore, necessary aims were to develop (iii) a

sedimentological profile of the lake sediments, (iv) a high-resolution chronology and age-depth model, and (v) an understanding of the autochthonous or allochthonous origin of the sedimentary organic matter.

1.2 Objectives of the thesis

The thesis focuses mainly on reconstructing the hydrological and temperature history of Garba Guracha in the Bale Mountains. The basis for such reconstructions is a high-resolution chronology and age depth model and an understanding of the autochthonous or allochthones origin of the sedimentary organic matter. Due to the unavailability of the Garba Guracha lake sediment core of TIERCELIN ET AL. (2008) and UMER ET AL. (2007), a new sediment core had to be retrieved. In 2017, replicate sediment cores (BAL GGU17 1A and 1B) were taken using a Livingstone corer in 1 m overlapping sections, yielding 1550 cm of sediment in each core.

The following research questions and associated objectives arise:

- What is the time frame and age-depth function of the 2017 sediments?

O1 - Development of a robust and high-resolution chronology and age-depth function

  - Dating of different compounds using well-established (bulk sediment, charcoal, ^{210}Pb) and the innovative compound-class-specific ^{14}C dating of *n*-alkanes
  - Establishment of an age-depth model using a Bayesian modelling framework
  - Validation of the chronology and age-depth model using tephra layers as external age control

- What is the origin of the organic material in the Garba Guracha sediment core?

O2 - Source identification of organic matter input into Garba Guracha sediments

  - Analyses of total carbon, total nitrogen, δ^{13}C, δ^{15}N and calculating the C/N ratio
  - Quantification of leaf wax lipids-derived *n*-alkanes and hemicellulose-derived sugars

- Why and how has the hydrology of Garba Guracha changed?

O3 - Reconstruction of the hydrological history of Garba Guracha.

  - Measurement of $\delta^{18}O_{sugar}$ and $\delta^{2}H_{n\text{-alkane}}$ to reconstruct δ^{18}O of lake and/or leaf water
  - Cross-validation using δ^{18}O analyses of diatom to reconstruct δ^{18}O of lake water

- Why and how has the mean annual temperature of Garba Guracha changed?

O4 - Reconstruction of the temperature variation of Garba Guracha

  - Establishment of a regional/local modern temperature calibration
  - Analyses of brGDGT of the Garba Guracha core sediments

- How does the reconstructed climate history of Garba Guracha relate to other climate records in eastern Africa?

O5 - Comparing the Garba Guracha climate record regionally in order to understand the main mechanisms driving the past climate variability.

1.3 Background – The Bale Mountains and biomarker

1.3.1 Study area and archive

The Bale Mountains belong to the Bale-Arsi Massif, situated east of the Main Ethiopian Rift (Fig. 1.1). The massif is located between 39.5 ° to 40 ° longitude (E) and between 6.7 ° to 7. 2 ° latitude (N) with an altitudinal range of ~ 3000 m (1400 - 4377 m a. s. l.) (HILLMAN, 1986). The Bale Mountains encompass an area of 2600 km^2 and are topographically diverse. Northward descending rivers have incised deep valley structures in the north and northeast of the plateau, like the Togona Valley. From the southern side, the steep Harenna Escarpment rises up from the surrounding low lands (1400 - 3800 m a. s. l.) (OSMASTON ET AL., 2005) to the interjacent high Sanetti Plateau. The volcanic plateau extends over 600 km^2 between ~ 3800 to ~ 4200 m a. s. l. Consisting of trachyte, alkali basalt and tuffs with rhyolites, the plateau was formed 40 million years ago by solidified horizontal lava on top of older volcanic material (UHLIG & UHLIG, 1991; WILLIAMS, 2016). The plateau and the valleys were repeatedly glaciated in the past, especially during the Last Glacial Maximum (GROOS ET AL., 2020,2021; OSSENDORF ET AL., 2019), resulting in distinct moraine and lake structures like Garba Guracha.

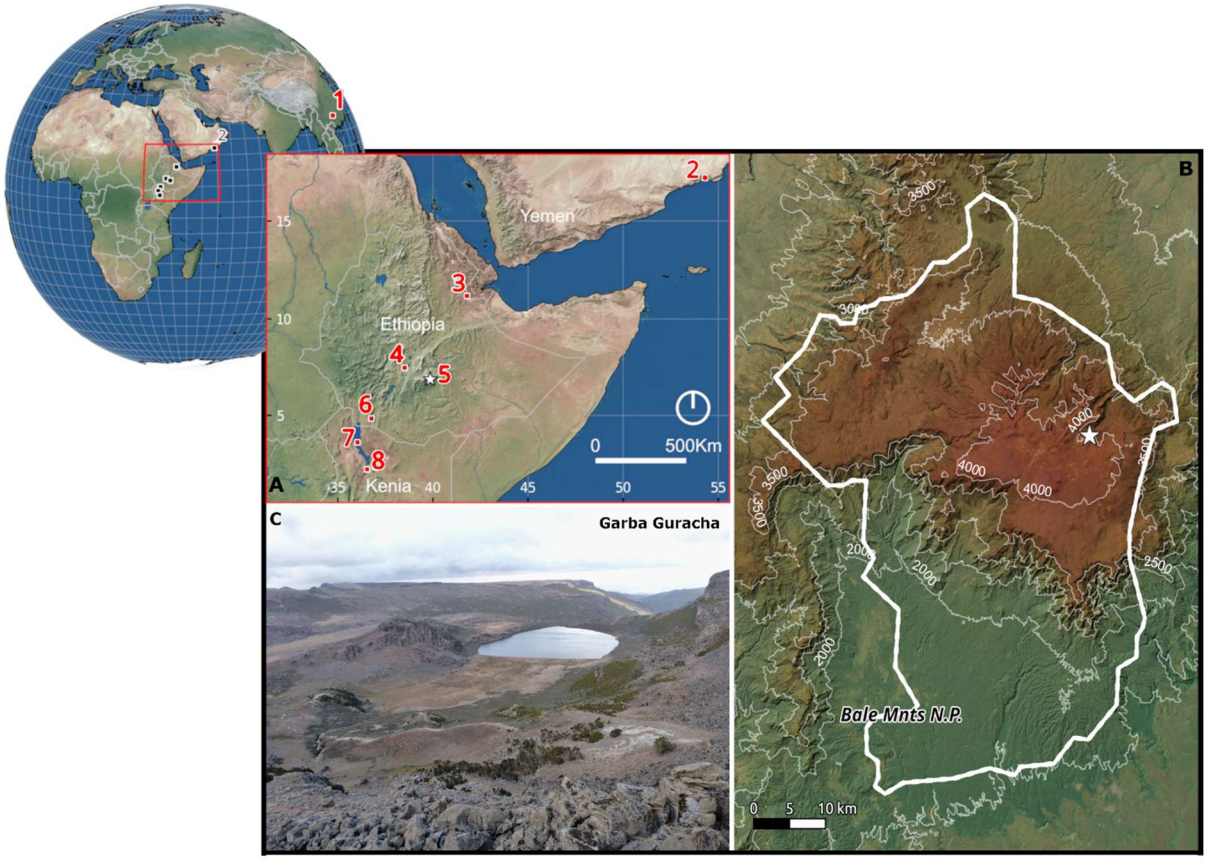

Figure 1.1: Study area - A) Overview of the region: (1) Dongge Caves, (2) Qunf Cave, (3) Lake Abhè, (4) Ziway-Shala, (5) Garba Guracha (this study), (6) Chew Bahir, (7) Lake Turkana, (8) Paleolake Suguta; B) Garba Guracha (white star) in the Bale Mountains National Park (thick white line); C) glacial cirque of the Garba Guracha catchment.

The north-facing glacial cirque Garba Guracha (6.875781 °N, 39.878075 °E), situated in a side valley of the Togona Valley, was described for the first time by WERDECKER (1962) and is located between the *Ericaceous* and afro-alpine vegetation belts. In the local Oromo language, Garba Guracha means "Black Lake" (TIERCELIN ET AL., 2008), and therefore this thesis uses Garba Guracha and not Lake Garba Guracha. UMER ET AL. (2007) and TIERCELIN ET AL. (2008) took a sediment core from Garba Guracha, focusing on pollen and sedimentological analyses and described the small catchment (0.15 km^2) in more detail. It is located at 3950 m a. s. l. and extends to about 500 x 300 m in size with a maximum water depth of 6 m. Steep cliffs border the catchment on the southern and southeastern sides. On the northern side, the lake has an outlet over a boulder-covered rock bar entering the Togona Valley. The southern shoreline consists of well-sorted clean sands due to strong northern winds and associated wave occurrence. Located south of the lake, a marshy alluvial plain is fed by several springs. Basaltic lavas form the carbonate-poor bedrock of the Garba Guracha catchment (LÖFFLER, 1978; UHLIG & UHLIG, 1991), while the cirque base is formed by trachytic tuff (TIERCELIN ET AL., 2008).

The regional climate of eastern Africa

Current climatic conditions in eastern Africa vary significantly due to its complex topography and the influence of the Intertropical Convergence Zone (ITCZ), the Congo Air Boundary (CAB), Indian Ocean sea surface temperature and the Indian Summer Monsoon (ISM) and the El Niño-Southern Oscillation (NICHOLSON, 2017). All of these affect temperature and the distribution, amount and timing of rainfall in the region, resulting in a wide range of climatic conditions from the warm, dry and semi-arid conditions of northern Kenya, southeastern Ethiopia, Djibouti and Somalia to the cool, humid conditions of the western highlands (HOVE ET AL., 2011; LYON & VIGAUD, 2017; NICHOLSON, 2017). The seasonal climatic changes of eastern Africa are driven mainly by interannual atmospheric circulation changes of the CAB and the latitudinal migration of the tropical rain belt and the ITCZ between 10 ° North and South of the equator. During the northern hemisphere summer, the CAB migrates eastward (DAVIES ET AL., 1985; HILLS, 1979; NAKAMURA, 1968). The extent of the eastward migration depends on the West-East atmospheric pressure gradient between Africa and India and the intensity of the ISM (WAGNER ET AL., 2018). Strong ISM conditions prevent Indian Ocean air masses from entering deep into the African continent, shifting the CAB further East (CAMBERLIN, 1997).

In the past, especially in the last 16.000 years, the region experienced strong climatic changes. While relatively cold temperatures and northeastern winds prevailed during the deglaciation and the northern hemisphere Younger Dryas (YD), the increasing northern summer insolation led to a land-ocean temperature gradient, causing a strengthening of the monsoonal systems. Additionally to the high monsoon intensity, a northward shift in the mean position of the tropical rain belt and an eastward migration of the CAB might have been responsible for enhanced humidity in the region as early as ~ 15 cal ka BP, causing recorded high stands of East African lakes (GASSE, 2000; JUNGINGER ET AL., 2014; LEZINE ET AL., 2014). This prolonged pluvial phase, termed the African Humid Period (AHP) (DEMENOCAL ET AL., 2000), lasted until ~ 5 cal ka BP. Humid conditions were particularly intense between north Africa and 10 °S in eastern Africa (GASSE, 2000), creating large lake systems whose remnants today

are periodic, shallow and alkaline. The shift towards the current relatively dry conditions in eastern Africa started around 4.5 cal ka BP with the termination of the AHP and is recorded in lake level drops and overall drier climatic conditions.

The climate of the Bale Mountains

The climate of the Bale Mountains varies spatially and temporarily and is, expectedly, affected by the orographic differences in altitude and north-south exposure and by changing atmospheric air mass movements in the course of the year (KIDANE ET AL., 2012; UHLIG & UHLIG, 1991). The Bale Mountains experience a four months dry season (November to February) and a bimodal wet season (March to October) lasting eight months (KIDANE ET AL., 2012). The bimodal rainfall pattern is associated with the convergence of northeast and southwest winds due to the northern and southern location of the ITCZ between June and September and between October and March, respectively (TIERCELIN ET AL., 2008). The highest monthly rainfalls are related to the convergence of southwest air masses, leading to precipitation maxima in April/May and September/October (LEMMA ET AL., 2020; WOLDU ET AL., 1989). At the altitude of Garba Guracha, 1097 mm of annual rainfall and 4.9 °C mean annual temperature were measured in 2017 (Angesso climate station). The afro-alpine regions near Garba Guracha are characterised by frequent frost and large diurnal temperature differences of 40 °C (-15 °C to + 26 °C) (HILLMAN, 1988).

1.3.2 A short introduction to selected biomarkers applied in environmental geochemistry

In the last decades, biomarker proxies have advanced paleoclimate and paleolimnological research. Biomarkers are organic remains of plants and other organisms that yield information about climate and environmental conditions during the time of their synthesis (CASTAÑEDA & SCHOUTEN, 2011; DIEFENDORF & FREIMUTH, 2017; FICKEN ET AL., 2000; HEPP ET AL., 2016; LENG & BARKER, 2006).

Hemicellulose-derived sugars and *n*-alkanes - compound-specific $\delta^{18}O$/ $\delta^{2}H$

One part of the cell structure of plants is hemicellulose. Hemicellulose is built up by monosaccharides, which consist of non-cyclic or cyclic carbohydrate chains with one carbonyl group and several hydroxyl groups (TUTHORN ET AL., 2014; ZECH ET AL., 2013). *n*-Alkanes, straight-chained hydrocarbons without functional groups, are part of the epicuticular leaf wax layers (EGLINTON & HAMILTON, 1967). Hemicellulose-derived sugars and *n*-alkanes are source-specific and synthesised by aquatic and terrestrial plants. Aquatic plants and algae produce the monosaccharide fucose in higher abundance, and in contrast, terrestrial plants predominantly synthesise arabinose and xylose (HEPP ET AL., 2016). While terrestrial plants produce *n*-alkanes with 25 (*n*-C_{25}) to 35 (*n*-C_{35}) carbon atoms predominantly, aquatic plants synthesise *n*-alkanes with 21 (*n*-C_{21}) to 25 (*n*-C_{25}) carbon atoms (CASTAÑEDA & SCHOUTEN, 2011; EGLINTON & EGLINTON, 2008; FICKEN ET AL., 2000).

n-Alkanes and hemicellulose-derived sugars are valuable proxies in paleoclimatology due to the incorporation of the isotopic composition (corresponding to $\delta^{18}O$ and $\delta^{2}H$) of source water during biosynthesis. In terrestrial settings, the isotopic composition of source water (corresponding to $\delta^{18}O/\delta^{2}H_{leaf\ water}$) is derived from soil water and shallow groundwater, which is directly linked to the isotopic composition of precipitation (SACHSE ET AL., 2012; SPRENGER & TETZLAFF, 2017). The original isotopic composition of source water is further overprinted by the evaporative enrichment of soil water (ε_{SW}) and the transpirative enrichment of plant leaf water (ε_{Et}) (CORMIER ET AL., 2018; LIU & LIU, 2016; LIU ET AL., 2016; SACHSE ET AL., 2012). In aquatic settings, the isotopic composition of source water ($\delta^{18}O/\delta^{2}H_{lake\ water}$) is altered by the different water sources (groundwater, ice/snow melting, precipitation, surface runoff) and evaporative enrichment of the lake water (ε_{LW}) (HEPP ET AL., 2015; SACHSE ET AL., 2012; SPRENGER & TETZLAFF, 2017). During the biosynthesis of *n*-alkanes and hemicellulose-derived monosaccharides in aquatic and terrestrial environments, the source water signature is further modified by a biosynthetic fractionation factor (ε_{bio}).

A ε_{bio} of ~ +27 ‰ to +29 ‰ is assumed to enrich the compound-specific oxygen isotopic composition of hemicellulose-derived sugars compared to the source water (HEPP ET AL., 2020,2021; LEMMA ET AL., 2021; TUTHORN ET AL., 2015). *n*-Alkanes in terrestrial plants are depleted by ε_{bio} of ~ −160 ‰, and the ε_{bio} for aquatic n-alkanes ranges between -160 ‰ and -105 ‰ (MÜGLER ET AL., 2008; SACHSE ET AL., 2012; SESSIONS ET AL., 1999). While the ε_{bio} of *n*-alkanes depends on the hydrogen origin from NADPH or leaf water, the variability of ε_{bio} in general is influenced by differences in plant physiological metabolisms, environmental conditions, and vegetation types (CORMIER ET AL., 2018; FREIMUTH ET AL., 2017; GRIEPENTROG ET AL., 2019; LEHMANN ET AL., 2017; LIU ET AL., 2017a; LIU & AN, 2019; SCHMIDT ET AL., 2003). The $\delta^{18}O$ and $\delta^{2}H$ values are presented in the usual δ-notation versus the Vienna Standard Mean Ocean Water (VSMOW).

Branched glycerol dialkyl glycerol tetraether

Branched glycerol dialkyl glycerol tetraethers (brGDGTs) are membrane-spanning bacterial lipids. BrGDGTs occur with different numbers of methyl groups and found as tetra- (I), penta- (II), or hexamethylated compounds. Additionally, different numbers of cyclopentyl moieties (none (a), one (b), or two (c)) appear (Fig. 1.2). The outer methyl group can be positioned either on the α and/or C5 (5-methyl compounds) or C6 (6-methyl compounds, indicated by a prime notation) location (DE JONGE ET AL., 2014a). These different forms of methylation (MBT) and cyclisation of branched tetraethers (CBT) correlate with the measured mean annual air temperature (MAT) and pH values (WEIJERS ET AL., 2007b).

Even though the first identification of GDGT compounds was made by DAMSTÉ ET AL. (2000), the producing bacterial communities are yet not fully known. It has been proposed that Acidobacteria produce brGDGTs both in cultures and in the environment (DE JONGE ET AL., 2019,2021; SINNINGHE DAMSTÉ ET AL., 2018). Supporting this, a recent study found that certain brGDGTs were produced by Acidobacteria under oxygen limitations (HALAMKA ET AL., 2021). Nevertheless, the good correlation between brGDGT abundances and MAT has been proven by several modern calibration studies applied to different settings (i.e. soils and lakes) (DE

JONGE ET AL., 2014b; DEARING CRAMPTON-FLOOD ET AL., 2020; RUSSELL ET AL., 2018; WEIJERS ET AL., 2007a). After analytical advances, separating 5 and 6-methyl isomers was possible, improving the temperature calibrations further. Based on these calibrations, continental paleo-temperature records have been successfully reconstructed in marine river outflow, lacustrine sediments and terrestrial archives such as loess sequences and paleosoils (GARELICK ET AL., 2022; LOOMIS ET AL., 2015,2017; MORRISSEY ET AL., 2018; SCHREUDER ET AL., 2016; ZENG & YANG, 2019).

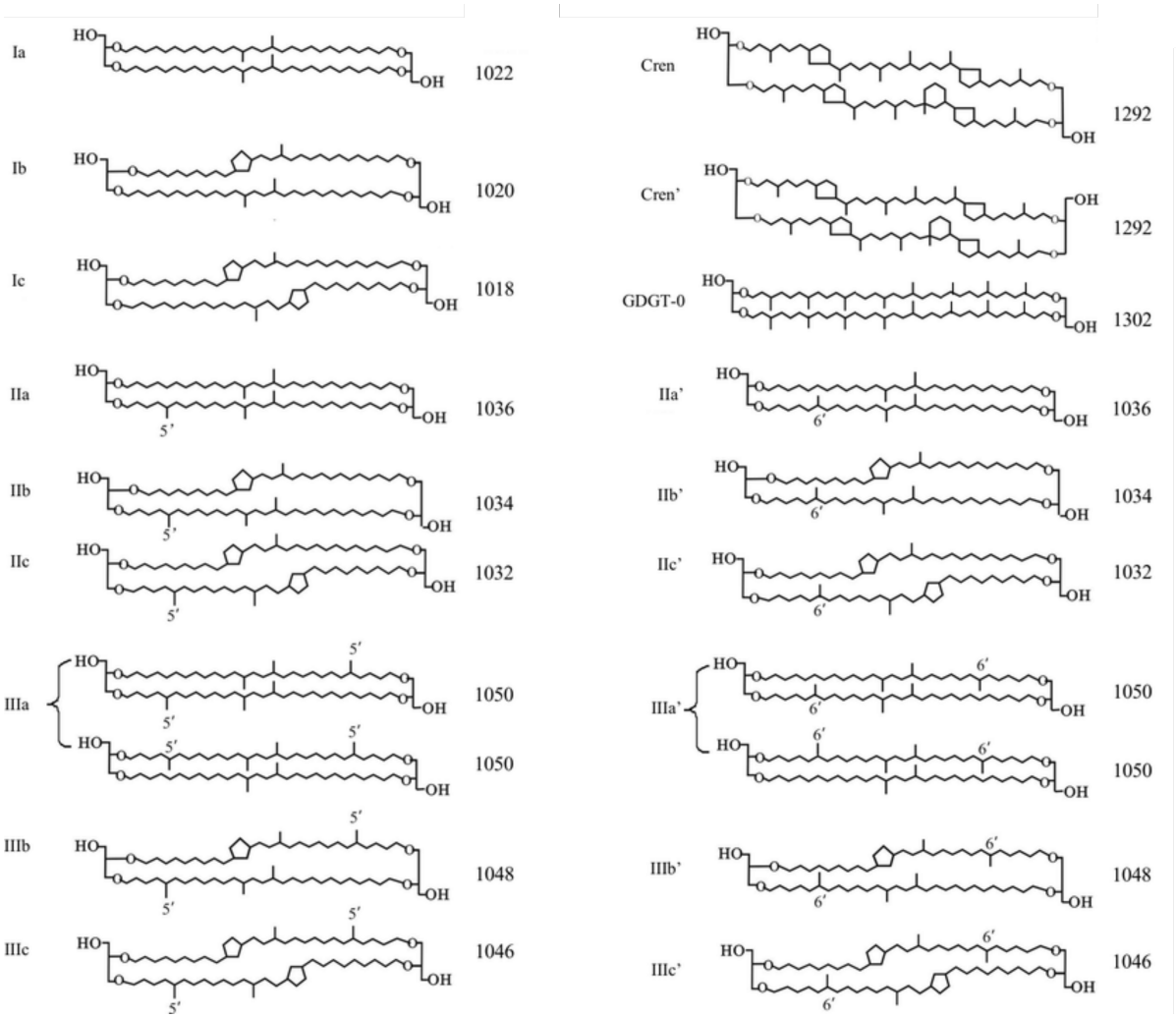

Figure 1.2: Chemical structures of branched GDGTs (I-III), GDGT-0 and crenarchaeol (GUO ET AL., 2020).

1.4 Methods used in the thesis

To accomplish the objectives, a series of field and laboratory analyses were carried out. The methods used are introduced here briefly, but for a more detailed description, the reader is referred to the respective methodology chapters of the included publications.

All analyses were performed on the replicate cores (BAL-GGU17-1A and 1B). The cores were shipped and stored at 4 ºC at the Research Core Facility of the IPE-CSIC (Zaragoza, Spain). The 1550 cm long cores were sampled in 10 cm intervals to create a continuous record with smoothed variability but without loss of information. Biomarker analyses were limited to the

upper part of the cores (< 950 cm) due to the required amount of organic matter that was only present in those sections.

1.4.1 Monosaccharide sugar biomarkers

After extraction using hydrolysis (4 M trifluoroacetic acid), the dissolved monosaccharide sugar biomarkers were filtered, evaporated, and then further purified using XAD-7 and DOWEX 50WX8 columns to remove humic-like compounds and cations, respectively (AMELUNG ET AL., 1996).

- Quantification

  In order to quantify the individual monosaccharide sugars (arabinose, fucose, galactose, glucose, mannose, rhamnose, ribose and xylose), a derivatisation (methyloxime-trimethylsilyl-derivatisation) following the method of ANDREWS (1989) was conducted. The quantification was achieved by measurements using a Gas Chromatograph with Flame-Ionization Detection (GC-FID) (Shimadzu, Kyoto, Japan).

  The abundance of monosaccharide sugars is used to identify their aquatic or terrestrial source. Based on the ratio $\frac{fucose}{(arabinose+xylos\ )}$ (HEPP ET AL., 2016)*, terrestrial plants and mosses are characterised by values < 0.1, while aquatic plants and algae are characterised by ratios > 0.1.*

- Isotopic composition

  Samples were derivatised with methylboronic acid (MBA) for 1 hour at 60 °C (KNAPP, 1979) to ensure the GC volatility of the monosaccharides arabinose, fucose, xylose and rhamnose (GROSS & GLASER, 2004). The samples were measured in triplicates using a Trace GC 2000 coupled to a Delta V Advantage isotope ratio mass spectrometer (IRMS) via an ^{18}O-pyrolysis reactor (GC IsoLink) and a ConFlow IV interface (all devices from Thermo Fisher Scientific, Bremen, Germany) (ZECH & GLASER, 2009).

  The oxygen isotopic composition of sugar molecules depends on fractionation processes linked to temperature, air mass source and trajectory, and global ice volume. The oxygen atoms, incorporated during the biosynthesis of the sugar molecules, yield climatic information (see Section 1.3.2).

1.4.2 Total lipid extraction for *n*-alkane and brGDGTs analyses

The total lipid extract (TLE) was obtained for compound-specific radiocarbon dating (Chapter 2), *n*-alkane analyses and brGDGT measurements (Chapter 3 and 4) using a soxhlet system. The TLE was seperated into three fractions of different polarity using aminopropyl pipette columns (Supelco, 45 um) and solvents of increasing polarity (*n*-hexane; dichloromethane:methanol 1:1; diethyl ether:acetic acid 19:1) (HOU ET AL., 2008; SCHÄFER ET AL., 2016).

- Radiocarbon dating

  The *n*-alkane fraction of the TLE was purified using $AgNO_3$-coated silica and zeolite. After the zeolite was dissolved in hydrofluoric acid, the *n*-alkanes were obtained by liquid-liquid extraction with *n*-hexane.

- Quantification

  The *n*-alkanes were quantified using a GC-2010 series gas chromatograph coupled with a flame ionisation detector (GC-FID; Shimadzu, Kyoto, Japan) at the Institute of Agronomy and Nutritional Sciences, Soil Biogeochemistry, Martin-Luther-University Halle-Wittenberg.

  The abundance of n-alkane chain lengths is used to identify the producing plant community. Grasses tend to produce the n-alkanes nC_{31} and nC_{33}, whereas shrubs and trees produce predominantly nC_{27} and nC_{29}. Aquatic organisms produce nC_{23} and nC_{25}. Based on the ratio $P_{aq}=(\frac{(nC_{23}+nC_{25})}{(nC_{23}+nC_{25}+nC_{29}+nC_{31})}$ (FICKEN ET AL., 2000)*, terrestrial plants are characterised by values < 0.1, while ratios between 0.4 and 1 characterise aquatic plants.*

- Isotopic composition

  Compound-specific *n*-alkane δ^2H measurements were performed using the coupling of a TRACE GC Ultra and a Delta V Plus IRMS (Thermo Fisher Scientific, Bremen, Germany). Co-analysing *n*-alkane standard mixtures with known isotope composition (supplied by A. Schimmelmann, University of Indiana) was used to calibrate the $\delta^2H_{n\text{-alkane}}$ results and check the precision of the GC-IRMS system. Routinely, standard mixtures with known isotopic composition were measured, and the stability of the H^+3 factor was evaluated and ensured.

  Similar to sugar molecules, the isotopic composition of n-alkanes depends on fractionation processes linked to air mass source and trajectory, temperature and global ice volume. The hydrogen atoms, incorporated during the biosynthesis of the n-alkanes, yield climatic information (see Section 1.3.2).

1.4.3 Branched Glycerol Dialkyl Glycerol Tetraether analyses

Prior to measurement, a standard was added to the brGDGT containing fraction, and the sample was filtered using a 0.45 um polytetrafluoroethylene (PTFE) filter. GDGTs were measured at the ETH Zurich using a high-performance liquid chromatograph (Agilent 1260) coupled to a quadrupole mass spectrometer configured for atmospheric pressure chemical ionisation (HPLC-APCI-MS). The purification and separation were achieved following the method described by HOPMANS ET AL. (2016) and quantified following the method described by HUGUET ET AL. (2006).

The membrane lipid-derived branched glycerol dialkyl glycerol tetraethers are used to reconstruct temperatures because the composition of differently synthesised isomers

correlates with mean annual air temperature and pH in soils, peats and lakes (see Section 1.4.2).

1.4.4 Biogeochemical analyses

Bulk sediment samples were packed in tin boats to be analysed for total nitrogen (N), total carbon (TC), and stable carbon and nitrogen isotopic composition ($\delta^{13}C$ and $\delta^{15}N$, respectively). The analyses were carried out at the Institute of Agronomy and Nutritional Sciences, Soil Biogeochemistry, Martin-Luther-University Halle-Wittenberg. For the measurements, a EuroVector EA 3000 elemental analyser (Hekatech, Wegberg, Germany) coupled via a Conflow III Interface to a Delta V Advantage isotope ratio mass spectrometer (IRMS; both from Thermo Fisher Scientific, Bremen, Germany) was used.

*The $\delta^{13}C$ values help to distinguish the source of organic matter. During photosynthesis, a natural isotope fractionation occurs depending on the photosynthetic pathway and environmental regime (terrestrial or aquatic). The lowest $\delta^{13}C$ values (-25 ‰ to -35 ‰) correspond to C_3 vascular plants, less negative (-16 ‰ to -10 ‰) for C_4 plants and most positive (> -12 ‰) for algae and aquatic plants (*Brenner et al., 2006; O'Leary, 1988*). Due to different amounts of carbon-rich lignin and cellulose in aquatic and terrestrial plants, the total organic carbon/nitrogen (TOC/N) ratio can also be used similarly to $\delta^{13}C$ to detect the origin of OM. Aquatic-produced organic matter is characterised by values < 10 (*Meyers, 2003*), and terrestrial higher plants by higher TOC/N values (> 20) (*Meyers, 1994*). The use of $\delta^{15}N$ in lake sediments is problematic due to various sources of nitrogen and fractionation during diagenesis and denitrification* (Brenner et al., 1999; Hepp et al., 2019b).

1.4.5 Radiocarbon dating

Carbonates were removed from bulk sediment and charcoal samples and washed with ultrapure water to pH neutrality. Prior to ^{14}C measurements, the samples were transferred in tin capsules. Also the purified *n*-alkanes were transferred into tin capsules by dissolving them in dichloromethane (DCM). The DCM was evaporated before ^{14}C measurements. A MIni CArbon DAting System (MICADAS) AMS coupled online to an elemental analyzer (Vario MICRO cube from Elementar) was used for the ^{14}C measurements at the LARA AMS Laboratory, University of Bern (Szidat et al., 2014). ^{14}C ages were calibrated to cal ka BP with the IntCal13 calibration curve (Reimer et al., 2013).

1.4.6 Age-depth model

The age-depth model is based on the Bayesian approach implemented rbacon v2.2 (Blaauw et al., 2011) available for R (R Core Team, 2021). The age-depth model was created using the IntCal13 calibration curve (Reimer et al., 2013).

Analyses in collaboration

Some analyses were carried out in collaboration, and the results were used for this doctoral thesis. These methods are, therefore, only very briefly mentioned here:

Smear slide petrography

To identify sedimentary facies and sedimentological changes, small portions of sample material (n = 60) were visually analysed for mineralogical features using a light microscope following the LACCORE guide. These analyses were performed at the Pyrenean Institute of Ecology-CSIC (Zaragoza, Spain).

XRF scanning

The XRF analysis was performed using an Itrax™ core scanner at Aberystwyth University. Applied standard scanning procedure was undertaken following CROUDACE ET AL. (2006).

Tephra analysis

The major element concentrations of tephra shards were determined using a Cameca SX-100 WDS electron microprobe (EPMA) at the Department of Earth Sciences, University of Cambridge. Additionally, trace element concentrations of the glass shards were measured using a Thermo Scientific iCapQ coupled to a Teledyne G2 Excimer laser (LA-ICP-MS) in the iCRAG laboratory, Trinity College Dublin.

Radiometric Dating

^{210}Pb, ^{226}Ra, ^{137}Cs, and ^{241}Am measurements were performed at the Environmental Radiometric Facility at University College London using an ORTEC HPGe GWL (APPLEBY ET AL., 1986). The results were corrected for the self-absorption effect of low energy gamma rays (APPLEBY ET AL., 1992), and ^{210}Pb dates were calculated following APPLEBY (2001).

Spheroidal carbonaceous particle (SCP) analysis

For SCP analysis, the highly purified sample was placed in suspension in water (ROSE, 1994). A known fraction of the suspension was evaporated, and the SCPs enumerated using a light microscope at 400x magnification. Standard criteria for SCP identification were followed (ROSE, 2008).

Diatom $\delta^{18}O$ analyses

The extraction, purification and correction for contamination of diatoms were done following the method described by CHAPLIGIN ET AL. (2010). The oxygen isotopic composition of purified diatom samples was measured using a PDZ Europa 2020 mass spectrometer at the AWI Potsdam ISOLAB Facility.

1.5 Structure of the thesis

This cumulative thesis is based on three scientific articles published or under review in international peer-reviewed journals. The thesis consists of six chapters embedding the three articles into a broader scientific context

Chapter 1 introduces the motivation of the thesis, provides a brief overview of the study area, states the objectives of the thesis and briefly mentions the methods used to achieve these.

Chapter 2 is a research article named “Revisiting afro-alpine Lake Garba Guracha in the Bale Mountains of Ethiopia: rationale, chronology, geochemistry, and paleoenvironmental implications.” that was published in the Journal of Paleolimnology. The article highlights the new research at Garba Guracha, the establishment of a high resolution, multi-component chronology, the organic matter source identification using biomarker and stable isotopes and the reconstruction of the catchment development since the deglaciation.

Chapter 3 is a research article entitled “The Holocene lake-evaporation history of the afro-alpine Lake Garba Guracha in the Bale Mountains, Ethiopia, based on $\delta^{18}O$ records of sugar biomarker and diatoms.” published in Quaternary Research. The article focuses on the reconstruction of the hydrological history of Garba Guracha and the methodological comparison of $\delta^{18}O$ of sugars and diatoms, improving the understanding of the allochthonous and autochthonous biomarker synthesis.

Chapter 4 is a research article published in the open discussion journal Biogeosciences. The title is “A Holocene temperature (brGDGT) record from Garba Guracha, a high-altitude lake in Ethiopia.”. The article focuses on the reconstruction of the thermal history of Garba Guracha and the methodological improvement of local brGDGT calibrations in a high-altitude setting.

Chapter 5 presents a synthesis of the main findings of the three research articles in the context of the analytical processes and the research questions. The implications of the main findings on the climatic and environmental history of Garba Guracha and the Bale Mountains are discussed.

Chapter 6 summarises the thesis's most important findings, implications and conclusions and offers an outlook of future research ideas and necessary developments.

1.6 References

AMELUNG, W., CHESHIRE, M. V, & GUGGENBERGER, G. (1996): Determination of neutral and acidic sugars in soil by capillary gas-liquid chromatography after trifluoroacetic acid hydrolysis. - Soil Biology and Biochemistry, **28**, 1631–1639.

ANDREWS, M. A. (1989): Capillary gas-chromatographic analysis of monosaccharides: Improvements and comparisons using trifluoroacetylation and trimethylsilylation of sugar O-benzyl- and O-methyl-oximes. - Carbohydrate Research, **194**, 1–19.

APPLEBY, P. G. (2001): Chronostratigraphic Techniques in Recent Sediments BT - Tracking Environmental Change Using Lake Sediments: Basin Analysis, Coring, and Chronological Techniques. - In W. M. Last & J. P. Smol (Eds.), (pp. 171–203). - Dordrecht: Springer Netherlands.

APPLEBY, P. G., NOLAN, P. J., GIFFORD, D. W., GODFREY, M. J., OLDFIELD, F., ANDERSON, N. J., & BATTARBEE, R. W. (1986): ^{210}Pb dating by low background gamma counting. - Hydrobiologia, **143**, 21–27.

APPLEBY, P. G., RICHARDSON, N., & NOLAN, P. J. (1992): Self-absorption corrections for well-type germanium detectors. - Nuclear Instruments and Methods in Physics Research Section B: Beam Interactions with Materials and Atoms, **71**, 228–233.

ARNAUD, F., POULENARD, J., GIGUET-COVEX, C., WILHELM, B., RÉVILLON, S., JENNY, J.-P., REVEL, M., ENTERS, D., BAJARD, M., FOUINAT, L., DOYEN, E., SIMONNEAU, A., PIGNOL, C., CHAPRON, E., VANNIÈRE, B., & SABATIER, P. (2016): Erosion under climate and human pressures: An alpine lake sediment perspective. - Quaternary Science Reviews, **152**, 1–18.

BAHAGA, T. K., MENGISTU TSIDU, G., KUCHARSKI, F., & DIRO, G. T. (2015): Potential predictability of the sea-surface temperature forced equatorial East African short rains interannual variability in the 20th century. - Quarterly Journal of the Royal Meteorological Society, **141**, 16–26.

BERKE, M. A., JOHNSON, T. C., WERNE, J. P., SCHOUTEN, S., & SINNINGHE DAMSTÉ, J. S. (2012): A mid-Holocene thermal maximum at the end of the African Humid Period. - Earth and Planetary Science Letters, **351**–**352**, 95–104.

BEZU, A. (2020): Analyzing Impacts of Climate Variability and Changes in Ethiopia: A Review. - American Journal of Modern Energy, **6**, 65–76.

BINI, M., ZANCHETTA, G., PERŞOIU, A., CARTIER, R., CATALÀ, A., CACHO, I., DEAN, J. R., DI RITA, F., DRYSDALE, R. N., FINNÈ, M., ISOLA, I., JALALI, B., LIRER, F., MAGRI, D., MASI, A., MARKS, L., MERCURI, A. M., PEYRON, O., SADORI, L., SICRE, M.-A., WELC, F., ZIELHOFER, C., & BRISSET, E. (2019): The 4.2 ka BP Event in the Mediterranean region: an overview. - Clim. Past, **15**, 555–577.

BLAAUW, M., CHRISTENY, J. A., & CHRISTEN, J. A. (2011): Flexible paleoclimate age-depth models using an autoregressive gamma process. - Bayesian Analysis, **6**, 457–474.

BLOM, R. G., FARR, T. G., FEYNMANN, J., RUZMAIKIN, A., & PAILLOU, P. (2009): The green Sahara: Climate change, hydrologic history and human occupation. - In 2009 IEEE Radar Conference (pp. 1–4).

BRENNER, M., WHITMORE, T. J., CURTIS, J. H., HODELL, D. A., & SCHELSKE, C. L. (1999): Stable isotope ($\delta^{13}C$ and $\delta^{15}N$) signatures of sedimented organic matter as indicators of historic lake trophic state. - Journal of Paleolimnology, **22**, 205–221.

BRENNER, M., HODELL, D. A., LEYDEN, B. W., CURTIS, J. H., KENNEY, W. F., GU, B., & NEWMAN, J. M. (2006): Mechanisms for organic matter and phosphorus burial in sediments of a shallow, subtropical, macrophyte-dominated lake. - Journal of Paleolimnology, **35**, 129–148.

CAMBERLIN, P. (1997): Rainfall Anomalies in the Source Region of the Nile and Their Connection with the Indian Summer Monsoon. - Journal of Climate, **10**, 1380–1392.

CASTAÑEDA, I. S., & SCHOUTEN, S. (2011): A review of molecular organic proxies for examining modern and ancient lacustrine environments. - Quaternary Science Reviews, **30**, 2851–2891.

CASTAÑEDA, I. S., SCHOUTEN, S., PÄTZOLD, J., LUCASSEN, F., KASEMANN, S., KUHLMANN, H., & SCHEFUß, E. (2016): Hydroclimate variability in the Nile River Basin during the past 28,000 years. - Earth and Planetary Science Letters, **438**, 47–56.

CATALAN, J., CAMARERO, L., FELIP, M., PLA, S., VENTURA, M., BUCHACA, T., BARTUMEUS, F., MENDOZA, G. DE, MIRÓ, A., CASAMAYOR, E., MEDINA-SÁNCHEZ, J., BACARDIT, M., ALTUNA, M., BARTRONS, M., & QUIJANO, D. (2006): High mountain lakes: Extreme habitats and witnesses of environmental changes. - Limnetica, **25**, 551–584.

CATALAN, J., PLA-RABÉS, S., WOLFE, A. P., SMOL, J. P., RÜHLAND, K. M., ANDERSON, N. J., KOPÁČEK, J., STUCHLÍK, E., SCHMIDT, R., KOINIG, K. A., CAMARERO, L., FLOWER, R. J., HEIRI, O., KAMENIK, C., KORHOLA, A., LEAVITT, P. R., PSENNER, R., & RENBERG, I. (2013): Global change revealed by palaeolimnological records from remote lakes: a review. - Journal of Paleolimnology, **49**, 513–535.

CHAPLIGIN, B., MEYER, H., FRIEDRICHSEN, H., MARENT, A., SOHNS, E., & HUBBERTEN, H.-W. (2010): A high-performance, safer and semi-automated approach for the $\delta^{18}O$ analysis of diatom silica and new methods for removing exchangeable oxygen. - Rapid Communications in Mass Spectrometry, **24**, 2655–2664.

CORMIER, M.-A., WERNER, R. A., SAUER, P. E., GRÖCKE, D. R., LEUENBERGER, M. C., WIELOCH, T., SCHLEUCHER, J., & KAHMEN, A. (2018): ^{2}H-fractionations during the biosynthesis of carbohydrates and lipids imprint a metabolic signal on the $\delta^{2}H$ values of plant organic compounds. - New Phytologist, **218**, 479–491.

COSTA, K., RUSSELL, J., KONECKY, B., & LAMB, H. (2014): Isotopic reconstruction of the African Humid Period and Congo Air Boundary migration at Lake Tana, Ethiopia. - Quaternary Science Reviews, **83**, 58–67.

CROUDACE, I., RINDBY, A., & GUY ROTHWELL, R. (2006): ITRAX: Description and Evaluation of a New Multi-Function X-ray Core Scanner. - Geological Society, London, Special Publications, **267**, 51–63.

DAMSTÉ, J. S. S., HOPMANS, E. C., PANCOST, R. D., SCHOUTEN, S., & GEENEVASEN, J. A. J. (2000): Newly discovered non-isoprenoid glycerol dialkyl glycerol tetraether lipids in sediments. - Chemical Communications, 1683–1684.

DAVIES, T. D., VINCENT, C. E., & BERESFORD, A. K. C. (1985): July-August rainfall in West-Central Kenya. - Journal of Climatology, **5**, 17–33.

DE JONGE, C., HOPMANS, E. C., ZELL, C. I., KIM, J.-H., SCHOUTEN, S., & SINNINGHE DAMSTÉ, J. S. (2014a): Occurrence and abundance of 6-methyl branched glycerol dialkyl glycerol tetraethers in soils: Implications for palaeoclimate reconstruction. - Geochimica et Cosmochimica Acta, **141**, 97–112.

DE JONGE, C., STADNITSKAIA, A., HOPMANS, E. C., CHERKASHOV, G., FEDOTOV, A., & SINNINGHE DAMSTÉ, J. S. (2014b): In situ produced branched glycerol dialkyl glycerol tetraethers in suspended particulate matter from the Yenisei River, Eastern Siberia. - Geochimica et Cosmochimica Acta, **125**, 476–491.

DE JONGE, C., RADUJKOVIĆ, D., SIGURDSSON, B. D., WEEDON, J. T., JANSSENS, I., & PETERSE, F. (2019): Lipid biomarker temperature proxy responds to abrupt shift in the bacterial community composition in geothermally heated soils. - Organic Geochemistry, **137**.

DE JONGE, C., KURAMAE, E. E., RADUJKOVIĆ, D., WEEDON, J. T., JANSSENS, I. A., & PETERSE, F. (2021): The influence of soil chemistry on branched tetraether lipids in mid- and high latitude soils: Implications for brGDGT- based paleothermometry. - Geochimica et Cosmochimica Acta, **310**, 95–112.

DEARING CRAMPTON-FLOOD, E., TIERNEY, J. E., PETERSE, F., KIRKELS, F. M. S. A., & SINNINGHE DAMSTÉ, J. S. (2020): BayMBT: A Bayesian calibration model for branched glycerol dialkyl glycerol tetraethers in soils and peats. - Geochimica et Cosmochimica Acta, **268**, 142–159.

DEMENOCAL, P., ORTIZ, J., GUILDERSON, T., ADKINS, J., SARNTHEIN, M., BAKER, L., & YARUSINSKY, M. (2000): Abrupt onset and termination of the African Humid Period: - Quaternary Science Reviews, **19**, 347–361.

DIEFENDORF, A. F., & FREIMUTH, E. J. (2017): Extracting the most from terrestrial plant-derived n-alkyl lipids and their carbon isotopes from the sedimentary record: A review. - Organic Geochemistry, **103**, 1–21.

DIRO, G. T., GRIMES, D. I. F., & BLACK, E. (2011): Teleconnections between Ethiopian summer rainfall and sea surface temperature: part I—observation and modelling. - Climate Dynamics, **37**, 103–119.

EGLINTON, G., & HAMILTON, R. J. (1967): Leaf Epicuticular Waxes. - Science, **156**, 1322 LP – 1335.

EGLINTON, T. I., & EGLINTON, G. (2008): Molecular proxies for paleoclimatology. - Earth and Planetary Science Letters, **275**, 1–16.

ENDRIS, H. S., LENNARD, C., HEWITSON, B., DOSIO, A., NIKULIN, G., & PANITZ, H.-J. (2016): Teleconnection responses in multi-GCM driven CORDEX RCMs over Eastern Africa. - Climate Dynamics, **46**, 2821–2846.

FICKEN, K. J., LI, B., SWAIN, D. L., & EGLINTON, G. (2000): An n-alkane proxy for the sedimentary input of submerged/floating freshwater aquatic macrophytes. - Organic Geochemistry, **31**, 745–749.

FREIMUTH, E. J., DIEFENDORF, A. F., & LOWELL, T. V (2017): Hydrogen isotopes of n-alkanes and n-alkanoic acids as tracers of precipitation in a temperate forest and implications for paleorecords. - Geochimica et Cosmochimica Acta, **206**, 166–183.

GARELICK, S., RUSSELL, J., RICHARDS, A., SMITH, J., KELLY, M., ANDERSON, N., JACKSON, M. S., DOUGHTY, A., NAKILEZA, B., IVORY, S., DEE, S., & MARSHALL, C. (2022): The dynamics of warming during the last deglaciation in high-elevation regions of Eastern Equatorial Africa. - Quaternary Science Reviews, **281**, 107416.

GASSE, F. (2000): Hydrological changes in the African tropics since the Last Glacial Maximum. - Quaternary Science Reviews, **19**, 189–211.

GRIEPENTROG, M., DE WISPELAERE, L., BAUTERS, M., BODÉ, S., HEMP, A., VERSCHUREN, D., & BOECKX, P. (2019): Influence of plant growth form, habitat and season on leaf-wax n-alkane hydrogen-isotopic signatures in equatorial East Africa. - Geochimica et Cosmochimica Acta, **263**, 122–139.

GROOS, A. R., NIEDERHAUSER, J., WRAASE, L., HÄNSEL, F., NAUSS, T., AKÇAR, N., & VEIT, H. (2020): Implications of present ground temperatures and relict stone stripes in the Ethiopian Highlands for the palaeoclimate of the tropics. - Earth Surf. Dynam. Discuss., **2020**, 1–37.

GROOS, A., AKÇAR, N., YESILYURT, S., MIEHE, G., VOCKENHUBER, C., & VEIT, H. (2021): Nonuniform Late Pleistocene glacier fluctuations in tropical Eastern Africa. - Science Advances, **7**.

GROSS, S., & GLASER, B. (2004): Minimization of carbon addition during derivatization of monosaccharides for compound-specific $\delta^{13}C$ analysis in environmental research. - Rapid Communications in Mass Spectrometry, **18**, 2753–2764.

GUO, J., GLENDELL, M., MEERSMANS, J., KIRKELS, F., MIDDELBURG, J. J., & PETERSE, F. (2020): Assessing branched tetraether lipids as tracers of soil organic carbon transport through the Carminowe Creek catchment (southwest England). - Biogeosciences, **17**, 3183–3201.

HALAMKA, T. A., MCFARLIN, J. M., YOUNKIN, A. D., DEPOY, J., DILDAR, N., & KOPF, S. H. (2021): Oxygen limitation can trigger the production of branched GDGTs in culture. - Geochemical Perspectives Letters, **19**, 36–39.

HEPP, J., TUTHORN, M., ZECH, R., MÜGLER, I., SCHLÜTZ, F., ZECH, W., & ZECH, M. (2015): Reconstructing

lake evaporation history and the isotopic composition of precipitation by a coupled δ^2H–$\delta^{18}O$ biomarker approach. - Journal of Hydrology, **529**, 622–631.

HEPP, J., RABUS, M., ANHÄUSER, T., BROMM, T., LAFORSCH, C., SIROCKO, F., GLASER, B., & ZECH, M. (2016): A sugar biomarker proxy for assessing terrestrial versus aquatic sedimentary input. - Organic Geochemistry, **98**, 98–104.

HEPP, J., WÜTHRICH, L., BROMM, T., BLIEDTNER, M., SCHÄFER, I. K., GLASER, B., ROZANSKI, K., SIROCKO, F., ZECH, R., & ZECH, M. (2019): How dry was the Younger Dryas? Evidence from a coupled δ^2H–$\delta^{18}O$ biomarker paleohygrometer applied to the Gemündener Maar sediments, Western Eifel, Germany. - Clim. Past, **15**, 713–733.

HEPP, J., SCHÄFER, I. K., LANNY, V., FRANKE, J., BLIEDTNER, M., ROZANSKI, K., GLASER, B., ZECH, M., EGLINTON, T. I., & ZECH, R. (2020): Evaluation of bacterial glycerol dialkyl glycerol tetraether and δ^2H–$\delta^{18}O$ biomarker proxies along a central European topsoil transect. - Biogeosciences, **17**, 741–756.

HEPP, J., MAYR, C., ROZANSKI, K., SCHÄFER, I. K., TUTHORN, M., GLASER, B., JUCHELKA, D., STICHLER, W., ZECH, R., & ZECH, M. (2021): Validation of a coupled $\delta^2H_{n\text{-}alkane}$ – $\delta^{18}O_{sugar}$ paleohygrometer approach based on a climate chamber experiment. - Biogeosciences, **18**, 5363–5380.

HILLMAN, J. (1986): Conservation in Bale Mountains National Park, EthiopiaOryx (Vol. 20).

HILLMAN, J. (1988): The Bale Mountains National Park Area, Southeast Ethiopia, and Its ManagementMountain Research and Development (Vol. 8).

HILLS, R. C. (1979): The Structure of the Inter-Tropical Convergence Zone in Equatorial Africa and Its Relationship to East African Rainfall. - Transactions of the Institute of British Geographers, **4**, 329–352.

HOPMANS, E. C., SCHOUTEN, S., & SINNINGHE DAMSTÉ, J. S. (2016): The effect of improved chromatography on GDGT-based palaeoproxies. - Organic Geochemistry, **93**, 1–6.

HOU, J., D'ANDREA, W. J., & HUANG, Y. (2008): Can sedimentary leaf waxes record D/H ratios of continental precipitation? Field, model, and experimental assessments. - Geochimica et Cosmochimica Acta, **72**, 3503–3517.

HOVE, H., ECHEVERRIA, D., & PARRY, J.-E. (2011): Review of current and planned adaptation action: East Africa. - International Institute for Sustainable Development, Winnipeg.

HUGHES, A. C., ORR, M. C., MA, K., COSTELLO, M. J., WALLER, J., PROVOOST, P., YANG, Q., ZHU, C., & QIAO, H. (2021): Sampling biases shape our view of the natural world. - Ecography, **44**, 1259–1269.

HUGUET, C., KIM, J. H., DAMSTÉ, J. S. S., & SCHOUTEN, S. (2006): Reconstruction of sea surface temperature variations in the Arabian Sea over the last 23 kyr using organic proxies (TEX86 and $U_{37}K'$). - Paleoceanography, **21**.

INDEJE, M., SEMAZZI, F. H. M., & OGALLO, L. J. (2000): ENSO signals in East African rainfall seasons.

- International Journal of Climatology, **20**, 19–46.

IPCC (2021): Climate Change 2021: The Physical Science Basis. Contribution of Working Group I to the Sixth Assessment Report of the Intergovernmental Panel on Climate Change [Masson-Delmotte, V., P. Zhai, A. Pirani, S.L. Connors, C. Péan, S. Berger, N. Caud, Y. Chen,. Cambridge University Press.

JAESCHKE, A., THIENEMANN, M., SCHEFUß, E., URBAN, J., SCHÄBITZ, F., WAGNER, B., & RETHEMEYER, J. (2020): Holocene Hydroclimate Variability and Vegetation Response in the Ethiopian Highlands (Lake Dendi). - Frontiers in Earth Science, **8**, 1–14.

JUNGINGER, A., ROLLER, S., OLAKA, L. A., & TRAUTH, M. H. (2014): The effects of solar irradiation changes on the migration of the Congo Air Boundary and water levels of paleo-Lake Suguta , Northern Kenya Rift , during the African Humid Period (15 – 5 ka BP). - Palaeogeography, Palaeoclimatology, Palaeoecology, **396**, 1–16.

KIDANE, Y., STAHLMANN, R., & BEIERKUHNLEIN, C. (2012): Vegetation dynamics, and land use and land cover change in the Bale Mountains, Ethiopia. - Environmental Monitoring and Assessment, **184**, 7473–7489.

KNAPP, D. R. (1979): Handbook of Analytical Derivatization Reactions. - New York, Chichester, Brisbane, Toronto, Singapore: John Wiley & Sons.

LEHMANN, M. M., GAMARRA, B., KAHMEN, A., SIEGWOLF, R. T. W., & SAURER, M. (2017): Oxygen isotope fractionations across individual leaf carbohydrates in grass and tree species. - Plant, Cell & Environment, **40**, 1658–1670.

LEMMA, B., KEBEDE GURMESSA, S., NEMOMISSA, S., OTTE, I., GLASER, B., & ZECH, M. (2020): Spatial and temporal ^{2}H and ^{18}O isotope variation of contemporary precipitation in the Bale Mountains, Ethiopia. - Isotopes in Environmental and Health Studies, **56**, 122–135.

LEMMA, B., BITTNER, L., GLASER, B., KEBEDE, S., NEMOMISSA, S., ZECH, W., & ZECH, M. (2021): $\delta^{2}H_{n\text{-alkane}}$ and $\delta^{18}O_{sugar}$ biomarker proxies from leaves and topsoils of the Bale Mountains, Ethiopia, and implications for paleoclimate reconstructions. - Biogeochemistry.

LENG, M. J., & BARKER, P. A. (2006): A review of the oxygen isotope composition of lacustrine diatom silica for palaeoclimate reconstruction. - Earth-Science Reviews, **75**, 5–27.

LEZINE, A.-M., BASSINOT, F., PETERSCHMITT, J. Y. J.-Y., LÉZINE, A. M., BASSINOT, F., & PETERSCHMITT, J. Y. J.-Y. (2014): Orbitally-induced changes of the Atlantic and Indian monsoons over the past 20,000 years: New insights based on the comparison of continental and marine records. - Bulletin de La Societe Geologique de France, **185**, 3–12.

LIU, H., & LIU, W. (2016): n-Alkane distributions and concentrations in algae, submerged plants and terrestrial plants from the Qinghai-Tibetan Plateau. - Organic Geochemistry, **99**, 10–22.

LIU, H. T., SCHÄUFELE, R., GONG, X. Y., & SCHNYDER, H. (2017): The $\delta^{18}O$ and $\delta^{2}H$ of water in the leaf

growth-and-differentiation zone of grasses is close to source water in both humid and dry atmospheres. - New Phytologist, **214**, 1423–1431.

LIU, J., & AN, Z. (2019): Variations in hydrogen isotopic fractionation in higher plants and sediments across different latitudes: Implications for paleohydrological reconstruction. - The Science of the Total Environment, **650**, 470–478.

LIU, J., LIU, W., AN, Z., & YANG, H. (2016): Different hydrogen isotope fractionations during lipid formation in higher plants: Implications for paleohydrology reconstruction at a global scale. - Scientific Reports, **6**, 19711.

LÖFFLER, H. (1978): Limnology and paleolimnological data on the Bale Mountain Lakes. - Verth, International Verein. Limnology, **20**, 1131–1138.

LOOMIS, S. E. S. E., RUSSELL, J. M., LADD, B., STREET-PERROTT, F. A. A., & SINNINGHE DAMSTÉ, J. S. J. S. (2012): Calibration and application of the branched GDGT temperature proxy on East African lake sediments. - Earth and Planetary Science Letters, **357**–**358**, 277–288.

LOOMIS, S. E., RUSSELL, J. M., & LAMB, H. F. (2015): Northeast African temperature variability since the Late Pleistocene. - Palaeogeography, Palaeoclimatology, Palaeoecology, **423**, 80–90.

LOOMIS, S. E., RUSSELL, J. M., VERSCHUREN, D., MORRILL, C., DE CORT, G., SINNINGHE DAMSTÉ, J. S., OLAGO, D., EGGERMONT, H., STREET-PERROTT, F. A., & KELLY, M. A. (2017): The tropical lapse rate steepened during the Last Glacial Maximum. - Science Advances, **3**.

LYON, B., & VIGAUD, N. (2017, June 22): Unraveling East Africa's Climate Paradox. - Climate Extremes.

MEYERS, P. A. (1994): Preservation of elemental and isotopic source identification of sedimentary organic matter. - Chemical Geology, **114**, 289–302.

MEYERS, P. A. (2003): Applications of organic geochemistry to paleolimnological reconstructions: a summary of examples from the Laurentian Great Lakes. - Organic Geochemistry, **34**, 261–289.

MORRISSEY, A., & SCHOLZ, C. A. (2014): Paleohydrology of Lake Turkana and its influence on the Nile River system. - Palaeogeography, Palaeoclimatology, Palaeoecology, **403**, 88–100.

MORRISSEY, A., SCHOLZ, C. A., & RUSSELL, J. M. (2018): Late Quaternary TEX_{86} paleotemperatures from the world's largest desert lake, Lake Turkana, Kenya. - Journal of Paleolimnology, **59**, 103–117.

MÜGLER, I., SACHSE, D., WERNER, M., XU, B., WU, G., YAO, T., & GLEIXNER, G. (2008): Effect of lake evaporation on δD values of lacustrine n-alkanes: A comparison of Nam Co (Tibetan Plateau) and Holzmaar (Germany). - Organic Geochemistry, **39**, 711–729.

NAKAMURA, K. (1968): Equatorial westerlies over East Africa and their climatological significance. - Geographical Review of Japan, **41**, 359–373.

NEUKOM, R., BARBOZA, L. A., ERB, M. P., SHI, F., EMILE-GEAY, J., EVANS, M. N., FRANKE, J., KAUFMAN, D. S., LÜCKE, L., REHFELD, K., SCHURER, A., ZHU, F., BRÖNNIMANN, S., HAKIM, G. J., HENLEY, B. J., LJUNGQVIST, F. C., MCKAY, N., VALLER, V., VON GUNTEN, L., & CONSORTIUM, P. 2K (2019): Consistent multidecadal variability in global temperature reconstructions and simulations over the Common Era. - Nature Geoscience, **12**, 643–649.

NIANG, I., C. RUPPEL, O., ABDRABO, M., ESSEL, A., LENNARD, C., PADGHAM, J., URQUHART, P., ADELEKAN, I., ARCHIBALD, S., BALINGA, M., BARKHORDARIAN, A., BATTERSBY, J., BILIR, E., BURKE, M., CHAHED, M., CHATTERJEE, M., CHINEKE, T., DESCHEEMAEKER, K., HOURIA, D., & LEARY, N. (2014): Chapter 22 Africa. In: Climate Change 2014: Impacts, Adaptation, and Vulnerability. Part B: Regional Aspects. Contribution of Working Group II to the Fifth Assessment Report of the Intergovernmental Panel on Climate Change. - (pp. 1199–1265).

NICHOLSON, S. E. (2017): Climate and climatic variability of rainfall over eastern Africa. - Reviews of Geophysics, **55**, 590–635.

O'LEARY, M. H. (1988): Carbon Isotopes in Photosynthesis. - BioScience, **38**, 328–336.

OGALLO, L. J. (1988): Relationships between seasonal rainfall in East Africa and the Southern Oscillation. - Journal of Climatology, **8**, 31–43.

OSMASTON, H. A., MITCHELL, W. A., & OSMASTON, J. A. N. (2005): Quaternary glaciation of the Bale Mountains, Ethiopia. - Journal of Quaternary Science, **20**, 593–606.

OSSENDORF, G., GROOS, A., BROMM, T., GIRMA TEKELEMARIAM, M., GLASER, B., LESUR, J., SCHMIDT, J., AKÇAR, N., BEKELE, T., BELDADOS, A., DEMISSEW, S., HADUSH KAHSAY, T., P NASH, B., NAUSS, T., NEGASH, A., NEMOMISSA, S., VEIT, H., VOGELSANG, R., ZERIHUN, W., & MIEHE, G. (2019): Middle Stone Age foragers resided in high elevations of the glaciated Bale Mountains, Ethiopia. - Science, **365**, 583–587.

OTTO-BLIESNER, B. L., RUSSELL, J. M., CLARK, P. U., LIU, Z., OVERPECK, J. T., KONECKY, B., DEMENOCAL, P., NICHOLSON, S. E., HE, F., & LU, Z. (2014): Coherent changes of southeastern equatorial and northern African rainfall during the last deglaciation. - Science, **346**, 1223–1227.

R CORE TEAM (2021): R: A Language and Environment for Statistical Computing. - . - Vienna, Austria. Retrieved from https://www.r-project.org/

REIMER, P. J. P. J., BARD, E., BAYLISS, A., BECK, J. W. W., BLACKWELL, P. G. P. G., BRONK RAMSEY, C., BUCK, C. E. C. E., CHENG, H., EDWARDS, R. L. L., FRIEDRICH, M., TURNEY, C. S. M. C. S. M., VAN DER PLICHT, J. (2013): IntCal13 and Marine13 Radiocarbon Age Calibration Curves 0–50,000 Years cal BP. - Radiocarbon, **55**, 1869–1887.

ROPELEWSKI, C. F., & HALPERT, M. S. (1987): Global and Regional Scale Precipitation Patterns Associated with the El Niño/Southern Oscillation. - Monthly Weather Review, **115**, 1606–1626.

ROSE, N. L. (1994): A note on further refinements to a procedure for the extraction of carbonaceous fly-ash particles from sediments. - Journal of Paleolimnology, **11**, 201–204.

ROSE, N. L. (2008): Quality control in the analysis of lake sediments for spheroidal carbonaceous particles. - Limnology and Oceanography: Methods, **6**, 172–179.

RUSSELL, J. M., HOPMANS, E. C., LOOMIS, S. E., LIANG, J., & SINNINGHE DAMSTÉ, J. S. (2018): Distributions of 5- and 6-methyl branched glycerol dialkyl glycerol tetraethers (brGDGTs) in East African lake sediment: Effects of temperature, pH, and new lacustrine paleotemperature calibrations. - Organic Geochemistry, **117**, 56–69.

SACHSE, D., BILLAULT, I., BOWEN, G. J., CHIKARAISHI, Y., DAWSON, T. E., FEAKINS, S. J., FREEMAN, K. H., MAGILL, C. R., MCINERNEY, F. A., VAN DER MEER, M. T. J., POLISSAR, P., ROBINS, R. J., SACHS, J. P., SCHMIDT, H.-L., SESSIONS, A. L., WHITE, J. W. C., WEST, J. B., & KAHMEN, A. (2012): Molecular Paleohydrology: Interpreting the Hydrogen-Isotopic Composition of Lipid Biomarkers from Photosynthesizing Organisms. - Annual Review of Earth and Planetary Sciences, **40**, 221–249.

SCHÄFER, I. K., LANNY, V., FRANKE, J., EGLINTON, T. I., ZECH, M., VYSLOUŽILOVÁ, B., & ZECH, R. (2016): Leaf waxes in litter and topsoils along a European transect. - Soil, **2**, 551–564.

SCHMIDT, H.-L., WERNER, R. A., & EISENREICH, W. (2003): Systematics of ^{2}H patterns in natural compounds and its importance for the elucidation of biosynthetic pathways. - Phytochemistry Reviews, **2**, 61–85.

SCHREUDER, L. T., BEETS, C. J., PRINS, M. A., HATTÉ, C., & PETERSE, F. (2016): Late Pleistocene climate evolution in Southeastern Europe recorded by soil bacterial membrane lipids in Serbian loess. - Palaeogeography, Palaeoclimatology, Palaeoecology, **449**, 141–148.

SESSIONS, A. L., BURGOYNE, T. W., SCHIMMELMANN, A., & HAYES, J. M. (1999): Fractionation of hydrogen isotopes in lipid biosynthesis. - Organic Geochemistry, **30**, 1193–1200.

SINNINGHE DAMSTÉ, J. S., RIJPSTRA, W. I. C., FOESEL, B. U., HUBER, K. J., OVERMANN, J., NAKAGAWA, S., KIM, J. J., DUNFIELD, P. F., DEDYSH, S. N., & VILLANUEVA, L. (2018): An overview of the occurrence of ether- and ester-linked iso-diabolic acid membrane lipids in microbial cultures of the Acidobacteria: Implications for brGDGT paleoproxies for temperature and pH. - Organic Geochemistry, **124**, 63–76.

SPRENGER, M., & TETZLAFF, D. (2017): Soil water stable isotopes reveal evaporation dynamics at the soil–plant–atmosphere interface of the critical zone. - Hydrol. Earth Syst. Sci., **21**, 3839–3858.

SZIDAT, S., A SALAZAR, G., VOGEL, E., BATTAGLIA, M., WACKER, L., SYNAL, H.-A., & TÜRLER, A. (2014): 14C Analysis and Sample Preparation at the New Bern Laboratory for the Analysis of Radiocarbon with AMS (LARA). - Radiocarbon, **56**, 561–566.

THOMPSON, R. S. (2004): The role of paleoclimatic studies in assessing climate change. - Eos, Transactions American Geophysical Union, **85**, 436.

TIERCELIN, J. J., GIBERT, E., UMER, M., BONNEFILLE, R., DISNAR, J. R., LÉZINE, A. M., HUREAU-MAZAUDIER, D., TRAVI, Y., KERAVIS, D., & LAMB, H. F. (2008): High-resolution sedimentary record of the

last deglaciation from a high-altitude lake in Ethiopia. - Quaternary Science Reviews, **27**, 449–467.

TIERNEY, J. E., & RUSSELL, J. M. (2007): Abrupt climate change in southeast tropical Africa influenced by Indian monsoon variability and ITCZ migration. - Geophysical Research Letters, **34**.

TIERNEY, J. E., & DEMENOCAL, P. B. (2013): Abrupt Shifts in Horn of Africa Hydroclimate Since the Last Glacial Maximum. - Science, **342**, 843 LP – 846. Retrieved from http://science.sciencemag.org/content/342/6160/843.abstract

TIERNEY, J. E., RUSSELL, J. M., HUANG, Y., DAMSTÉ, J. S. S., HOPMANS, E. C., & COHEN, A. S. (2008): Northern Hemisphere Controls on During the Past 60,000 Years. - Science Magazine, **322**, 252–255.

TIERNEY, J. E., LEWIS, S. C., COOK, B. I., LEGRANDE, A. N., & SCHMIDT, G. A. (2011a): Model, proxy and isotopic perspectives on the East African Humid Period. - Earth and Planetary Science Letters, **307**, 103–112.

TIERNEY, J. E., RUSSELL, J. M., SINNINGHE DAMSTÉ, J. S., HUANG, Y., & VERSCHUREN, D. (2011b): Late Quaternary behavior of the East African monsoon and the importance of the Congo Air Boundary. - Quaternary Science Reviews, **30**, 798–807.

TIERNEY, J. E., SMERDON, J. E., ANCHUKAITIS, K. J., & SEAGER, R. (2013): Multidecadal variability in East African hydroclimate controlled by the Indian Ocean. - Nature, **493**, 389–392.

TIERNEY, J. E., PAUSATA, F. S. R., & DEMENOCAL, P. B. (2017): Rainfall regimes of the Green Sahara. - Science Advances, **3**.

TRAUTH, M. H., FOERSTER, V., JUNGINGER, A., ASRAT, A., LAMB, H. F., & SCHAEBITZ, F. (2018): Abrupt or gradual? Change point analysis of the late Pleistocene–Holocene climate record from Chew Bahir, southern Ethiopia. - Quaternary Research, **90**, 321–330.

TUTHORN, M., ZECH, M., RUPPENTHAL, M., OELMANN, Y., KAHMEN, A., VALLE, H. F. DEL, WILCKE, W., GLASER, B., MAYR, C., TUTHORN, M., LEIBER, K., GLASER, B., LEIBER-SAUHEITL, K., GLASER, B., ZECH, M., RUPPENTHAL, M., OELMANN, Y., KAHMEN, A., VALLE, H. F. DEL, WILCKE, W., & GLASER, B. (2014): Oxygen isotope ratios ($^{18}O/^{16}O$) of hemicellulose-derived sugar biomarkers in plants, soils and sediments as paleoclimate proxy II: Insight from a climate transect study. - Geochimica et Cosmochimica Acta, **126**, 624–634.

TUTHORN, M., ZECH, R., RUPPENTHAL, M., OELMANN, Y., KAHMEN, A., DEL VALLE, H. F., EGLINTON, T., ROZANSKI, K., AND ZECH, M.: Coupling δ^2H and $\delta^{18}O$ biomarker results yields information on relative humidity and isotopic composition of precipitation - A climate transect validation study, 12, 3913–3924, https://doi.org/10.5194/bg-12-3913-2015, 2015.

Uhlig, S., & Uhlig, K. (1991): Studies on the Altitudinal Zonation of Forests and Alpine Plants in the Central Bale Mountains, EthiopiaMountain Research and Development (Vol. 11).

UMER, M., LAMB, H. F., BONNEFILLE, R., LÉZINE, A. M., TIERCELIN, J. J., GIBERT, E., CAZET, J. P., & WATRIN, J. (2007): Late Pleistocene and Holocene vegetation history of the Bale Mountains, Ethiopia. - Quaternary Science Reviews, **26**, 2229–2246.

WAGNER, B., WENNRICH, V., VIEHBERG, F., JUNGINGER, A., KOLVENBACH, A., RETHEMEYER, J., SCHAEBITZ, F., & SCHMIEDL, G. (2018): Holocene rainfall runoff in the central Ethiopian highlands and evolution of the River Nile drainage system as revealed from a sediment record from Lake Dendi. - Global and Planetary Change, **163**, 29–43.

WEIJERS, J. W. H., SCHEFUß, E., SCHOUTEN, S., & DAMSTÉ, J. S. S. (2007a): Coupled thermal and hydrological evolution of tropical Africa over the last deglaciation. - Science, **315**, 1701–1704.

WEIJERS, J. W. H., SCHOUTEN, S., VAN DEN DONKER, J. C., HOPMANS, E. C., & SINNINGHE DAMSTÉ, J. S. (2007b): Environmental controls on bacterial tetraether membrane lipid distribution in soils. - Geochimica et Cosmochimica Acta, **71**, 703–713.

WERDECKER, J. (1962): Eine Durchquerung des Goba-Massivs in Südäthiopien. - , **Hermann vo**, 132–144.

WILLIAMS, F. M. (2016): The Southeastern Highlands and the Ogaden. - In F. M. Williams (Ed.), Understanding Ethiopia: Geology and Scenery (pp. 153–170). - Cham: Springer International Publishing.

WOLDU, Z., FEOLI, E., & NIGATU, L. (1989): Partitioning an elevation gradient of vegetation from southeastern Ethiopia by probabilistic methods. - Plant Ecology, **81**, 189–198.

WORLD METEOROLOGICAL ORGANIZATION (WMO) (2021): State of the Climate in Africa 2020. Retrieved from https://library.wmo.int/doc_num.php?explnum_id=10914

ZECH, M., & GLASER, B. (2009): Compound-specific $\delta^{18}O$ analyses of neutral sugars in soils using gas chromatography-pyrolysis-isotope ratio mass spectrometry: problems, possible solutions and a first application. - Rapid Communications in Mass Spectrometry, **23**, 3522–3532.

ZECH, M., SAURER, M., TUTHORN, M., RINNE, K., WERNER, R. A., SIEGWOLF, R., GLASER, B., & JUCHELKA, D. (2013): A novel methodological approach for $\delta^{18}O$ analysis of sugars using gas chromatography-pyrolysis-isotope ratio mass spectrometry. - Isotopes in Environmental and Health Studies, **49**, 492–502.

ZEGEYE, H. (2018): Climate change in Ethiopia: impacts, mitigation and adaptation. - International Journal of Research in Environmental Studies, **5**, 18–35.

ZENG, F., & YANG, H. (2019): Temperature changes reconstructed from branched GDGTs on the central Loess Plateau during the past 130–5 ka. - Quaternary International, **503**, 3–9.

Chapter 2

Revisiting afro-alpine Lake Garba Guracha in the Bale Mountains of Ethiopia: rationale, chronology, geochemistry, and paleoenvironmental implications

L. Bittner[1,2], M. Bliedtner[3], D. Grady[4], G. Gil-Romera[4,5], C. Martin-Jones[6,7], B. Lemma[1], B. Mekonnen[8,1], H. F. Lamb[4], H. Yang[9], B. Glaser[1], S. Szidat[10], G. Salazar[10], N. L. Rose[9], L. Opgenoorth[11], G. Miehe[12], W. Zech[8], M. Zech[2]

[1] Institute of Agronomy and Nutritional Sciences, Soil Biogeochemistry, Martin-Luther-Universität Halle-Wittenberg, Halle (Saale), Germany
[2] Heisenberg Chair of Physical Geography with focus on paleoenvironmental research, Institute of Geography, Technical University of Dresden, Dresden, Germany
[3] Department of Physical Geography, Institute of Geography, Friedrich-Schiller-University Jena, Jena, Germany
[4] Department of Geography and Earth Sciences, Aberystwyth University, Aberystwyth, UK
[5] Department of Geo-environmental Processes and Global Change, Pyrenean Institute of Ecology, CSIC, Zaragoza, Spain
[6] Department of Geography, University of Cambridge, Cambridge CB2 3EN, UK
[7] Limnology Unit, Department of Biology, Ghent University, B-9000 Gent, Belgium
[8] Institute of Soil Science and Soil Geography, University of Bayreuth, D-95440 Bayreuth, Germany
[9] Environmental Change Research Centre, University College London, Gower Street, London WC1E 6BT, UK
[10] Department of Chemistry and Biochemistry & Oeschger Centre for Climate Change Research, University of Bern, Bern, Switzerland
[11] Department of Ecology, University of Marburg, Marburg, Germany

Abstract

Previous paleolimnological studies demonstrated that the sediments of Garba Guracha, situated at 3950 m a. s. l. in the afro-alpine zone of the Bale Mountains of Ethiopia, provide a complete Late Glacial and Holocene paleoclimate and environmental archive. We revisited Garba Guracha in order to retrieve new sediment cores and to apply new environmental proxies, e.g. charcoal, diatoms, biomarkers, and stable isotopes. Our chronology is established using ^{210}Pb dating and radiocarbon dating of bulk sedimentary organic matter, bulk *n*-alkanes, and charcoal. Although bedrock was not reached during coring, basal ages confirm that sedimentation started at the earliest ~ 16 cal ka BP. The absence of a systematic age offset for the *n*-alkanes suggests that "pre-aging" is not a prominent issue in this lake, which is characterised by a very small afro-alpine catchment. X-ray fluorescence scans and total organic carbon contents show a prominent transition from minerogenic to organic-rich sediments around 11 cal ka BP coinciding with the Holocene onset. While an unambiguous terrestrial versus aquatic source identification seems challenging, the *n*-alkane-based P_{aq} proxy, TOC/N ratios, $\delta^{13}C$ values, and the sugar biomarker patterns suggest a predominantly autochthonous organic matter source. Supraregional climate events, such as the African Humid Period (AHP), the Younger Dryas (YD), a 6.5 cal ka BP short drying event, and the 4.2 cal ka BP transition to overall drier climate are recorded in our archive. The Garba Guracha record suggests that northern hemisphere forcings played a role in the Eastern African highland paleoclimate.

2.1 Introduction

Eastern Africa, and Ethiopia in particular, has received much attention from archaeologists and paleoclimatologists (LAMB ET AL., 2018; VIEHBERG ET AL., 2018). This may be attributed to Quaternary climatic changes being widely acknowledged to have played a role in the early history of modern humans in Africa. Climatic extremes may have caused human populations to take refuge in the Ethiopian highlands (BRANDT ET AL., 2012), including the Bale Mountains (Fig. 2.1). OSSENDORF ET AL. (2019) recently highlighted that Middle Stone Age foragers occupied a rock shelter at 3469 m a. s. l. from 47 to 31 cal ka BP, during times of the largest extent of the glaciation in the Bale Mountains.

Earlier studies of the Quaternary climate and environmental history of the Bale Mountains include OSMASTON ET AL. (2005) on glacial geology, KUZMICHEVA ET AL. (2017) on pollen and hyrax deposits and GIL-ROMERA ET AL. (2019) on pollen and charcoal. UMER ET AL. (2007) and TIERCELIN ET AL. (2008) studied the sedimentary record of Garba Guracha at 3950 m a. s. l., using sedimentological, geochemical and pollen analyses, showing that Garba Guracha is one of the longest, most continuous high-resolution Late Quaternary environmental archives from highland Africa.

Recently, the importance of compound-specific ^{14}C dating in lake sediments has been shown by DOUGLAS ET AL. (2014) and GIERGA ET AL. (2016). The occurrence or nonoccurrence of age differences between organic matter components provides valuable information for the catchment itself and for the interpretation of proxies, especially in a multi-proxy approach.

The rationale for revisiting Garba Guracha was (i) to make this archive accessible by retrieving new sediment cores, (ii) to examine age offsets in the organic matter components by applying bulk *n*-alkane dating and (iii) to apply charcoal, diatom, biomarker or stable isotope analyses, not made in previous studies of the Garba Guracha cores. Together with non-pollen palynomorph and renewed pollen analyses, these new analyses provide proxy records of paleofire, limnology, vegetation, climate, and human environments. In this paper, we describe the sedimentary sequence and evaluate the organic matter origin of the new (2017) cores, establish a robust chronology with the first tephra correlations and present the first biogeochemical and biomarker results.

2.1.1 Study site

Garba Guracha is located in the Bale Mountains of the Bale-Arsi Massif, situated east of the Main Ethiopian Rift (Fig. 2.1). The highest plateau of the Bale Mountains is the Sanetti Plateau at an altitude between ~ 3800 to ~ 4200 m a. s. l. and an area of 600 km^2 bordered by a steep escarpment to the south (OSMASTON ET AL., 2005). The north and northeast are characterised by valley structures deeply incised by northward descending rivers. The volcanic plateau overlies older volcanic material and was formed by solidified horizontal lava consisting of alkali basalt, trachyte, and tuffs with rhyolites (UHLIG & UHLIG, 1991; WILLIAMS, 2016).

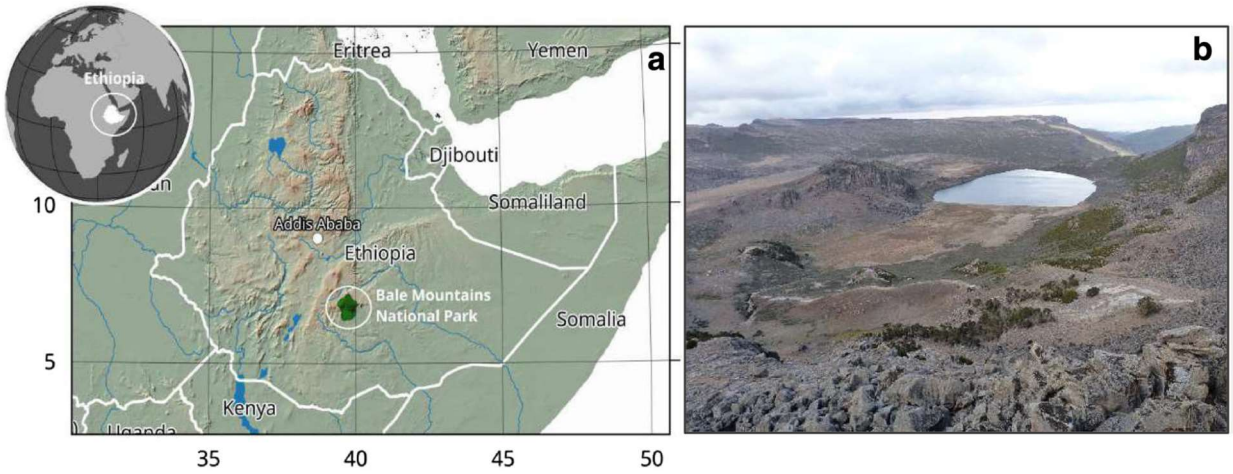

Figure 2.1: (a) Map of the study area (Bale Mountains National Park) situated east of the Ethiopian Rift Valley in Ethiopia, Eastern Africa (made by Dr. Miguel Sevilla-Callejo); (b) Garba Guracha catchment and glacial cirque.

The plateau and the valleys were locally glaciated during the Last Glacial Maximum (OSMASTON ET AL., 2005; OSSENDORF ET AL., 2019). The glacial cirque Garba Guracha (6.875781 °N, 39.878075 °E) was first described by Werdecker (1962) and has also been described in detail by UMER ET AL. (2007) and TIERCELIN ET AL. (2008). It is located at 3950 m a. s. l., extends to about 500 x 300 m in size, has a maximum water depth of 6 m and a very small watershed (0.15 km^2). The bedrock of the Garba Guracha catchment consists mainly of basaltic lavas. The cirque base is formed by trachytic tuff, which outcrops only on the southern and southeastern slopes (TIERCELIN ET AL., 2008). The catchment bedrock is carbonate-poor (LÖFFLER, 1978; UHLIG & UHLIG, 1991). The northeast-facing cirque lies between the Ericaceous and afro-alpine vegetation belts, which are continuous on the northeastern side into the Togona Valley. The lake has an outlet during the rainy season. A marshy alluvial plain fed by several springs extends to the south of the lake.

The climate of the Bale Mountains varies from north to south due to differences in altitude, aspect and continental hot air masses (KIDANE ET AL., 2012; UHLIG & UHLIG, 1991). The mean annual temperature at Dinsho (7.105016 °N 39.776001 °E, 3207 m a. s. l., 25 km NNW of Garba Guracha) is 11.8 °C, and the mean minimum temperature for the coldest month is 0.6 °C (HILLMAN, 1986). Ten newly installed climate stations across the Bale Mountains have provided modern climate data since 2017. The results from 2017 show a mean annual temperature of 4.9 °C at the Angesso Station (6.8964 °N, 39.9085 °E, 3949 m a. s. l.), which is located 4 km northeast of Garba Guracha.

UHLIG (1988) and MIEHE & MIEHE (1994) state that two moisture sources, the Indian Ocean monsoon and the equatorial westerlies, bring precipitation to the Bale Mountains. High seasonality characterises the rainfall pattern with a dry season from November to February and a bimodal wet season from March to October. Precipitation maxima occur in April/May and September/October, respectively (WOLDU ET AL., 1989). The highest monthly rainfall, related to the convergence of southwest and northeast air masses, occurs in the months of July to September. Mean annual precipitation increases with altitude from 925 mm at Goba (elevation 2720 m a. s. l.) to Chorchora with 1086 mm at 3500 m a. s. l. At higher elevations,

the mean annual precipitation decreases again (852 mm at Konteh, 4050 m a. s. l.) (UMER ET AL., 2007). Recently installed climate stations support this finding, with annual precipitation in the year 2017 decreasing from 1097 mm at Angesso Station (elevation 3949 m a. s. l.) to 711 mm at the EWCP Station (elevation 4124 m a. s. l.) and even further to 468 mm at Tulu Dimtu (elevation 4385 m a. s. l.) (2017, unpublished data). The afro-alpine regions, including the Sanetti Plateau, are characterised by strong diurnal temperature differences between day and night. HILLMAN (1988) reported on a diurnal temperature range of 40 °C (-15 °C to + 26 °C).

2.2 Material and Methods

In February 2017, we retrieved two overlapping sediment cores using a Livingstone piston corer from a raft anchored at 4.8 m water depth. The replicate cores (BAL-GGU17-1A and BAL-GGU17-1B) were taken in sequential 1 m sections, with core 1B sections taken to overlap those of core 1A by 70 cm. Sediments at and below the water-sediment interface (Section BAL-GGU17-1A-1L (65 cm)) were sub-sampled at 1 cm intervals in the field. A maximum sediment depth of 1550 cm was reached, similar to the depth (1582 cm) achieved by TIERCELIN ET AL. (2008). Unfortunately, that core was not available for further analyses. The bottom four sections of each of our cores were difficult to retrieve and extrude due to densely compacted sediments, coarse sand, and gravel. Bedrock or glacial diamicts were not reached. In the laboratory, the cores were split, described and stored at 4 °C. Sampling for chronological controls and proxy analyses was carried out on core BAL-GGU17-1B as its extrusion was more complete than core BAL-GGU17-1A.

2.2.1 Chronology and dating

Radiocarbon dating

For radiocarbon dating, we took a total of 31 samples, comprising 18 bulk sediment samples, 8 bulk *n*-alkane and 5 charcoal samples from the top 9 meters of the BAL-GGU17-1B core (Table A.1). Bulk *n*-Alkane and bulk sediment samples were taken at the same depths to test for age offsets.

Bulk sediment and charcoal samples were weighed into glass centrifuge vials and treated with 1N HCl for 8 hrs at 60 °C to remove carbonates from the samples. They were subsequently washed and rinsed with ultrapure water to pH neutrality. Samples were then packed in tin boats (Elementar, 6 x 6 x 12) for ^{14}C measurements.

For bulk *n*-alkane dating, the total lipid extract (TLE) was obtained by constant rinsing with solvent (dichloromethane:methanol in a ratio of 9:1) using a soxhlet system. After rotary evaporation, the TLE was dissolved again with *n*-hexane and transferred onto aminopropyl pipette columns (Supelco, 45 um). The different fractions of the TLE (nonpolar fraction, including *n*-alkanes; polar fraction, including alcohols; acids) were selectively eluted from the columns using three solvents of increasing polarity (*n*-hexane; dichloromethane:methanol 1:1; diethyl ether:acetic acid 19:1). The *n*-alkane fraction was then loaded onto $AgNO_3$-coated silica

and zeolite pipette columns (Geokleen 5A, GHGeochemical Services) for further purification. The zeolite with the trapped *n*-alkanes was dried in an oven (12 hrs, 40 °C). After dissolving the zeolite in hydrofluoric acid, the *n*-alkanes were recovered using liquid-liquid extraction with *n*-hexane. Prior to ^{14}C-measurements, the *n*-alkanes were transferred with dichloromethane (DCM) into tin capsules (Elementar, Art. Nr. 05001727, 3.5× 5.5× 0.1 mm), and the DCM was subsequently evaporated using a heating plate at 40 °C.

^{14}C measurements were performed at the MIni CArbon DAting System (MICADAS) AMS coupled online to an elemental analyzer (Vario MICRO cube from Elementar) at the LARA AMS Laboratory, University of Bern (SZIDAT ET AL., 2014). Results were reported as fraction modern (F^{14}C), which is the activity ratio of a sample normalised to the modern reference material Oxalic Acid II (National Institute of Standards and Technology). F^{14}C results were corrected for cross and constant contamination following the contamination drift model of SALAZAR ET AL. (2015). Constant contamination for the bulk *n*-alkanes was obtained from 10 combined tin capsules that yielded 0.94 µg carbon for a single cap with F^{14}C values of 0.8145. Constant contamination for the bulk sediment and charcoal samples was obtained from 10 combined tin boats that yield 1.41 µg carbon for a single boat with F^{14}C values of 0.7390. ^{14}C ages were calibrated to cal yr BP with the IntCal13 calibration curve (REIMER ET AL., 2013).

Radiometric Dating

The dried sediment samples of the surface core BAL-GGU17-1A-1L were analysed for ^{210}Pb, ^{226}Ra, ^{137}Cs, and ^{241}Am by direct gamma assay in the Environmental Radiometric Facility at University College London using an ORTEC HPGe GWL series well-type coaxial low background intrinsic germanium detector. Lead-210 was determined via its gamma emissions at 46.5 keV and ^{226}Ra by the 295 keV and 352 keV gamma rays emitted by its daughter isotope ^{214}Pb following 3 weeks storage in sealed containers to allow radioactive equilibration. Cesium-137 and ^{241}Am were measured by their emissions at 662 keV and 59.5 keV (APPLEBY ET AL., 1986). The absolute efficiencies of the detector were determined using calibrated sources and sediment samples of known activity. Corrections were made for the effect of self-absorption of low energy gamma rays within the sample (APPLEBY ET AL., 1992).

Lead-210 dates were calculated using the CRS (constant rate of ^{210}Pb supply) dating model (APPLEBY, 2001). The CRS dating model places 1963 depth at 14.5 cm, which is considerably deeper than the depth suggested by the ^{137}Cs and ^{241}Am records. The corrected CRS chronologies and sediment accumulation rates were calculated by using the sediments at 7.5 cm as formed in 1963 (Table A.1).

Spheroidal carbonaceous particle (SCP) analysis

Spheroidal carbonaceous particles (SCPs) are a component of fly-ash produced only from the high temperature industrial combustion of coal-series and oil fuels. SCP concentration profiles provide an additional means to provide independent dates at the regional scale while the rapid increase in SCP accumulation in the 1950s appears to be a global signal (ROSE, 2015). SCP analysis involved sequential removal of unwanted sediment fractions using nitric, hydrofluoric and hydrochloric acids resulting in a final suspension in water (ROSE, 1994). A known fraction

of this suspension was then evaporated onto a coverslip, mounted onto a glass slide, and the SCPs enumerated under a light microscope at 400x magnification. Standard criteria for SCP identification were followed (ROSE, 2008). Analytical blanks and SCP reference material (ROSE, 2008) were included with all sample digestions. The detection limit for the technique is typically less than 100 g $DM^{-1,}$ and calculated concentrations generally have an accuracy of approximately ± 45 g DM^{-1}.

Tephra analysis

Three tephra layers (GGT-1, GGT-2, and GGT-3) were identified in the Garba Guracha sediments. These were geochemically fingerprinted to test whether they could be matched to the tephra layers that MARTIN-JONES ET AL. (2017) observed and dated in sediment cores from the Main Ethiopian Rift lakes, Tilo, Awassa, and Chamo. The oldest tephra layer GGT-3 has yet to be analysed but may provide a further tie point to regional lakes in the future.

Samples were collected from across the entire thickness of the tephra and, in order to isolate glass shards for geochemical analysis, the samples were wet sieved to > 25 µm and separated using a solution of sodium polytungstate to a density of > 1.95 g ccm^{-1}. Shards from each tephra were mounted in an epoxy resin block which was ground and polished to reveal the interior of the glass for analysis. First, the shards were analysed for major element concentrations using a Cameca SX-100 WDS electron microprobe (EPMA) at the Department of Earth Sciences, University of Cambridge. The analysis was set up to minimise alkali element migration through using a 10 µm defocused beam set at 6 nA and 15 kV and counting Na for 10s, Cl and P for 30 s and all other elements for 30 s. A series of mineral standards were used to calibrate the instrument and concentrations were quantified using the PAP absorption correction method. Data presented in the text and figures have been normalised to 100 % to account for variable secondary hydration of the glass; for the unprocessed data see Table A.2.

Second, the glass shards were analysed for their trace element concentrations using a Thermo Scientific iCapQ coupled to a Teledyne G2 Excimer laser (LA-ICP-MS) in the iCRAG laboratory, Trinity College Dublin. The shards were analysed with 40 μm^2 laser spots, with the laser firing at 5 Hz and counting for 40 s on both the sample and the blank. Counts were calibrated against assays of NIST612 with the average ^{29}Si concentration for each tephra layer (obtained via EPMA) used as an internal standard. Data were reduced using Iolite3.4, using Ca correction as advocated by TOMLINSON ET AL. (2010).

For each analytical session with the EPMA and the LA-ICP-MS, the MPI-DING basaltic, andesitic and rhyolitic natural glass standards (JOCHUM ET AL., 2006) were analysed in order to monitor instrument accuracy.

Age-depth model

For establishing an age-depth model, we used the Bayesian approach implemented in the package Bacon v 2.2 (BLAAUW ET AL., 2011) available for R (CRAN, 2017). Bacon calibrates all ^{14}C dates simultaneously according to the stratigraphic principle (BLAAUW ET AL., 2007) applying the IntCal13 calibration curve (REIMER ET AL., 2013). This Bayesian method defines accumulation rates using a gamma autoregressive semi-parametric model with several subdivisions along

the sediment that can be set up as a prior to the model (parameter α and thick, respectively). This serves as a smoothness factor for the aging series, followed by a self-adjusting Markov Chain Monte Carlo (MCMC) building a robust-to-outliers age model (BLAAUW ET AL., 2011). The Bayesian approach aims to build a realistic age-depth relationship that often implies no linear deposition.

2.2.2 XRF scanning

XRF analysis for both cores was performed at Aberystwyth University using the Itrax™ core scanner. Standard scanning procedure for an Itrax scanner was undertaken (Itrax scanner specifications and procedures outlined in (CROUDACE ET AL., 2006). Scan settings were 30 kV, 45 mA using a step size of 500 µm for the Garba Guracha cores. XRF and X-ray exposure times were set to 15 seconds and 200 milliseconds, respectively, for both cores. Fine-tuning of the detector parameters was performed before each scan to match the actual and fitted spectra and minimise the mean square error (MSE) value. As a result, MSE values were maintained below 2 (mean = 1.59 ± 0.3). Following the calibration of scanner settings, a layer of 1.5 µm thick film was used to cover the core to minimise moisture loss during scanning.

Significant changes in water and organic content may lead to inaccurate detection of some elements, resulting in downcore changes in raw element profiles unrelated to sediment geochemistry (LÖWEMARK ET AL., 2011). Consequently, to minimise the effects of sediment-water and organic content, normalization of raw element data by the total scatter (both the incoherent and coherent data, equivalent to Compton and Rayleigh scattering, respectively) is commonly used (KYLANDER ET AL., 2011). Normalization of the peak area data was achieved using the total scatter.

Due to low and noisy signals, only K, Ca, Ti, Fe, and Rb could be evaluated robustly and were further considered for interpretation. The surface core (BAL-GGU17-1A-1L), as well as two core sections of BAL-GGU17-AB and 1B from 1245 cm to 1485 cm sediment depth, were not scanned because of high water content and coarse and gravel material, respectively. Therefore, the results presented in this study are missing the top 20 cm and 240 cm near the core base.

2.2.3 Biogeochemical analyses

Total carbon (TC), total nitrogen (N) and stable carbon and nitrogen isotopic composition ($\delta^{13}C$ and $\delta^{15}N$, respectively) were determined for 110 mixed sediment samples covering roughly 10 cm intervals. The analyses were carried out on dried and ground samples at the Institute of Agronomy and Nutritional Sciences, Soil Biogeochemistry, Martin-Luther-University Halle-Wittenberg using an EuroVector EA 3000 elemental analyzer (Hekatech, Wegberg, Germany) coupled via a Conflow III Interface to a Delta V Advantage isotope ratio mass spectrometer (IRMS; both from Thermo Fisher Scientific, Bremen, Germany). The results were calibrated using standard materials with known total carbon, nitrogen, ^{13}C and ^{15}N contents (IAEA N_2, IAEA CH_6, IAEA NO_3, IAEA CH_7, IAEA 305A, USGS 41). Following the international standard

regulations (COPLEN 2011; ^{13}C: Vienna Pee Dee Belemnite, VPDB; ^{15}N: atmospheric N_2, Air) all isotope results are reported in the common δ-notation. Concerning total carbon, please note that (i) the bedrock in the catchment is reported to be carbonate-poor/free and (ii) we performed Scheibler analyses (ALLISON, 1960) on several sediment test samples that yielded 0 % inorganic carbon content. Given that, moreover, our TC record is in excellent agreement with the TOC record of TIERCELIN ET AL. (2008), we use the term TOC instead of TC from here on for our record.

2.2.4 *n*-Alkane and sugar quantification

The *n*-alkanes from the extracted TLEs were quantified using a GC-2010 series gas chromatograph coupled with a flame ionization detector (GC-FID; Shimadzu, Kyoto, Japan). For linear calibration, a C8 – C40 saturated *n*-alkane standard mixture (Supelco 49452-U) was repeatedly analysed in each batch at different concentrations (10 µg ml^{-1}, 50 µg ml^{-1} and 100 µg ml^{-1}). All work was carried out at the Institute of Agronomy and Nutritional Sciences, Soil Biogeochemistry, Martin-Luther-University Halle-Wittenberg.

Sugar biomarkers were extracted following the method described by Zech and Glaser (2009). Briefly, the monosaccharides were hydrolytically extracted from the homogenised samples using 4 M trifluoroacetic acid at 105 °C for 4 h (AMELUNG ET AL., 1996). The monosaccharides were then filtered over glass fiber filters, evaporated and further purified over XAD-7 and DOWEX 50WX8 columns. After freeze-drying, the samples were derivatised (methyloxime-trimethylsilyl-derivatisation). The derivatization follows the method of (ANDREWS, 1989) to enable a quantification of a large range of sugars (arabinose (ara), fucose (fuc), galactose, glucose, mannose, rhamnose, ribose and xylose (xyl)). The quantification of these sugars was also carried out on a GC-FID (Shimadzu, Kyoto, Japan). Note that for this study, only the sugar results for ara, fuc, and xyl are evaluated.

2.3 Results

2.3.1 The sedimentary sequence – Master core and lithofacies

A master core of the overlapping BAL-GGU17-1A and 1B cores (Fig. 2.2) was created by visual correlation of several XRF elements like Ti, Fe, Rb, and K using Stratfit (SAGNOTTI & CARICCHI, 2018). Stratfit combines all core sections into one depth model. Additionally, the core sections were checked for contaminated parts, especially at the top and the bottom of individual core sections. The master core consists mainly of sections of the BAL-GGU17-1B core due to less contamination or disturbance than in core 1A. Only in the lower part of the sequence, a few 1A core sections were used instead of 1B core sections (Fig. 2.2).

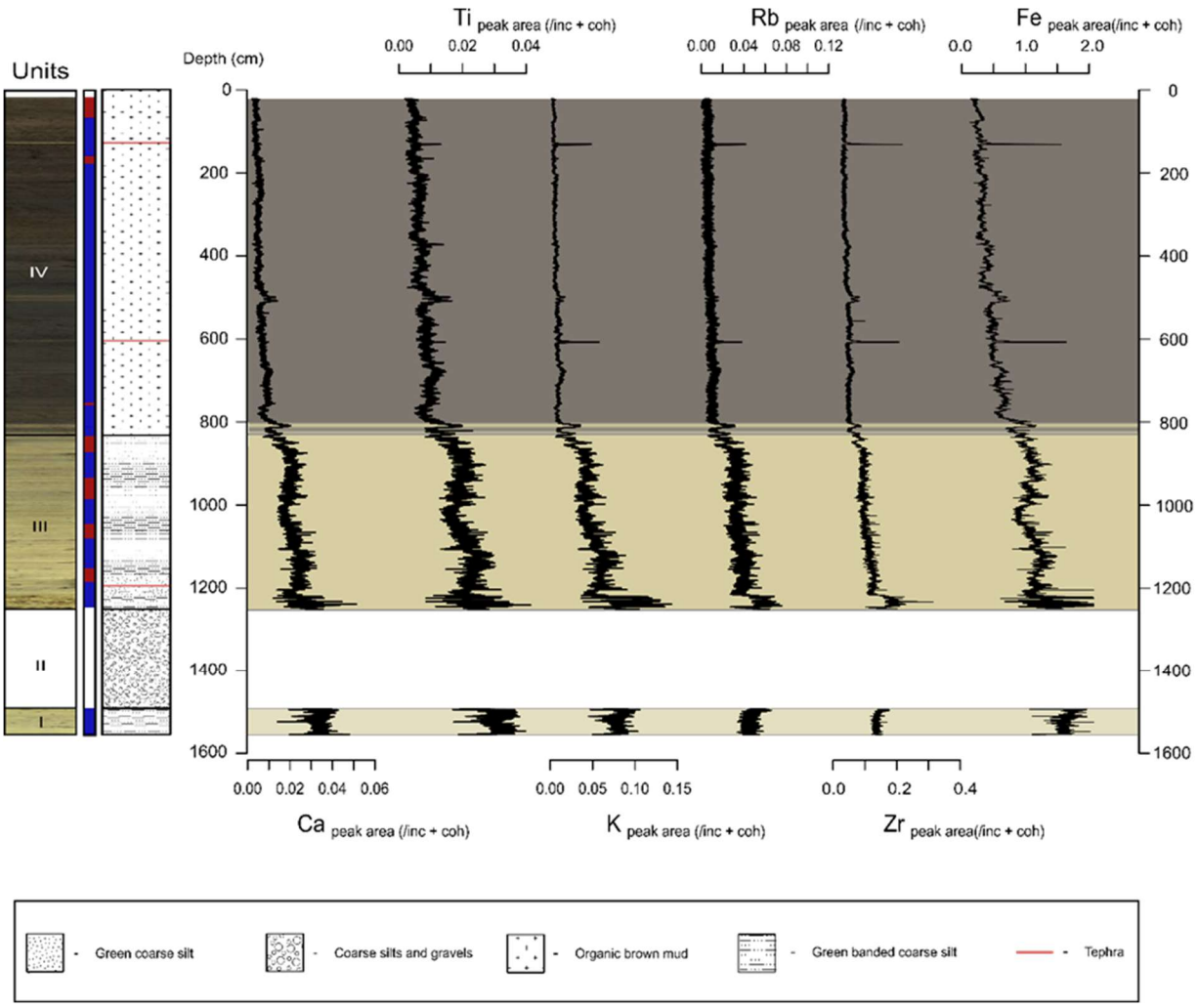

Figure 2.2: Lithostratigraphy (Master core: 1B = blue; 1A = red) and XRF data for calcium (Ca), titan (Ti), potassium (K), rubidium (Rb), zirconium (Zr) and iron (Fe).

The sedimentary sequence of core GGU17 consists of green banded siliciclastic fine material interbedded with layers of coarser material and gravel in the lower part (Fig. 2.2). It can be divided into 4 lithostratigraphic units:

- Unit 1 (1552-1476 cm) contains greenish banded siliciclastic coarse sand.
- Unit 2 (1476 – 1276 cm) is comprised of two meters of highly coarse silt and gravel.
- Unit 3 (1276-1476 cm) consists mostly of green banded siliciclastic material mostly coarse silt with amorphous organic matter (OM) intersected with one layer of fine silt between 1219-1166 cm and a layer of coarse sand at 1031-966 cm. The diatom content of this unit is about 10 %.
- Unit 4 (838-70 cm) consists of nearly 8 m of dark brown massive organic mud with varying diatom content. This unit is intersected by a small layer of green-greyish massive siliciclastic fine silt at 828 cm and two layers of organic poor, finer sediments at 496 cm and 505 cm.

Three tephra layers have been identified at 129 cm, 604 cm, and 1198 cm depth, respectively. A fourth tephra layer mentioned by TIERCELIN ET AL. (2008) (~ 340 cm) was not detected.

2.3.2 Chronology

Tephra age

Two grey tephra layers were analysed as part of this study. They occur at 129 cm and 604 cm depth in the Garba Gurache core (Fig. 2.2), are no more than 1 cm in thickness and contain clear, bubble wall and pumiceous glass shards. According to the Garba Gurache age model, tephra GGT-1 has a modelled age of 1.2 -1.6 cal ka BP and GGT-2 has an age of 7.8 - 8.1 cal ka BP. Glass shards in both tephra layers have a similar rhyolitic composition (Fig. A.3), however, GGT-1 can be distinguished from GGT-2 based on its higher Ba concentrations.

Lead-210 Activity and SCP

Total ^{210}Pb activity reaches equilibrium with supported ^{210}Pb at a depth around 52 cm of the core. Unsupported ^{210}Pb activities, calculated by subtracting ^{226}Ra activity (as supported ^{210}Pb) from total ^{210}Pb activity, decline overall irregularly with depth (Table A.2, Fig. A.1 and A.2). The unsupported ^{210}Pb activity profile shows two different sections: the top 19 cm section and the rest of the core. Within each individual section, unsupported ^{210}Pb activities decline more or less exponentially with depth, suggesting a relatively uniform sedimentation rate within the sections. However, as the decline gradients in the two sections are different, sedimentation rates might have changed at around 19 cm depth.

The ^{137}Cs activity versus depth (Fig. A.3) shows a well-resolved peak at 7.5 cm. Such a ^{137}Cs peak has been found in other records from Eastern Africa (PANIZZO ET AL., 2008; STOOF-LEICHSENRING ET AL., 2011). It is almost certain that this peak was derived from the 1963 fallout maximum of the atmospheric testing of nuclear weapons. A ^{241}Am activity at 7.5 cm suggests the fallout of nuclear weapon testing, although one single point is not sufficient for dating (Table A.3, Fig. A.1 and A.2).

SCP concentrations increase above detection limit at 11.5 cm and increase rapidly to a peak of almost 1000 g^{-1} (per gram dry mass) at 4.5 cm. Outside Europe and North America, such a profile is common, with the initial increase representing 1950 ±5 years (ROSE, 2015). This would place 1950 ±5 at 12 cm depth, in good agreement with the ^{210}Pb chronology.

Radiocarbon dating

The 7-bulk *n*-alkane and 14 bulk sediment samples yielded sufficient carbon amounts of up to 138 µg for ^{14}C dating (Table A.1). Except for one *n*-alkane sample (low carbon mass of 16 µg), the bulk *n*-alkane and the bulk sediment samples obtained from the same core centimeters yielded similar ages without any systematic age offset. Additionally, there is no age offset for the three charcoal ^{14}C ages. Apart from macrocharcoal particles (> 150 microns particles), we found no other terrestrial macrofossils suitable for ^{14}C dating.

Age-depth model and sedimentation rate

To develop an age-depth model (Fig. 2.3), we combined the ^{210}Pb, bulk sediment, bulk *n*-alkane and charcoal radiocarbon ages into a Bayesian modelling framework (BLAAUW, 2010; BLAAUW ET AL., 2011). Note that a preliminary version of this age-model underlies the paleoenvironmental dataset published by GIL-ROMERA ET AL. (2019). All ^{14}C ages with a carbon mass smaller than 19 µg were rejected and not used for our age-depth model. Additionally, two ages that are not in stratigraphic order and three bulk sediment ^{14}C ages at the core top, which have an age offset to the ^{210}Pb dating, were excluded but are displayed in Fig. 2.3. According to the dating results and the established age-depth model, sedimentation in Garba Guracha started at about 15.9 cal ka BP.

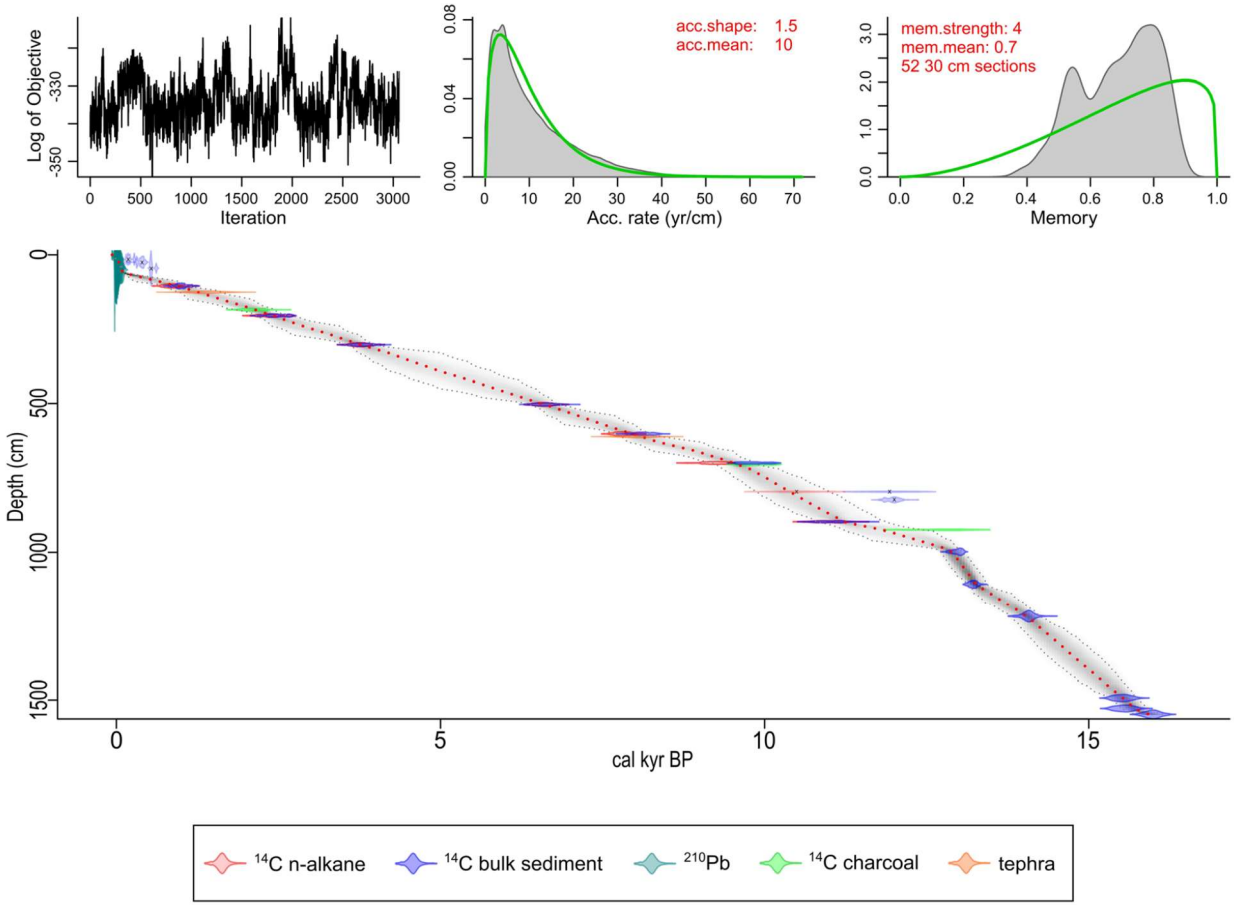

Figure 2.3: Age-depth model for the GG sedimentary record. The model was created using Bacon (BLAAUW AND CHRISTEN 2011). Top left: The log-likelihood of the model fit for the saved iterations of the model, Top middle: prior and posterior distribution of accumulation rate, and Top right: prior and posterior distribution of the autocorrelation in accumulation rates (memory). In the bottom left: The accumulation rate (cm/yr) per time (cal. Yr. BP). The main panel displays the depth (x-axis) and age (y-axis) scale. The probability distribution of the calibrated ages are represented as violin plots (modelled ages (blue), non-modeled ages (pink) and tephra ages (68% probability) of TT1 and CHT2 (red). The probability of age ranges for any given depth is displayed in the grey shaded sections, and the dotted lines around it represent the 95% highest probability density. Datings are shown in different colours. Shaded violin plots marked with "x" show datings excluded from the age-depth model. In the lower-left corner, the sedimentation rate with a mean sedimentation rate (dotted red line) is displayed.

The mean sedimentation rate (MSR) for our BAL-GGU17-AB core is 1.25 mm a^{-1} (Fig. 2.3). The highest average values of 2.90 mm a^{-1} are recorded between 1110-990 cm with maximum values of 5 mm a^{-1}. A second maximum is present from 900 to 720 cm with a sedimentation rate of 1.27 mm a^{-1}. In between these maxima, a marked sedimentation minimum with decreased rates by up to 75 % characterises the time period from 12.8 cal ka BP to 11.3 cal ka BP. From 720 cm on, the sedimentation rate constantly decreases until the present day, with a mean sedimentation rate of 0.70 mm a^{-1}.

Establishing a robust chronology/sedimentation rate for the uppermost decimetres of the core is challenging because the combination of the two chronological methods provides us with a significant change in sedimentation rate that is most likely unrepresentative of the true sedimentation process. But since the modelled age is coherent with the sedimentation pattern of previous sections, and there is no significant change in any other proxies, we assume the radiocarbon-Cs/Pb age-transition to be valid. Therefore, MSR for the topmost 65 cm is 5.4 mm a^{-1}.

2.3.3 Geochemistry

XRF scanning

The XRF scanning of the elements Rb, K, Ti, Fe, Ca, and Zr yielded the highest values in the lower part of the core with a stepwise decrease at 1200 cm and 800 cm to relatively low amounts. (Fig. 2.2). All these elements have a very high correlation coefficient of $r > 0.93$. At 500 cm, an increase of Ca, Ti, and Fe coincide with low TOC values. Two short peaks in Zr, Rb, K and Fe reflect the tephra layers at 604 cm and 129 cm, respectively.

Organic geochemistry and stable isotope results

TOC values for the Garba Guracha master core range from 0.3 % to 21.4 % (Fig. 2.4). Low TOC persists until 840 cm. Above that depth, TOC values constantly increase until 355 cm, with maxima at 630 cm (19.2 %) and 430 cm (21.4 %) and a minimum at 500 cm of 8 %. At 355 cm, TOC rapidly decreases to values < 10 %.

The TOC/N ratios range from 2.8 to 14.9. The lowest values prevail from the bottom of the core until 840 cm. Until 355 cm, relatively high ratios of up to 15 occur with short minima at 700 and 500 cm (9.5 and 6.5 cal ka BP). Maxima characterise the depth between 640 and 610 and 460 and 355 cm.

The $\delta^{13}C$ values range between -22.7 ‰ and -13.9 ‰. A decline in $\delta^{13}C$ to the lowest values (-22 ‰) coincides with an increase in TOC and TOC/N at 840 cm, followed by generally increasing values until 420 cm with a strong decrease at 600 cm. A small overall decrease continues to160 cm. This interval includes a strong maximum of -16.3 ‰ at 340 cm and a weaker one (-16.8 ‰) at 355 cm. An increase is visible from 160 cm to the top of the core.

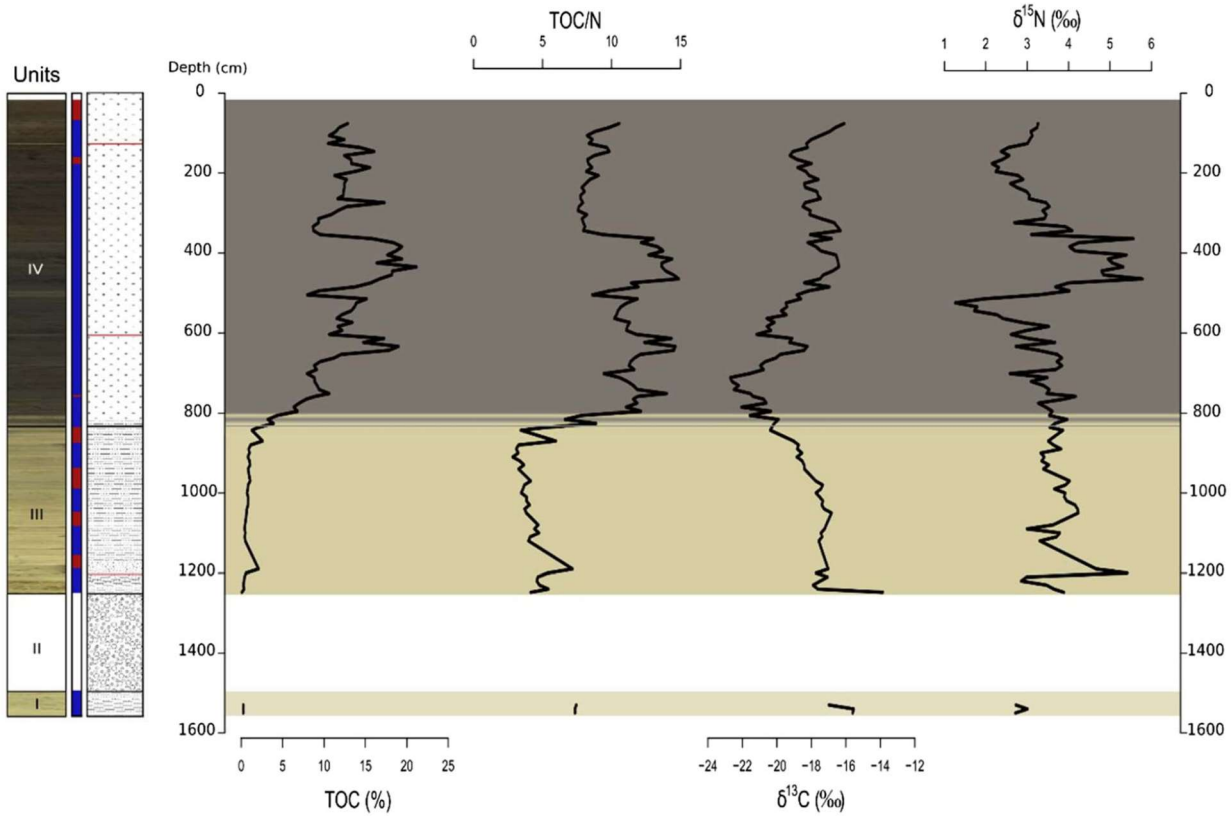

Figure 2.4: Total organic carbon (TOC), carbon to nitrogen ratio (TOC/N) and stable carbon and nitrogen isotopic composition ($\delta^{13}C$ and $\delta^{15}N$).

The $\delta^{15}N$ values range from 1.3 ‰ to 5.8 ‰. From the bottom of the core to around 55 cm, values stay stable around 3 ‰ to 4 ‰. A decrease with a minimum (1.3 ‰) at 525 cm is followed by a maximum between 500 and 355 cm (4 - 5.8 ‰). Values decrease again until 170 cm.

P_{aq} and sugar ratios

Using the quantification of *n*-alkanes and sugar biomarkers, different ratios can be calculated to distinguish between terrestrial versus aquatic sources (Fig. 2.5). Calculated ratios in this study cover the first 940 cm of the core due to insufficient organic matter content in the lower parts.

A common ratio for *n*-alkanes to differentiate aquatic macrophyte input versus emergent and terrestrial vegetation input is the P_{aq} proxy (FICKEN ET AL., 2000), defined as

$$P_{\mathrm{aq}} = \frac{(n_{C23} + n_{C25})}{(n_{C23} + n_{C25} + n_{C29} + n_{C31})} \qquad \text{[Eq. 1]}$$

The P_{aq} ratio values range between 0.04 and 0.57 (Fig. 2.6). Highest values are present between 940 and 780 cm (up to 0.57), with one minimum at 840 cm (0.33). A shift to lower values occurs with a minimum at 750 cm (0.22) and a maximum at 500 cm (0.41). Like the TOC and TOC/N values, the P_{aq} decreases drastically at 355 cm. Followed by a phase of low values until 260 cm. The last 260 cm have intermediate values with a minimum at 155 cm (0.04).

HEPP ET AL. (2016) developed two sugar biomarker ratios defined as fuc/(ara+xyl) and fuc/(ara+xyl).

The fuc/(ara+xyl) ratios range from 0.2 to 0.8 (Fig. 2.6). The highest values concur with the highest values of the P_{aq} ratio from 940 to 780 cm with a maximum at 795 cm (0.5). A more abrupt shift to lower values occurs at 770 cm. Low values proceed until 260 cm, with a maximum at 485 cm (0.6) and a minimum at 720 cm (0.3). After a maximum at 235 cm (0.5), the lowest values of the core prolong between 235 and 145 cm. The last 140 cm are characterised by a strong increase with a maximum at 85 cm (0.58).

The (fuc+xyl)/ara ratios range between 0.7 and 3 (Fig. 2.6). The ratio correlates well with the fuc/(ara+xyl) ratio for the top 235 cm with minima at 145 and 195 cm. The highest values are reached between 390 and 490 cm (up to 3). Low values at 690 to 740 cm correlate well with the fuc/(ara+xyl) ratio. However, underneath 770 cm, when the fuc/(ara+xyl) ratio shows the highest values, the (fuc+xyl)/ara ratio displays conditions with values between 1.3 and 1.9.

2.4 Discussion

2.4.1 Chronology

Tephra correlation

Rhyolitic tephras, of similar composition to the Gurba Gurache tephras, have also been documented in Holocene sediment cores from the Main Ethiopian Rift lakes Tilo and Chamo (MARTIN-JONES ET AL., 2017). Fourteen tephra layers were identified in the < 10 cal ka BP Lake Tilo sequence by MARTIN-JONES ET AL. (2017), who geochemically correlated two of these horizons (TT-2 and TT-13) to two tephra layers occurring within sediments from Lake Chamo, 170 km to the south. MARTIN-JONES ET AL. (2017) suggested that the Corbetti caldera (~ 40 km east of Lake Tilo), which erupts tephras of a distinct composition in comparison to other Ethiopian Rift volcanoes, is the source of the tephras found at lakes Tilo and Chamo. FONTIJN ET AL. (2018) later correlated TT-2 and TT-13 to their on-land equivalents in outcrops within the Corbetti caldera, confirming this as the source for these two eruptions.

To test if the Garba Guracha tephras were also deposited by eruptions from Corbetti (~ 120 km to the west of our site), we compared the glass composition of GGT-1 and GGT-2 with the Tilo and Chamo tephras (Fig. A.3). Tephra GGT-1 matches the composition of the Tilo tephra TT-2, which is dated at Lake Tilo to 1.3 - 1.5 cal ka BP. MARTIN-JONES ET AL. (2017) geochemically correlated TT-2 to the youngest of the Chamo tephras CHT-1 (1.5 - 1.9 cal ka BP), and this deposit represents Corbetti's most recent highly explosive eruption. Tephra GGT-2 has a similar composition to glass within the Tilo tephra TT-13 (dated at Tilo to 8.3 - 8.7 cal ka BP), which correlates to CHT-2 at Lake Chamo and where it is dated to 7.8 – 8.3 cal ka BP. GGT-1 and GGT-2 glass do, however, contain lower concentrations of Zr, Th, and Ba than the Tilo and Chamo tephra glass shards. These eruptions may have tapped a compositionally stratified magma chamber resulting in wide-ranging tephra compositions. Garba Guracha is

the first distal site to the east of Corbetti for which we have glass data, and if wind direction changed mid-eruption, this could explain why we have a slightly different tephra compositions deposited in this new location.

Although the Corbetti tephras are compositionally zoned, making their recognition in different locations more challenging, the existing evidence for the widespread dispersal of tephras TT-2 and TT-13 supports our tentative geochemical correlations to the distal tephra layers preserved at Garba Guracha. Here we use these tephra correlations as an external test of the Garba Guracha age model. Whilst the tephra layers recorded in lakes Tilo and Chamo have greater uncertainties than the Garba Guracha tephras, these horizons act as useful markers around which we can compare environmental indicators recorded in the different lakes. Our correlations to the well-dated Garba Guracha record allow us to refine the ages of these two highly explosive Holocene eruptions from the Corbetti caldera.

Age-depth model

The 2017 Garba Guracha core covers the range from the present day to ~ 15.9 cal ka BP. TIERCELIN ET AL. (2008) suggested the minimum age of deglaciation to be ~ 16.7 cal ka BP. Exposure dating (15 ± 1 cal ka BP) of boulders and glacial features in the Togona Valley (downhill from Garba Guracha) support a later minimum age of deglaciation (OSSENDORF ET AL., 2019; GROOS ET AL., unpublished data). The modelled ages for the two tephra layers at 129 and 604 cm depths are 1.2 - 1.6 and 7.8 - 8.1 cal ka BP, respectively. These tephra ages compare well with the ages of their geochemical correlatives (Fig. 2.3). The independent chronological context provided by the tephra layers on the Garba Guracha age model not only underlines the robustness of the age model but also allows us to conclude that the offset between ^{14}C bulk sediment and ^{210}Pb ages in the top of the core (Table A.1) is not a systematic age offset. Due to the fact that the ^{210}Pb ages are supported by SCP, and a hard water effect of the ^{14}C ages can be ruled out, we hypothesise the input of pre-aged terrestrial organic matter after ~ 1 cal ka BP.

An old carbon input could also explain the stratigraphically inconsistent older ^{14}C bulk sediment ages at 794 and 821 cm. Interestingly an n-alkane date at 794 cm (9.7 - 11.2 cal ka BP), which has been excluded due to low carbon mass, suggests a younger age more in agreement with the current age-depth model (Fig. 2.3). Higher runoff after 11.3 cal ka BP (i.e. after the YD period) might have led to an input of old terrestrial organic matter with low *n*-alkane content (less vegetation during the YD cold phase). Therefore, bulk sediment could be more strongly pre-aged than the *n*-alkane component.

In the literature, pre-aging effects have been described for bulk sediment (SIROCKO ET AL., 2013) and *n*-alkanes (DOUGLAS ET AL., 2014; GIERGA ET AL., 2016) because terrestrial material/biomarkers can be stored in soils for a long period before being transported into the sediment (RAYMOND & BAUER, 2001). In soils or sediments, *n*-alkanes can be preserved due to their chemical inertness, resistance against degradation and low water solubility (EGLINTON & EGLINTON, 2008). If the catchment area does not yield old carbon pools and the residence times for biomarkers are short, bulk *n*-alkane dating that was previously undertaken by (HAAS ET AL.,

2017; HÄGGI ET AL., 2014; ZECH ET AL., 2017) is hence corroborated as a valuable tool for dating lacustrine sediments in addition to compound-specific *n*-alkane ^{14}C dating (GIERGA ET AL., 2016).

The small Garba Guracha catchment with poorly developed soils favours rapid sedimentation and *n*-alkane deposition without considerable pre-aging effects. A contribution of aeolian transported plant-waxes cannot be completely discounted, despite the negligible old carbon input. Yet, for most parts of the core, our ^{14}C results suggest that (i) either the terrestrial *n*-alkanes have a very short residence time in the catchment and/or (ii) the *n*-alkanes are primarily of the same allochthonous/autochthonous origin as the bulk sedimentary organic matter.

2.4.2 Origin of organic matter

Distinguishing between allochthonous (terrestrial) versus autochthonous (aquatic) OM is a crucial issue in paleolimnological studies (BRENNER ET AL., 1999; MEYERS, 2003). For instance, TOC/N ratios < 10 (MEYERS, 2003) are frequently used as indicators for primarily autochthonous-derived OM. By contrast, terrestrial higher plants (due to a higher amount of carbon-rich lignin and cellulose) are typically characterised by higher TOC/N ratios (> 20) (MEYERS, 1994). It should be acknowledged, however, that degradation and mineralization of terrestrial OM result in lower TOC/N ratios, as well as in more positive $\delta^{13}C$ values (ZECH ET AL., 2007). In a study by MEKONNEN ET AL. (2019), it is shown that the leaves of *Erica* in the Bale Mountains have very high TOC/N ratios of about 55, whereas A_h horizons underneath *Erica* yielded TOC/N ratios of around 17. The TOC/N ratios of the Garba Guracha core reveal a wide range from 2.8 to 14.9 (Fig. 2.6). While a predominantly allochthonous OM input can be excluded, a partial terrestrial OM input cannot be ruled out for the Early to Mid-Holocene. At the same time, the planktonic microalgae *Botryococcus braunii* became more abundant during the Early and Mid-Holocene, with a clear maximum from 6.5 to 4.2 cal ka BP (UMER ET AL., 2007) (Fig. 2.6). *B. braunii* is known for unusually high TOC/N ratios compared to other algae (LENG & MARSHALL, 2004). This is confirmed by a *B. braunii* sample that we cultivated, which yielded a TOC/N ratio of 18 and a $\delta^{13}C$ value of -13.8 ‰. Higher TOC/N values due to a strong abundance of *B. braunii* may, therefore, be misinterpreted as an increase in allochthonous OM input.

According to BRENNER ET AL. (2006) and O'LEARY (1988), C3 vascular plants are characterised by $\delta^{13}C$ values ranging between -25 ‰ and -35 ‰. By contrast, C4 plants are characterised by less negative $\delta^{13}C$ values ranging between -16 ‰ to -10 ‰, and algae can produce $\delta^{13}C$ values up to -12 ‰. Given that there is no evidence hitherto for the occurrence of C4 plants in our catchment (MEKONNEN ET AL., 2019), the overall relatively positive $\delta^{13}C$ values of Garba Guracha (≥-22.7 ‰, Fig. 2.6) support a dominant autochthonous OM input. The use of $\delta^{15}N$ as a proxy for OM origin can be problematic due to various possible nitrogen sources, the discrimination during denitrification and diagenesis (BRENNER ET AL., 1999; HEPP ET AL., 2019b).

Apart from bulk sedimentary OM, source identification can be done on a molecular level, too. Concerning *n*-alkane biomarkers, FICKEN ET AL. (2000) introduced the P_{aq} index based

on the finding that submerged and floating aquatic plants from a lake on Mt. Kenya are characterised by values between 0.4 and 1, whereas terrestrial plants yielded values lower than 0.1. According to this proxy, aquatic-derived *n*-alkanes dominate the YD sediments, a mixture of aquatic- and terrestrial-derived *n*-alkanes dominate the Early and Mid-Holocene sediments, and terrestrial-derived *n*-alkanes dominate at least partly the Late Holocene sediments (Fig. 2.6). However, we recommend caution when using the P_{aq} proxy, because there is increasing evidence for potentially erroneous interpretations. While HEPP ET AL. (2018, and references therein) emphasised the high production of the 'aquatic' n-alkane nC_{23} by birch rendering the P_{aq} proxy invalid in European Late Glacial sedimentary archives, BAAS ET AL. (2000) and TARASOV ET AL. (2013) report on high nC_{23} and nC_{25} concentrations of *Sphagnum* species, a fern and a sedge species. Moreover, the P_{aq} interpretation for the Late Holocene part of Garba Guracha is clearly in contradiction with the TOC/N and $\delta^{13}C$ interpretation (Fig. 2.6). At the current state of research, an unambiguous terrestrial versus aquatic source identification of the *n*-alkane record of Garba Guracha hence seems challenging.

Concerning the sugar biomarkers, HEPP ET AL. (2016) found terrestrial plants and mosses to be characterised by fuc/(ara+xyl) ratios < 0.1, whereas algae are characterised by ratios > 0.1. The results for Garba Guracha (Fig. 2.6) thus suggest a predominantly aquatic (algae) origin of the sugars. This finding can also be nicely illustrated in a ternary diagram (Fig. 2.5) and highlights that the interpretation of predominantly aquatic-derived sugars is in good agreement with the 'aquatic' TOC/N and $\delta^{13}C$ interpretation.

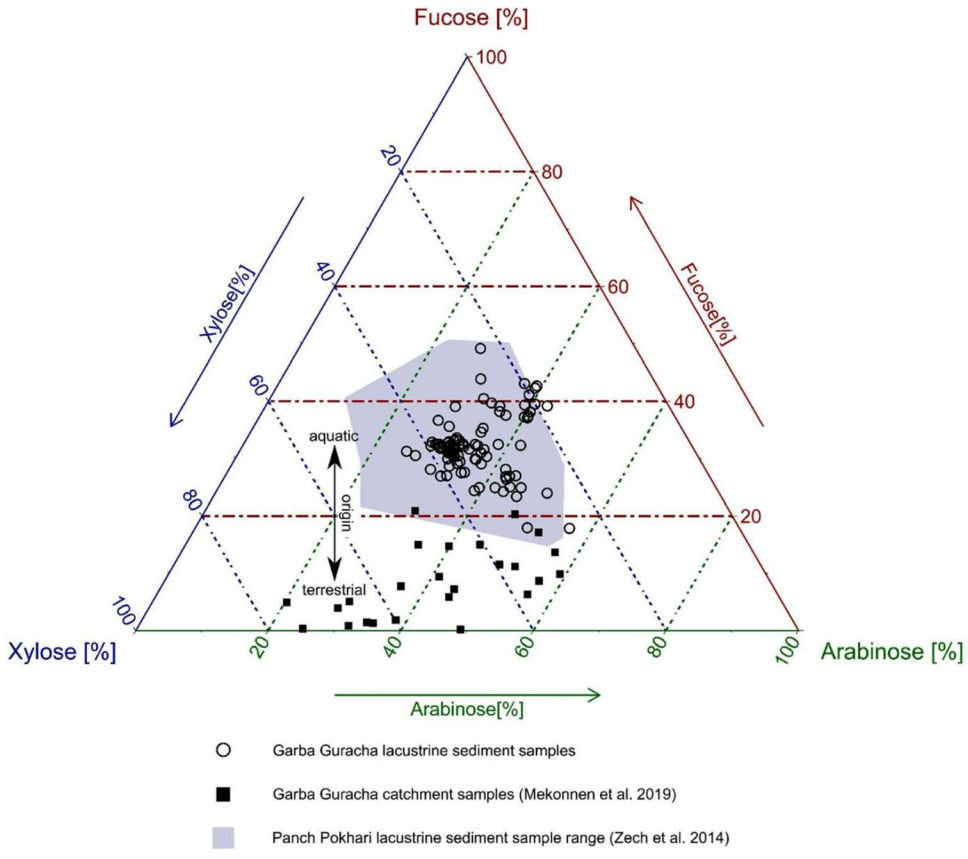

Figure 2.5: Ternary diagram illustrating the relative contributions of ara, fuc and xyl in the Garba Guracha sedimentary record. For comparison, plant, organic layer and topsoil samples from the Garba Guracha catchment are included (MEKONNEN ET AL., 2019).

2.4.3 Environmental implications

Phase 1: (1548 - 995 cm; 16 – 12.8 cal ka BP)

The highest values of the elements Rb, K, Ti, Fe, and Zr used to detect changes in minerogenic/lithogenic influx (KYLANDER ET AL., 2011) likely represent relatively high minerogenic input attributable to glacial retreat in the catchment. In contrast to TIERCELIN ET AL. (2008), we found no evidence for low sedimentation rates prevailing during the early Late Glacial; instead, we found high mean sedimentation rates of up to 1.86 mm a^{-1}. This implies a fast-filling glacial cirque, potentially fed by a melting glacier forced by rising temperatures. Sparse vegetation in the catchment (GIL-ROMERA ET AL., 2019; UMER ET AL., 2007) and low algal productivity in the meltwater-fed lake could have been a small OM source represented by low TOC values of up to 1 %. Low TOC/N values of 5 and relatively positive $\delta^{13}C$ values (-19 ‰ to 14 ‰) point to aquatic algae as the dominant OM source (BRENNER ET AL., 2006; MEYERS, 2003).

At ~ 14 cal ka BP an increasing mean sedimentation rate of up to 2.2 mm a^{-1} was dominated by detrital input as represented by high but decreased K, Rb, Ti, and Zr values which suggest continued, rapid in-filling of the lake fed by glacier retreat. Here our data and interpretation agree with TIERCELIN ET AL. (2008) in that the strong rise in sedimentation rate is due to stronger glacial recession probably caused by increasing temperatures and/or higher precipitation.

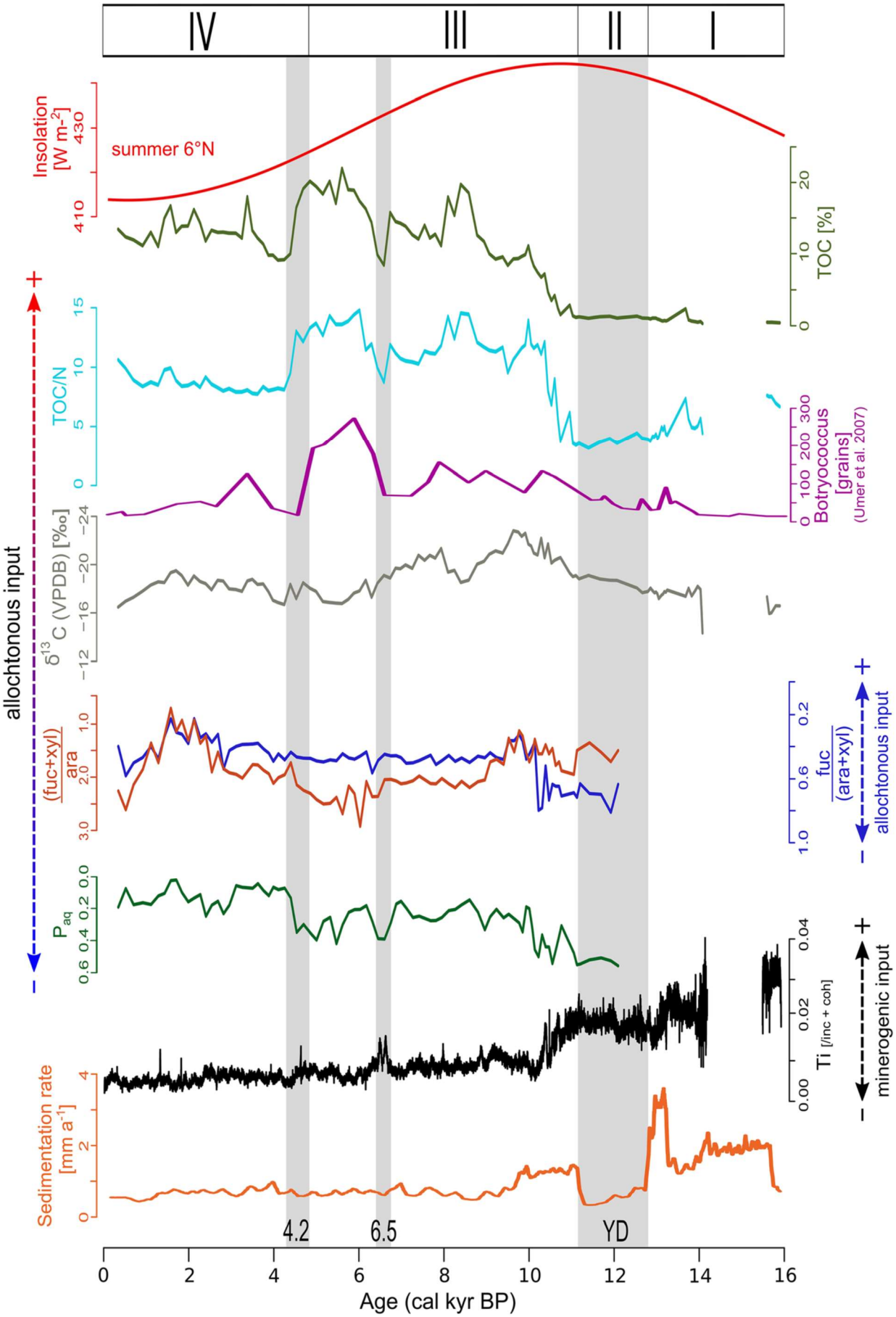

Figure 2.6: Summer insolation (LASKAR ET AL., 2004), TOC, TOC/N, Botryococcus braunii (UMER ET AL., 2007), $\delta^{13}C$, (fuc + xyl)/ara, fuc/(ara + xyl), P_{aq}, titan element and calculated sedimentation rate.

Phase 2: (995 - 900 cm, 12.8 – 11.2 cal ka BP)

During this interval, sedimentation rates decreased dramatically by nearly 75 % to 0.60 mm a^{-1}, indicating either a drier or colder climate. Cold conditions may have favoured a longer season of ice-cover on the lake, whereas dry conditions would be associated with less runoff into the lake. In either scenario, we would expect to see not only a change in sedimentation but also a lower OM input into the lake. This is supported by low TOC values and decreased dominance of *Erica* heathlands, which, as revealed in the Garba Guracha pollen data, dominated the local vegetation during this phase (GIL-ROMERA ET AL., 2019; UMER ET AL., 2007). Additionally, aquatic production would likely have been reduced due to lower insolation during ice cover and lower input of nutrients.

This dry or/and cold period coincides with the YD in the Greenland ice cores (ALLEY, 2000). The more precise timing of this phase of low sedimentation rate due to our robust and higher resolution chronology allows us to re-address previous discussions of the YD at Garba Guracha (TIERCELIN ET AL., 2008). Younger Dryas-like conditions have been described in Eastern Africa before (ROBERTS ET AL., 1993; TALBOT ET AL., 2007). MARSHALL ET AL. (2011) suggest likewise a phase of low sedimentation rate for Lake Tana during the YD due to reduced precipitation and runoff. During the YD, a weakening of the North Atlantic Deep Water formation, linked to increased freshwater input, is thought to have caused a sea surface temperature anomaly with reduced precipitation in the tropics and associated lake low stands (STREET-PERROTT & PERROTT, 1990). Climate modelling results (BROCCOLI ET AL., 2006; CHIANG & BITZ, 2005) support the idea of NICHOLSON (1982) that an interhemispheric thermal gradient forces the ITCZ south of the equator. A more recent modelling approach suggests a period of dry north winds during cold phases like Heinrich event 1 or YD (MOHTADI ET AL., 2014). Dry conditions coinciding with the YD have been reconstructed in several Eastern African lakes, including Lake Victoria (STAGER ET AL., 2002; TALBOT & LÆRDAL, 2000), Lake Suguta (JUNGINGER ET AL., 2014), the Ziway–Shala basin (GILLESPIE ET AL., 1983), and Lake Albert (BEUNING ET AL., 1997).

Phase 3: (900 - 340 cm, 11.2 – 4.5 cal ka BP)

From the beginning of this phase until 10.8 cal ka BP, the mean sedimentation rate more than doubled to 1.37 mm a^{-1}. The reason for this may have been increasing temperatures due to higher insolation (Fig. 2.6) and increasing precipitation resulting in a stronger runoff. Both are supported by increasing TOC values and a higher hydrogen index (TIERCELIN ET AL., 2008), pointing to more favourable conditions for aquatic and terrestrial OM production. Additionally, a change in OM production is recorded by an increasing TOC/N ratio from less than 5 to around 12. However, the input of eroded old organic matter (formed during phase 2) cannot be ruled out.

After 10.8 cal ka BP the sedimentation rate decreased slightly to 1.25 mm a^{-1} until 9.8 cal ka BP and in a second step more strongly to 0.72 mm a^{-1}. Additionally, lower Ti, Fe, Ca, K, and Rb counts and a TOC increase of up to 18 % indicate less minerogenic input and higher organic matter production. This change may be indicative of the progression of the catchment from a glacier-dominated catchment without vegetation to a cirque lake catchment with soil development and vegetation cover.

A drop in TOC and TOC/N ratios coincides with the 8.2 ka event in the northern hemisphere, known as a short cold spell (BOND ET AL., 1997; DANSGAARD ET AL., 1993). For this most pronounced climate shift in the Holocene, a period of drought has been reconstructed for the Ziway-Shala system (GILLESPIE ET AL., 1983), Lake Malawi (GASSE ET AL., 2002), and Lake Tilo (LENG ET AL., 1999). THOMPSON ET AL. (2002) found a maximum in wind-blown fluoride derived from dry lake basins in the Kilimanjaro ice record at ~ 8.4 cal ka BP.

A pronounced TOC minimum with a drop to 10 % coinciding with a tephra layer at 7.9 cal ka BP is followed by a phase of decreased TOC with a minimum of 8 % at 6.5 cal ka BP. At 6.5 cal ka BP a small maximum of higher minerogenic input marked by higher Rb, Ti, Ca and K counts concur with two organic-poor layers in the core. Additionally, P_{aq}, fuc/(ara + xyl) and (fuc + xyl)/ara indicate a lower terrestrial OM input, which is supported by the reduced vegetation cover at that time in the lake's catchment (GIL-ROMERA ET AL., 2019). These findings represent a drought period, which is in agreement with an arid period found in a speleothem record in southern Oman (FLEITMANN ET AL., 2007).

Between 6 cal ka BP and 4.5 cal ka BP, the highest OM production (TOC ~ 20 %) of the core occurs. It coincides with the highest abundance of *B. braunii* (UMER ET AL., 2007), which could explain the highest TOC/N values of the entire core rather than an increased allochthonous OM input. A higher allochthonous OM input is contradicted by positive delta ^{13}C values in this phase which accompany a *B. braunii* increase. Blooms of *B. braunii* are associated with phosphorus availability due to high inwash (HUANG & HONG, 1999). This could point to a phase of increased nutrient availability and stronger aquatic productivity.

Phase 4 (340 - 70 cm, 4.5 – 0.3 cal ka BP)

Contemporaneous with a strong decrease of *B. braunii* (UMER ET AL., 2007), TOC and the TOC/N ratio drop massively to 7 % and 8, respectively. Less favourable conditions for OM in the Garba Guracha record coincide with a known drought phase due to a weak monsoon in the Indian ocean records (FLEITMANN & MATTER, 2009; NAKAMURA ET AL., 2016) and aridity in North Africa (GASSE, 2000; MARCHANT & HOOGHIEMSTRA, 2004).

The 4.5 ka drought event is followed by a period of increased precipitation as evidenced by a slightly increased mean sedimentation rate to 0.85 mm a^{-1} for around 1000 years before it decreases to 0.66 mm a^{-1}. TOC is around 15 % with some variations and TOC/N decreases to 7-9. At 1.5 cal ka BP minima in the P_{aq}, $\delta^{13}C$ and sugar ratios point to an increased terrestrial OM production followed by an increase in aquatic production until the Little Ice Age at ~ 0.6 cal ka BP represented in the sugar biomarker ratios.

The high-altitude Garba Guracha archive reflects local and supraregional climate changes beginning with deglaciation at around 15.9 cal ka BP pointing to a temperature increase as a consequence of rising insolation (LASKAR ET AL., 2011). This temperature increase may have been even stronger than low-land ecosystems (LOOMIS ET AL., 2017). Increasing temperatures and precipitation at the beginning of phase 3 led not only to favourable conditions for OM production after the YD (phase 2) but also to prolonged humid conditions (phase 3) due to an enhancement of East and West African monsoon intensity in contrast to the reduced monsoonal activity during the YD (UMER ET AL., 2007) and a change in atmospheric

circulation (COSTA ET AL., 2014; JUNGINGER ET AL., 2014; TIERNEY ET AL., 2011b). This coincides with the AHP (DEMENOCAL ET AL., 2000) and rising lake levels in Eastern Africa (GASSE, 2000; JUNGINGER ET AL., 2014; LEZINE ET AL., 2014). A shift to arid conditions at 4.5 cal ka BP may mark a late termination of the AHP in the Garba Guracha record and may indicate a late response of a high-altitude aquatic system. However, *Erica* pollen already decreased at 5.2 cal ka BP (GIL-ROMERA ET AL., 2019). A return to wetter conditions between 2.5 and 1.5 cal ka BP concurs with rising lake levels in the Horn of Africa region (LEZINE ET AL., 2014).

2.4.4 Comparison with lake level and other records

Garba Guracha appears to have reacted sensitively to local and supraregional climate changes. Despite favourable conditions for OM production are indicated by TOC and TOC/N, we should be careful when interpreting TOC and TOC/N as climate proxies because local factors may overprint supraregional climate change effects on these proxies. For example, a TOC decrease at 7.9 cal ka BP coincides with a volcanic eruption (GGT-1 tephra), and TOC increases may be explained for instance by high algal production (UMER ET AL., 2007).

However, the inferred timing of favourable conditions in the Early to Mid-Holocene for OM production (TOC and TOC/N) shows similarities with a TOC record from Lake Turkana (MORRISSEY & SCHOLZ, 2014) and coincides with lake level fluctuations of Lake Turkana (BECK ET AL., 2019; BLOSZIES ET AL., 2015; GARCIN ET AL., 2012), Lake Suguta (JUNGINGER ET AL., 2014), Chew Bahir (FOERSTER ET AL., 2012), Lake Abhé (GASSE, 2000), Lake Dendi (WAGNER ET AL., 2018), and Lake Ziway-Shala (GILLESPIE ET AL., 1983). The offset shown in our record at the Holocene onset may be altitude-related as during deglaciation, high-altitude climate records might be buffered due to slow melting of the remaining ice in the catchment, especially given the northward aspect of Garba Guracha (TIERCELIN ET AL., 2008). Several minima in our TOC and TOC/N record coincide with drought phases in other Eastern African and Oman records at 10.7 cal ka BP (JUNGINGER ET AL., 2014; WAGNER ET AL., 2018), 8.2 cal ka BP (COSTA ET AL., 2014; GARCIN ET AL., 2012; GASSE, 2000; JUNGINGER ET AL., 2014) and 6.5 cal ka BP (FLEITMANN ET AL., 2007). The decrease of TOC and TOC/N values at 4.5 cal ka BP concurs better with the North-Ethiopian lake records (Lake Ziway-Shala (GILLESPIE ET AL., 1983) and Lake Abhé (GASSE, 2000)) than with the South-Ethiopian lake records (JUNGINGER ET AL., 2014).

Moreover, it has been shown that the timing of the AHP termination depends not only on the archive but on the investigated proxy (CASTAÑEDA ET AL., 2016). This holds true for the Garba Guracha archive with the decline of *Erica* pollen already beginning at 5.2 cal ka BP (GIL-ROMERA ET AL., 2019), 700 years earlier than the TOC and TOC/N records. An AHP termination at 5.2 cal ka BP would concur with South-Ethiopian lake records (JUNGINGER ET AL., 2014).

The different response of lake records in Eastern Africa during the Holocene might be explained, despite local factors, by two possible mechanisms: (1) an increase of atmospheric moisture depending on the ITCZ shift and thus on insolation and (2) an eastward shift of the Congo Air Boundary due to an enhanced pressure gradient between India and Eastern Africa (CASTAÑEDA ET AL., 2016; COSTA ET AL., 2014; JUNGINGER ET AL., 2014; TIERNEY ET AL., 2011b). Due to the blurring of local factors on TOC and TOC/N and the different timing of proxies in

connection with the AHP termination, further research, and other proxies, especially water isotopes, may be needed to help disentangle the conflicting evidence.

2.5 Conclusions

Garba Guracha provides one of the best dated Late Glacial – Holocene continuous high-altitude records in Eastern Africa. It offers a relatively small, undisturbed catchment where global and local climate influences can be studied. New sedimentary data and a more detailed and robust chronology give new insights into the sedimentary history and the catchment dynamics of Garba Guracha.

The chronology of the Garba Guracha record spans the last ca. 16 cal ka BP. Bulk sediment and bulk *n*-alkane dates are in good agreement with charcoal and tephra ages. *n*-Alkane ages show no age offset to ^{14}C bulk sediment dating. We propose that a pre-aging effect for terrestrial *n*-alkanes or terrestrial material, in general, is negligible for most of the record due to short residence times for terrestrial material in the small catchment area and due to the high lake productivity. We conclude that our chronology is robust and that dating of bulk *n*-alkanes is a valuable tool for lake sediment dating in small catchment areas. The Garba Guracha sedimentary archive records the environmental change from deglaciation to a precipitation-fed lake. The record shows well-known climate changes such as the YD and the arid $\sim$ 6.5 and $\sim$ 4.2 ka events. The occurrence of these events clearly shows regional and northern hemispheric influence on the high-altitude Eastern African ecosystems. Since the Holocene onset, organic-rich sediments point to climatic conditions favourable for aquatic biomass production due to higher temperatures and increased precipitation.

The high-resolution environmental and chronological data presented in this study, alongside the uniqueness of the GG site, allow us to pick out the complexity of past climates in the Ethiopian Rift and highlands. Our data suggest similarities between GG and other sites in the region, but clearly there are temporal and spatial variations in how the past climate changes are manifested. Future proxy publications and further study using a wider network of sites, may enable us to understand leads and lags in the past climates of Eastern Africa in greater depth.

2.6 Acknowledgements

This research was funded by the German Research Council (DFG) in the framework of the joint Ethio-European DFG Research Unit 2358 “The Mountain Exile Hypothesis. How humans benefited from and re-shaped African high-altitude ecosystems during Quaternary climate changes”. We thank the Ethiopian Wildlife Conservation Authority for permitting our research in the Bale Mountains National Park. We are grateful to the project coordination, the Philipps University Marburg, University of Addis Abeba, the Frankfurt Zoological Society, the Ethiopian Wolf Project, the Bale Mountains National Park, and the related staff members, especially Katinka Thielsen, Mekbib Fekadu, Bahru Zinaye Asegahegn, Elias Tadesse, Ermias Getachew,

and Terefe Endale, for their logistic assistance during our fieldwork. CMJ was supported by the Geography Laboratories, Cambridge, and thanks Iris Buisman (Cambridge) and Emma Tomlinson (Trinity College, Dublin) for guidance with tephra analysis. We thank the team of the Soil Biogeochemistry Department at Martin Luther University Halle Saale for the support during lab work, in particular, Marianne Benesch and Heike Maennike.

2.7 References

ALLEY, R. B. (2000): The Younger Dryas cold interval as viewed from central Greenland. - Quaternary Science Reviews, **19**, 213–226.

ALLISON, L. E. . (1960): Wet combustion apparatus and procedure for organic and inorganic carbon in soils. - Soil Science of America, **24**, 36–40.

AMELUNG, W., CHESHIRE, M. V, & GUGGENBERGER, G. (1996): Determination of neutral and acidic sugars in soil by capillary gas-liquid chromatography after trifluoroacetic acid hydrolysis. - Soil Biology and Biochemistry, **28**, 1631–1639.

ANDREWS, M. A. (1989): Capillary gas-chromatographic analysis of monosaccharides: Improvements and comparisons using trifluoroacetylation and trimethylsilylation of sugar O-benzyl- and O-methyl-oximes. - Carbohydrate Research, **194**, 1–19.

APPLEBY, P. G. (2001): Chronostratigraphic Techniques in Recent Sediments BT - Tracking Environmental Change Using Lake Sediments: Basin Analysis, Coring, and Chronological Techniques. - In W. M. Last & J. P. Smol (Eds.), (pp. 171–203). - Dordrecht: Springer Netherlands.

APPLEBY, P. G., NOLAN, P. J., GIFFORD, D. W., GODFREY, M. J., OLDFIELD, F., ANDERSON, N. J., & BATTARBEE, R. W. (1986): ^{210}Pb dating by low background gamma counting. - Hydrobiologia, **143**, 21–27.

APPLEBY, P. G., RICHARDSON, N., & NOLAN, P. J. (1992): Self-absorption corrections for well-type germanium detectors. - Nuclear Instruments and Methods in Physics Research Section B: Beam Interactions with Materials and Atoms, **71**, 228–233.

BAAS, M., PANCOST, R., VAN GEEL, B., & SINNINGHE DAMSTÉ, J. S. (2000): A comparative study of lipids in Sphagnum species. - Organic Geochemistry, **31**, 535–541.

BECK, C. C., FEIBEL, C. S., WRIGHT, J. D., & MORTLOCK, R. A. (2019): Onset of the African Humid Period by 13.9 kyr BP at Kabua Gorge, Turkana Basin, Kenya. - Holocene, **29**, 1011–1019.

BEUNING, K. R. M., TALBOT, M. R., & KELTS, K. (1997): A revised 30,000-year paleoclimatic and paleohydrologic history of Lake Albert, East Africa. - Palaeogeography, Palaeoclimatology, Palaeoecology, **136**, 259–279.

BLAAUW, M. (2010): Methods and code for 'classical' age-modelling of radiocarbon sequences. - Quaternary Geochronology, **5**, 512–518.

BLAAUW, M., BAKKER, R., CHRISTEN, J. A., HALL, V. A., & VAN DER PLICHT, J. (2007): A Bayesian Framework for Age Modeling of Radiocarbon-Dated Peat Deposits: Case Studies from the Netherlands. - Radiocarbon, **49**, 357–367.

BLAAUW, M., CHRISTENY, J. A., & CHRISTEN, J. A. (2011): Flexible paleoclimate age-depth models using an autoregressive gamma process. - Bayesian Analysis, **6**, 457–474.

BLOSZIES, C., FORMAN, S. L., & WRIGHT, D. K. (2015): Water level history for Lake Turkana, Kenya in the past 15,000 years and a variable transition from the African Humid Period to Holocene aridity. - Global and Planetary Change, **132**, 64–76.

BOND, G., SHOWERS, W., CHESEBY, M., LOTTI, R., ALMASI, P., DEMENOCAL, P., PRIORE, P., CULLEN, H., HAJDAS, I., & BONANI, G. (1997): A Pervasive Millennial-Scale Cycle in North Atlantic Holocene and Glacial Climates. - Science, **278**, 1257 LP – 1266.

BRANDT, S. A., FISHER, E. C., HILDEBRAND, E. A., VOGELSANG, R., AMBROSE, S. H., LESUR, J., & WANG, H. (2012): Early MIS 3 occupation of Mochena Borago Rockshelter, Southwest Ethiopian Highlands: Implications for Late Pleistocene archaeology, paleoenvironments and modern human dispersals. - Quaternary International, **274**, 38–54.

BRENNER, M., WHITMORE, T. J., CURTIS, J. H., HODELL, D. A., & SCHELSKE, C. L. (1999): Stable isotope ($\delta^{13}C$ and $\delta^{15}N$) signatures of sedimented organic matter as indicators of historic lake trophic state. - Journal of Paleolimnology, **22**, 205–221.

BRENNER, M., HODELL, D. A., LEYDEN, B. W., CURTIS, J. H., KENNEY, W. F., GU, B., & NEWMAN, J. M. (2006): Mechanisms for organic matter and phosphorus burial in sediments of a shallow, subtropical, macrophyte-dominated lake. - Journal of Paleolimnology, **35**, 129–148.

BROCCOLI, A. J., DAHL, K. A., & STOUFFER, R. J. (2006): Response of the ITCZ to Northern Hemisphere cooling. - Geophysical Research Letters, **33**.

CASTAÑEDA, I. S., SCHOUTEN, S., PÄTZOLD, J., LUCASSEN, F., KASEMANN, S., KUHLMANN, H., & SCHEFUß, E. (2016): Hydroclimate variability in the Nile River Basin during the past 28,000 years. - Earth and Planetary Science Letters, **438**, 47–56.

CHIANG, J. C. H., & BITZ, C. M. (2005): Influence of high latitude ice cover on the marine Intertropical Convergence Zone. - Climate Dynamics, **25**, 477–496.

COPLEN, T. B. (2011): Guidelines and recommended terms for expression of stable-isotope-ratio and gas-ratio measurement results. - Rapid Communications in Mass Spectrometry, **25**, 2538–2560.

COSTA, K., RUSSELL, J., KONECKY, B., & LAMB, H. (2014): Isotopic reconstruction of the African Humid Period and Congo Air Boundary migration at Lake Tana, Ethiopia. - Quaternary Science Reviews, **83**, 58–67.

CROUDACE, I., RINDBY, A., & GUY ROTHWELL, R. (2006): ITRAX: Description and Evaluation of a New Multi-Function X-ray Core Scanner. - Geological Society, London, Special

Publications, **267**, 51–63.

DANSGAARD, W., JOHNSEN, S. J., CLAUSEN, H. B., DAHL-JENSEN, D., GUNDESTRUP, N. S., HAMMER, C. U., HVIDBERG, C. S., STEFFENSEN, J. P., SVEINBJÖRNSDOTTIR, A. E., JOUZEL, J., & BOND, G. (1993): Evidence for general instability of past climate from a 250-kyr ice-core record. - Nature, **364**, 218–220. Retrieved from https://doi.org/10.1038/364218a0

DEMENOCAL, P., ORTIZ, J., GUILDERSON, T., ADKINS, J., SARNTHEIN, M., BAKER, L., & YARUSINSKY, M. (2000): Abrupt onset and termination of the African Humid Period: - Quaternary Science Reviews, **19**, 347–361.

DOUGLAS, P. M. J. J., PAGANI, M., EGLINTON, T. I., BRENNER, M., HODELL, D. A., CURTIS, J. H., MA, K. F., & BRECKENRIDGE, A. (2014): Pre-aged plant waxes in tropical lake sediments and their influence on the chronology of molecular paleoclimate proxy records. - Geochimica et Cosmochimica Acta, **141**, 346–364.

EGLINTON, T. I., & EGLINTON, G. (2008): Molecular proxies for paleoclimatology. - Earth and Planetary Science Letters, **275**, 1–16.

FICKEN, K. J., LI, B., SWAIN, D. L., & EGLINTON, G. (2000): An n-alkane proxy for the sedimentary input of submerged/floating freshwater aquatic macrophytes. - Organic Geochemistry, **31**, 745–749.

FLEITMANN, D., BURNS, S. J., MANGINI, A., MUDELSEE, M., KRAMERS, J., VILLA, I., NEFF, U., AL-SUBBARY, A. A., BUETTNER, A., HIPPLER, D., & MATTER, A. (2007): Holocene ITCZ and Indian monsoon dynamics recorded in stalagmites from Oman and Yemen (Socotra). - Quaternary Science Reviews, **26**, 170–188.

FLEITMANN, D., & MATTER, A. (2009): The speleothem record of climate variability in Southern Arabia. - Comptes Rendus - Geoscience, **341**, 633–642.

FOERSTER, V., JUNGINGER, A., LANGKAMP, O., GEBRU, T., ASRAT, A., UMER, M., LAMB, H. F., WENNRICH, V., RETHEMEYER, J., NOWACZYK, N., TRAUTH, M. H., & SCHAEBITZ, F. (2012): Climatic change recorded in the sediments of the Chew Bahir basin, southern Ethiopia, during the last 45,000 years. - Quaternary International, **274**, 25–37.

FONTIJN, K., MCNAMARA, K., ZAFU TADESSE, A., PYLE, D. M., DESSALEGN, F., HUTCHISON, W., MATHER, T. A., & YIRGU, G. (2018): Contrasting styles of post-caldera volcanism along the Main Ethiopian Rift: Implications for contemporary volcanic hazards. - Journal of Volcanology and Geothermal Research, **356**, 90–113.

GARCIN, Y., MELNICK, D., STRECKER, M. R. M. R., OLAGO, D., & TIERCELIN, J.-J. J.-J. (2012): East African mid-Holocene wet–dry transition recorded in palaeo-shorelines of Lake Turkana, northern Kenya Rift. - Earth and Planetary Science Letters, **331**–**332**, 322–334.

GASSE, F. (2000): Hydrological changes in the African tropics since the Last Glacial Maximum. - Quaternary Science Reviews, **19**, 189–211.

GASSE, F., BARKER, P., & JOHNSON, T. C. (2002): A 24,000 yr Diatom Record from the Northern Basin of Lake Malawi BT - The East African Great Lakes: Limnology, Palaeolimnology and Biodiversity. - In E. O. Odada & D. O. Olago (Eds.), (pp. 393–414). - Dordrecht: Springer Netherlands.

GIERGA, M., HAJDAS, I., VAN RADEN, U. J., GILLI, A., WACKER, L., STURM, M., BERNASCONI, S. M., & SMITTENBERG, R. H. (2016): Long-stored soil carbon released by prehistoric land use: Evidence from compound-specific radiocarbon analysis on Soppensee lake sediments. - Quaternary Science Reviews, **144**, 123–131.

GIL-ROMERA, G., ADOLF, C., BENITO BLAS, M., BITTNER, L., JOHANSSON, M., GRADY, D., LAMB, H., LEMMA, B., FEKADU, M., GLASER, B., MEKONNEN, B., SEVILLA-CALLEJO, M., ZECH, M., ZECH, W., & MIEHE, G. (2019): Long-term fire resilience of the Ericaceous Belt, Bale Mountains, Ethiopia. - Biology Letters, **15**, 20190357.

GILLESPIE, R., STREET-PERROTT, F. A., & SWITSUR, R. (1983): Post-glacial arid episodes in Ethiopia have implications for climate prediction. - Nature, **306**, 680–683.

HAAS, M., BLIEDTNER, M., BORODYNKIN, I., SALAZAR, G., SZIDAT, S., EGLINTON, T. I., & ZECH, R. (2017): Radiocarbon dating of leaf waxes in the Loess-Paleosol sequence Kurtak, central Siberia. - Radiocarbon, **59**, 165–176.

HÄGGI, C., ZECH, R., MCINTYRE, C., ZECH, M., & EGLINTON, T. I. (2014): On the stratigraphic integrity of leaf-wax biomarkers in loess paleosols. - Biogeosciences, **11**, 2455–2463.

HEPP, J., RABUS, M., ANHÄUSER, T., BROMM, T., LAFORSCH, C., SIROCKO, F., GLASER, B., & ZECH, M. (2016): A sugar biomarker proxy for assessing terrestrial versus aquatic sedimentary input. - Organic Geochemistry, **98**, 98–104.

HEPP, J., WÜTHRICH, L., BROMM, T., BLIEDTNER, M., SCHÄFER, I. K., GLASER, B., ROZANSKI, K., SIROCKO, F., ZECH, R., & ZECH, M. (2019): How dry was the Younger Dryas? Evidence from a coupled δ^2H–$\delta^{18}O$ biomarker paleohygrometer applied to the Gemündener Maar sediments, Western Eifel, Germany. - Clim. Past, **15**, 713–733.

HILLMAN, J. (1986): Conservation in Bale Mountains National Park, EthiopiaOryx (Vol. 20).

HILLMAN, J. (1988): The Bale Mountains National Park Area, Southeast Ethiopia, and Its ManagementMountain Research and Development (Vol. 8).

HUANG, B., & HONG, H. (1999): Alkaline Phosphatase Activity and Utilization of Dissolved Organic Phosphorus by Algae in Subtropical Coastal Waters. - Marine Pollution Bulletin, **39**, 205–211.

JOCHUM, K. P., STOLL, B., HERWIG, K., WILLBOLD, M., HOFMANN, A. W., AMINI, M., AARBURG, S., ABOUCHAMI, W., HELLEBRAND, E., … WOODHEAD, J. D. (2006): MPI-DING reference glasses for in situ microanalysis: New reference values for element concentrations and isotope ratios. - Geochemistry, Geophysics, Geosystems, **7**.

JUNGINGER, A., ROLLER, S., OLAKA, L. A., & TRAUTH, M. H. (2014): The effects of solar irradiation changes on the migration of the Congo Air Boundary and water levels of paleo-Lake Suguta , Northern Kenya Rift , during the African Humid Period (15 – 5 ka BP). - Palaeogeography, Palaeoclimatology, Palaeoecology, **396**, 1–16.

KIDANE, Y., STAHLMANN, R., & BEIERKUHNLEIN, C. (2012): Vegetation dynamics, and land use and land cover change in the Bale Mountains, Ethiopia. - Environmental Monitoring and Assessment, **184**, 7473–7489.

KUZMICHEVA, E., JEBESSA DEBELLA, H., KHASANOV, B., KRYLOVICH, O., GIRMAY, W., VASYUKOV, D., YIRGA, S., & SAVINETSKY, A. (2017): Ecosystem histroy of the Bale Mountains. - Ethiop. J. Biol. Sci, **16**, 61–94.

KYLANDER, M. E., AMPEL, L., WOHLFARTH, B., & VERES, D. (2011): High-resolution X-ray fluorescence core scanning analysis of Les Echets (France) sedimentary sequence: new insights from chemical proxies. - Journal of Quaternary Science, **26**, 109–117.

LAMB, H. F., BATES, C. R., BRYANT, C. L., DAVIES, S. J., HUWS, D. G., MARSHALL, M. H., ROBERTS, H. M., & TOLAND, H. (2018): 150,000-year palaeoclimate record from northern Ethiopia supports early, multiple dispersals of modern humans from Africa. - Scientific Reports, **8**, 1077.

LASKAR, J., ROBUTEL, P., JOUTEL, F., GASTINEAU, M., CORREIA, A. C. M., & LEVRARD, B. (2004): A long-term numerical solution for the insolation quantities of the Earth . - A&A, **428**, 261–285. Retrieved from https://doi.org/10.1051/0004-6361:20041335

LASKAR, J., FIENGA, A., GASTINEAU, M., & MANCHE, H. (2011): La2010: a new orbital solution for the long-term motion of the Earth⋆. - A&A, **532**. Retrieved from https://doi.org/10.1051/0004-6361/201116836

LENG, M. J., LAMB, A. L., LAMB, H. F., & TELFORD, R. J. (1999): Palaeoclimatic implications of isotopic data from modern and early Holocene shells of the freshwater snail Melanoides tuberculata, from lakes in the Ethiopian Rift Valley. - Journal of Paleolimnology, **21**, 97–106.

LENG, M. J., & MARSHALL, J. D. (2004): Palaeoclimate interpretation of stable isotope data from lake sediment archives. - Quaternary Science Reviews, **23**, 811–831.

LEZINE, A.-M., BASSINOT, F., PETERSCHMITT, J. Y. J.-Y., LÉZINE, A. M., BASSINOT, F., & PETERSCHMITT, J. Y. J.-Y. (2014): Orbitally-induced changes of the Atlantic and Indian monsoons over the past 20,000 years: New insights based on the comparison of continental and marine records. - Bulletin de La Societe Geologique de France, **185**, 3–12.

LÖFFLER, H. (1978): Limnology and paleolimnological data on the Bale Mountain Lakes. - Verth, International Verein. Limnology, **20**, 1131–1138.

LOOMIS, S. E., RUSSELL, J. M., VERSCHUREN, D., MORRILL, C., DE CORT, G., SINNINGHE DAMSTÉ, J. S., OLAGO, D., EGGERMONT, H., STREET-PERROTT, F. A., & KELLY, M. A. (2017): The tropical lapse rate steepened during tLoomis SE, Russell JM, Verschuren D, Morrill C, De Cort G, Sinninghe

Damsté JS, Olago D, EggermLoomis SE, Russell JM, Verschuren D, Morrill C, De Cort G, Sinninghe Damsté JS, Olago D, Eggermont H, Street-Perrott F. - Science Advances, **3**, e1600815.

LÖWEMARK, L., CHEN, H.-F., YANG, T.-N., KYLANDER, M., YU, E.-F., HSU, Y.-W., LEE, T.-Q., SONG, S.-R., & JARVIS, S. (2011): Normalizing XRF-scanner data: A cautionary note on the interpretation of high-resolution records from organic-rich lakes. - Journal of Asian Earth Sciences, **40**, 1250–1256.

MARCHANT, R., & HOOGHIEMSTRA, H. (2004): Rapid environmental change in African and South American tropics around 4000 years before present: a review. - Earth-Science Reviews, **66**, 217–260.

MARSHALL, M. H. M. H., LAMB, H. F. H. F., HUWS, D., DAVIES, S. J. S. J., BATES, R., BLOEMENDAL, J., BOYLE, J., LENG, M. J. M. J., UMER, M., & BRYANT, C. (2011): Late Pleistocene and Holocene drought events at Lake Tana, the source of the Blue Nile. - Global and Planetary Change, **78**, 147–161.

MARTIN-JONES, C. M., LANE, C. S., PEARCE, N. J. G., SMITH, V. C., LAMB, H. F., SCHAEBITZ, F., VIEHBERG, F., BROWN, M. C., FRANK, U., & ASRAT, A. (2017): Recurrent explosive eruptions from a high-risk Main Ethiopian Rift volcano throughout the Holocene. - Geology, **45**, 1127–1130. Retrieved from http://dx.doi.org/10.1130/G39594.1

MEKONNEN, B., ZECH, W., GLASER, B., LEMMA, B., BROMM, T., NEMOMISSA, S., BEKELE, T., & ZECH, M. (2019): Chemotaxonomic patterns of vegetation and soils along altitudinal transects of the Bale Mountains, Ethiopia, and implications for paleovegetation reconstructions – Part 1: stable isotopes and sugar biomarkers. - E&G Quaternary Sci. J., **68**, 177–188.

MEYERS, P. A. (1994): Preservation of elemental and isotopic source identification of sedimentary organic matter. - Chemical Geology, **114**, 289–302.

MEYERS, P. A. (2003): Applications of organic geochemistry to paleolimnological reconstructions: a summary of examples from the Laurentian Great Lakes. - Organic Geochemistry, **34**, 261–289.

MIEHE, S., & MIEHE, G. (1994): Ericaceous forests and heathlands in the Bale mountains of South Ethiopia : ecology and man's impact (G. Miehe & 1952-, Eds.). - Reinbek: Reinbek : Warnke.

MOHTADI, M., PRANGE, M., OPPO, D. W., DE POL-HOLZ, R., MERKEL, U., ZHANG, X., STEINKE, S., & LÜCKGE, A. (2014): North Atlantic forcing of tropical Indian Ocean climate. - Nature, **509**, 76–80.

MORRISSEY, A., & SCHOLZ, C. A. (2014): Paleohydrology of Lake Turkana and its influence on the Nile River system. - Palaeogeography, Palaeoclimatology, Palaeoecology, **403**, 88–100.

NAKAMURA, A., YOKOYAMA, Y., MAEMOKU, H., YAGI, H., OKAMURA, M., MATSUOKA, H., MIYAKE, N., OSADA, T., ADHIKARI, D. P., DANGOL, V., IKEHARA, M., MIYAIRI, Y., & MATSUZAKI, H. (2016): Weak monsoon event at 4.2 ka recorded in sediment from Lake Rara, Himalayas. - Quaternary

International, **397**, 349–359.

NICHOLSON, S. E. (1982): Pleistocene and Holocene climates in Africa. - Nature, **296**, 779.

O'LEARY, M. H. (1988): Carbon Isotopes in Photosynthesis. - BioScience, **38**, 328–336.

OSMASTON, H. A., MITCHELL, W. A., & OSMASTON, J. A. N. (2005): Quaternary glaciation of the Bale Mountains, Ethiopia. - Journal of Quaternary Science, **20**, 593–606.

OSSENDORF, G., GROOS, A., BROMM, T., GIRMA TEKELEMARIAM, M., GLASER, B., LESUR, J., SCHMIDT, J., AKÇAR, N., BEKELE, T., BELDADOS, A., DEMISSEW, S., HADUSH KAHSAY, T., P NASH, B., NAUSS, T., NEGASH, A., NEMOMISSA, S., VEIT, H., VOGELSANG, R., ZERIHUN, W., & MIEHE, G. (2019): Middle Stone Age foragers resided in high elevations of the glaciated Bale Mountains, Ethiopia. - Science, **365**, 583–587.

PANIZZO, V. N., MACKAY, A. W., SSEMMANDA, I., TAYLOR, R., ROSE, N., & LENG, M. J. (2008): A 140-year record of recent changes in aquatic productivity in a remote, tropical alpine lake in the Rwenzori Mountain National Park, Uganda. - Journal of Paleolimnology, **40**, 325–338.

RAYMOND, P. A., & BAUER, J. E. (2001): Riverine export of aged terrestrial organic matter to the North Atlantic Ocean. - Nature, **409**, 497–500. Retrieved from https://doi.org/10.1038/35054034

REIMER, P. J. P. J., BARD, E., BAYLISS, A., BECK, J. W. W., BLACKWELL, P. G. P. G., BRONK RAMSEY, C., BUCK, C. E. CHENG, H., EDWARDS, R. L. L., FRIEDRICH, M., TURNEY, C. S. M. C. S. M., & VAN DER PLICHT, J. (2013): IntCal13 and Marine13 Radiocarbon Age Calibration Curves 0–50,000 Years cal BP. - Radiocarbon, **55**, 1869–1887.

ROBERTS, N., TAIEB, M., BARKER, P., DAMNATI, B., ICOLE, M., & WILLIAMSON, D. (1993): Timing of the younger dryas event in East Africa from lake-level changes. - Nature, **366**, 146–148.

ROSE, N. L. (1994): A note on further refinements to a procedure for the extraction of carbonaceous fly-ash particles from sediments. - Journal of Paleolimnology, **11**, 201–204.

ROSE, N. L. (2008): Quality control in the analysis of lake sediments for spheroidal carbonaceous particles. - Limnology and Oceanography: Methods, **6**, 172–179.

ROSE, N. L. (2015): Spheroidal Carbonaceous Fly Ash Particles Provide a Globally Synchronous Stratigraphic Marker for the Anthropocene. - Environmental Science & Technology, **49**, 4155–4162.

SAGNOTTI, L., & CARICCHI, C. (2018): StratFit: An Excel Workbook for correlation of multiple stratigraphic trendsAnnals of Geophysics (Vol. 61).

SALAZAR, G., ZHANG, Y., AGRIOS, K., & SZIDAT, S. (2015): Development of a method for fast and automatic radiocarbon measurement of aerosol samples by online coupling of an elemental analyzer with a MICADAS AMS. - Nuclear Instruments and Methods in Physics Research Section B: Beam Interactions with Materials and Atoms, **111**.

SIROCKO, F., DIETRICH, S., VERES, D., GROOTES, P. M., SCHABER-MOHR, K., SEELOS, K., NADEAU, M.-J., KROMER, B., ROTHACKER, L., RÖHNER, M., KRBETSCHEK, M., APPLEBY, P., HAMBACH, U., ROLF, C., SUDO, M., & GRIM, S. (2013): Multi-proxy dating of Holocene maar lakes and Pleistocene dry maar sediments in the Eifel, Germany. - Quaternary Science Reviews, **62**, 56–76.

STAGER, J. C., MAYEWSKI, P. A., & MEEKER, L. D. (2002): Cooling cycles, Heinrich event 1, and the desiccation of Lake Victoria. - Palaeogeography, Palaeoclimatology, Palaeoecology, **183**, 169–178.

STOOF-LEICHSENRING, K. R., JUNGINGER, A., OLAKA, L. A., TIEDEMANN, R., & TRAUTH, M. H. (2011): Environmental variability in Lake Naivasha, Kenya, over the last two centuries. - Journal of Paleolimnology, **45**, 353–367.

STREET-PERROTT, F. A., & PERROTT, R. A. (1990): Abrupt climate fluctuations in the tropics: the influence of Atlantic Ocean circulation. - Nature, **343**, 607–612.

SZIDAT, S., A SALAZAR, G., VOGEL, E., BATTAGLIA, M., WACKER, L., SYNAL, H.-A., & TÜRLER, A. (2014): ^{14}C Analysis and Sample Preparation at the New Bern Laboratory for the Analysis of Radiocarbon with AMS (LARA). - Radiocarbon, **56**, 561–566.

TALBOT, M. R., & LÆRDAL, T. (2000): The Late Pleistocene - Holocene palaeolimnology of Lake Victoria, East Africa, based upon elemental and isotopic analyses of sedimentary organic matter. - Journal of Paleolimnology, **23**, 141–164.

TALBOT, M. R., FILIPPI, M. L., JENSEN, N. B., & TIERCELIN, J.-J. (2007): An abrupt change in the African monsoon at the end of the Younger Dryas. - Geochemistry, Geophysics, Geosystems, **8**, n/a-n/a.

TARASOV, P. E., MÜLLER, S., ZECH, M., ANDREEVA, D., DIEKMANN, B., & LEIPE, C. (2013): Last glacial vegetation reconstructions in the extreme-continental eastern Asia: Potentials of pollen and n-alkane biomarker analyses. - Quaternary International, **s 290–291**, 253–263.

THOMPSON, L. G., MOSLEY-THOMPSON, E., DAVIS, M. E., HENDERSON, K. A., BRECHER, H. H., ZAGORODNOV, V. S., MASHIOTTA, T. A., LIN, P.-N., MIKHALENKO, V. N., HARDY, D. R., & BEER, J. (2002): Kilimanjaro Ice Core Records: Evidence of Holocene Climate Change in Tropical Africa. - Science, **298**, 589 LP – 593.

TIERCELIN, J. J., GIBERT, E., UMER, M., BONNEFILLE, R., DISNAR, J. R., LÉZINE, A. M., HUREAU-MAZAUDIER, D., TRAVI, Y., KERAVIS, D., & LAMB, H. F. (2008): High-resolution sedimentary record of the last deglaciation from a high-altitude lake in Ethiopia. - Quaternary Science Reviews, **27**, 449–467.

TIERNEY, J. E., RUSSELL, J. M., SINNINGHE DAMSTÉ, J. S., HUANG, Y., & VERSCHUREN, D. (2011): Late Quaternary behavior of the East African monsoon and the importance of the Congo Air Boundary. - Quaternary Science Reviews, **30**, 798–807.

TOMLINSON, E., THORDARSON, T., MÜLLER, W., THIRLWALL, M., & MENZIES, M. (2010): Microanalysis of tephra by LA-ICP-MS — Strategies, advantages and limitations assessed using the

Thorsmörk ignimbrite (Southern Iceland). - Chemical Geology, **279**, 73–89.

UHLIG, S. K. (1988): Mountain Forests and the Upper Tree Limit on the Southeastern Plateau of Ethiopia. - Mountain Research and Development, **8**, 227–234.

UHLIG, S., & UHLIG, K. (1991): Studies on the Altitudinal Zonation of Forests and Alpine Plants in the Central Bale Mountains, EthiopiaMountain Research and Development (Vol. 11).

UMER, M., LAMB, H. F., BONNEFILLE, R., LÉZINE, A. M., TIERCELIN, J. J., GIBERT, E., CAZET, J. P., & WATRIN, J. (2007): Late Pleistocene and Holocene vegetation history of the Bale Mountains, Ethiopia. - Quaternary Science Reviews, **26**, 2229–2246.

VIEHBERG, F. A., JUST, J., DEAN, J. R., WAGNER, B., FRANZ, S. O., KLASEN, N., KLEINEN, T., LUDWIG, P., ASRAT, A., LAMB, H. F., LENG, M. J., RETHEMEYER, J., MILODOWSKI, A. E., CLAUSSEN, M., & SCHÄBITZ, F. (2018): Environmental change during MIS4 and MIS 3 opened corridors in the Horn of Africa for Homo sapiens expansion. - Quaternary Science Reviews, **202**, 139–153.

WAGNER, B., WENNRICH, V., VIEHBERG, F., JUNGINGER, A., KOLVENBACH, A., RETHEMEYER, J., SCHAEBITZ, F., & SCHMIEDL, G. (2018): Holocene rainfall runoff in the central Ethiopian highlands and evolution of the River Nile drainage system as revealed from a sediment record from Lake Dendi. - Global and Planetary Change, **163**, 29–43.

WERDECKER, J. (1962): Eine Durchquerung des Goba-Massivs in Südäthiopien. - , **Hermann vo**, 132–144.

WILLIAMS, F. M. (2016): The Southeastern Highlands and the Ogaden. - In F. M. Williams (Ed.), (pp. 153–170). - Cham: Springer International Publishing.

WOLDU, Z., FEOLI, E., & NIGATU, L. (1989): Partitioning an elevation gradient of vegetation from southeastern Ethiopia by probabilistic methods. - Plant Ecology, **81**, 189–198.

ZECH, M., & GLASER, B. (2009): Compound-specific $\delta^{18}O$ analyses of neutral sugars in soils using gas chromatography-pyrolysis-isotope ratio mass spectrometry: problems, possible solutions and a first application. - Rapid Communications in Mass Spectrometry, **23**, 3522–3532.

ZECH, M., ZECH, R., & GLASER, B. (2007): A 240,000-year stable carbon and nitrogen isotope record from a loess-like palaeosol sequence in the Tumara Valley, Northeast Siberia. - Chemical Geology, **242**, 307–318.

ZECH, M., KREUTZER, S., ZECH, R., GOSLAR, T., MESZNER, S., MCINTYRE, C., HÄGGI, C., EGLINTON, T., FAUST, D., & FUCHS, M. (2017): Comparative ^{14}C and OSL dating of loess-paleosol sequences to evaluate post-depositional contamination of n-alkane biomarkers. - Quaternary Research, **87**, 180–189.

Chapter 3

The Holocene lake-evaporation history of the afro-alpine Lake Garba Guracha in the Bale Mountains, Ethiopia, based on $\delta^{18}O$ records of sugar biomarker and diatoms

Lucas Bittner[1,2], Graciela Gil-Romera[3,4] David Grady[5], Henry F. Lamb[5,6], Eva Lorenz[1], Mikaela Weiner[7], Hanno Meyer[7], Tobias Bromm[2], Bruno Glaser[2], Michael Zech[1]

[1] Heisenberg Chair of Physical Geography with focus on paleoenvironmental research, Institute of Geography, Technische Universität Dresden, 01069 Dresden, Germany
[2] Institute of Agronomy and Nutritional Sciences, Soil Biogeochemistry, Martin-Luther-University Halle-Wittenberg, 06108 Halle (Saale), Germany
[3] Department of Ecology, Philipps-Marburg University, 35037 Marburg, Germany
[4] Department of Geo-environmental Processes and Global Change, Pyrenean Institute of Ecology, CSIC, 50059 Zaragoza, Spain
[5] Department of Geography and Earth Sciences, Aberystwyth University, Aberystwyth SY23 3DB, UK
[6] Department of Botany, School of Natural Sciences, Trinity College Dublin, Dublin 2, Ireland.
[7] Alfred Wegener Institute Helmholtz Centre for Polar and Marine Research, Polar Terrestrial Environmental Systems, TelegrafenbergA45, 14473 Potsdam, Germany

Abstract

In eastern Africa, there are few long, high-quality records of environmental change at high altitudes, inhibiting a broader understanding of regional climate change. We investigated a Holocene lacustrine sediment archive from Lake Garba Guracha, Bale Mountains, Ethiopia, (3,950 m a. s. l.), and reconstructed high-altitude lake evaporation history using $\delta^{18}O$ records derived from the analysis of compound-specific sugar biomarkers and diatoms. The $\delta^{18}O_{diatom}$ and $\delta^{18}O_{fuc}$ records are clearly correlated and reveal similar ranges (7.9 ‰ and 7.1 ‰, respectively). The lowest $\delta^{18}O$ values occurred between 10 - 7 cal ka BP and were followed by a continuous shift towards more positive $\delta^{18}O$ values. Due to the aquatic origin of the sugar biomarker and similar trends of $\delta^{18}O_{diatom}$, we suggest that our lacustrine $\delta^{18}O_{fuc}$ record reflects $\delta^{18}O_{lake\ water}$. Therefore, without completely excluding the influence of the 'amount-effect' and the 'source-effect', we interpret our record to reflect primarily the precipitation-to-evaporation ratio (P/E). We conclude that precipitation increased at the beginning of the Holocene, leading to an overflowing lake between ~ 10 and ~ 8 cal ka BP, indicated by low $\delta^{18}O_{lake\ water}$ values, which are interpreted as reduced evaporative enrichment. This is followed by a continuous trend towards drier conditions, indicating at least a seasonally closed lake system.

3.1 Introduction

The climate of eastern Africa is driven by the position of the tropical rain belt. Increasing north hemisphere insolation during northern hemisphere summer forces the tropical rain belt and ITCZ northward and the Congo Air Boundary (CAB) migrates eastward (DAVIES ET AL., 1985; HILLS, 1979; NAKAMURA, 1968). The eastward extent of CAB movement is related to the seasonal changes of Indian Summer Monsoon (ISM) strength (CAMBERLIN, 1997). Moreover, an increased W-E atmospheric pressure gradient between Africa and India during the northern hemisphere summer enhances the ISM (WAGNER ET AL., 2018). The enhanced ISM redirects Indian Ocean air masses towards India preventing them from penetrating deeply into eastern Africa. Therefore, the convergence zone of Indian Ocean air masses and Congo Basin air masses shifts to the east (COSTA ET AL., 2014).

In the past, in addition to the effects described above, an increased land-ocean temperature gradient caused strengthening of the West African Monsoon and ISM. The interaction of monsoon intensity and eastward migration of the CAB may have been responsible for enhanced moisture in the region, thereby generating a water level rise in eastern African lakes (JUNGINGER ET AL., 2014; LEZINE ET AL., 2014). Additionally, increased lake levels may have been driven by a northward shift in the mean position of the tropical rain belt during the early Holocene northern hemisphere summer insolation maximum (GASSE, 2000). These processes led to a more pluvial early-mid Holocene (12 - 5 cal ka BP), termed the African Humid Period (AHP) (DEMENOCAL ET AL., 2000), which was particularly intense in North Africa and extended south to 10 °S in eastern Africa (GASSE, 2000). While the general mechanisms for

the orbitally forced AHP are well understood, the spatial and temporal patterns are intensively debated.

Due to the complexity of atmospheric circulation in eastern Africa, it is not surprising that the reconstructed timing of the AHP differs across sites. The termination of the AHP has been described as rapid (COLLINS ET AL., 2017), as synchronous and abrupt (TIERNEY & DEMENOCAL, 2013), or asynchronous and gradual (COSTA ET AL., 2014; FOERSTER ET AL., 2012; VAN DER LUBBE ET AL., 2017). However, the inferred timing of the AHP termination may depend largely on the analysed proxy (CASTAÑEDA ET AL., 2016) and the type of archive. Furthermore, in addition to a variable climate, the scarce and patchy paleoenvironmental records of Northern and eastern Africa supply insufficient data for comprehensive climate reconstruction. The hydrological history of eastern Africa has been reconstructed mainly from low-elevation sites.

High-altitude lakes have proved to be excellent sensors of environmental change (CATALAN ET AL., 2006,2013). They incorporate information about changes in the catchment, including varying erosion, often without significant anthropogenic disturbance or desiccation (ARNAUD ET AL., 2016). In eastern Africa, high-altitude paleolimnological research has been carried out at Lake Ashenge (2442 m a. s. l.; MARSHALL ET AL., 2009), Lake Dendi (2840 m a. s. l.; WAGNER ET AL., 2018), Sacred Lake (2350 m a. s. l. on Mount Kenya; BARKER ET AL., 2001, 2011; STREET-PERROTT ET AL., 2008; LOOMIS ET AL., 2015, 2017), and Lake Garba Guracha (3950 m a. s. l. on the Bale Mountains; UMER ET AL., 2007; TIERCELIN ET AL., 2008; BITTNER ET AL., 2020).

Paleolimnological research has advanced in recent decades by the use of stable isotope ratios as environmental indicators. The oxygen isotope composition ($\delta^{18}O$) of biogenic compounds and autochthonous carbonates has been established as a valuable paleoclimate proxy because the value of $\delta^{18}O$ in water, which is incorporated into biogenic and autochthonous compounds, depends on fractionation processes linked to temperature, air mass source and trajectory, and global ice volume.

Oxygen isotope composition has been determined for several Quaternary records in eastern Africa: for example, $\delta^{18}O_{ice\ cores}$ (THOMPSON ET AL., 2002), $\delta^{18}O_{carbonate}$ (LAMB ET AL., 2005), $\delta^{18}O_{diatom}$ (BARKER ET AL., 2001,2007,2011; LAMB ET AL., 2005), and $\delta^{18}O_{sugar}$ (HEPP ET AL., 2017). $\delta^{18}O_{sugar}$ has been successfully applied to several other paleolimnological archives (HEPP ET AL., 2015,2019b; TUTHORN ET AL., 2014). In contrast to this relatively new proxy (ZECH & GLASER, 2009), numerous $\delta^{18}O_{diatom}$ records have been published, proving the potential for reconstructing past climate changes from biogenic silica ($\delta^{18}O_{diatom}$) (BARKER ET AL., 2004,2007,2011; CARTIER ET AL., 2019; KOSTROVA ET AL., 2019; LAMB ET AL., 2005; LENG ET AL., 2001; NARANCIC ET AL., 2016; WILSON ET AL., 2014).

At Garba Guracha, early work by UMER ET AL. (2007) and TIERCELIN ET AL. (2008) focused on sedimentological, geochemical, and pollen analyses. Their work indicates that Garba Guracha is one of the longest, most continuous high-resolution Late Quaternary environmental archives from highland Africa. With a new core, BITTNER ET AL. (2020) established a higher resolution chronology and analysed XRF and biomarkers. GIL-ROMERA ET AL. (2019) carried out charcoal and pollen analyses on the same core to show that fire has been a constant disturbance at millennial time scales in the Afromontane vegetation of the Bale Mountains, driving the long-term ecological dynamics of *Erica* spp.

Here we present the first record in eastern Africa of lake-level variation derived from the oxygen isotope composition of sugar biomarkers and diatoms and the first high-altitude, long-term oxygen isotope record from above 3500 m a. s. l. in Ethiopia. We compare the results of well-established $\delta^{18}O_{diatom}$ analyses with the more novel $\delta^{18}O_{sugar}$ analyses (ZECH & GLASER, 2009) to gain more detailed knowledge regarding the $\delta^{18}O_{sugar}$ proxy and interpretations of the proxy from the archive itself. Our main aims are: (i) to determine the allochthonous versus autochthonous source of the analysed sugar biomarkers, (ii) to use $\delta^{18}O_{diatom}$ analyses to test and corroborate the $\delta^{18}O_{sugar}$ results, (iii) to describe the hydrological history of high-altitude Garba Guracha, and (iv) to consider the implications of our data for understanding regional paleoclimate.

3.1.1 Regional setting

Study area

Garba Guracha is situated in the Bale Mountains of the Bale-Arsi Massif, located east of the Main Ethiopian Rift (Fig. 3.1).

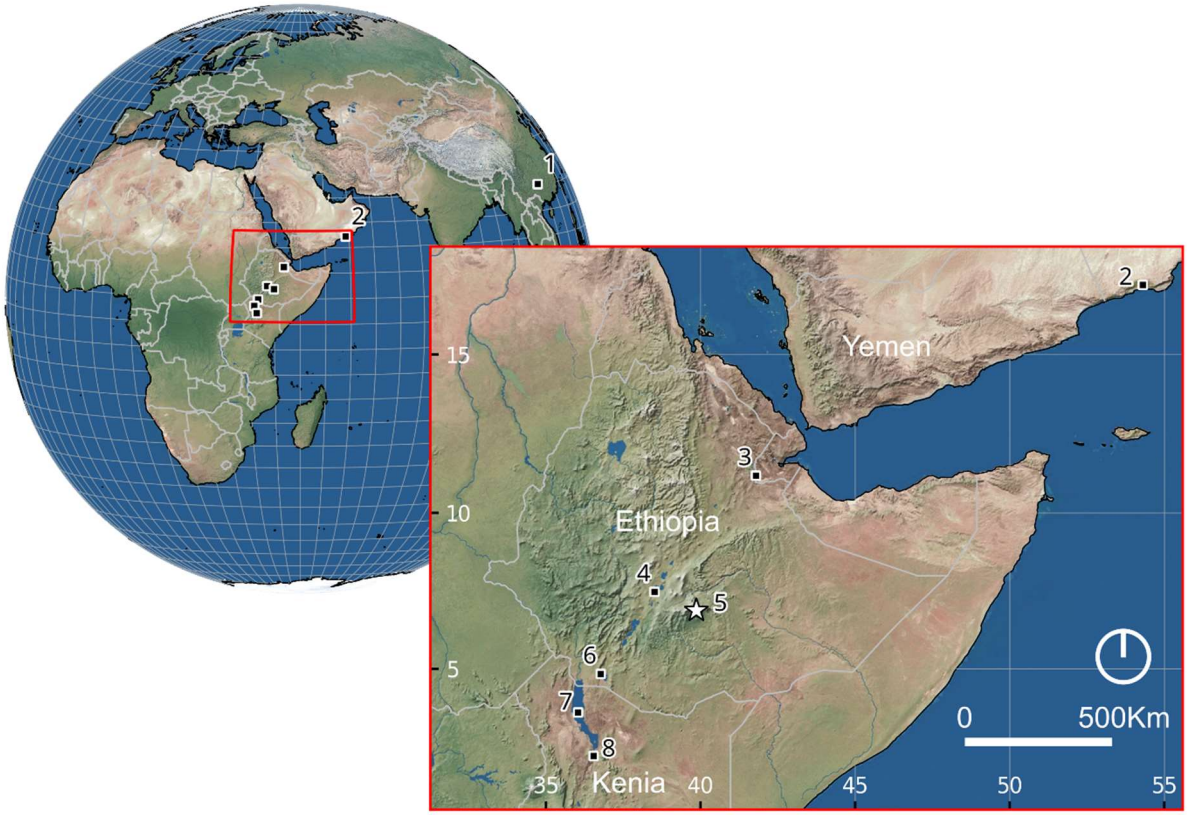

Figure 3.1: Overview of the region: (1) Dongge caves, (2) Qunf cave, (3) Lake Abhè, (4) Ziway-Shala, (5) Garba Guracha (this study), (6) Chew Bahir, (7) Lake Turkana, (8) Paleolake Suguta.

The Sanetti Plateau is the highest plateau in the Bale Mountains at an altitude between ~ 3800 and ~ 4200 m a. s. l., encompassing an area of 600 km^2, bordered by a steep escarpment to the south (OSMASTON ET AL., 2005). Deep valleys incised by northward

descending rivers characterise the northern slopes. The volcanic plateau is formed of solidified horizontal lava consisting of alkali basalt, trachyte, and tuffs with rhyolites, overlying older volcanic material (UHLIG & UHLIG, 1991; WILLIAMS, 2016). During the Last Glacial Maximum, the plateau and the valleys were locally glaciated (GROOS ET AL., 2020,2021; OSMASTON ET AL., 2005; OSSENDORF ET AL., 2019). The glacial cirque Garba Guracha (6.875781 °N, 39.878075 °E) was first mentioned by WERDECKER (1962) and was described in detail by UMER ET AL. (2007) and TIERCELIN ET AL. (2008). It is located at 3950 m a. s. l., has a maximum water depth of 6 m, a very small watershed (0.15 km^2), and extends to ~ 500 x 300 m in area. The catchment bedrock is carbonate-poor (LÖFFLER, 1978; UHLIG & UHLIG, 1991). The lake has an outlet during the rainy season. A marshy alluvial plain fed by several springs extends to the south of the lake.

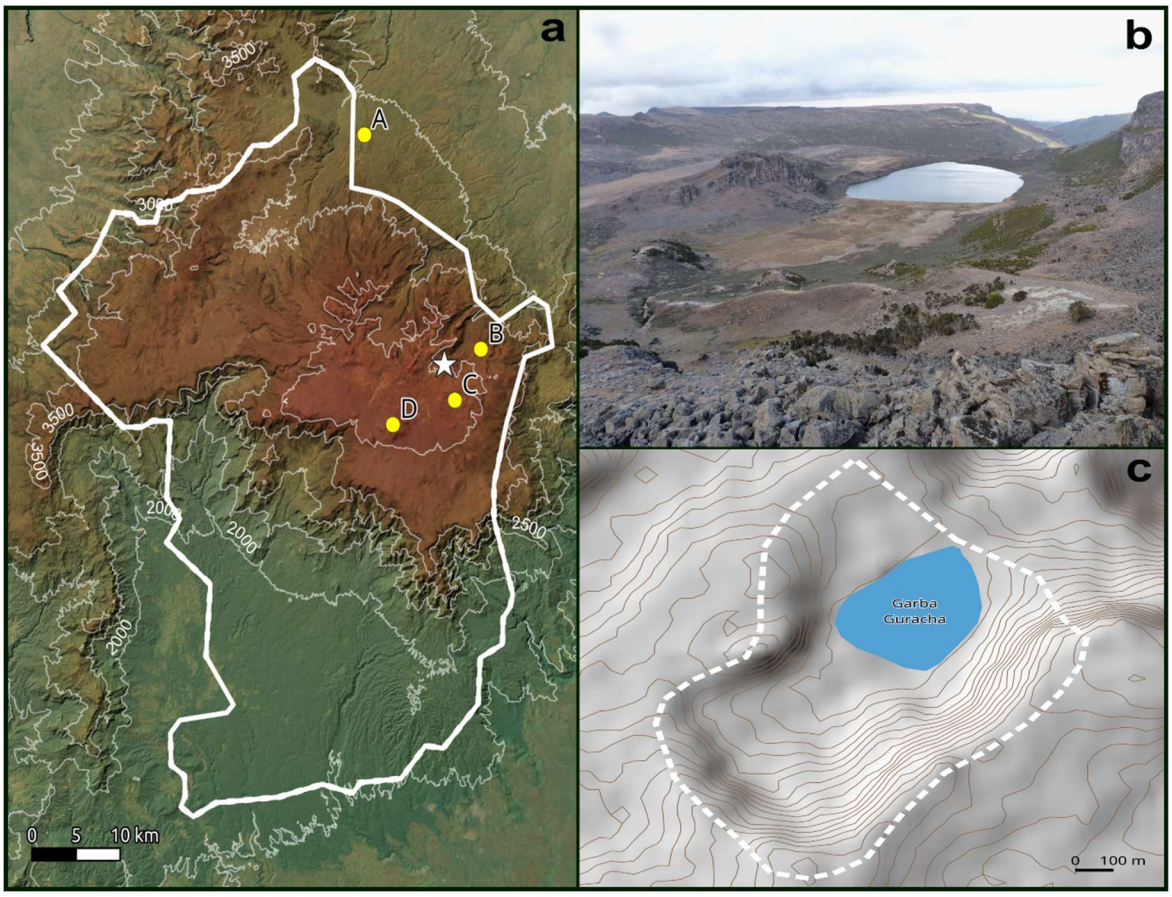

Figure 3.2: Location of the study area. (a) Bale Mountain National Park (thick white line); climate stations: (A) Dinsho, (B) Angesso station, (C) EWCP station, (D) Tulu Dimtu; (b) northeastward view over the glacial cirque of the Garba Guracha catchment; (c) Garba Guracha catchment structure and watershed (dashed white line).

Climate

The climate of the Bale Mountains differs from north to south due to differences in altitude, aspect, and continental air masses (KIDANE ET AL., 2012; UHLIG & UHLIG, 1991). The mean annual temperature at Dinsho (Fig. 3.2a A) is 11.8 °C, and the mean minimum temperature for the coldest month is 0.6 °C (HILLMAN, 1986). Ten newly installed climate stations across the Bale Mountains have provided climate data since 2017. The results from 2017 show a mean annual temperature of 4.9 °C at the Angesso Station (Fig. 3.2a B), which is located 4 km northeast of Garba Guracha.

Precipitation in the Bale Mountains originates from two moisture sources, the Indian Ocean monsoon, and the Equatorial Westerlies (MIEHE & MIEHE, 1994; UHLIG, 1988). A dry season from November to February and a bimodal wet season from March to October define the climate. Precipitation maxima occur in April/May and September/October, respectively (LEMMA ET AL., 2020; WOLDU ET AL., 1989). The highest monthly rainfalls (July to September) are related to the convergence of southwest air masses. In 2017, Angesso Station (3949 m a. s. l.) (Fig. 3.2a B) recorded 1097 mm while 711 mm were registered at the EWCP Station (elevation 4124 m a. s. l.) (Fig. 3.2a C) and 468 mm at Tulu Dimtu (4385 m a. s. l.) (Fig. 3.2a D). Garba Guracha (3950 m a. s. l.) lies at a similar altitude to the Angesso Station. The afro-alpine regions, including the Sanetti Plateau, are characterised by strong diurnal temperature differences between day and night (-15 °C to +26 °C) (HILLMAN, 1988).

3.2 Material and methods

3.2.1 Material and sampling

In February 2017, we retrieved two overlapping sediment cores using a Livingstone piston corer from a raft anchored at 4.8 m water depth. A maximum sediment depth of 1550 cm was reached with an organic-rich upper part (0 - 900 cm) (Fig. 3) and an organic-poor lower part (900 - 1550 cm). For radiocarbon dating, we took a total of 31 samples, comprising 18 bulk sediment samples, 8 bulk *n*-alkane, and 5 charcoal samples. More details on sediment and chronology can be found in BITTNER ET AL. (2020). For sugar biomarker analyses (n = 80), the organic-rich upper core sections (top 900 cm, compressed to ~ 800 cm during coring) were sampled at contiguous 10 cm intervals, each sample representing ca. 103 years of sedimentation. This sampling technique enabled us to create a continuous record where variability is smoothed, but without missing information. Nineteen of those samples were later selected for diatom analyses.

3.2.2 Compound-specific $\delta^{18}O$ analyses of sugar biomarkers

Sugar biomarker extraction was done at the Institute of Agricultural and Nutritional Sciences, Soil Biogeochemistry, Martin-Luther-University Halle-Wittenberg following the method described by ZECH & GLASER (2009). Briefly, monosaccharides were extracted from the homogenised samples by hydrolysis using 4 M trifluoroacetic acid at 105 °C for 4 hours (AMELUNG ET AL., 1996). The dissolved monosaccharides were first filtered over glass fiber filters, evaporated, and then further cleaned by transferring them with H_2O onto XAD-7 columns and finally over DOWEX 50WX8 columns. After freeze-drying, the samples were derivatised with methylboronic acid (MBA) for 1 hour at 60 °C (KNAPP, 1979). The derivatised samples were measured in triplicates on a Trace GC 2000 coupled to a Delta V Advantage IRMS via an ^{18}O-pyrolysis reactor (GC IsoLink) and a ConFlow IV interface (all devices from Thermo Fisher Scientific, Bremen, Germany). Sugar standards with known $\delta^{18}O$ values, containing

arabinose (ara), fucose (fuc), and xylose (xyl), were measured in various concentrations after every six sample triplicates (ZECH & GLASER, 2009). Correction of the sample $\delta^{18}O$ values was applied for possible amount dependency and drift during a sample batch and for the hydrolytically exchangeable oxygen atoms of the carbonyl group (ZECH & GLASER, 2009). The $\delta^{18}O$ values of the monosaccharides are presented in the usual δ-notation versus the Vienna Standard Mean Ocean Water (VSMOW).

3.2.3 $\delta^{18}O$ analyses of diatoms

Nineteen sediment samples were processed for diatom oxygen isotope ($\delta^{18}O_{diatom}$) analyses (Table B.1). Two g of dry sediment were used to purify samples using a multi-step cleaning procedure. Sediment samples were first treated with 35 % H_2O_2 on a heating plate at 50 °C for 72 hours to remove organic matter, adding 10 % HCl at 50 °C to eliminate carbonates, then washed pH neutral. The subsequent heavy liquid separation was carried out with sodium polytungstate (SPT; $3Na_2WO_4 \cdot 9WO_3 \cdot H_2O$) heavy liquid solutions with decreasing densities (2.50 - 2.05 g/ml) and subsequent centrifuging at 2500 rpm for 30 minutes, leading to the separation of diatoms from heavier detrital contaminants. Decreasing densities were subsequently used to properly separate diatoms from the mineral particles of the terrigenous fraction. Different diatom species have slightly different densities, which makes this step-wise separation procedure necessary in order not to lose any diatoms during heavy liquid separation. This detritus was retained for contamination assessment and used for $\delta^{18}O_{diatom}$ correction following CHAPLIGIN ET AL. (2010). Diatom samples were washed in ultra-pure water at 2500 rpm for 20 minutes and sieved through a 3 µm filter. Sixteen of the purified diatom samples (n = 19) yielded enough material (> 1.5 mg) to be measured for $\delta^{18}O$ at the AWI Potsdam ISOLAB Facility.

To remove exchangeable oxygen, inert Gas Flow Dehydration (iGFD) and heating to 1100 °C under Argon gas (following CHAPLIGIN ET AL., 2010) was applied. Dehydrated samples were then quantitatively reacted to liberate O_2 by laser fluorination under BrF_5 atmosphere (CLAYTON & MAYEDA, 1963). Sample oxygen was directly measured against a calibrated oxygen reference with a PDZ Europa 2020 mass spectrometer. The working standard BFC ($\delta^{18}O$ = 29.0 ± 0.3 ‰; CHAPLIGIN ET AL., 2011) was used for calibration (this study: $\delta^{18}O$ = +28.88 ± 0.24 ‰; n = 10) for controlling both accuracy and precision of the isotope analyses. The long-term analytical reproducibility (1σ) is ± 0.25 ‰ (CHAPLIGIN ET AL., 2010). All measured diatom $\delta^{18}O$ values were corrected for contamination, mainly due to clay particles (Fig. B.7), using a geochemical mass-balance approach (CHAPLIGIN ET AL., 2012). Contamination was calculated for all samples individually and corrected following the method described in CHAPLIGIN ET AL. (2012). Briefly, we calculated the correction following Equation 2 in CHAPLIGIN ET AL. (2012):

$$\delta^{18}O_{corr} = \delta^{18}O_{measured} + (\%cont. \times \delta^{18}O_{cont.})$$

where $\delta^{18}O_{measured}$ is the isotopic composition of the sample after purification, %cont. is the contamination percentage left in the purified sample and $\delta^{18}O_{cont.}$ is the isotopic composition of the contaminants (i.e., the heavy [mineral] fraction).

3.3 Results

3.3.1 $\delta^{18}O_{fuc}$ record of Garba Guracha

Compound-specific $\delta^{18}O$ values for the sugar biomarker fucose reveal a total range from +24.7 to +36.2 ‰ (Fig. 3.3, Table B.2).

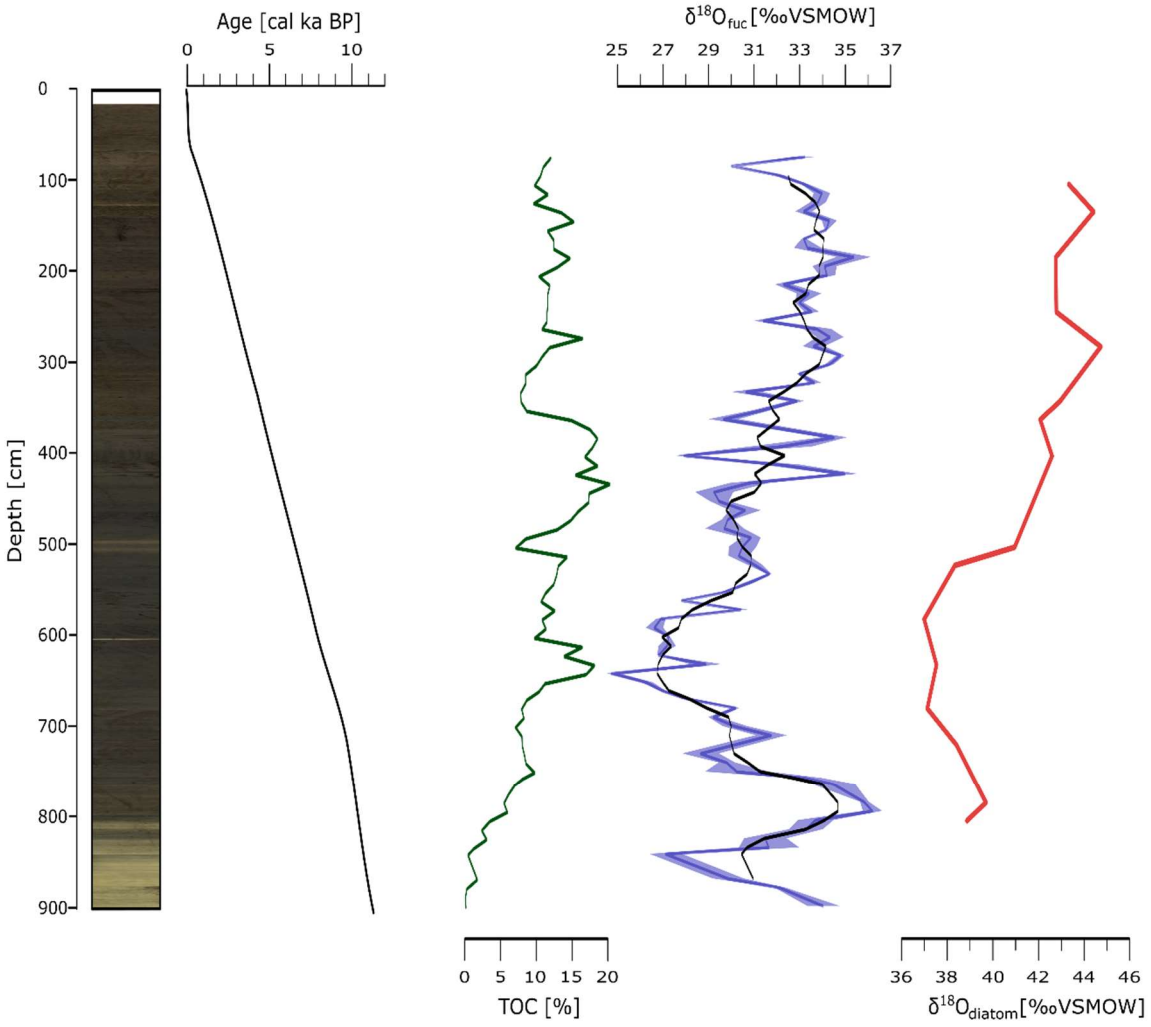

Figure 3.3: Depth profiles of age and TOC (BITTNER ET AL., 2020), $\delta^{18}O_{fuc}$ (blue), and $\delta^{18}O_{diatom}$ (purple) (this study). The black line shows the running mean of 5. Stacked core photos are shown on the left and shaded areas indicate the standard error range

The mean standard error for fucose was ± 1.4 ‰. The $\delta^{18}O$ values of fucose increase from 840 cm (11 cal ka BP) and begin to decrease at ~ 800 cm (10.5 cal ka BP) showing minima between 665 and 535 cm (9 and 7 cal ka BP). Thereafter, a continuous trend towards more

positive $\delta^{18}O$ values of fucose is apparent until 290 cm (3.5 cal ka BP). Above this depth, stable values continue with the exception of one pronounced minimum at ~ 85 cm (0.5 cal ka BP).

In detail, the Early Holocene reveals centennial-scale $\delta^{18}O_{fucose}$ shifts with minima at 840 and 750 cm (10.9 and 10.2 cal ka BP), and a maximum at 800 cm (10.6 cal ka BP). The phase of lowest $\delta^{18}O_{fuc}$ values is interrupted by a short maximum at 635 cm (8.4 cal ka BP). The Late Holocene reveals major fluctuations of $\delta^{18}O_{fuc}$ between 425 and 370 cm (5.5 and 4.6 cal ka BP). Moreover, a maximum at 290 cm (3.5 cal ka BP), a minimum at 85 cm (0.5 cal ka BP), and numerous centennial-scale variations are visible in the Late Holocene. However, the variability of $\delta^{18}O$ is highest during the Early Holocene and decreases towards the Late Holocene.

3.3.2 $\delta^{18}O_{diatom}$ record of Garba Guracha

For most of the 16 diatom samples, duplicate or triplicate oxygen isotope analyses yielded a mean (max) standard deviation of ± 0.26 ‰ (± 0.51 ‰: Table B.1). One sample could only be measured once due to low diatom content after the separation procedure. In general, the $\delta^{18}O_{diatom}$ values span a range of 7.9 ‰ (Fig. 3.3). Like the $\delta^{18}O_{sugar}$ data, the $\delta^{18}O_{diatom}$ values decrease above 750 cm (10 cal ka BP), with lowest values co-occurring between 665 and 535 cm (9 and 7 cal ka BP) ($\delta^{18}O_{diatom}$ ~ +37 ‰). An overall increasing trend between 535 and 285 cm (7 and 3.5 cal ka BP) is interrupted by a decrease between 425 and 370 cm (5.5 and 4.6 cal ka BP). More less-positive values follow the maximum at 285 cm (3.5 cal ka BP) ($\delta^{18}O_{diatom}$ = +44.8 ‰) until 140 cm. A small maximum at 140 cm (1.5 cal ka BP) and subsequent decreasing values are similar to the $\delta^{18}O_{sugar}$ record.

3.4 Discussion

3.4.1 The Garba Guracha $\delta^{18}O_{sugar}$ record - lake or leaf water?

A crucial issue for the interpretation of $\delta^{18}O_{sugar}$ records is the aquatic (autochthonous) or terrestrial (allochthonous) origin of the sedimentary sugar biomarkers. Plant-derived sugar biomarkers, modified by a biosynthetic fractionation factor (ε_{bio}), can either reflect lake water $\delta^{18}O$ ($\delta^{18}O_{lake\ water}$) or terrestrial leaf water $\delta^{18}O$ ($\delta^{18}O_{leaf\ water}$) origin. In the case of Garba Guracha, a high aquatic organic matter content of the sediments can be inferred from several proxies. First, relatively positive $\delta^{13}C$ values of > - 23 ‰ and a low TOC/N ratio of < 15 indicate a high aquatic organic matter content (BITTNER ET AL., 2020). Second, the sugar biomarker quantification pattern indicates a high relative abundance of fucose in the Garba Guracha sediments. Fucose is a major component of phytoplankton, zooplankton, and bacteria (OGIER ET AL., 2001), as well as of aquatic plants (HEPP ET AL., 2016). In terrestrial vascular plants, fucose is produced in low concentrations, according to HEPP ET AL. (2016) who developed two ratios, fuc/(ara + xyl) and (fuc + xyl)/ara, to distinguish between aquatic (> 0.10) and terrestrial (≤ 0.10) input. In our data, both ratios suggest that the sediments of Garba Guracha contain sugar

biomarkers that are principally of aquatic origin (BITTNER ET AL., 2020, Fig. 3.6). While a partial terrestrial contribution of sugar biomarkers to the sediments cannot be fully excluded, the terrestrial contribution, especially of fucose, can be neglected. We therefore interpret our $\delta^{18}O_{fuc}$ data as a record of changes in $\delta^{18}O_{lake\ water}$.

3.4.2 The Garba Guracha $\delta^{18}O_{diatom}$ record

$\delta^{18}O_{lake\ water}$ and temperature at the time of frustule formation define the $\delta^{18}O_{diatom}$ composition of aquatic diatoms (LABEYRIE, 1974; LECLERC & LABEYRIE, 1987; LENG & BARKER, 2006). Some processes in the incorporation of oxygen isotopes into diatom silica (summarised by BIRD ET AL., 2020) still require a better understanding, such as (1) species-specific fractionation (BAILEY ET AL., 2014), (2) post-mortem alteration of the oxygen isotopic composition (TYLER ET AL., 2017), and (3) the effect of diagenesis on oxygen isotope fractionation and exchange (DODD ET AL., 2012). However, $\delta^{18}O_{diatom}$ analyses have been applied successfully to many archives as a proxy for P/E to identify wet and dry conditions (MEYER ET AL., 2015; POLISSAR ET AL., 2006), moisture source (MEYER ET AL., 2015; POLISSAR ET AL., 2006), $\delta^{18}O_{precipitation}$ (BAILEY ET AL., 2015; MACKAY ET AL., 2013; MORLEY ET AL., 2005), hydrological changes (KOSTROVA ET AL., 2019; NARANCIC ET AL., 2016), and temperature (KOSTROVA ET AL., 2014). The interpretation of $\delta^{18}O_{diatom}$ as a proxy for temperature is difficult due to the variability of $\delta^{18}O_{precipitation}$ and, especially in warm and/or dry environments, due to evaporative enrichment. These factors may have a more significant influence on $\delta^{18}O_{diatom}$ than temperature (LENG & BARKER, 2006). Especially in the tropics, where inter-annual and seasonal temperature variability is low, $\delta^{18}O_{diatom}$ generally has been interpreted as a proxy for precipitation amount (BARKER ET AL., 2007; COLE ET AL., 1999; LAMB ET AL., 2005). BARKER ET AL. (2001) suggested that the $\delta^{18}O_{diatom}$ record of Small Hall Tarn and Simba Tarn at Mount Kenya represents the moisture balance of lake-level stands and overflows.

For reconstructing the $\delta^{18}O_{lake\ water}$, several calibration studies for modern diatoms (BRANDRISS ET AL., 1998; CRESPIN ET AL., 2010; DODD & SHARP, 2010; MOSCHEN ET AL., 2005) and one for sedimentary diatoms (LECLERC & LABEYRIE, 1987) have been published. The temperature-coefficient of these studies is quite similar (-0.16 ‰/°C to -0.29 ‰/°C), although offsets of several per mil between the regression lines are present. Explanations suggested by CRESPIN ET AL. (2010) include (1) an under- or overestimation of temperature or $\delta^{18}O_{lake\ water}$ in the calibration, (2) incomplete accounting for exchangeable oxygen, and (3) post-mortem ^{18}O enrichment of sedimentary diatoms (SCHMIDT ET AL., 2001). To account for post-mortem ^{18}O enrichment, we reconstructed the $\delta^{18}O_{lake\ water}$ of the Garba Guracha sedimentary diatoms using the equation of LECLERC & LABEYRIE (1987). Taking into consideration a mean annual T_{air} of ~ 4.9 °C (min: 3.5 °C, max: 6.0 °C) in 2017, measured at the closest meteorological station (Angesso), which is at the same altitude as Lake Garba Guracha, an isotope fractionation factor α in the system (silica-water) of 1.0435 ± 0.004 can be calculated (after LECLERC & LABEYRIE, 1987). The calculated value is subject to some uncertainty due to the lack of more recent $\delta^{18}O_{diatom}$ values, an incomplete record of modern $\delta^{18}O_{lake\ water}$ variability, and an underestimation of frustule growth temperature by using mean annual air temperature.

Based on these factors, the measured most recent (931 cal years BP) $\delta^{18}O_{diatom}$ of ~ +43.4 ‰ at Lake Garba Guracha leads to a calculated "modern" $\delta^{18}O_{lake\ water}$ value of +0.8 ± 0.3 ‰, which is lower than the measured $\delta^{18}O_{lake\ water}$ of +4.7 ‰ at the end of the 2017 dry season, representing strong ^{18}O enrichment of lake water (LEMMA ET AL., 2020). For comparison, precipitation in 2017 yielded a mean $\delta^{18}O$ value of -4.5 ‰ (max -6.2 ‰, min -1.9 ‰). The reconstructed $\delta^{18}O_{lake\ water}$ value of +0.8 ‰ for the uppermost diatom sample is hence a reasonable estimated value between those of modern precipitation (-4.5 ‰) and the seasonally enriched lake water (+4.7 ‰) (LEMMA ET AL., 2020).

3.4.3 Comparison of reconstructed $\delta^{18}O_{lake\ water}$ from $\delta^{18}O_{fuc}$ versus $\delta^{18}O_{diatom}$

The predominantly aquatic origin of sugar biomarkers in the Garba Guracha sediments, as discussed earlier, leads to the conclusion that the isotopic composition of the fucose sugar biomarkers primarily represents $\delta^{18}O_{lake\ water}$ modified by ε_{bio}, the biosynthetic fractionation factor. ε_{bio} can be estimated as +29 ‰ between aquatic cellulose $\delta^{18}O$ and $\delta^{18}O_{lake\ water}$ (MAYR ET AL., 2015). An ε_{bio} of +29 ‰ may slightly underestimate the fractionation factor of aquatic hemicellulose, as is known for terrestrial cellulose and hemicellulose (HEPP ET AL., 2019a; TUTHORN ET AL., 2014; ZECH ET AL., 2014). The slight offset derives from the loss of the relatively ^{18}O-depleted oxygen atom attached to C-6 during 6-deoxyhexose (fucose) biosynthesis (C-6 decarboxylation; ALTERMATT & NEISH, 1956; BURGET ET AL., 2003; HARPER & BAR-PELED, 2002). This is supported by the findings of WATERHOUSE ET AL. (2013) that ~ 80 % of the oxygen atoms at the C-6 position are isotopically exchanged during cellulose synthesis. Similarly, the Garba Guracha $\delta^{18}O_{diatom}$ record can be interpreted as $\delta^{18}O_{lake\ water}$ due to a lesser influence of temperature in tropical regions, as discussed previously.

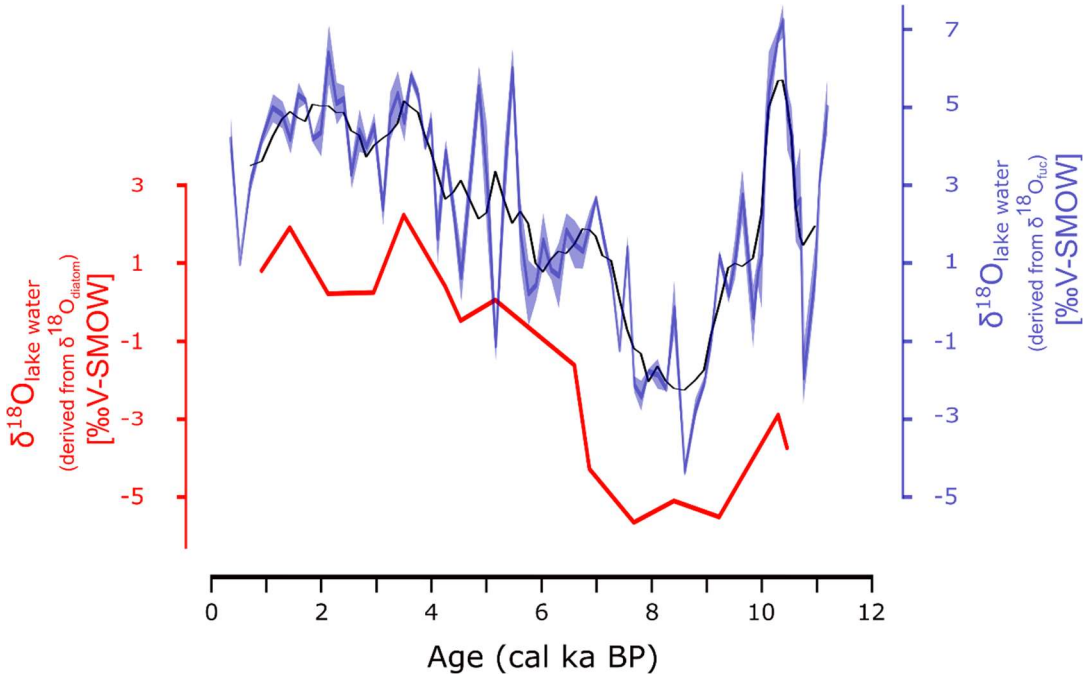

Figure 3.4: Comparison of the $\delta^{18}O_{lake\ water}$ derived from diatom and fucose of Garba Guracha. The black line shows the running mean of 5 and shaded areas the standard error range.

The reconstructed $\delta^{18}O_{lake\ water}$ values of sugar biomarker and diatoms are consistent after correction for ε_{bio} (+29 ‰) (MAYR ET AL., 2015) and temperature-dependent fractionation during diatom growth (LECLERC & LABEYRIE, 1987), respectively (Fig. 3.4).

Additionally, the $\delta^{18}O_{diatom}$ and $\delta^{18}O_{fuc}$ ranges of the 16 analysed samples are similar (7.9 ‰ and 7.1 ‰, respectively). Despite the rather small number of analyses, the aquatic $\delta^{18}O_{diatom}$ and $\delta^{18}O_{fuc}$ show identical trends during the Holocene (Fig. 3.3), pointing to a common source of $\delta^{18}O_{fuc}$ and $\delta^{18}O_{diatom}$. Therefore, we conclude that the $\delta^{18}O_{diatom}$ record corroborates the $\delta^{18}O_{fuc}$ record to reflect primarily $\delta^{18}O_{lake\ water}$ and, moreover, that $\delta^{18}O_{fuc}$ of aquatic sugar biomarker is a valuable proxy for $\delta^{18}O_{lake\ water}$ in the Garba Guracha sedimentary archive.

3.4.4 Paleoclimatic significance and proxy interpretation

Past variations of $\delta^{18}O_{lake\ water}$ reflect past changes in $\delta^{18}O_{precipitation}$ and evaporative ^{18}O enrichment of lake water. In the tropics, $\delta^{18}O_{precipitation}$ values in paleo-archives and rainfall records have been interpreted to represent changes in the amount of precipitation—depleted $\delta^{18}O$ values indicating high amounts of precipitation (amount effect; DANSGAARD, 1964; ROZANSKI ET AL., 1993). However, besides amount effect, the history of the entire moist air mass, including source region (source effect), the air mass convection (altitude effect), (re)evaporative history (recycling), and transport distance (continental effect), must be considered (SHARP, 2017). Moreover, $\delta^{18}O_{precipitation}$ is influenced by temperature (temperature effect; ROZANSKI ET AL., 1993). However, temperature changes in the tropics, especially during the Holocene, were rather small (BERKE ET AL., 2012b), implying that the temperature effect is negligible (ROZANSKI ET AL., 1993; VUILLE ET AL., 2005).

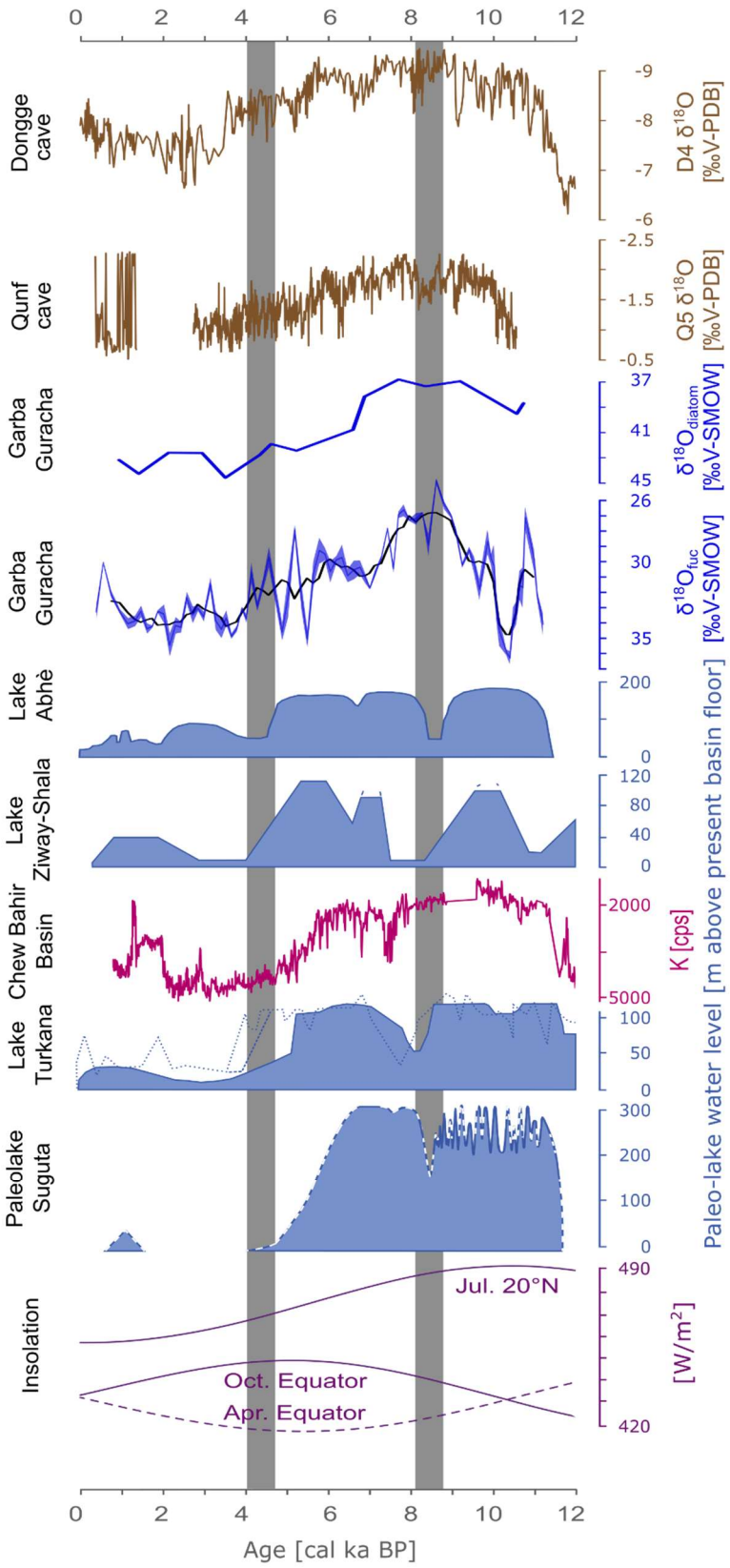

Figure 3.5: Comparison of lake level reconstructions in eastern Africa and $\delta^{18}O$ records for the past 12,000 years (adapted from JUNGINGER ET AL., 2014). Dongge cave (DYKOSKI ET AL., 2005), Qunf cave (FLEITMANN ET AL., 2003), Garba Guracha (this study), Lake Abhè (GASSE, 2000), Lake Ziway-Shala (GILLESPIE ET AL., 1983), Chew Bahir Basin (FOERSTER ET AL., 2012), Lake Turkana (GARCIN ET AL., 2012; filled curve), (JOHNSON ET AL., 1991; dotted curve), (BROWN & FULLER, 2008; dashed curve), Paleolake Suguta (JUNGINGER ET AL., 2014), and insolation variations (LASKAR ET AL., 2004)

The relatively small temperature effect means that $\delta^{18}O_{precipitation}$ is predominantly influenced by the amount and the source effect in eastern Africa. For the tropics in general, high-resolution $\delta^{18}O$ speleothem records, such as those of FLEITMANN ET AL. (2003) and DYKOSKI ET AL. (2005) (Fig. 3.5), are generally interpreted as mainly reflecting variations in the intensity of the monsoon systems (amount effect)—East Asian Summer (EASM) and the ISM. Overall trends of Qunf cave $\delta^{18}O$ (FLEITMANN ET AL., 2003) and Dongee cave $\delta^{18}O$ (DYKOSKI ET AL., 2005) are in agreement with our $\delta^{18}O$ records (Fig. 3.5). Monsoon intensity in eastern Africa may have played an essential role in controlling the stable isotope composition of precipitation, as recorded in our Bale Mountain archive and reconstructed $\delta^{18}O$ values. However, modern data suggest that the amount effect alone does not explain the $\delta^{18}O_{precipitation}$ pattern in eastern Africa (COSTA ET AL., 2014; LEMMA ET AL., 2020). Therefore, COSTA ET AL. (2014) question the primary influence of the amount effect for Lake Tana, Ethiopia, and suggest that an Atlantic moisture source (Congo Basin) is responsible for both past and current depleted $\delta^{18}O_{precipitation}$ values. Back trajectories for modern precipitation at Lake Tana show an average contribution from Congo Basin air masses of 13 %. The primary source is the Indian Ocean (80 %) with only a minor contribution of 7 % from the Mediterranean and Red Sea (COSTA ET AL., 2014). In contrast, other climate studies for Ethiopia have found only minor (VISTE & SORTEBERG, 2013) or no air mass contribution from the Congo Basin (LEVIN ET AL., 2009). However, a recent study by FINNEY ET AL. (2020) suggests that despite the low air mass contribution, westerly winds are responsible for a disproportionally high amount of rainfall in eastern Africa. For the Bale Mountains, a recent back-trajectory study found air mass contributions principally from the Indian Ocean and the Mediterranean and Red Sea but no evidence for any contribution or even an isotopic depletion due to Congo Basin air masses (LEMMA ET AL., 2020).

Even if these air mass contributions are not now influencing rainfall in southeastern Ethiopia (LEVIN ET AL., 2009) or the Bale Mountains (LEMMA ET AL., 2020), a past change of atmospheric circulation could have exerted a significant effect on the isotopic composition of paleo records (JUNGINGER ET AL., 2014; TIERNEY ET AL., 2011a). We, however, have no further evidence to test potential past source contributions at our study site. A change in moisture source might explain some $\delta^{18}O$ variations in the Garba Guracha archive. However, because our ^{18}O records are of aquatic origin, unlike other records, we reconstructed $\delta^{18}O_{lake\ water}$, not $\delta^{18}O_{precipitation}$, and suggest an additional strong influence of evaporative enrichment in the Garba Guracha record.

In open lake systems, $\delta^{18}O_{precipitation}$ is the most crucial control on $\delta^{18}O_{lake\ water}$, whereas in closed lake systems, evaporative enrichment is the primary driver (HORTON ET AL., 2016; LAMB ET AL., 2002; TALBOT, 1990) (Fig. B.1). Garba Guracha in modern times, with a sill level at 6 m above the sediment surface at the lake's maximum depth, is an open lake during the wet season and a closed lake system during the dry season (Fig. B.6). Lake water samples taken during the dry season (+4.7 ‰, ± 0.6 ‰; February 2017) are enriched by at least 9.2 ‰ compared to the annual mean $\delta^{18}O_{precipitation}$ of -4.5 ‰ (Angesso station 2017; max: -1.9 ‰, min -6.2 ‰). This confirms that evaporative enrichment is able to explain a large part of the variability in the $\delta^{18}O_{fucose}$ record (range of 11.5 ‰). Therefore, the reconstructed $\delta^{18}O_{lake\ water}$

record of Garba Guracha likely represents changes from an open to a closed lake system and wet/dry phases, and can be interpreted in terms of precipitation-to-evaporation ratio (P/E).

3.4.5 Comparison with other records

11 - 7 cal ka BP

Our $\delta^{18}O_{fuc}$ record suggests a high P/E at the end of the Younger Dryas, shown by values increasing to a maximum at 11 cal ka BP. This is supported by a change from organic-poor to organic-rich sedimentation, indicating a shift to favorable growth conditions for aquatic algae (BITTNER ET AL., 2020). *Erica* expanded near the lake (GIL-ROMERA ET AL., 2019) at the onset of the Holocene (11.5 - 10 cal ka BP), which supports our interpretation of increased rainfall and rising P/E values. Along with such an increase, but lagged for some centuries (~ 10.7 cal ka BP), wildfires were triggered in the Garba Guracha catchment (GIL-ROMERA ET AL., 2019). This is possible evidence that rainfall seasonality was in place at this time, permitting dry phases favoring fire, and facilitated by enhanced biomass accumulation (GIL-ROMERA ET AL., 2019). MEYER ET AL., (2020) suggested a coincident wet phase (11 - 9.5 ka) in the Lake Chala region due to changes in the intensity of the monsoon system.

However, a maximum of $\delta^{18}O_{fuc}$ in the Garba Guracha sediments at 10.2 cal ka BP coincides with a lake level drop in Lake Turkana (BLOSZIES ET AL., 2015; JUNGINGER ET AL., 2014) and interrupts the trend towards more humid conditions (Fig. 3.5). Both $\delta^{18}O_{diatom}$ and $\delta^{18}O_{fuc}$, but especially $\delta^{18}O_{fuc}$, indicate a pronounced phase of depleted $\delta^{18}O$ values between 10 and 7 cal ka BP; suggesting a high P/E ratio due to increased rainfall amounts, a more permanent open lake phase with more constant overflow, and less evaporative enrichment. This is in agreement with the modeled overflow of Paleolake Suguta, Kenya, eastern Africa (JUNGINGER ET AL., 2014) (Fig. 3.5). JUNGINGER ET AL. (2014) suggested that the lake reached its sill level several times between 10 - 8.5 cal ka BP and overflowed more or less continuously from 8.5 cal ka BP until ~ 7 cal ka BP. Enhanced moisture transport into the region, indicated by reconstructed high lake levels and stronger runoff during the AHP, is well documented in the literature (BECK ET AL., 2019; FERSI ET AL., 2016; FOERSTER ET AL., 2012; JAESCHKE ET AL., 2020; LIU ET AL., 2017b; MOLOGNI ET AL., 2020; MORRISSEY & SCHOLZ, 2014; TIERNEY & DEMENOCAL, 2013; TIERNEY ET AL., 2011b; WAGNER ET AL., 2018)

A brief shift towards more positive $\delta^{18}O$ values is present in all records coinciding with the 8.2 cal ka BP event in the northern hemisphere, known as a short cold spell in Greenland with reduced precipitation (BOND ET AL., 1997; DANSGAARD ET AL., 1993). A period of low lake levels and drought has also been reconstructed in eastern Africa for the Ziway-Shala system (GILLESPIE ET AL., 1983), Lake Malawi (GASSE ET AL., 2002), Lake Turkana (GARCIN ET AL., 2012), Paleolake Suguta (JUNGINGER ET AL., 2014), Lake Abhè (GASSE, 2000), and Lake Tilo (LENG ET AL., 1999) at that time. THOMPSON ET AL. (2002) found a maximum in wind-blown fluoride derived from dry lake basins in the Kilimanjaro ice record at ~ 8.4 cal ka BP. However, the increase in $\delta^{18}O_{diatom}$ and $\delta^{18}O_{fuc}$ in Garba Guracha is rather small in comparison with the range of most regional records. This might be due to a muted precipitation change in our high-altitude

archive compared to lower altitude sites or due to a temperature change rather than a precipitation decrease.

After this drought phase, $\delta^{18}O_{diatom}$ and $\delta^{18}O_{fuc}$ decrease again, indicating a return to humid conditions and high lake levels (Fig. 3.5). With the start of declining boreal summer insolation at ~ 8.7 cal ka BP, the atmospheric circulation pattern changed, and the influence of the CAB decreased in eastern Africa (JUNGINGER ET AL., 2014; WAGNER ET AL., 2018). This can be seen in our record since 7 cal ka BP when $\delta^{18}O_{diatom}$ and $\delta^{18}O_{fuc}$ values start to increase, indicating a shift to decreased precipitation and stronger evaporative enrichment. The phase between 10 - 7 cal ka BP indicates an overall increase in moisture availability concurring with the AHP.

7 - 4 cal ka BP

Strong variability in $\delta^{18}O_{fuc}$ from 6 - 4 cal ka BP coincides with the termination of the AHP. The timing of the AHP termination has been debated, and seems to be related to individual proxy responses (CASTAÑEDA ET AL., 2016). *Erica* and fire experienced maxima and minima during this period at Garba Guracha, but consistently decreased towards absolute minima from 5.2 - 2.5 cal ka BP (GIL-ROMERA ET AL., 2019), while the *Botryococcus braunii* content (UMER ET AL., 2007) and TOC values drop later at 4.5 cal ka BP (BITTNER ET AL., 2020). This asynchronous proxy response may be related to the differential sensitivity of proxies to environmental change and individual drivers (CASTAÑEDA ET AL., 2016). Furthermore, differences in the timing of the response of various biological processes to climatic change make it difficult to assign cause and effect (e.g., perennial plants such as *Erica* may have declined, but seasonal organic matter production in the lake or transport into the lake could have continued, delaying any decline in TOC to later decades or centuries).

Despite strong variability, the mean trends in Garba Guracha $\delta^{18}O$ values indicate a continuous transition from a humid phase before 7 cal ka BP towards a more stable arid phase after 4 cal ka BP. The more positive $\delta^{18}O$ values after 4 cal ka BP suggest a dry climate with stronger evaporative enrichment and at least seasonally low lake levels.

In the regional context, contemporaneous decreases in lake levels have been found at north Ethiopian lakes Ziway-Shala and Abhé at ~ 4 - 4.5 cal ka BP (GASSE, 2000; GILLESPIE ET AL., 1983; KHALIDI ET AL., 2020). More southern lakes, including Paleolake Suguta, Lake Turkana, and Chew Bahir, show an earlier AHP termination at ~ 5 - 5.5 cal ka BP (FOERSTER ET AL., 2012; GARCIN ET AL., 2012; JUNGINGER ET AL., 2014).

4 cal ka BP to present

The most positive values of $\delta^{18}O_{diatom}$ in the entire record coincide with very positive $\delta^{18}O_{fuc}$ values at 3.5 cal ka BP, suggesting a reduced P/E ratio and a low lake level at Garba Guracha. After 3.5 cal ka BP, the $\delta^{18}O_{diatom}$ and $\delta^{18}O_{fuc}$ values decrease, indicating a higher P/E ratio and increased lake level. In response to wetter conditions at 2.5 cal ka BP, an expanding heathland and more active fires may have occurred (GIL-ROMERA ET AL., 2019). However, we cannot rule out a human origin for these fires, and subsequent re-expansion of *Erica* at particular areas within the basin because anthropogenically induced changes have been detected at lower

altitudes during this period (BONNEFILLE & MOHAMMED, 1994). Our findings are consistent with those of (GASSE & VAN CAMPO, 1994) who found a more humid phase in eastern Africa at ~ 2.5 cal ka BP. The diatom record of Lake Ashenge also shows a humid phase between 2.5 - 1.5 cal ka BP (MACHADO ET AL., 1998). Moreover, a data comparison presented by LEZINE ET AL. (2014) indicates increased humid conditions at the Horn of Africa between 3.5 - 1.5 cal ka BP.

During the last 1.5 cal ka BP, decreasing $\delta^{18}O_{fuc}$ and $\delta^{18}O_{diatom}$ values in Garba Guracha support a shift towards increased dryness at Lake Tana (documented by MARSHALL ET AL. (2011)). A minimum in $\delta^{18}O_{fuc}$ at 0.5 cal ka BP may coincide with the timing of the Little Ice Age (GROVE, 2004).

3.5 Conclusions

In eastern Africa, and especially in the Horn of Africa region, the relative scarcity of high-altitude climate proxy reconstructions inhibits understanding of regional climate change and ecosystem reaction during the Holocene and earlier. The continuous Garba Guracha archive with a high-resolution chronology allows us to present and interpret the first high-altitude (> 3500 m a. s. l.) $\delta^{18}O_{sugar}$ and $\delta^{18}O_{diatom}$ records from the Horn of Africa. Because of the small catchment area of Garba Guracha, the sugar biomarker fucose is primarily of aquatic origin. The similar trends of $\delta^{18}O_{fuc}$ and $\delta^{18}O_{diatom}$ results therefore indicate that $\delta^{18}O_{fuc}$ is a valuable proxy for $\delta^{18}O_{lake\ water}$.

Besides possible variation in the source effect, we conclude that in the case of reconstructed $\delta^{18}O_{lake\ water}$ record, the effect of evaporative enrichment has to be considered to gain a better understanding of eastern African climate change. We conclude that, in general, precipitation increased at the beginning of the Holocene, leading to a primarily open lake system between ~ 10 and ~ 8 cal ka BP, with lowest $\delta^{18}O_{lake\ water}$ values due to increased precipitation and reduced evaporative enrichment (lower P/E). When the lake was open and overflowing, the $\delta^{18}O_{lake\ water}$ was less affected by evaporative enrichment, so the evaporative signal did not overprint the precipitation source and amount effects in the $\delta^{18}O_{lake\ water}$ values.

At ~ 7 cal ka BP, a continuous shift towards drier conditions began, indicating a change towards a predominantly closed lake system. Small minima, representing phases of lower P/E, occurred at 10.8 cal ka BP, 10.2 cal ka BP, 3.5 cal ka BP, and 0.5 cal ka BP. At the temporal resolution of the Graba Guracha record, the 4.5 cal ka BP and 8.2 cal ka BP drought phases seen in eastern African lake records are not strongly imprinted in our isotope records and may point to a buffered and/or reduced response at high altitudes. Despite differences in apparent intensity, reconstructed dry and wet phases are broadly coincident with Rift Valley records, indicating similar climate controls. The Rift Valley records are influenced by eastward migration of the Congo Air Boundary, allowing Atlantic moisture to enter the region. However, the Garba Guracha record shows no evidence that the influence of Congo Basin air masses extended farther eastwards into the Bale Mountains in the past. Further studies are needed to disentangle the source and amount effects and evaporative enrichment in stable isotope records from eastern Africa.

3.6 Acknowledgements

This research was funded by the German Research Council (DFG) in the framework of the joint Ethio-European DFG Research Unit 2358 “The Mountain Exile Hypothesis. How humans benefited from and re-shaped African high-altitude ecosystems during Quaternary climate changes.” We are grateful to the project coordination, the Philipps University Marburg, University of Addis Ababa, the Frankfurt Zoological Society, the Ethiopian Wolf Conservation Programme, the Bale Mountains National Park, and the related staff members, especially Katinka Thielsen and Mekbib Fekadu for their logistic assistance during our fieldwork. We thank the Ethiopian Wildlife Conservation Authority for permitting our research in the Bale Mountains National Park. We thank the team of the Soil Biogeochemistry Department at Martin Luther University Halle Saale for support during lab work, in particular Marianne Benesch and Heike Maennike. We thank Dr. Miguel Sevillia-Callejo for creating the maps in Figure 1. We are grateful to two anonymous reviewers for their helpful and detailed work improving the publication.

3.7 References

ALTERMATT, H. A., & NEISH, A. C. (1956): The biosybnthesis of cell wall carbonhydrates: III. Further studies on formation of cellulose and xylan from labeled monosaccharides in wheat plants. - Canadian Journal of Biochemistry and Physiology, **34**, 405–413.

AMELUNG, W., CHESHIRE, M. V, & GUGGENBERGER, G. (1996): Determination of neutral and acidic sugars in soil by capillary gas-liquid chromatography after trifluoroacetic acid hydrolysis. - Soil Biology and Biochemistry, **28**, 1631–1639.

ARNAUD, F., POULENARD, J., GIGUET-COVEX, C., WILHELM, B., RÉVILLON, S., JENNY, J.-P., REVEL, M., ENTERS, D., BAJARD, M., FOUINAT, L., DOYEN, E., SIMONNEAU, A., PIGNOL, C., CHAPRON, E., VANNIÈRE, B., & SABATIER, P. (2016): Erosion under climate and human pressures: An alpine lake sediment perspective. - Quaternary Science Reviews, **152**, 1–18.

BAILEY, H. L., HENDERSON, A. C. G., SLOANE, H. J., SNELLING, A., LENG, M. J., & KAUFMAN, D. S. (2014): The effect of species on lacustrine $\delta^{18}O$ diatom and its implications for palaeoenvironmental reconstructions. - Journal of Quaternary Science, **29**, 393–400.

BAILEY, H. L., KAUFMAN, D. S., HENDERSON, A. C. G., & LENG, M. J. (2015): Synoptic scale controls on the $\delta^{18}O$ in precipitation across Beringia. - Geophysical Research Letters, **42**, 4608–4616.

BARKER, P. A., STREET-PERROTT, F. A., LENG, M. J., GREENWOOD, P. B., SWAIN, D. L., PERROTT, R. A., TELFORD, R. J., & FICKEN, K. J. (2001): A 14,000-Year Oxygen Isotope Record from Diatom Silica in Two Alpine Lakes on Mt. Kenya. - Science, **292**, 2307 LP – 2310.

BARKER, P. A., TALBOT, M. R., STREET-PERROTT, F. A., MARRET, F., SCOURSE, J., & ODADA, E. O. (2004): Late Quaternary climatic variability in intertropical Africa BT - Past Climate Variability through Europe and Africa. - In R. W. Battarbee, F. Gasse, & C. E. Stickley (Eds.), (pp. 117–

138). - Dordrecht: Springer Netherlands.

BARKER, P. A., LENG, M. J., GASSE, F., & HUANG, Y. (2007): Century-to-millennial scale climatic variability in Lake Malawi revealed by isotope records. - Earth and Planetary Science Letters, **261**, 93–103.

BARKER, P. A., HURRELL, E. R., LENG, M. J., WOLFF, C., COCQUYT, C., SLOANE, H. J., & VERSCHUREN, D. (2011): Seasonality in equatorial climate over the past 25 k.y. revealed by oxygen isotope records from Mount Kilimanjaro. - Geology, **39**, 1111–1114.

BECK, C. C., FEIBEL, C. S., WRIGHT, J. D., & MORTLOCK, R. A. (2019): Onset of the African Humid Period by 13.9 kyr BP at Kabua Gorge, Turkana Basin, Kenya. - Holocene, **29**, 1011–1019.

BERKE, M. A., JOHNSON, T. C., WERNE, J. P., SCHOUTEN, S., & SINNINGHE DAMSTÉ, J. S. (2012): A mid-Holocene thermal maximum at the end of the African Humid Period. - Earth and Planetary Science Letters, **351**–**352**, 95–104.

BIRD, M. I., HAIG, J., HADEEN, X., RIVERA-ARAYA, M., WURSTER, C. M., & ZWART, C. (2020): Stable isotope proxy records in tropical terrestrial environments. - Palaeogeography, Palaeoclimatology, Palaeoecology, **538**, 109445.

BITTNER, L., BLIEDTNER, M., GRADY, D., GIL-ROMERA, G., MARTIN-JONES, C., LEMMA, B., MEKONNEN, B., LAMB, H. F., YANG, H., GLASER, B., SZIDAT, S., SALAZAR, G., ROSE, N. L., OPGENOORTH, L., MIEHE, G., ZECH, W., & ZECH, M. (2020): Revisiting afro-alpine Lake Garba Guracha in the Bale Mountains of Ethiopia: rationale, chronology, geochemistry, and paleoenvironmental implications. - Journal of Paleolimnology.

BLOSZIES, C., FORMAN, S. L., & WRIGHT, D. K. (2015): Water level history for Lake Turkana, Kenya in the past 15,000 years and a variable transition from the African Humid Period to Holocene aridity. - Global and Planetary Change, **132**, 64–76.

BOND, G., SHOWERS, W., CHESEBY, M., LOTTI, R., ALMASI, P., DEMENOCAL, P., PRIORE, P., CULLEN, H., HAJDAS, I., & BONANI, G. (1997): A Pervasive Millennial-Scale Cycle in North Atlantic Holocene and Glacial Climates. - Science, **278**, 1257 LP – 1266.

BONNEFILLE, R., & MOHAMMED, U. (1994): Pollen-inferred climatic fluctuations in Ethiopia during the last 3000 years. - Palaeogeography, Palaeoclimatology, Palaeoecology, **109**, 331–343.

BRANDRISS, M. E., O'NEIL, J. R., EDLUND, M. B., & STOERMER, E. F. (1998): Oxygen Isotope Fractionation Between Diatomaceous Silica and Water. - Geochimica et Cosmochimica Acta, **62**, 1119–1125.

BROWN, F. H., & FULLER, C. R. (2008): Stratigraphy and tephra of the Kibish Formation, southwestern Ethiopia. - Journal of Human Evolution, **55**, 366–403.

BURGET, E. G., VERMA, R., MØLHØJ, M., & REITER, W.-D. (2003): The Biosynthesis of l-Arabinose in Plants : Molecular Cloning and Characterization of a Golgi-Localized UDP-d-Xylose 4-Epimerase Encoded by the MUR4 Gene of Arabidopsis. - The Plant Cell, **15**, 523–531.

CAMBERLIN, P. (1997): Rainfall Anomalies in the Source Region of the Nile and Their Connection with the Indian Summer Monsoon. - Journal of Climate, **10**, 1380–1392.

CARTIER, R., SYLVESTRE, F., PAILLÈS, C., SONZOGNI, C., COUAPEL, M., ALEXANDRE, A., MAZUR, J.-C., BRISSET, E., MIRAMONT, C., & GUITER, F. (2019): Diatom-oxygen isotope record from high-altitude Lake Petit (2200 m a.s.l.) in the Mediterranean Alps: shedding light on a climatic pulse at 4.2 ka. - Clim. Past, **15**, 253–263.

CASTAÑEDA, I. S., SCHOUTEN, S., PÄTZOLD, J., LUCASSEN, F., KASEMANN, S., KUHLMANN, H., & SCHEFUß, E. (2016): Hydroclimate variability in the Nile River Basin during the past 28,000 years. - Earth and Planetary Science Letters, **438**, 47–56.

CATALAN, J., CAMARERO, L., FELIP, M., PLA, S., VENTURA, M., BUCHACA, T., BARTUMEUS, F., MENDOZA, G. DE, MIRÓ, A., CASAMAYOR, E., MEDINA-SÁNCHEZ, J., BACARDIT, M., ALTUNA, M., BARTRONS, M., & QUIJANO, D. (2006): High mountain lakes: Extreme habitats and witnesses of environmental changes. - Limnetica, **25**, 551–584.

CATALAN, J., PLA-RABÉS, S., WOLFE, A. P., SMOL, J. P., RÜHLAND, K. M., ANDERSON, N. J., KOPÁČEK, J., STUCHLÍK, E., SCHMIDT, R., KOINIG, K. A., CAMARERO, L., FLOWER, R. J., HEIRI, O., KAMENIK, C., KORHOLA, A., LEAVITT, P. R., PSENNER, R., & RENBERG, I. (2013): Global change revealed by palaeolimnological records from remote lakes: a review. - Journal of Paleolimnology, **49**, 513–535.

CHAPLIGIN, B., MEYER, H., FRIEDRICHSEN, H., MARENT, A., SOHNS, E., & HUBBERTEN, H.-W. (2010): A high-performance, safer and semi-automated approach for the $\delta^{18}O$ analysis of diatom silica and new methods for removing exchangeable oxygen. - Rapid Communications in Mass Spectrometry, **24**, 2655–2664.

CHAPLIGIN, B., LENG, M. J., WEBB, E., ALEXANDRE, A., DODD, J. P., IJIRI, A., LÜCKE, A., SHEMESH, A., ABELMANN, A., HERZSCHUH, U., LONGSTAFFE, F. J., MEYER, H., MOSCHEN, R., OKAZAKI, Y., REES, N. H., SHARP, Z. D., SLOANE, H. J., SONZOGNI, C., SWANN, G. E. A., SYLVESTRE, F., TYLER, J. J., & YAM, R. (2011): Inter-laboratory comparison of oxygen isotope compositions from biogenic silica. - Geochimica et Cosmochimica Acta, **75**, 7242–7256.

CHAPLIGIN, B., MEYER, H., BRYAN, A., SNYDER, J., & KEMNITZ, H. (2012): Assessment of purification and contamination correction methods for analysing the oxygen isotope composition from biogenic silica. - Chemical Geology, **300**–**301**, 185–199.

CLAYTON, R. N., & MAYEDA, T. K. (1963): The use of bromine pentafluoride in the extraction of oxygen from oxides and silicates for isotopic analysis. - Geochimica et Cosmochimica Acta, **27**, 43–52.

COLE, J. E., RIND, D., WEBB, R. S., JOUZEL, J., & HEALY, R. (1999): Climatic controls on interannual variability of precipitation $\delta^{18}O$: Simulated influence of temperature, precipitation amount, and vapor source region. - Journal of Geophysical Research: Atmospheres, **104**, 14223–14235.

COLLINS, J. A., PRANGE, M., CALEY, T., GIMENO, L., BECKMANN, B., MULITZA, S., SKONIECZNY, C., ROCHE, D., & SCHEFUß, E. (2017): Rapid termination of the African Humid Period triggered by northern high-latitude cooling. - Nature Communications, **8**.

COSTA, K., RUSSELL, J., KONECKY, B., & LAMB, H. (2014): Isotopic reconstruction of the African Humid Period and Congo Air Boundary migration at Lake Tana, Ethiopia. - Quaternary Science Reviews, **83**, 58–67.

CRESPIN, J., SYLVESTRE, F., ALEXANDRE, A., SONZOGNI, C., PAILLÈS, C., & PERGA, M.-E. (2010): Re-examination of the temperature-dependent relationship between $\delta^{18}O$ diatoms and $\delta^{18}O$ lake water and implications for paleoclimate inferences. - Journal of Paleolimnology, **44**, 547–557.

DANSGAARD, W. (1964): Stable isotopes in precipitation. - Tellus, **16**, 436–468.

DANSGAARD, W., JOHNSEN, S. J., CLAUSEN, H. B., DAHL-JENSEN, D., GUNDESTRUP, N. S., HAMMER, C. U., HVIDBERG, C. S., STEFFENSEN, J. P., SVEINBJÖRNSDOTTIR, A. E., JOUZEL, J., & BOND, G. (1993): Evidence for general instability of past climate from a 250-kyr ice-core record. - Nature, **364**, 218–220. Retrieved from https://doi.org/10.1038/364218a0

DAVIES, T. D., VINCENT, C. E., & BERESFORD, A. K. C. (1985): July-August rainfall in West-Central Kenya. - Journal of Climatology, **5**, 17–33.

DEMENOCAL, P., ORTIZ, J., GUILDERSON, T., ADKINS, J., SARNTHEIN, M., BAKER, L., & YARUSINSKY, M. (2000): Abrupt onset and termination of the African Humid Period: - Quaternary Science Reviews, **19**, 347–361.

DODD, J. P., & SHARP, Z. D. (2010): A laser fluorination method for oxygen isotope analysis of biogenic silica and a new oxygen isotope calibration of modern diatoms in freshwater environments. - Geochimica et Cosmochimica Acta, **74**, 1381–1390.

DODD, J. P., SHARP, Z. D., FAWCETT, P. J., BREARLEY, A. J., & MCCUBBIN, F. M. (2012): Rapid post-mortem maturation of diatom silica oxygen isotope values. - Geochemistry, Geophysics, Geosystems, **13**.

DYKOSKI, C. A., EDWARDS, R. L., CHENG, H., YUAN, D., CAI, Y., ZHANG, M., LIN, Y., QING, J., AN, Z., & REVENAUGH, J. (2005): A high-resolution, absolute-dated Holocene and deglacial Asian monsoon record from Dongge Cave, China. - Earth and Planetary Science Letters, **233**, 71–86.

FERSI, W., LÉZINE, A.-M., & BASSINOT, F. (2016): Hydro-climate changes over southwestern Arabia and the Horn of Africa during the last glacial–interglacial transition: A pollen record from the Gulf of Aden. - Review of Palaeobotany and Palynology, **233**, 176–185.

FINNEY, D. L., MARSHAM, J. H., WALKER, D. P., BIRCH, C. E., WOODHAMS, B. J., JACKSON, L. S., & HARDY, S. (2020): The effect of westerlies on East African rainfall and the associated role of tropical cyclones and the Madden–Julian Oscillation. - Quarterly Journal of the Royal Meteorological Society, **146**, 647–664.

FLEITMANN, D., BURNS, S. J., NEFF, U., MANGINI, A., & MATTER, A. (2003): Changing moisture sources over the last 330,000 years in Northern Oman from fluid-inclusion evidence in speleothems. - Quaternary Research, **60**, 223–232.

FOERSTER, V., JUNGINGER, A., LANGKAMP, O., GEBRU, T., ASRAT, A., UMER, M., LAMB, H. F., WENNRICH, V., RETHEMEYER, J., NOWACZYK, N., TRAUTH, M. H., & SCHAEBITZ, F. (2012): Climatic change recorded in the sediments of the Chew Bahir basin, southern Ethiopia, during the last 45,000 years. - Quaternary International, **274**, 25–37.

GARCIN, Y., MELNICK, D., STRECKER, M. R. M. R., OLAGO, D., & TIERCELIN, J.-J. J.-J. (2012): East African mid-Holocene wet–dry transition recorded in palaeo-shorelines of Lake Turkana, northern Kenya Rift. - Earth and Planetary Science Letters, **331**–**332**, 322–334.

GASSE, F. (2000): Hydrological changes in the African tropics since the Last Glacial Maximum. - Quaternary Science Reviews, **19**, 189–211.

GASSE, F., & VAN CAMPO, E. (1994): Abrupt post-glacial climate events in West Asia and North Africa monsoon domains. - Earth and Planetary Science Letters, **126**, 435–456.

GIL-ROMERA, G., ADOLF, C., BENITO BLAS, M., BITTNER, L., JOHANSSON, M. M. U., GRADY, D. D. A., LAMB, H. H. F., LEMMA, B., FEKADU, M., GLASER, B., MEKONNEN, B., SEVILLA-CALLEJO, M., ZECH, M., ZECH, W., MIEHE, G. (2019): Long-term fire resilience of the Ericaceous Belt, Bale Mountains, Ethiopia. - Biology Letters, **15**, 20190357.

GILLESPIE, R., STREET-PERROTT, F. A., & SWITSUR, R. (1983): Post-glacial arid episodes in Ethiopia have implications for climate prediction. - Nature, **306**, 680–683.

GROOS, A. R., NIEDERHAUSER, J., WRAASE, L., HÄNSEL, F., NAUSS, T., AKÇAR, N., & VEIT, H. (2020): Implications of present ground temperatures and relict stone stripes in the Ethiopian Highlands for the palaeoclimate of the tropics. - Earth Surf. Dynam. Discuss., **2020**, 1–37.

GROOS, A., AKÇAR, N., YESILYURT, S., MIEHE, G., VOCKENHUBER, C., & VEIT, H. (2021): Nonuniform Late Pleistocene glacier fluctuations in tropical Eastern Africa. - Science Advances, **7**.

GROVE, J. M. (2004): Little Ice Ages (2nd ed.). - London: Routledge.

HARPER, A. D., & BAR-PELED, M. (2002): Biosynthesis of UDP-xylose. Cloning and characterization of a novel Arabidopsis gene family, UXS, encoding soluble and putative membrane-bound UDP-glucuronic acid decarboxylase isoforms. - Plant Physiology, **130**, 2188–2198.

HEPP, J., TUTHORN, M., ZECH, R., MÜGLER, I., SCHLÜTZ, F., ZECH, W., & ZECH, M. (2015): Reconstructing lake evaporation history and the isotopic composition of precipitation by a coupled δ^2H-δ^{18}O biomarker approach. - Journal of Hydrology, **529**, 622–631.

HEPP, J., RABUS, M., ANHÄUSER, T., BROMM, T., LAFORSCH, C., SIROCKO, F., GLASER, B., & ZECH, M. (2016): A sugar biomarker proxy for assessing terrestrial versus aquatic sedimentary input. - Organic Geochemistry, **98**, 98–104.

HEPP, J., ZECH, R., ROZANSKI, K., TUTHORN, M., GLASER, B., GREULE, M., KEPPLER, F., HUANG, Y., ZECH, W.,

& ZECH, M. (2017): Late Quaternary relative humidity changes from Mt. Kilimanjaro, based on a coupled ^{2}H-^{18}O biomarker paleohygrometer approach. - Quaternary International, **438**, 116–130.

HEPP, J., GLASER, B., JUCHELKA, D., MAYR, C., ROZANSKI, K., SCHÄFER, I. K., STICHLER, W., TUTHORN, M., ZECH, R., & ZECH, M. (2019a): Validation of a coupled $\delta^{2}H_{n\text{-}alkane}$-$\delta^{18}O_{sugar}$ paleohygrometer approach based on a climate chamber experiment. - Biogeosciences Discuss., **2019**, 1–30.

HEPP, J., WÜTHRICH, L., BROMM, T., BLIEDTNER, M., SCHÄFER, I. K., GLASER, B., ROZANSKI, K., SIROCKO, F., ZECH, R., & ZECH, M. (2019b): How dry was the Younger Dryas? Evidence from a coupled $\delta^{2}H$–$\delta^{18}O$ biomarker paleohygrometer applied to the Gemündener Maar sediments, Western Eifel, Germany. - Clim. Past, **15**, 713–733.

HILLMAN, J. (1986): Conservation in Bale Mountains National Park, EthiopiaOryx (Vol. 20).

HILLMAN, J. (1988): The Bale Mountains National Park Area, Southeast Ethiopia, and Its ManagementMountain Research and Development (Vol. 8).

HILLS, R. C. (1979): The Structure of the Inter-Tropical Convergence Zone in Equatorial Africa and Its Relationship to East African Rainfall. - Transactions of the Institute of British Geographers, **4**, 329–352.

HORTON, T. W., DEFLIESE, W. F., TRIPATI, A. K., & OZE, C. (2016): Evaporation induced 18O and 13C enrichment in lake systems: A global perspective on hydrologic balance effects. - Quaternary Science Reviews, **131**, 365–379.

JAESCHKE, A., THIENEMANN, M., SCHEFUß, E., URBAN, J., SCHÄBITZ, F., WAGNER, B., & RETHEMEYER, J. (2020): Holocene Hydroclimate Variability and Vegetation Response in the Ethiopian Highlands (Lake Dendi). - Frontiers in Earth Science, **8**, 1–14.

JOHNSON, T. C., HALFMAN, J. D., & SHOWERS, W. J. (1991): Paleoclimate of the past 4000 years at Lake Turkana, Kenya, based on the isotopic composition of authigenic calcite. - Palaeogeography, Palaeoclimatology, Palaeoecology, **85**, 189–198.

JUNGINGER, A., ROLLER, S., OLAKA, L. A., & TRAUTH, M. H. (2014): The effects of solar irradiation changes on the migration of the Congo Air Boundary and water levels of paleo-Lake Suguta , Northern Kenya Rift , during the African Humid Period (15 – 5 ka BP). - Palaeogeography, Palaeoclimatology, Palaeoecology, **396**, 1–16.

KHALIDI, L., MOLOGNI, C., MÉNARD, C., COUDERT, L., GABRIELE, M., DAVTIAN, G., CAULIEZ, J., LESUR, J., BRUXELLES, L., CHESNAUX, L., REDAE, B. E., HAINSWORTH, E., DOUBRE, C., REVEL, M., SCHUSTER, M., & ZAZZO, A. (2020): 9000 years of human lakeside adaptation in the Ethiopian Afar: Fisher-foragers and the first pastoralists in the Lake Abhe basin during the African Humid Period. - Quaternary Science Reviews, **243**, 106459.

KIDANE, Y., STAHLMANN, R., & BEIERKUHNLEIN, C. (2012): Vegetation dynamics, and land use and land cover change in the Bale Mountains, Ethiopia. - Environmental Monitoring and

Assessment, **184**, 7473–7489.

KNAPP, D. R. (1979): Handbook of Analytical Derivatization Reactions. - New York, Chichester, Brisbane, Toronto, Singapore: John Wiley & Sons.

KOSTROVA, S. S., MEYER, H., CHAPLIGIN, B., TARASOV, P. E., & BEZRUKOVA, E. V (2014): The last glacial maximum and late glacial environmental and climate dynamics in the Baikal region inferred from an oxygen isotope record of lacustrine diatom silica. - Quaternary International, **348**, 25–36.

KOSTROVA, S. S., MEYER, H., BAILEY, H. L., LUDIKOVA, A. V, GROMIG, R., KUHN, G., SHIBAEV, Y. A., KOZACHEK, A. V, EKAYKIN, A. A., & CHAPLIGIN, B. (2019): Holocene hydrological variability of Lake Ladoga, northwest Russia, as inferred from diatom oxygen isotopes. - Boreas, **48**, 361–376.

LABEYRIE, L. (1974): New approach to surface seawater palaeotemperatures using 18O/16O ratios in silica of diatom frustules. - Nature, **248**, 40–42.

LAMB, H. F., KEBEDE, S., LENG, M. J., RICKETTS, D., TELFORD, R. J., & UMER, M. (2002): Origin and Isotopic Composition of Aragonite Laminae in an Ethiopian Crater Lake. - In The East African Great Lakes: Limnology, Palaeolimnology and Biodiversity (pp. 487–508).

LAMB, A., LENG, M., SLOANE, H., & TELFORD, R. (2005): A comparison of the palaeoclimate signals from diatom oxygen isotope ratios and carbonate oxygen isotope ratios from a low latitude crater lake. - Palaeogeography, Palaeoclimatology, Palaeoecology, **223**, 290–302.

LASKAR, J., ROBUTEL, P., JOUTEL, F., GASTINEAU, M., CORREIA, A. C. M., & LEVRARD, B. (2004): A long-term numerical solution for the insolation quantities of the Earth . - A&A, **428**, 261–285. Retrieved from https://doi.org/10.1051/0004-6361:20041335

LECLERC, A. J., & LABEYRIE, L. (1987): Temperature dependence of the oxygen isotopic fractionation between diatom silica and water. - Earth and Planetary Science Letters, **84**, 69–74.

LEMMA, B., KEBEDE GURMESSA, S., NEMOMISSA, S., OTTE, I., GLASER, B., & ZECH, M. (2020): Spatial and temporal ^{2}H and ^{18}O isotope variation of contemporary precipitation in the Bale Mountains, Ethiopia. - Isotopes in Environmental and Health Studies, **56**, 122–135.

LENG, M. J., LAMB, A. L., LAMB, H. F., & TELFORD, R. J. (1999): Palaeoclimatic implications of isotopic data from modern and early Holocene shells of the freshwater snail Melanoides tuberculata, from lakes in the Ethiopian Rift Valley. - Journal of Paleolimnology, **21**, 97–106.

LENG, M., BARNKER, P., GREENWOOD, P., ROBERTS, N., & REED, J. (2001): Oxygen isotope analysis of diatom silica and authigenic calcite from Lake Pinarbasi, Turkey. - Journal of Paleolimnology, **25**, 343–349.

LENG, M. J., & BARKER, P. A. (2006): A review of the oxygen isotope composition of lacustrine

diatom silica for palaeoclimate reconstruction. - Earth-Science Reviews, **75**, 5–27.

LEVIN, N. E., ZIPSER, E. J., & CEDING, T. E. (2009): Isotopic composition of waters from Ethiopia and Kenya: Insights into moisture sources for eastern Africa. - Journal of Geophysical Research Atmospheres, **114**, 1–13.

LEZINE, A.-M., BASSINOT, F., PETERSCHMITT, J. Y. J.-Y., LÉZINE, A. M., BASSINOT, F., & PETERSCHMITT, J. Y. J.-Y. (2014): Orbitally-induced changes of the Atlantic and Indian monsoons over the past 20,000 years: New insights based on the comparison of continental and marine records. - Bulletin de La Societe Geologique de France, **185**, 3–12.

LIU, X., RENDLE-BÜHRING, R., KUHLMANN, H., & LI, A. (2017): Two phases of the Holocene East African Humid Period: Inferred from a high-resolution geochemical record off Tanzania. - Earth and Planetary Science Letters, **460**, 123–134.

LÖFFLER, H. (1978): Limnology and paleolimnological data on the Bale Mountain Lakes. - Verth, International Verein. Limnology, **20**, 1131–1138.

MACHADO, M. J., PÉREZ-GONZÁLEZ, A., & BENITO, G. (1998): Paleoenvironmental Changes during the Last 4000 yr in the Tigray, Northern Ethiopia. - Quaternary Research, **49**, 312–321.

MACKAY, A. W., SWANN, G. E. A., FAGEL, N., FIETZ, S., LENG, M. J., MORLEY, D., RIOUAL, P., & TARASOV, P. (2013): Hydrological instability during the Last Interglacial in central Asia: a new diatom oxygen isotope record from Lake Baikal. - Quaternary Science Reviews, **66**, 45–54.

MARSHALL, M., LAMB, H., DAVIES, S., LENG, M., BEDASO, Z., UMER, M., & BRYANT, C. (2009): Climatic change in northern Ethiopia during the past 17,000 years: A diatom and stable isotope record from Lake Ashenge. - Palaeogeography Palaeoclimatology Palaeoecology, **279**.

MARSHALL, M. H. M. H., LAMB, H. F. H. F., HUWS, D., DAVIES, S. J. S. J., BATES, R., BLOEMENDAL, J., BOYLE, J., LENG, M. J. M. J., UMER, M., & BRYANT, C. (2011): Late Pleistocene and Holocene drought events at Lake Tana, the source of the Blue Nile. - Global and Planetary Change, **78**, 147–161.

MAYR, C., LAPRIDA, C., LÜCKE, A., MARTÍN, R. S., MASSAFERRO, J., RAMÓN-MERCAU, J., & WISSEL, H. (2015): Oxygen isotope ratios of chironomids, aquatic macrophytes and ostracods for lake-water isotopic reconstructions – Results of a calibration study in Patagonia. - Journal of Hydrology, **529**, 600–607.

MEYER, H., CHAPLIGIN, B., HOFF, U., NAZAROVA, L., & DIEKMANN, B. (2015): Oxygen isotope composition of diatoms as Late Holocene climate proxy at Two-Yurts Lake, Central Kamchatka, Russia. - Global and Planetary Change, **134**, 118–128.

MEYER, I., VAN DAELE, M., TANGHE, N., DE BATIST, M., & VERSCHUREN, D. (2020): Reconstructing East African monsoon variability from grain-size distributions: End-member modeling and source attribution of diatom-rich sediments from Lake Chala. - Quaternary Science Reviews, **247**, 106574.

MIEHE, S., & MIEHE, G. (1994): Ericaceous forests and heathlands in the Bale mountains of South Ethiopia : ecology and man's impact (G. Miehe & 1952-, Eds.). - Reinbek: Reinbek : Warnke.

MOLOGNI, C., REVEL, M., BLANCHET, C., BOSCH, D., DEVELLE, A.-L., ORANGE, F., LUC, B., KHALIDI, L., DUCASSOU, E., & MIGEON, S. (2020): Frequency of exceptional Nile flood events as an indicator of Holocene hydro-climatic changes in the Ethiopian Highlands. - Quaternary Science Reviews, **247**.

MORLEY, D. W., LENG, M. J., MACKAY, A. W., & SLOANE, H. J. (2005): Late glacial and Holocene environmental change in the Lake Baikal region documented by oxygen isotopes from diatom silica. - Global and Planetary Change, **46**, 221–233.

MORRISSEY, A., & SCHOLZ, C. A. C. A. (2014): Paleohydrology of Lake Turkana and its influence on the Nile River system. - Palaeogeography, Palaeoclimatology, Palaeoecology, **403**, 88–100.

MOSCHEN, R., LÜCKE, A., & SCHLESER, G. H. (2005): Sensitivity of biogenic silica oxygen isotopes to changes in surface water temperature and palaeoclimatology. - Geophysical Research Letters, **32**.

NAKAMURA, K. (1968): Equatorial westerlies over East Africa and their climatological significance. - Geographical Review of Japan, **41**, 359–373.

NARANCIC, B., PIENITZ, R., CHAPLIGIN, B., MEYER, H., FRANCUS, P., & GUILBAULT, J.-P. (2016): Postglacial environmental succession of Nettilling Lake (Baffin Island, Canadian Arctic) inferred from biogeochemical and microfossil proxies. - Quaternary Science Reviews, **147**, 391–405.

OGIER, S., DISNAR, J.-R., ALBÉRIC, P., & BOURDIER, G. (2001): Neutral carbohydrate geochemistry of particulate material (trap and core sediments) in an eutrophic lake (Aydat, France). - Organic Geochemistry, **32**, 151–162.

OSMASTON, H. A., MITCHELL, W. A., & OSMASTON, J. A. N. (2005): Quaternary glaciation of the Bale Mountains, Ethiopia. - Journal of Quaternary Science, **20**, 593–606.

OSSENDORF, G., GROOS, A., BROMM, T., GIRMA TEKELEMARIAM, M., GLASER, B., LESUR, J., SCHMIDT, J., AKÇAR, N., BEKELE, T., BELDADOS, A., DEMISSEW, S., HADUSH KAHSAY, T., P NASH, B., NAUSS, T., NEGASH, A., NEMOMISSA, S., VEIT, H., VOGELSANG, R., ZERIHUN, W., & MIEHE, G. (2019): Middle Stone Age foragers resided in high elevations of the glaciated Bale Mountains, Ethiopia. - Science, **365**, 583–587.

POLISSAR, P. J., ABBOTT, M. B., SHEMESH, A., WOLFE, A. P., & BRADLEY, R. S. (2006): Holocene hydrologic balance of tropical South America from oxygen isotopes of lake sediment opal, Venezuelan Andes. - Earth and Planetary Science Letters, **242**, 375–389.

ROZANSKI, K., ARAGUÁS-ARAGUÁS, L., & GONFIANTINI, R. (1993): Isotopic Patterns in Modern Global Precipitation. - Climate Change in Continental Isotopic Records.

SCHMIDT, M., BOTZ, R., RICKERT, D., BOHRMANN, G., HALL, S. R., & MANN, S. (2001): Oxygen isotopes of marine diatoms and relations to opal-A maturation11Associate editor: B. Taylor. - Geochimica et Cosmochimica Acta, **65**, 201–211.

SHARP, Z. (2017): Principles of Stable Isotope Geochemistry, 2nd Edition.

TALBOT, M. R. (1990): A review of the palaeohydrological interpretation of carbon and oxygen isotopic ratios in primary lacustrine carbonates. - Chemical Geology: Isotope Geoscience Section, **80**, 261–279.

THOMPSON, L. G., MOSLEY-THOMPSON, E., DAVIS, M. E., HENDERSON, K. A., BRECHER, H. H., ZAGORODNOV, V. S., MASHIOTTA, T. A., LIN, P.-N., MIKHALENKO, V. N., HARDY, D. R., & BEER, J. J. (2002): Kilimanjaro Ice Core Records: Evidence of Holocene Climate Change in Tropical Africa. - Science, **298**, 589 LP – 593.

TIERNEY, J. E., & DEMENOCAL, P. B. (2013): Abrupt Shifts in Horn of Africa Hydroclimate Since the Last Glacial Maximum. - Science, **342**, 843–846.

TIERNEY, J. E., LEWIS, S. C., COOK, B. I., LEGRANDE, A. N., & SCHMIDT, G. A. (2011a): Model, proxy and isotopic perspectives on the East African Humid Period. - Earth and Planetary Science Letters, **307**, 103–112.

TIERNEY, J. E., RUSSELL, J. M., SINNINGHE DAMSTÉ, J. S., HUANG, Y., & VERSCHUREN, D. (2011b): Late Quaternary behavior of the East African monsoon and the importance of the Congo Air Boundary. - Quaternary Science Reviews, **30**, 798–807.

TUTHORN, M., ZECH, M., RUPPENTHAL, M., OELMANN, Y., KAHMEN, A., VALLE, H. F. DEL, WILCKE, W., GLASER, B., MAYR, C., , LEIBER, K., LEIBER-SAUHEITL, K., ZECH, M., (2014): Oxygen isotope ratios ($^{18}O/^{16}O$) of hemicellulose-derived sugar biomarkers in plants, soils and sediments as paleoclimate proxy II: Insight from a climate transect study. - Geochimica et Cosmochimica Acta, **126**, 624–634.

TYLER, J. J., SLOANE, H. J., RICKABY, R. E. M., COX, E. J., & LENG, M. J. (2017): Post-mortem oxygen isotope exchange within cultured diatom silica. - Rapid Communications in Mass Spectrometry, **31**, 1749–1760.

UHLIG, S. K. (1988): Mountain Forests and the Upper Tree Limit on the Southeastern Plateau of Ethiopia. - Mountain Research and Development, **8**, 227–234.

UHLIG, S., & UHLIG, K. (1991): Studies on the Altitudinal Zonation of Forests and Alpine Plants in the Central Bale Mountains, EthiopiaMountain Research and Development (Vol. 11).

UMER, M., LAMB, H. F., BONNEFILLE, R., LÉZINE, A. M., TIERCELIN, J. J., GIBERT, E., CAZET, J. P., & WATRIN, J. (2007): Late Pleistocene and Holocene vegetation history of the Bale Mountains, Ethiopia. - Quaternary Science Reviews, **26**, 2229–2246.

VAN DER LUBBE, H. J. L., KRAUSE-NEHRING, J., JUNGINGER, A., GARCIN, Y., JOORDENS, J. C. A., DAVIES, G. R., BECK, C., FEIBEL, C. S., JOHNSON, T. C., & VONHOF, H. B. (2017): Gradual or abrupt? Changes in

water source of Lake Turkana (Kenya) during the African Humid Period inferred from Sr isotope ratios. - Quaternary Science Reviews, **174**, 1–12.

VISTE, E., & SORTEBERG, A. (2013): Moisture transport into the Ethiopian highlands. - International Journal of Climatology, **33**, 249–263.

VUILLE, M., WERNER, M., BRADLEY, R. S., & KEIMIG, F. (2005): Stable isotopes in precipitation in the Asian monsoon region. - Journal of Geophysical Research: Atmospheres, **110**.

WAGNER, B., WENNRICH, V., VIEHBERG, F., JUNGINGER, A., KOLVENBACH, A., RETHEMEYER, J., SCHAEBITZ, F., & SCHMIEDL, G. (2018): Holocene rainfall runoff in the central Ethiopian highlands and evolution of the River Nile drainage system as revealed from a sediment record from Lake Dendi. - Global and Planetary Change, **163**, 29–43.

WATERHOUSE, J., CHENG, S., JUCHELKA, D., J.LOADER, N., MCCARROLL, D., SWITSUR, V. R., & GAUTAM, L. (2013): Position-specific measurement of oxygen isotope ratios in cellulose: Isotopic exchange during heterotrophic cellulose synthesis. - Geochimica et Cosmochimica Acta, **112**, 178–191.

WERDECKER, J. (1962): Eine Durchquerung des Goba-Massivs in Südäthiopien. - , **Hermann vo**, 132–144.

WILLIAMS, F. M. (2016): The Southeastern Highlands and the Ogaden. - In F. M. Williams (Ed.), Understanding Ethiopia: Geology and Scenery (pp. 153–170). - Cham: Springer International Publishing.

WILSON, K. E., MASLIN, M. A., LENG, M. J., KINGSTON, J. D., DEINO, A. L., EDGAR, R. K., & MACKAY, A. W. (2014): East African lake evidence for Pliocene millennial-scale climate variability. - Geology, **42**, 955–958.

WOLDU, Z., FEOLI, E., & NIGATU, L. (1989): Partitioning an elevation gradient of vegetation from southeastern Ethiopia by probabilistic methods. - Plant Ecology, **81**, 189–198.

ZECH, M., & GLASER, B. (2009): Compound-specific $\delta^{18}O$ analyses of neutral sugars in soils using gas chromatography-pyrolysis-isotope ratio mass spectrometry: problems, possible solutions and a first application. - Rapid Communications in Mass Spectrometry, **23**, 3522–3532.

ZECH, M., TUTHORN, M., ZECH, R., SCHLÜTZ, F., ZECH, W., & GLASER, B. (2014): A 16-ka $\delta^{18}O$ record of lacustrine sugar biomarkers from the High Himalaya reflects Indian Summer Monsoon variability. - Journal of Paleolimnology, **51**, 241–251.

Chapter 4

A Holocene temperature (brGDGT) record from Garba Guracha, a high-altitude lake in Ethiopia.

Lucas Bittner[1], Cindy De Jonge[2], Graciela Gil-Romera[3,4], Henry F. Lamb[5,6], James M. Russell[7], Michael Zech[1]

[1] Heisenberg Chair of Physical Geography with focus on paleoenvironmental research, Institute of Geography, Technische Universität Dresden, Dresden, Germany
[2] Geological Institute, Department of Earth Sciences, ETH Swiss Federal Institute of Technology, 8092 Zurich, Switzerland
[3] Plant Ecology and Geobotany dept., Philipps-Marburg University, Marburg, Germany.
[4] Department of Geo-environmental Processes and Global Change, Pyrenean Institute of Ecology, CSIC, Zaragoza, Spain
[5] Department of Geography and Earth Sciences, Aberystwyth University, Aberystwyth, UK.
[6] Department of Botany, School of Natural Sciences, Trinity College Dublin, Dublin 2, Ireland
[7] Department of Geological Sciences, Brown University, USA

Abstract

Eastern Africa has experienced strong climatic changes since the last deglaciation (15,000 years ago). The driving mechanisms and teleconnections of these spatially complex climate variations are yet not fully understood. Although previous studies on lake systems have enhanced our knowledge of Holocene precipitation variation in eastern Africa, relatively few studies have reconstructed the terrestrial temperature history of eastern Africa from lake archives. Here, we present (i) a new branched glycerol dialkyl glycerol tetraether (brGDGT) temperature calibration that includes Bale Mountain surface sediments and (ii) a quantitative record of mean annual temperature (MAT) over the past 12 cal ka BP using brGDGTs in a sediment core collected from Garba Guracha (3950 m a.s.l.) in the Bale Mountains. After adding Bale Mountain surface sediment (n = 11) data to the existing East African lake dataset, additional variation in 6-methyl brGDGTs was observed, which necessitated modifying the MBT'_{5ME} calibration by adding 6-methyl brGDGT IIIa' (resulting in the MBT-Bale Mountain index, $r^2 = 0.93$, $p < 0.05$). Comparing the MBT'_{5ME} and the new MBT-Bale Mountain index, our high-altitude Garba Guracha temperature record shows that warming occurred shortly after the Holocene onset when the temperature increased by more than 3.0 °C in less than 600 years. The highest temperatures prevailed between 9 and 6 cal ka BP, followed by a temperature decrease until 1.4 cal ka BP. The reconstructed temperature history is linked to supraregional climatic changes associated with insolation forcing and the African Humid Period (AHP), as well as with local anomalies associated with catchment deglaciation and hydrology.

4.1 Introduction

The severity of the current climate change and its global implications have been widely discussed following the latest report from the Intergovernmental Panel for Climate Change (IPCC) (IPCC, 2021). Uncertainty in future climate projection highlights the need for the scientific community to use palaeoclimate to estimate climate baseline conditions prior to human impact on climate (NEUKOM ET AL., 2019). Although palaeoclimatology has become a central discipline in understanding current climate variability (THOMPSON, 2004), important areas of the planet remain understudied. A partial understanding of global climate complexity can lead to biased views of natural systems (HUGHES ET AL., 2021). This is the case for the African continent in general and northeastern Africa in particular. Current climatic conditions in eastern Africa vary significantly due to its complex topography and the influence of the Intertropical Convergence Zone (ITCZ), the Indian Monsoon and the El Niño-Southern Oscillation. All of these affect temperature and the distribution, amount and timing of rainfall in the region, resulting in a wide range of climatic conditions from the warm, dry and semi-arid conditions of northern Kenya, south-eastern Ethiopia, Djibouti and Somalia to the cool, humid conditions of the western highlands (HOVE ET AL., 2011; LYON & VIGAUD, 2017; NICHOLSON, 2017).

There is clear evidence indicating that, since the last glacial period, northern and eastern Africa experienced severe climatic changes (LOOMIS ET AL., 2015; TIERNEY ET AL., 2008,2011b,2017,2013; WAGNER ET AL., 2018). Three major climate events are the post-glacial warming (~ 15 ka BP), hydrological variability during the African Humid Period (AHP) (15 - 5 ka BP) (DEMENOCAL ET AL., 2000) that lead to the greening of the Saharan Desert (BLOM ET AL., 2009), and the drying period near the beginning of the Meghalayan (4.2 ka BP) (BINI ET AL., 2019). The intensity and the timing of these climatic changes varied regionally over northern and eastern Africa (CASTAÑEDA ET AL., 2016). While the driving mechanisms and the regional differences are complex and not fully understood, evidence supports the view that climatic changes in northern and eastern Africa were connected across the northern hemisphere (OTTO-BLIESNER ET AL., 2014; TIERNEY & RUSSELL, 2007; TIERNEY ET AL., 2013). These complex teleconnections and their global impact support the importance of understanding long-term climate drivers in eastern Africa. Such knowledge will lead to better assessments of the impacts and potential mitigation of the current and future climate change scenarios in this world's understudied yet critical region.

While several studies have reconstructed the precipitation history in northern and eastern Africa over the last 15 cal ka BP (BITTNER ET AL., 2021; COSTA ET AL., 2014; JAESCHKE ET AL., 2020; JUNGINGER ET AL., 2014; MORRISSEY & SCHOLZ, 2014; TIERNEY ET AL., 2011b; TRAUTH ET AL., 2018; WAGNER ET AL., 2018), only a few have reconstructed the regional temperature history in northern and eastern Africa (BERKE ET AL., 2012b; CASTAÑEDA ET AL., 2016; LOOMIS ET AL., 2017,2015,2012; MORRISSEY ET AL., 2018; TIERNEY ET AL., 2008,2016). Moreover, there is a lack of terrestrial temperature reconstructions, especially in the high altitudes and the Horn of Africa. The Bale Mountain, situated in the East of the Rift Valley, are a valuable study site with the potential to enhance the paleoclimatic knowledge in an understudied region.

For terrestrial archives, different methods have been developed and applied based on pollen, chironomids, and lipid biomarkers (BONNEFILLE ET AL., 1992; CHEDDADI ET AL., 1998; CHEVALIER & CHASE, 2015; EGGERMONT ET AL., 2010; SCHOUTEN ET AL., 2007; WU ET AL., 2007). Over the last 15 years, an innovative approach for temperature reconstructions emerged based on branched glycerol dialkyl glycerol tetraethers (brGDGTs), membrane-spanning bacterial lipids (DAMSTÉ ET AL., 2000). Several calibration studies in different settings (i.e. soils and lakes) have shown a correlation between brGDGT abundances and mean annual air temperature (MAT) (e.g. DE JONGE ET AL., 2014; DEARING CRAMPTON-FLOOD ET AL., 2020; RUSSELL ET AL., 2018; WEIJERS ET AL., 2007). These calibrations have been successfully used to quantitatively reconstruct continental temperature in marine river outflow and lacustrine sediments and terrestrial archives such as loess sequences and paleosoils (GARELICK ET AL., 2022; LOOMIS ET AL., 2015,2017; SCHREUDER ET AL., 2016; ZENG & YANG, 2019). Recently, global calibrations have been developed that suit cooler and more seasonal high-latitude lakes better (MARTÍNEZ-SOSA ET AL., 2021; RABERG ET AL., 2021).

The phylogenetic breadth of the brGDGT-producing bacteria is still poorly constrained, although members from the phylum Acidobacteria have been proposed to produce brGDGTs both in cultures and in the environment (DE JONGE ET AL., 2019,2021; SINNINGHE DAMSTÉ ET AL., 2018; VAN BREE ET AL., 2020; WEBER ET AL., 2018). A recent study by Halamka et al., 2021 reports

that Acidobacteria produce certain brGDGTs under oxygen limitation. Originally, WEIJERS ET AL. (2007b) found that the methylation (MBT) and cyclisation of branched tetraethers (CBT) correlate with the measured mean annual air temperature (MAT) and pH values, respectively. Following the analytical separation of 5 and 6-methyl isomers, DE JONGE ET AL. (2014) developed a new modified MBT'_{5ME} ratio. This resulted in a revised calibration that removed the pH dependence affecting the MBT/MAT correlation and improved the accuracy of MAT reconstructions in terrestrial/soil archives. As brGDGT distributions recovered from lake sediments showed a different MAT dependence compared to soils, RUSSELL ET AL. (2018) developed a MBT'_{5ME} temperature calibration for lake sediments in eastern Africa. However, compared to the dataset of RUSSELL ET AL. (2018), the brGDGT distribution of some Bale Mountain lake surface sediments are unique (BAXTER ET AL., 2019). Although the MBT'_{5ME} calibration by RUSSELL ET AL. (2018) is a valuable supra-regional metric for reconstructing lake temperature, an adjusted calibration might better account for local conditions in the Bale region.

In this study, we aim to (i) compare brGDGT distributions from lake surface sediments of the Bale Mountains (n = 11) (BAXTER ET AL., 2019) with the eastern African dataset (Russell et al., 2018), (ii) develop a new ratio that captures the unique variation in the Bale Mountains and compare the accuracy of this calibrated ratio with the MBT'_{5ME}, and (iii) reconstruct the first Horn of Africa high altitude paleotemperature record in the Bale Mountains using the sedimentary record of Garba Guracha (3950 m a.s.l.) and (iv) compare this Garba Guracha temperature record with other records in the region.

4.1.1 Regional setting

Study area

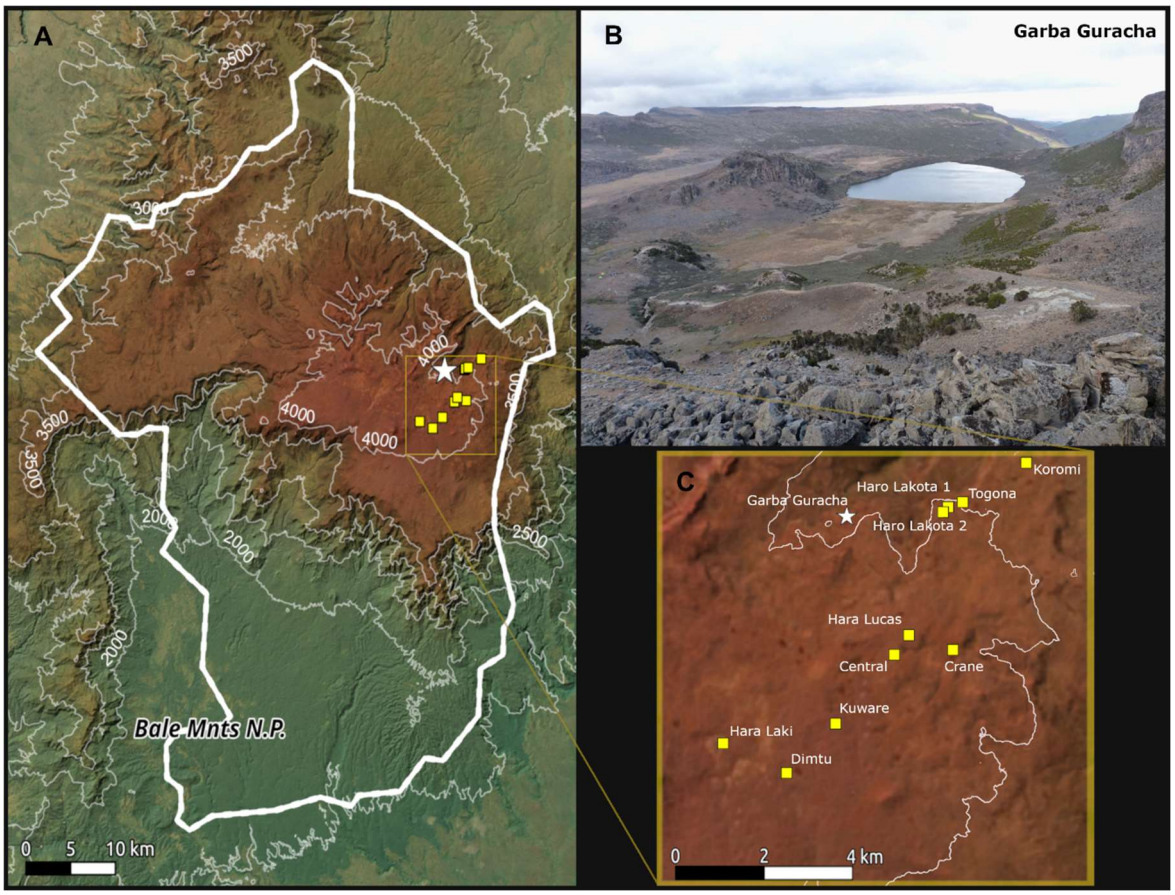

Figure 4.1: Location of the study area. (A) Bale Mountain National Park (thick white line), (B) a northeastward view over the glacial cirque of the Garba Guracha catchment (BITTNER ET AL., 2021), and (C) Bale Mountain lakes in the dataset (yellow) - The map was created by the authors using QGis 3.24 Tisler. All map layers are CC-by-SA v4.0, Image is from Bing Image / DigitalGlobe © Microsoft, DEM is from NASA/JPL SRTM (http://www.jpl.nasa.gov/srtm/), and the Bale Mountains National Park boundaries are from © OpenStreetMap contributors 2019. Distributed under the Open Data Commons Open Database License (ODbL) v1.0.

Garba Guracha (6.875781 °N, 39.878075 °E; Fig. 4.1) and all other lakes in this study are located east of the Main Ethiopian Rift in the Bale Mountains of the Bale-Arsi Massif. More specifically, they are situated on the Sanetti Plateau, the highest plateau in the Bale Mountains, between ~ 3800 to ~ 4200 m.a.s.l. and an area of 600 km^2 (OSMASTON ET AL., 2005). Solidified horizontal lava consisting of tuffs with rhyolites, alkali basalt, and trachyte formed the volcanic plateau (UHLIG & UHLIG, 1991; WILLIAMS, 2016). The plateau and the valleys were partially glaciated at the Last Glacial Maximum (GROOS ET AL., 2020,2021; OSMASTON ET AL., 2005; OSSENDORF ET AL., 2019). The glacial cirque Garba Guracha was first mentioned by WERDECKER (1962) and was also described in depth by UMER ET AL. (2007) and TIERCELIN ET AL. (2008). With a maximum water depth of 6 m and a very small catchment area, the lake is located at 3950 m above sea level (0.15 km^2; Fig. 4.1). The bedrock of the catchment is carbonate-poor (LÖFFLER, 1978; UHLIG & UHLIG, 1991). An outlet towards the Togona Valley is present during the rainy

season at the lake's northern end. A swampy alluvial plain fed by multiple springs stretches along the lake's southern shore.

Climate

The climate of the Bale Mountains varies spatially and temporally, affected by the orographic differences in altitude, a north-south exposure and by changing atmospheric air mass movements over the course of the year (KIDANE ET AL., 2012; UHLIG & UHLIG, 1991). The Bale Mountains experience a four-month dry season (November to February) and a long wet season with complex orographic rainfall patterns (March to October) (KIDANE ET AL., 2012; WOLDU ET AL., 1989). The complexity of the rainfall pattern is associated with the convergence of northeast and southwest winds due to the northern and southern location of the ITCZ between June and September and between October and March, respectively (KIDANE ET AL., 2012; TIERCELIN ET AL., 2008). The Equatorial Westerlies and the Indian Ocean monsoon act as two moisture sources for the precipitation in the Bale Mountains (MIEHE & MIEHE, 1994; UHLIG, 1988). With 1000-1500 mm per year, the southern part of Bale Mountain experiences the highest precipitation amount, whereas the northern region, including Garba Guracha, only receives 800-1000 mm (WOLDU ET AL., 1989). Temperatures vary seasonally, with the lowest temperatures in the dry season and the highest temperatures in the rainy season (HILLMAN, 1988). The Afro-Alpine regions, including the Sanetti Plateau, are characterised by diurnal temperature differences between day and night (-15 to +26 °C) (HILLMAN, 1988). Across the Bale Mountains, climate data has been collected since 2017 with a mean annual temperature of 4.9 °C (max. 6 °C; min. 3.4 °C) at the Angesso Station, located at the same altitude 4 km northeast of Garba Guracha. The mean annual temperature at Garba Guracha is 5.4 °C (BAXTER ET AL., 2019).

4.2 Material and Methods

4.2.1 Material and Sampling

In this study, we used the published data of 76 surface sediment samples from eastern African lakes. The data of these lakes, located mainly in Ethiopia, Uganda and Kenya, were published by LOOMIS ET AL. (2014, 2011, 2012), RUSSELL ET AL. (2018), EGGERMONT ET AL. (2011) and BAXTER ET AL. (2019). The environmental data for the 11 lakes in the Bale Mountains were published by EGGERMONT ET AL. (2011) and BAXTER ET AL. (2019), and the corresponding MAT is based on a calculated lapse rate supported by local climate station data (LOOMIS ET AL., 2012; RUSSELL ET AL., 2018).

At the Garba Guracha site, two overlapping sediment cores were retrieved in February 2017, at a water depth of 4.8 m using a Livingstone piston corer. A maximum sediment depth of 1550 cm was reached, covering an organic matter-rich upper section (0-900 cm) and an organic matter-poor bottom one (900-1550 cm). This study focuses on the last 12.3 cal ka BP covering the 0-950 cm, with a mean sedimentation rate of 15 years/cm (more details on

sediment properties and chronology can be found in BITTNER ET AL. (2020)). We sampled at contiguous 10 cm intervals (average ~ 100 years of sedimentation). Thirty-five samples were selected for brGDGT analyses.

4.2.2 Sample preparation and analysis

The total lipid extracts (TLE) of the surface sediment samples were extracted using an accelerated solvent extractor (ASE) with dichloromethane:methanol in a ratio of 9:1 (LOOMIS ET AL., 2012). The brGDGTs were purified and separated according to their polarity. The samples were quantified following the method described by HUGUET ET AL. (2006).

The TLE of the downcore sediments was obtained using a soxhlet system by constant rinsing (24h) with solvent (dichloromethane:methanol in a ratio of 9:1). After rotary evaporation, the TLE was redissolved in *n*-hexane and transferred onto a pipette column filled with aminopropyl silica gel (Supelco, 45 um). Solvents of increasing polarity (*n*-hexane, dichloromethane/methanol 2:1; diethyl ether/acetic acid 19:1) were used to selectively elute the fractions of the TLE (nonpolar fraction A; two polar fractions B and C, including brGDGTs). Fraction B contained 98-99 %, while fraction C contained 1-2 % of all brGDGTs. All results refer to the brGDGTs contained in fraction B. Before measurement, a C_{46} brGDGT standard was added, and the extract dried, redissolved in n-hexane/isopropanol (99:1) and filtered using a 0.45 um polytetrafluoroethylene (PTFE) filter. The measurements of the GDGTs (dissolved in n-hexane/IPA (99:1)) were done at ETH Zurich using a high-performance liquid chromatograph (Agilent 1260) coupled to a quadrupole mass spectrometer configured for atmospheric pressure chemical ionisation (HPLC-APCI-MS). The separation of the GDGTs was achieved by two silica columns at 45 °C (modified after HOPMANS ET AL. (2016)) with a flow rate of 0.2ml/min and an injection volume of 10 µl. Compound-peak integrations of *m/z* 1292, 1050, 1048, 1046, 1046, 1034, 1032, 1022, 1020, 1018 and 744 were performed according to previously published methods (HOPMANS ET AL., 2016).

4.2.3 BrGDGTs – structure, statistical methods and proxy calculation

BrGDGTs can be present as tetra- (I), penta- (II), or hexamethylated (III) compounds with different numbers of cyclopentyl moieties (none (a), one (b), or two (c)). The outer methyl group can be positioned on the α and/or ω C5 (5-methyl compounds) or C6 (6-methyl compounds, indicated by a prime notation) location (DE JONGE ET AL., 2014a). To interpret the GDGT composition of the samples, we used the BIT, MBT', MBT'_{5ME}, and CBT'.

We calculated the BIT index following the equation of HOPMANS ET AL. (2004):

$$BITindex = (Ia + IIa + IIIa + IIa' + IIIa')/(Ia + IIa + IIIa + IIa' + IIIa' + crenarchaeol) \quad \text{[Eq. 1]}$$

DE JONGE ET AL. (2014) showed that the MBT' ratio (PETERSE ET AL., 2012) contains 5- and 6-methyl compounds that are explicitly mentioned here:

$$MBT' = (Ia + Ib + Ic)/(Ia + Ib + Ic + IIa + IIa' + IIb + IIb' + IIc + IIc' + IIIa + IIIa') \quad \text{[Eq. 2]}$$

By removing the 6-methyl isomers from the equation, DE JONGE ET AL. (2014) improved the temperature calibration further:

$$MBT'_{5ME} = (Ia + Ib + Ic)/(Ia + Ib + Ic + IIa + IIb + IIc + IIIa) \quad \text{[Eq. 3]}$$

The cyclisation of branched tetraethers (CBT') is calculated following the equation from DE JONGE ET AL. (2014a):

$$CBT' = {}^{10}log\,(Ic + IIa' + IIb' + IIc' + IIIa' + IIIb' + IIIc')/(Ia + IIa + IIIa) \quad \text{[Eq. 4]}$$

RUSSELL ET AL. (2018) defined a calculation for surface water pH:

$$Surface\ water\ pH = 8.95 + 2.65 * CBT' \quad \text{[Eq. 5]}$$

Lake water conductivity can be calculated using Eq. 12 of RABERG ET AL. (2021):

$$\begin{aligned} ln(conductivity) = {} & 6.62 + 8.87 * (Ib/(Ia + Ib + Ic)) \\ & + 5.12 * ((IIa'/(IIa + IIb + IIc + IIa' + IIb' + IIc'))^2) \\ & + 10.64 * ((IIa/(IIa + IIb + IIc + IIa' + IIb' + IIc'))^2) \\ & - 8.59 * (IIa/(IIa + IIb + IIc + IIa' + IIb' + IIc')) \\ & - 4.32 * ((IIIa'/(IIIa + IIIb + IIIc + IIIa' + IIIb' + IIIc'))^2) \\ & - 5.31 * ((IIIa/(IIIa + IIIb + IIIc + IIIa' + IIIb' + IIIc'))^2) \\ & - 142.67 * ((IIIb/(IIIa + IIIb + IIIc + IIIa' + IIIb' + IIIc'))^2) \end{aligned} \quad \text{[Eq. 6]}$$

The fractional abundance of any individual brGDGT compound (i) was defined as:

$$f(i) = i/(Ia + Ib + Ic + IIa + IIa' + IIb + IIb' + IIc + IIc' + IIIa + IIIa' + IIIb + IIIb' + IIIc + IIIc') \quad \text{[Eq. 7]}$$

4.2.4 Quantitative data analyses

Numerical analyses in this paper have been performed with Excel and R 4.1.0 (R CORE TEAM, 2021). Results are displayed using the arithmetic mean and standard deviations using the notation ±. To explore the correlations between brGDGTs and MAT, we used linear regressions and the reported Pearson correlation values (r^2), where correlations were considered significant when the p-value < 0.05. We performed a Principal Component Analysis (PCA) of brGDGTs from i) the calibration dataset and ii) the Garba Guracha record, based on standardised and scaled fractional abundance. The ordination methods provide a simple yet effective way to visualise the variability within the distribution of the brGDGTs. PCA was performed with the R package *factoextra* (KASSAMBARA & MUNDT, 2020).

4.3 Result

4.3.1 BrGDGT patterns of surface sediments from lakes in the Bale Mountains

To frame the downcore variation in Garba Guracha in the current environmental settings, we have expanded the dataset of RUSSELL ET AL. (2018) by 11 Bale Mountain lake surface sediment samples (Table C.1 and C.2) (DATA FROM BAXTER ET AL., 2019). Due to the missing values of IIc, IIc', IIIb, IIIb', IIIc and IIIc' in the manuscript by RUSSELL ET AL. (2018), we excluded these isomers in the Bale Mountain data from the PCA to allow direct comparison of the PCAs (see Fig. C.1 for different PCA including all isomers). The highest fractional abundances of brGDGTs in these surface sediments are (i) IIIa with a mean of 22 % (±5), (ii) IIa with a mean of 22 % (±7) and (iii) IIIa' with a mean of 16 % (±12) (Fig. 4.2A, Table C.2).

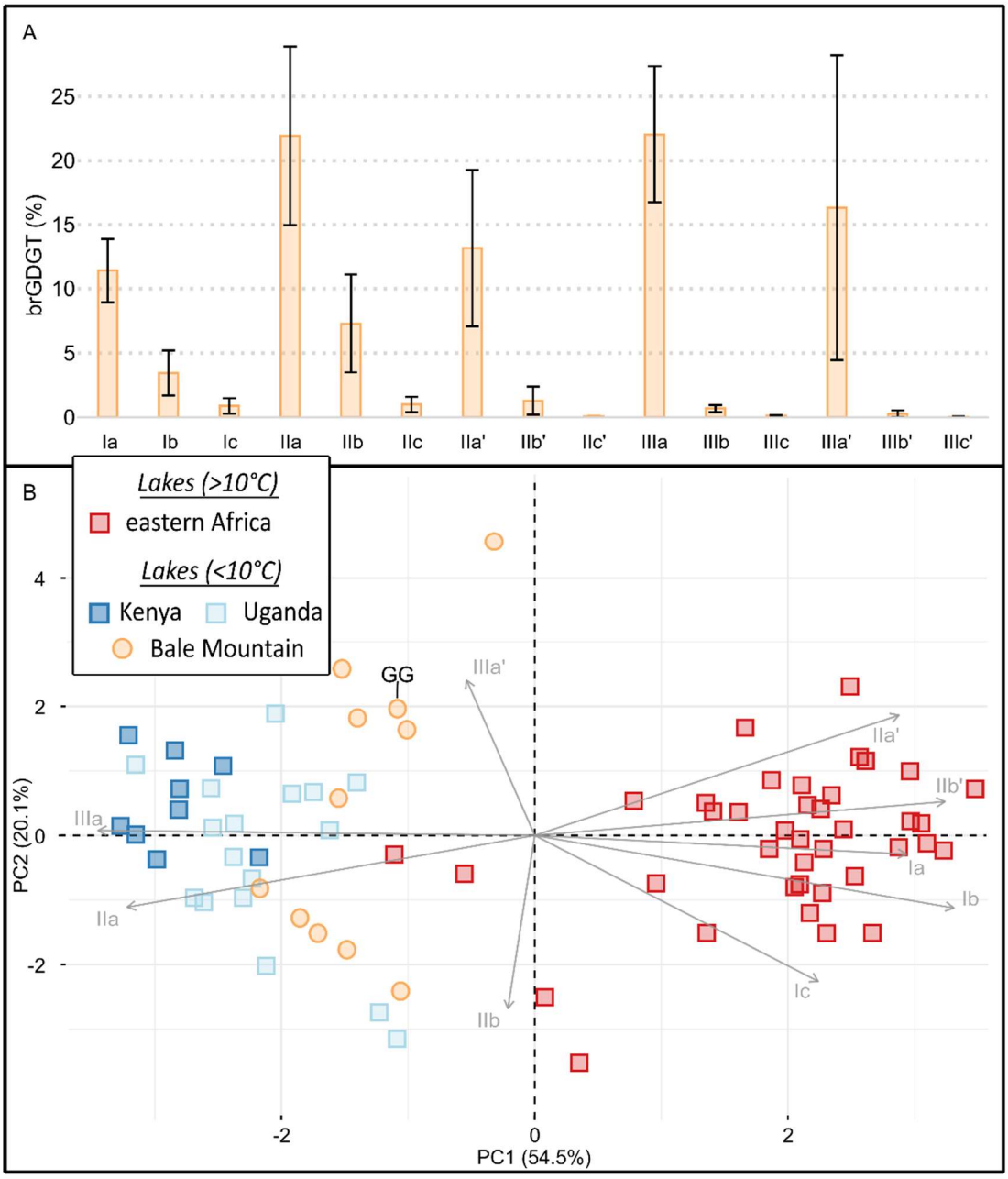

Figure 4.2: (A) Barplot of average brGDGT percentages in Bale Mountain lake surface sediments (BAXTER ET AL., 2019), with standard deviation, plotted as error flags, and (B) PCA of brGDGTs of eastern African lakes with regional pattern; data from RUSSELL ET AL. (2018) and BAXTER ET AL. (2019) - lakes > 10 °C (red) and lakes < 10 °C (Bale Mountain - orange, Kenya - blue and Uganda - light blue); Garba Guracha (GG).

The PCA of brGDGTs shows some differences between the East African lake dataset and the Bale Mountain lakes (Fig. 4.2B). IIIa and IIa have negative loadings, and IIa', IIb', Ia, Ib and Ic have positive loading on PC1. PC2 shows negative loadings from IIb and positive loading from IIIa' and IIa'. The Bale Mountain lakes have a negative score on PC1, consistent with their location in a cool climate. The similar distribution of tetra-, penta- and hexamethylated brGDGTs in surface sediments, illustrates a shared dominant lake-derived provenance as the East African lake dataset, as soil-derived brGDGTs are characterised by a larger fractional abundance of brGDGTs Ia (RUSSELL ET AL., 2018). At the same time, the Bale Mountain lakes

have a wide dispersion on PC2, illustrating additional variation of brGDGTs. Regional differences in the brGDGT isomer abundances, especially in Bale Mountain surface sediments, are further supported by variations in the degree of cyclisation (DC') and CBT' ratio values in the eastern African lake surface sediment data (RUSSELL ET AL., 2018; BAXTER ET AL., 2019) (Fig. C.2). Specifically, on PC2, a decrease IIb and an increase of IIIa' is visible in some of the Bale Mountain lakes, including Garba Guracha (highlighted in Fig. 4.2B).

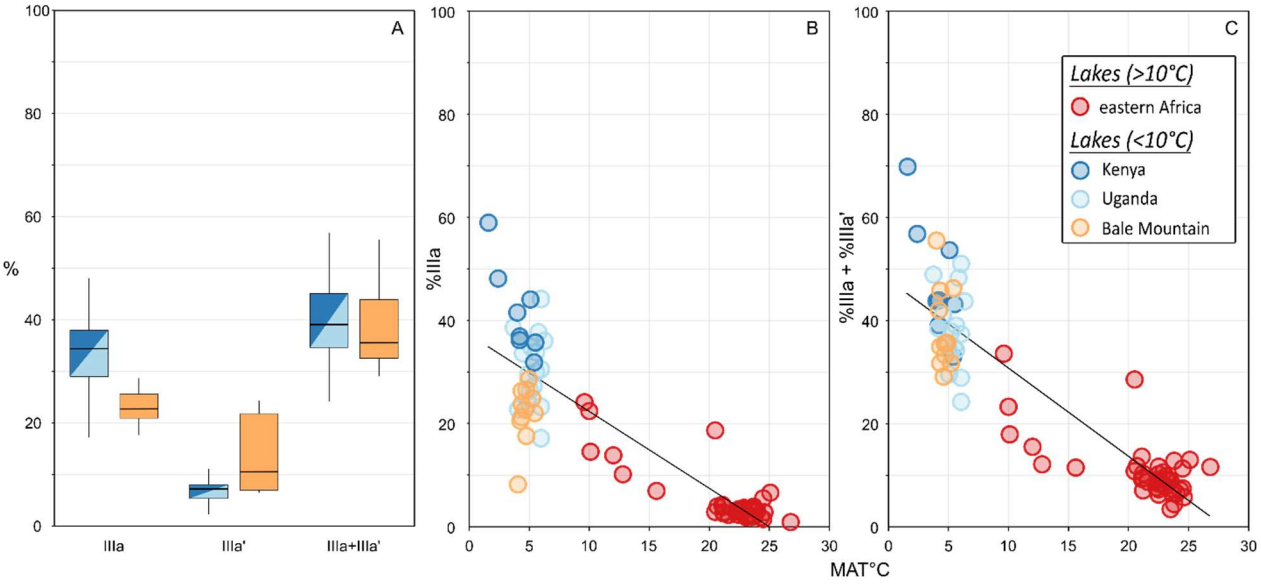

Figure 4.3: (A) Abundance (%) of IIIa and IIIa'; (B) Linear correlation between IIIa (%) and MAT (r^2 = 0.78) and (C) IIIa + IIIa' (%) to MAT (r^2 = 0.82) - data from RUSSELL ET AL. (2018) and BAXTER ET AL. (2019) - lakes > 10 °C (red) and lakes < 10 °C (Bale Mountain - orange, Kenya - blue and Uganda - light blue).

Compared to similar high-altitude lakes (above 3500 m and MAT < 10 °C) in eastern Africa (Kenya and Uganda lakes previously published in the East African lake dataset (RUSSELL ET AL., 2018)), the percentage of IIIa and IIa is lower, and the percentage of IIIa' and IIa' is higher in the Bale Mountain lakes (Fig. 4.3). Interestingly, the combined percentage of these 5 and 6-methyl isomers is similar (Fig. 4.3A).

We hypothesise that the 6-methyl compound (IIa' and IIIa') might be produced instead of their 5-methyl counterparts (IIa and IIIa), resulting in their higher fractional abundance in some of the Bale Mountain lakes (Fig. 4.3A). This is supported by our observation that, in the East African lake dataset, the correlation of %IIIa to MAT (r^2 = 0.78) is slightly improved by adding %IIIa' to r^2 = 0.82 (Fig. 4.3B, C). Narrowing the temperature range, (MAT< 10 °C), the improvement remains significant: the correlation of %IIIa to MAT (r^2 = 0.11; p-value < 0.001) is improved by adding %IIIa' to r^2 = 0.31 (p-value < 0.001) (Fig. C.3). Although the production of IIIa' at the expense of IIIa is poorly understood in lacustrine settings the isomerisation of brGDGTs can be affected by the conductivity and salinity of the lake water (RABERG ET AL., 2021; WANG ET AL., 2021). As IIIa is a major component of the MBT'_{5ME} ratio, the hypothesised production of IIIa' at the expense of IIIa could have the potential to influence MBT'_{5ME} values. Indeed, MBT'_{5ME} values of the Bale Mountain lakes range from 0.20 to 0.37, with a mean of 0.24 (±0.05). As the MAT range of Bale Mountain lakes is limited (4 - 5.4 °C), the range of

MBT'_{5ME} is larger than expected of the measured MAT relative to similar eastern African lakes in the East African lake dataset (MBT'_{5ME} = 0.17 to 0.25 with a mean of 0.22 ± 0.02; MAT = 4 - 5.4 °C) (RUSSELL ET AL., 2018).

4.3.2 BrGDGT patterns of the Garba Guracha sediment core

In general, the sediments of the Garba Guracha are characterised by a high input of aquatic organic matter. Several analysed proxies used to identify the source of organic matter indicate a predominantly aquatic production ($\delta^{13}C$, TOC/N, P_{aq}, sugar quantification ratios) (BITTNER ET AL., 2020,2021). The composition of brGDGTs in the sediment of Lake Garba Gurahca is inconsistent with the soil samples in Bale Mountain, indicating different producing communities (Fig. C.4, Table C.3). These findings are concurrent with the results of RUSSELL ET AL. (2018) that brGDGTs in eastern African lake sediments are dominantly lake-derived. Therefore, we suggest that most brGDGTs in the Garba Guracha sediment archive are also of aquatic origin.

In the Garba Guracha sediments, both branched and isoprenoid GDGTs are present. The BIT index ranges between 0.8 and 1 (mean = 0.98, ± 0.04). Only the oldest samples (12-10 cal ka BP) have a lower BIT index value of 0.8 to 0.9 (Table C.4). Tetramethylated brGDGTs in the sediment core represent on average 19.5 %, pentamethylated brGDGTs 44 %, and hexamethylated brGDGTs 36.5 % (Table C.4). The highest fractional abundances are (i) IIIa with a mean of 21 % (±5), (ii) IIa with a mean of 20 % (±3) and (iii) Ia with a mean of 15 % (±3). The MBT'_{5ME} ranges from 0.20 to 0.35 with a mean of 0.28 (±0.04) (Table C.5). The CBT' ratio ranges from 0.06 to -0.54 with a mean of 0.27 (±0.18) (Table C.4).

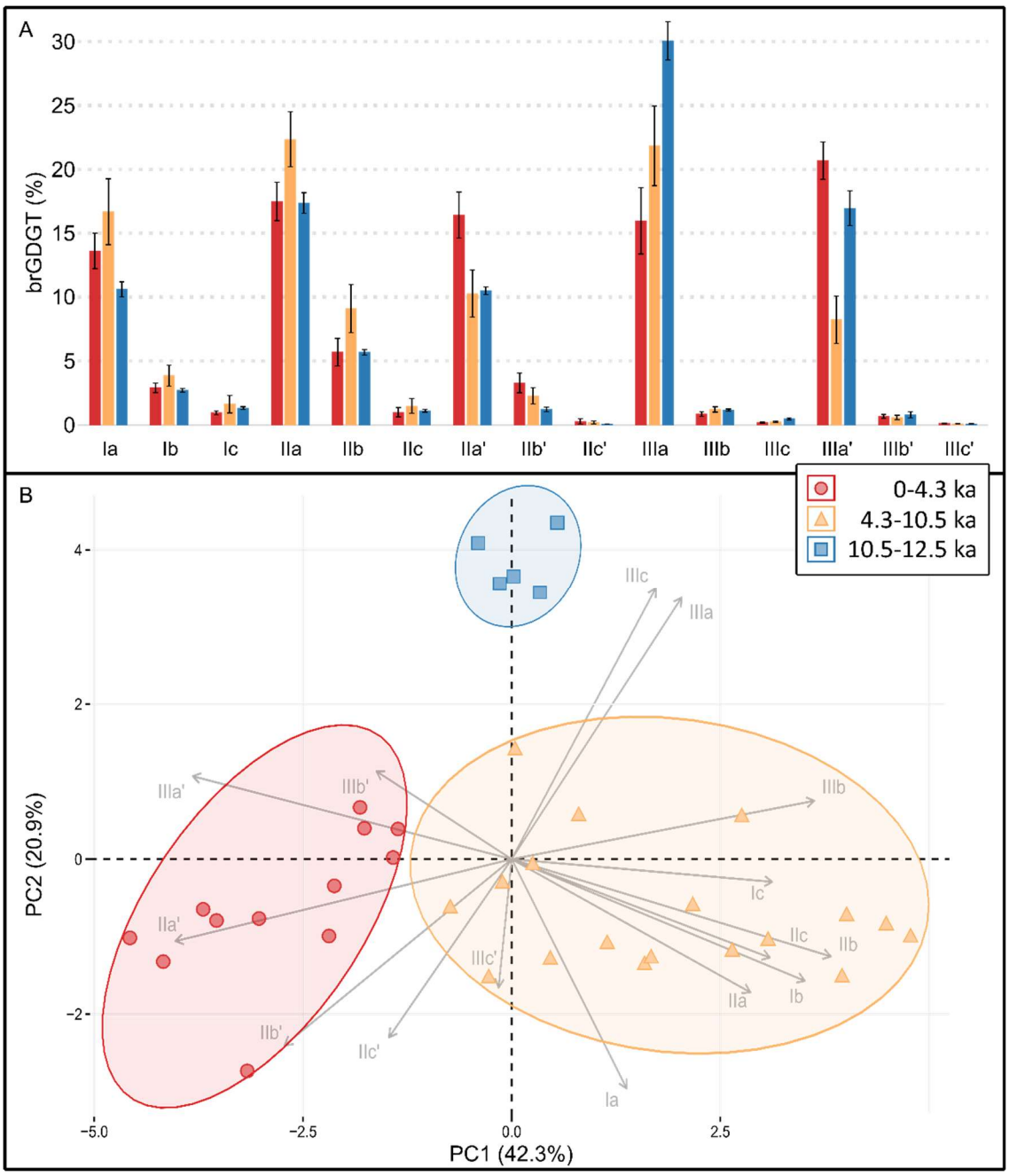

Figure 4.4: (A) barplot of average brGDGT percentages in the Garba Guracha sediment core, with standard deviation, plotted as error flags; (B) PCA of brGDGTs of the Garba Guracha sediment core; data from 0 to 4.3 cal ka BP (red), data from 4.3 to 10.5 cal ka BP (orange) and data from 10.5 to 12.5 cal ka BP (blue).

A PCA of all downcore brGDGTs distributions (Fig. 4.4A) shows that the first two components explain 63.2 % of the variance. On PC1 (42.3 %), all 6-methyl isomers have negative loadings, while 5-methyl isomers show positive loadings. PC2 (20.9 %) shows positive loadings of all hexamethylated brGDGTs and negative loadings of all penta- and tetramethylated brGDGTs. The PCA reveals changes in brGDGT composition with core depth when the data points are grouped using the following age cut-offs: (0-4.3 cal ka BP; 4.3-10.5 cal ka BP; 10.5-12.5 cal ka BP) (Fig. 4.4A). In phase 1 (12.5 – 10.5 cal ka BP), IIIa, IIIa' and IIa have the highest mean abundances of 30 %, 17 %, and 17 %, respectively. In phase 2 (10.5 – 4.3 cal ka BP), the mean abundance of IIIa and IIIa' are decreased by around 9 %, while IIa, IIb

and Ia increase. In phase 3 (4.3 - 0 cal ka BP), the mean abundances of IIIa decrease by 6 % further. Conversely, the mean abundance of IIIa' increases again by 12 %. The same holds true for IIa (-5 %) and IIa' (+6 %). The mean abundance of Ia increases further by 3 % (Fig. 4.4B).

The unusually high abundance of brGDGTs IIIa' compared to IIIa observed in surface sediments of Bale Mountains lakes (Fig. 4.2A) is also visible in the Garba Guracha record and the relative abundance of IIIa' varies with depth. High amounts of IIIa' appear until 10.8 cal ka BP followed by low percentage (< 10 %) until 4.5 cal ka BP. The highest abundance of IIIa' with up to 22 % occurs after 4.5 cal ka BP until the recent past. The changing abundances of IIIa' in our record coincide with changes in CBT' (Fig. 4.5). The variability in the 6-methyl brGDGTs reflects the largest part of the variation in this dataset, reflected by the good agreement (r^2 = 0.77, $p < 0.001$) between the fractional abundance of brGDGTs IIIa' and the sample loadings on PC1.

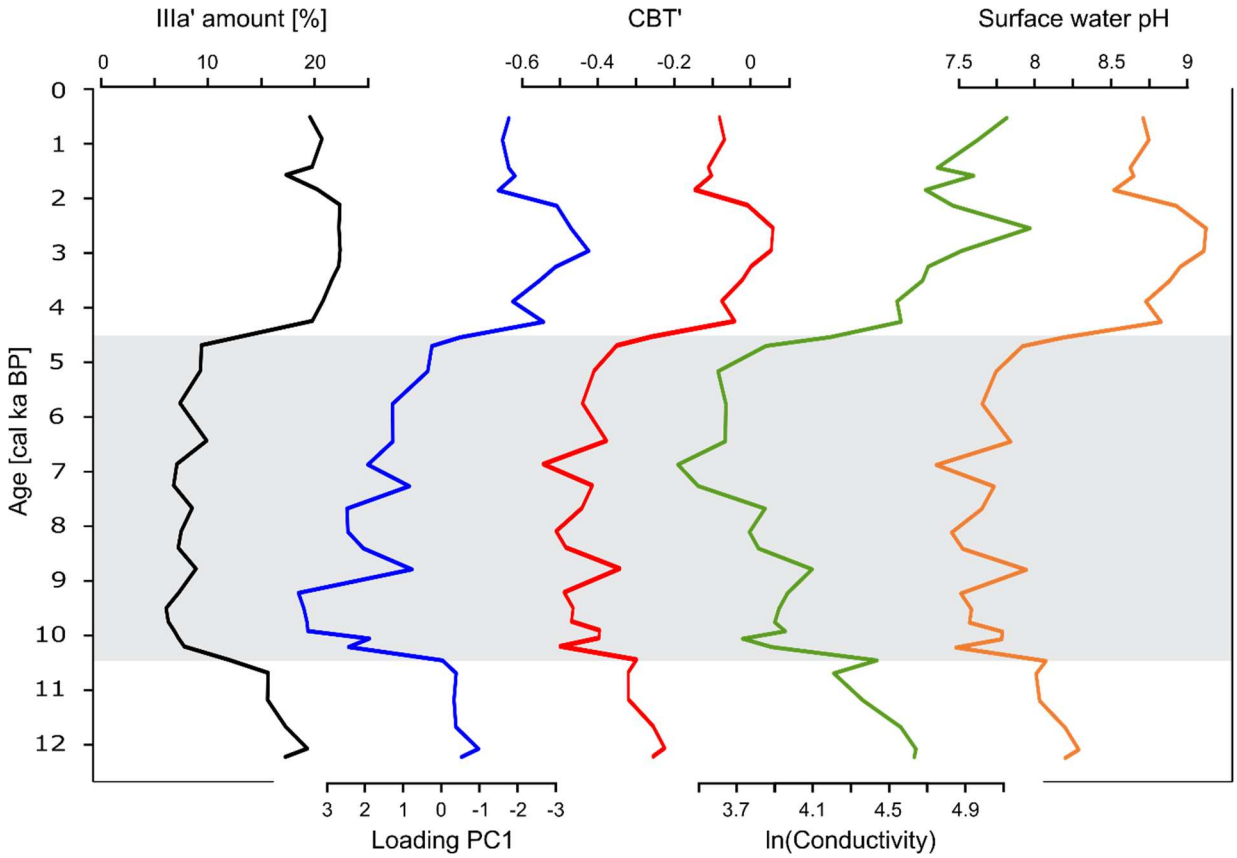

Figure 4.5: Downcore functions for IIIa' amount, the PC1 loading, CBT', ln(conductivity) (Eq. 12 in RABERG ET AL., 2021), and surface water pH of the Garba Guracha brGDGT record.

4.4 Discussion

4.4.1 Possible MAT calibration functions inferred from the expanded eastern African surface sediment dataset

Table 4.1: Temperature calibrations – Ratios, calibration dataset, r^2, and root-mean-square-error (RMSE) in °C - East African Lake dataset (EAL), East African Lakes + Bale Mountain lakes (EAL_{BM})

Ratio	Calibration dataset	r^2	RMSE °C
MBT'_{5ME} (Ia+Ib+Ic)/(Ia+Ib+Ic+IIa+IIb+IIc+IIIa)	EAL (n = 65)	0.92	2.41
	EAL_{BM} (n = 76)	0.92	2.41
MBT'_{5ME} + IIIa' (Ia+Ib+Ic)/(Ia+Ib+Ic+IIa+IIb+IIc+IIIa+IIIa') [Eq. 8]	EAL_{BM} (n = 76)	0.93	2.38
Simplified MBT'_{5ME} + IIa'&IIIa' Ia/(Ia+IIa+IIIa+IIa'+IIIa') [Eq. 9]	EAL_{BM} (n = 76)	0.84	3.48
Simplified MBT'_{5ME} + IIIa' Ia/(Ia+IIa+IIIa+IIIa') [Eq. 10]	EAL_{BM} (n = 76)	0.91	2.59

We added the GDGT distribution data of 11 surface sediments from Bale Mountain lakes (BAXTER ET AL., 2019) to the existing data of RUSSELL ET AL. (2018) and applied the MBT'_{5ME} calibration (Table 4.1). Here, the original dataset (n = 65) is referred to as East African Lakes "EAL", while the extended dataset (n = 76) is referred to as East African Lakes + Bale Mountain lakes (EAL_{BM}). The linear correlation between the MBT'_{5ME} and MAT was almost identical after adding the 11 Bale Mountain lake samples (EAL r^2 = 0.92, EAL_{BM} r^2 = 0.92). In the tropical Bale Mountain, the freezing of lakes is extremely rare, due in part to the intense year-round insolation, and MAT is equal to MAF. To test whether the unique brGDGT distribution in some Bale Mountain lakes (Fig. 4.2) affected the temperature correlation, we applied various calibrations to account for the increased abundance of IIIa' (and to a lesser extent IIa'). In the EAL_{BM} dataset, the application of this ratio has a lower r^2 of 0.84 and a higher RMSE of 3.48 °C compared to the MBT'_{5ME} (Table 4.1: Eq. 9). As brGDGT IIIa' specifically was shown to increase in Bale Mountain sediments and improved the correlation with MAT (Fig. 4.3B, C), we investigated alternative ratios that incorporate this compound but exclude IIa'. Table 4.1 and Fig. 4.6 summarise the correlation coefficients of the MBT'_{5ME} (r^2 = 0.92, RMSE of 2.41 °C), an MBT'_{5ME} ratio that includes IIIa' (Eq. 10) with r^2 = 0.93 and RMSE of 2.38 °C and the simplified ratio that includes only the major brGDGTs compounds (Eq. 10: r^2 = 0.91 and an RMSE of 2.59 °C).

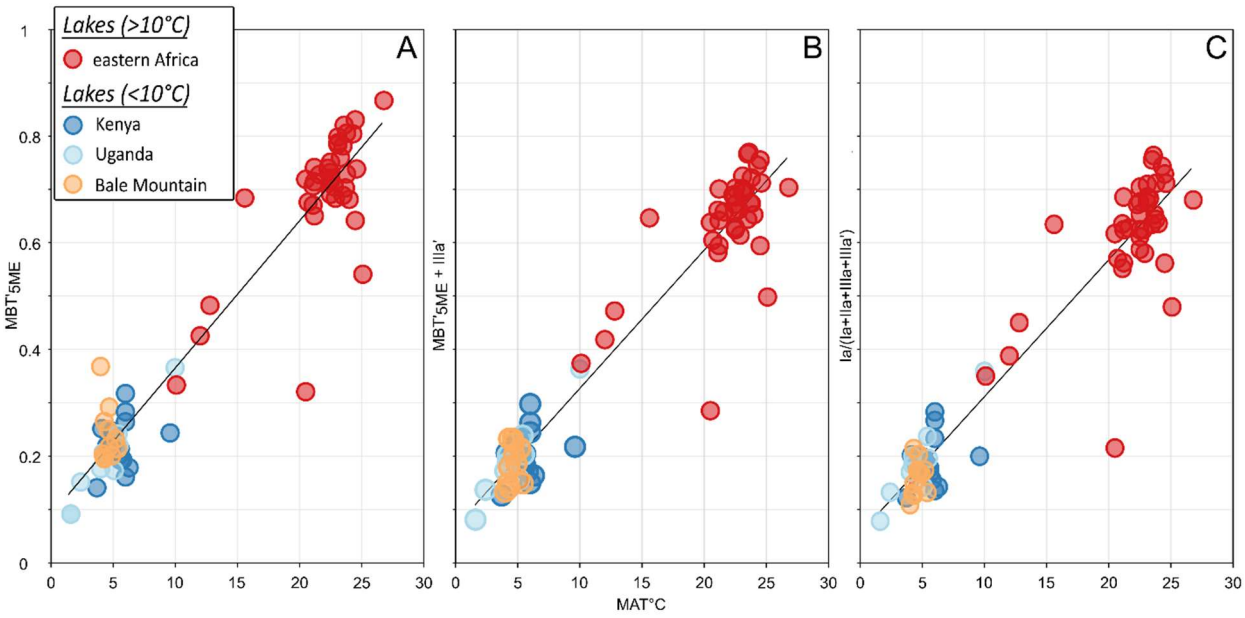

Figure 4.6: Correlations EAL_{BM} datasets, (A) MBT'_{5ME} (r^2 = 0.92; RMSE of 2.41); (B) MBT'_{5ME} + IIIa' (r^2 = 0.93; RMSE of 2.38).); (C) Ia/(Ia+IIa+IIIa+IIIa') (r^2 = 0.91; RMSE of 2.59) - data from RUSSELL ET AL. (2018) and BAXTER ET AL. (2019) - lakes > 10 °C (red) and lakes < 10 °C (Bale Mountain - yellow, Kenya - blue and Uganda - light blue)

The results of the calibrations Ia/(Ia+IIa+IIIa+IIIa') (MAT = -0.773 + 35.646 x Ia/(Ia+IIa+IIIa+IIIa')) and MBT'_{5ME} + IIIa' (MAT = -1.4734 + 35.777 x MBT'_{5ME} + IIIa') applied to the Garba Guracha sediment core are very similar and correlate well (r^2 = 0.97) (Fig. 4.7, purple and green curves, respectively). Therefore, we will only discuss the best performing calibrations developed using the EAL_{BM} dataset MBT'_{5ME} (MAT = -1.8299 + 33.304 x MBT'_{5ME}) and the MBT'_{5ME} + IIIa' calibration to the downcore distributions.

4.4.2 Paleotemperature reconstructions for the Garba Guracha sedimentary record - comparison of the different calibrations

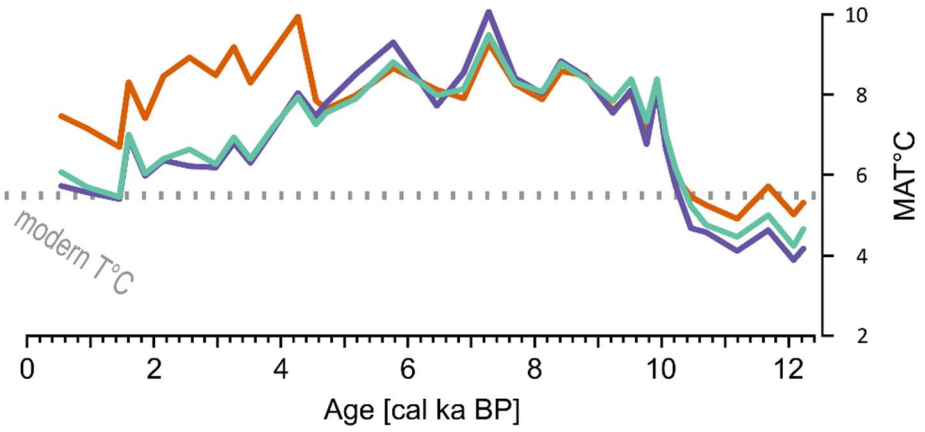

Figure 4.7: Reconstructed temperatures of the Garba Guracha sedimentary record. MBT'_{5ME} (orange); Ia/(Ia+IIa+IIIa+IIIa') (purple); MBT'_{5ME} + IIIa' (turquoise).

We evaluate the downcore trend in GG sediments to compare the performance of both calibrations, revealing periods of agreement (10-4.2 ka BP) and a period of temperature offset (since 4.2 ka BP). Using established and newly developed ratios and calibrations ($MBT`_{5ME}$ +IIIa' and MBT'_{5ME} EAL_{BM}) resulted in similar absolute values and comparable temperature trends, principally in the early and mid-Holocene. Reconstructed temperatures range from 4.9 to 10.0 °C (MBT'_{5ME}) and 4.2 to 9.5 °C (MBT'_{5ME} + IIIa') (Fig. 4.7). Despite a slightly different range in temperature (4.4 and 5.3 °C), the trends of both calibrations are similar between 12 and 4.7 cal ka BP. The lowest MATs (< 5 °C) occurred between 12.2 cal ka BP (950 cm) and 10.5 cal ka BP (800 cm). MAT increased rapidly by 3.5 °C between 10.5 cal ka BP (800 cm) and ca. 10 cal ka BP (700 cm). During the early to mid-Holocene, a thermal maximum occurred between 10 and 5.7 cal ka BP (440 cm), with the highest MAT values reaching ca. 10 °C. At ~ 6.5 cal ka BP, the MAT decreased for both calibrations. The temperature drop coincides with organic-poor layers in the sediment core formed during a drought, associated with low monsoonal intensity (BITTNER ET AL., 2020). A strong offset between the calibrations appeared at 4.2 cal ka BP, at a moment when temperatures are expected to decrease in phase with insolation (Fig. 4.7). Using the MBT'_{5ME}, we reconstruct a sudden temperature rise (Fig. 4.7) that contrasts with the temperature decrease when using the MBT'_{5ME} + IIIa' calibration. The offset coincides with a known drought phase and is accompanied by shifts of many proxies (TOC, $\delta^{13}C$, TOC/N, *Erica spp*, charcoal) in the Garba Guracha sediments (BITTNER ET AL., 2020; GIL-ROMERA ET AL., 2019). The changing conditions in the Garba Guracha catchment during this drought phase, especially the decline of the *Erica* shrubland (GIL-ROMERA ET AL., 2019), might have increased the surface water pH (Fig. 4.5). A change in the lake water chemistry is supported changes in the reconstructed surface water pH (7.3 - 9.1) and conductivity (30 - 189; reported in Fig. 4.5 as ln(conductivity)) of the lake water (Fig. 4.5; calibrations from RUSSEL ET AL., 2018 and RABERG ET AL., 2021). In the last years, studies have suggested that the change in brGDGT composition captured by the CBT' may change due to shifting bacterial communities in soils and lakes (DE JONGE ET AL., 2019; VAN BREE ET AL., 2020; WEBER ET AL., 2018). Previously, pH, conductivity and salinity-dependent brGDGTs composition, sometimes driven by community changes, have been shown to affect MBT'_{5ME} values in soils and lake sediments (DE JONGE ET AL., 2021; RABERG ET AL., 2021; WANG ET AL., 2021), and we propose that a similar effect can be seen in Garba Guracha.

Hence, we suggest that MBT'_{5ME} systematically overestimates the temperatures of Garba Guracha during the late Holocene after 4 cal ka BP. A systematic offset is further supported by continuously and similarly decreasing reconstructed temperatures using both calibrations until the top of the core with a shared maximum at 150 cm (1.6 cal ka BP). We suggest that the production of IIIa' at the expense of IIIa is increased during dryer intervals, possibly caused by a change in lake water chemistry and/or bacterial communities. We conclude that a temperature calibration including IIIa' allows to reconstruct MAT in Garba Guracha sediments more accurately, as it accounts for the unique and variable production of IIIa' in Bale Mountain lakes.

4.4.3 Paleotemperature reconstructions for the Garba Guracha sedimentary record – regional comparison

In contrast to precipitation reconstructions based on δ^2H in eastern Africa (GARELICK ET AL., 2021), the temperature records do not show a clear meridional, north-south temperature change, nor an east-west pattern. The reconstructed overall temperature ranges are, however, consistent with the elevations of the lake archives. The amplitude of temperature change over the last 13 ka at Garba Guracha is ~ 6 °C. Similar amplitudes of change have been reconstructed at other high-altitude sites (Lake Mahoma and Lake Rutundu) (GARELICK ET AL., 2022; LOOMIS ET AL., 2017), whereas equatorial records at lower elevations yield lower temperature amplitudes (Lake Victoria and Lake Tanganyika) (BERKE ET AL., 2012a; TIERNEY ET AL., 2008), and higher temperature amplitudes are also recorded in northeast African Lake Tana (LOOMIS ET AL., 2015). In fact, Garba Guracha has some of the highest amplitude temperature changes of all of the sites during the Holocene, perhaps because it combines high elevation with a slightly higher latitude than other terrestrial African temperature records.

Deglacial warming

Overall, the recorded temperature trends in Garba Guracha are in phase with northern summer insolation variability (Fig. 4.8). This is reasonable because air temperature and insolation are closely connected (HUYBERS, 2006). However, the coldest MATs (< 5 °C) were recorded before 10.5 cal ka BP even though the northern hemisphere summer (20 °N) insolation maxima occurred already 12 cal ka BP (Fig. 4.8). TIERCELIN ET AL. (2008) argue that in Garba Guracha, ice remained in the catchment until ~ 10 cal ka BP due to topographical conditions, especially the north-facing exposition of the valley. The remaining ice in the basin might have (i) reduced the temperature of the lake water by inflow of cold melt water and (ii) buffered the air temperature warming caused by increasing insolation. Indeed, rising temperatures were recorded in other eastern African records as early as 21 cal ka BP (Lake Mahoma) (GARELICK ET AL., 2022) and in Ethiopia as early as 14 cal ka BP (Lake Tana) (LOOMIS ET AL., 2015; TIERNEY ET AL., 2016).

Similar to Lake Tana, but ~ 4000 years later, MAT (°C) in the Garba Guracha record experienced an abrupt increase of ca. 3.5 °C in just ca. 600 years, from 10.5 to 9.9 cal ka BP. Simultaneously with the rise in temperature, BITTNER ET AL. (2021) found an increase in P/E, indicating higher moisture availability based on depleting values of reconstructed $\delta^{18}O_{lake\ water}$. At Lake Tana, LOOMIS ET AL. (2015) and COSTA ET AL. (2014) attribute a similar connection between warmer temperature and depleted water isotopes (δ^2H) since 13.8 cal ka BP to the penetration of warm Congo Basin air masses resulting in weaker easterly trade winds and a strengthening of the southwesterly winds and the Somali Jet. The connection between Congo Basin air masses and eastern Africa is supported by the absence of cold temperatures associated with the YD in both the Congo Basin temperature record (WEIJERS ET AL., 2007a) and Lake Tana (LOOMIS ET AL., 2015). However, in the Garba Guracha record, lower temperatures prevailed 4000 years longer than in Lake Tana (LOOMIS ET AL., 2015). Although catchment glaciers could have caused these conditions in Garba Guracha, the low temperatures are

accompanied by a reduced sedimentation rate between 12.8 and 11.3 cal ka BP (BITTNER ET AL., 2020), pointing to climatic influences associated with YD times (ALLEY, 2000). Indeed, other records from the Horn of Africa indicate dry conditions associated with the YD period, like Lake Ashenge (MARSHALL ET AL., 2009) and the marine record of the Gulf of Aden (TIERNEY & DEMENOCAL, 2013). Therefore, we suggest that, at least for some periods, the climate drivers operating in the Garba Guracha region might have been different from other parts of eastern Africa. The time lag between Lake Tana and Garba Guracha could be explained by a slow eastwards advance of the Congo Air Boundary and different climatic conditions at the sites. However, with the current data, we are unable to precisely distinguish between north hemisphere YD forcing, remaining ice in the lake catchment, or regional atmospheric circulation change affecting the Garba Guracha record.

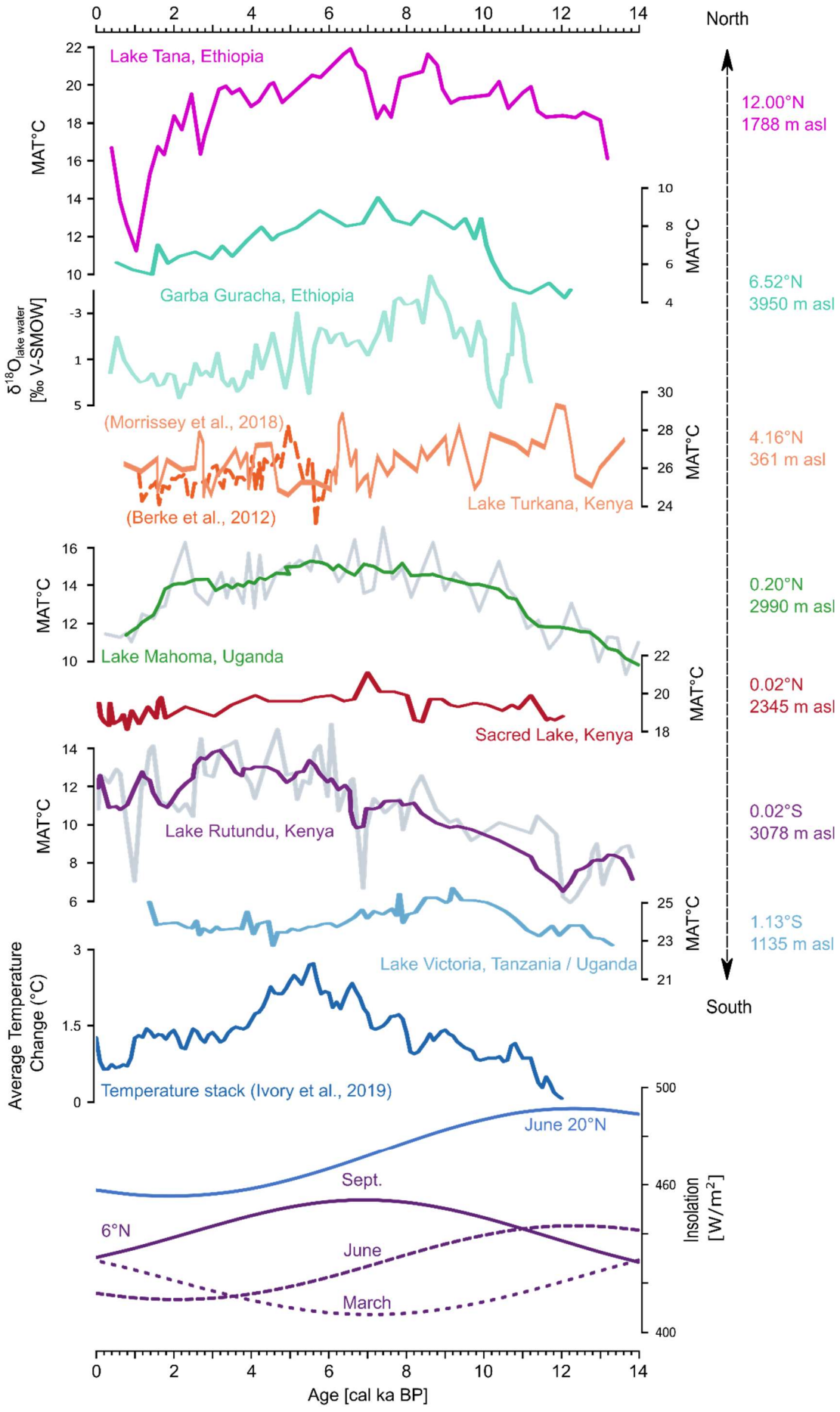
North
South
Lake Tana, Ethiopia
MAT°C
12.00°N
1788 m asl
Garba Guracha, Ethiopia
$\delta^{18}O_{lake\ water}$ [‰ V-SMOW]
6.52°N
3950 m asl
(Morrissey et al., 2018)
(Berke et al., 2012)
Lake Turkana, Kenya
4.16°N
361 m asl
Lake Mahoma, Uganda
0.20°N
2990 m asl
Sacred Lake, Kenya
0.02°N
2345 m asl
Lake Rutundu, Kenya
0.02°S
3078 m asl
Lake Victoria, Tanzania / Uganda
1.13°S
1135 m asl
Average Temperature Change (°C)
Temperature stack (Ivory et al., 2019)
June 20°N
Sept.
6°N
June
March
Insolation [W/m²]
Age [cal ka BP]

Figure 4.8: Comparison of records. MAT: Lake Tana (LOOMIS ET AL., 2015); Garba Guracha (this study); $\delta^{18}O_{lake\ water}$ as reconstructed from the aquatic sugar biomarker fucose (BITTNER ET AL., 2021); Lake Turkana (BERKE ET AL., 2012b; MORRISSEY ET AL., 2018); Lake Mahoma (GARELICK ET AL., 2022); Sacred Lake (LOOMIS ET AL., 2012); Lake Rutundu (LOOMIS ET AL., 2017); Lake Victoria (BERKE ET AL., 2012a); eastern Africa temperature stack (IVORY & RUSSELL, 2018); and insolation 6 °N and June 20 °N (LASKAR ET AL., 2004).

Warm temperatures during the African Humid Period in eastern Africa

Regardless of the cause, the ~ 10.5 cal ka BP rise in MAT is associated with an abrupt increasing moisture availability and changes of vegetation around Garba Guracha (GIL-ROMERA ET AL., 2021; UMER ET AL., 2007). Vegetation and fire dynamics around Garba Guracha responded dynamically to the changing climatic conditions, evidencing the sensitivity of the afromontane-afroalpine plant communities to increasing temperature. As MAT increased between 11 and 10 cal ka BP, the ericaceous belt expanded (GIL-ROMERA ET AL., 2021). The rising temperature and increasing P/E (BITTNER ET AL., 2021) were accompanied by the expansion of the afroalpine vegetation cover (GIL-ROMERA ET AL., 2021; MIEHE & MIEHE, 1994). An immediate consequence of the temperature rise and increasing moisture availability was biomass accumulation, as evidenced by the change from organic matter-poor to organic matter-rich sedimentation (BITTNER ET AL., 2020) and the expansion of heathlands (GIL-ROMERA ET AL., 2019). Under an increasing MAT and extending biomass, fire activity was very intense at this time (GIL-ROMERA ET AL., 2019).

The thermal maximum of the Garba Guracha record spanned from 9 to 5.8 cal ka BP, with the highest reconstructed temperatures occurring at 7 cal ka BP. A similar mid-Holocene thermal optimum has been recorded at Sacred Lake (7 cal ka BP) and Lake Tana (7 cal ka BP) (Fig. 4.8). However, the highest temperatures of Lake Victoria occurred at 9 cal ka BP, and of Lake Rutundu, Lake Malawi and Lake Tanganyika at 5 cal ka BP (BERKE ET AL., 2012a; GARELICK ET AL., 2022; LOOMIS ET AL., 2017,2015,2012; POWERS ET AL., 2005; TIERNEY ET AL., 2008). At Lake Turkana, the thermal optimum occurred at 6.4 cal ka BP (MORRISSEY ET AL., 2018) or 5 cal ka BP (BERKE ET AL., 2012b). A new temperature reconstruction from Lake Mahoma (GARELICK ET AL., 2022) and a temperature stack including temperature reconstructions from Sacred Lake, Lake Malawi, Lake Tanganyika, Lake Rutundu, and the Congo Basin by IVORY & RUSSELL (2018) showed the highest temperatures between ~ 7 and ~ 4.5 cal ka BP. The timing of the highest reconstructed temperatures at these sites is not related to greenhouse gas radiative forcing or insolation forcing (LOOMIS ET AL., 2015). LOOMIS ET AL. (2015) point out that the Lake Tana and Sacred Lake temperature maxima lag northern hemisphere summer insolation, and Lake Malawi and Lake Tanganyika lead peak southern summer insolation. In the case of Garba Guracha, the highest temperatures coincide with local maximum September insolation at the sites latitude of 6 °N (LASKAR ET AL., 2004) (Fig. 4.8). This matches the suggestion of BERKE ET AL. (2012a) that the thermal optimum of several eastern African lakes might be determined by local solar irradiance from Sep to Dec (maximum at ~ 6 cal ka BP) (Fig. 4.8) rather than northern hemisphere summer solar irradiance. The restratification processes of eastern African lakes in these months and associated epilimnetic heating might explain the increased warming of lake water (BERKE ET AL., 2012b). However, modelling studies do not support this hypothesis (DEE ET AL., 2021).

In addition to local insolation changes, local changes in P/E could have the potential to modify the lake water temperature. During the Early and Mid-Holocene, reconstructed high temperatures occurred during the African Humid Period, accompanied by the wettest phase of Garba Guracha (BITTNER ET AL., 2021) and rising lake levels in the region (GASSE, 2000; JUNGINGER ET AL., 2014), indicating higher amounts of precipitation due to an intensification of the monsoon system. A modelling study (TIERNEY ET AL., 2011a) proposes that during the AHP, the precipitation increase occurred mainly in June, July, and August (JJA), shortening the duration of annual drought phases in eastern Africa. Increased relative humidity would reduce evaporation, limiting the evaporative cooling of the lake water. Less evaporation, either due to shorter drought phases or generally higher precipitation, would increase the temperature and cause less positive $\delta^{18}O_{lake\ water}$ values, as suggested for Garba Guracha (BITTNER ET AL., 2021).

The highest temperatures of the Holocene continued until 5.8 cal ka BP, interrupted only by a short drop in temperature after 7 cal ka BP. This is in agreement with the Sacred Lake temperature record (LOOMIS ET AL., 2012). Lake Tana experienced a shift towards colder conditions a bit earlier, from 7.5 to 7 cal ka BP (LOOMIS ET AL., 2015).

Cooling in the Late Holocene

After 5.8 cal ka BP, the MAT continuously decreased by ~ 3.6 °C until recent times, coinciding with the summer insolation decline and decreasing temperatures of equatorial lakes (IVORY & RUSSELL, 2018), Lake Tana (LOOMIS ET AL., 2015) and the marine Gulf of Aden record (TIERNEY ET AL., 2016). The general decreasing temperature trend is also supported by $\delta^{18}O_{lake\ water}$, pollen and charcoal results showing a decrease in moisture availability and fire activity at Garba Guracha (BITTNER ET AL., 2021; GIL-ROMERA ET AL., 2019). Furthermore, an upwards shift of the lower and dry forests during this time reinforces the idea of more intense evapotranspiration due to the decrease in moisture availability (GIL-ROMERA ET AL., 2021). A drop in TOC and decreasing $\delta^{13}C$ values (BITTNER ET AL., 2020) support overall shifting catchment conditions.

During the last two thousand years, we observed that the increasing temperature trend concurred with an abrupt increase in the main woody communities and enhanced fire activities around Garba Guracha (GIL-ROMERA ET AL., 2021). However, we cannot discard human influence favoring both woody encroachment and fire activity.

The strong connection of temperature, P/E and insolation across the Holocene shows that the Garba Guracha temperatures might have been affected by local radiation, possibly in interplay with insolation-driven atmospheric circulation changes and their impacts on air mass source, cloud cover and evaporation. As current global warming continues, the intense warming of landmasses could lead to a major and complex restructuring of the atmospheric circulation system in the future, affecting eastern Africa and possibly even larger regions beyond via teleconnections.

4.5 Conclusions

Eastern African climatic history is spatially very diverse, and the driving mechanisms are complex and not fully understood. In eastern Africa, temperature reconstructions are generally sparse, especially in the high altitudes of the Horn of Africa. In this study, we used brGDGT from a high-altitude sedimentary record of the Bale Mountains (Lake Garba Guracha, Southwestern Ethiopia) to produce the first temperature reconstruction for the Horn of Africa.

The composition of brGDGT isomers in sediment records is affected by several influences, mainly by MAT, but in addition by lake water chemistry (pH and conductivity) and bacterial community, resulting in locally unique brGDGT compositions. For instance, in some of the Bale Mountain lakes, the abundance of a specific isomer IIIa' is uncommonly high in surface sediments. However, the summed abundance of IIIa and IIIa' is similar to other comparable lake archives in eastern Africa. We suspect that in the case of the Bale Mountains, changes in the lake's water chemistry (pH and conductivity) or bacterial community are responsible for the high production of IIIa' at the expense of IIIa under drier conditions. By including the 6-methyl isomer in a temperature calibration, we were able to enhance the correlation with MAT. Therefore, we conclude that 6-methyl isomers have an impact on temperature reconstructions, highlighting their inclusion in a Bale Mountain-specific temperature calibration. Using surface sediment data from Bale Mountain lakes and the East African lake database, the best performing temperature calibration is a modified MBT'_{5ME} including IIIa’.

With the use of the new calibration, the Garba Guracha MAT record reflects insolation variability as one of the main climatic drivers at millennial scales. Additional factors such as glacier and permafrost melting during deglaciation and the regional atmospheric circulation likely play a prominent role on shorter time scales. These additional mechanisms partly explain the asynchronicity between the Garba Guracha MAT record in the high altitude afro-alpine region of the Horn of Africa and other eastern African lake records. Further research is necessary to understand the influences on and the origin of brGDGTs producing communities, especially at high altitudes.

4.6 Acknowledgements

This research was funded by the German Research Council (DFG: ZE 844/10–1) in the framework of the joint Ethio-European DFG Research Unit 2358 "The Mountain Exile Hypothesis. How humans benefited from and reshaped African high-altitude ecosystems during Quaternary climate changes". We are grateful to the project coordination, the Philipps University Marburg, the University of Addis Abeba, the Frankfurt Zoological Society, the Ethiopian Wolf Project, the Bale Mountains National Park, and the related staff members, especially Katinka Thielsen and Mekbib Fekadu, for their logistic assistance during our fieldwork. We thank the Ethiopian Wildlife Conservation Authority for permitting our research in the Bale Mountains National Park.

4.7 References

ALLEY, R. B. (2000): The Younger Dryas cold interval as viewed from central Greenland. - Quaternary Science Reviews, **19**, 213–226.

BAXTER, A. J., HOPMANS, E. C., RUSSELL, J. M., & SINNINGHE DAMSTÉ, J. S. (2019): Bacterial GMGTs in East African lake sediments: Their potential as palaeotemperature indicators. - Geochimica et Cosmochimica Acta, **259**, 155–169.

BERKE, M. A., JOHNSON, T. C., WERNE, J. P., GRICE, K., SCHOUTEN, S., & SINNINGHE DAMSTÉ, J. S. (2012a): Molecular records of climate variability and vegetation response since the Late Pleistocene in the Lake Victoria basin, East Africa. - Quaternary Science Reviews, **55**, 59–74.

BERKE, M. A., JOHNSON, T. C., WERNE, J. P., SCHOUTEN, S., & SINNINGHE DAMSTÉ, J. S. (2012b): A mid-Holocene thermal maximum at the end of the African Humid Period. - Earth and Planetary Science Letters, **351**–**352**, 95–104.

BINI, M., ZANCHETTA, G., PERŞOIU, A., CARTIER, R., CATALÀ, A., CACHO, I., DEAN, J. R., DI RITA, F., DRYSDALE, R. N., FINNÈ, M., ISOLA, I., JALALI, B., LIRER, F., MAGRI, D., MASI, A., MARKS, L., MERCURI, A. M., PEYRON, O., SADORI, L., SICRE, M.-A., WELC, F., ZIELHOFER, C., & BRISSET, E. (2019): The 4.2 ka BP Event in the Mediterranean region: an overview. - Clim. Past, **15**, 555–577.

BITTNER, L., BLIEDTNER, M., GRADY, D., GIL-ROMERA, G., MARTIN-JONES, C., LEMMA, B., MEKONNEN, B., LAMB, H. F., YANG, H., GLASER, B., SZIDAT, S., SALAZAR, G., ROSE, N. L., OPGENOORTH, L., MIEHE, G., ZECH, W., & ZECH, M. (2020): Revisiting afro-alpine Lake Garba Guracha in the Bale Mountains of Ethiopia: rationale, chronology, geochemistry, and paleoenvironmental implications. - Journal of Paleolimnology.

BITTNER, L., GIL-ROMERA, G., GRADY, D., LAMB, H. F., LORENZ, E., WEINER, M., MEYER, H., BROMM, T., GLASER, B., & ZECH, M. (2021): The Holocene lake-evaporation history of the afro-alpine Lake Garba Guracha in the Bale Mountains, Ethiopia, based on $\delta^{18}O$ records of sugar biomarker and diatoms. - Quaternary Research, 1–14.

BLOM, R. G., FARR, T. G., FEYNMANN, J., RUZMAIKIN, A., & PAILLOU, P. (2009): The green Sahara: Climate change, hydrologic history and human occupation. - In 2009 IEEE Radar Conference (pp. 1–4).

BONNEFILLE, R., CHALIÉ, F., GUIOT, J., & VINCENS, A. (1992): Quantitative estimates of full glacial temperatures in equatorial Africa from palynological data*. - Climate Dynamics, **6**, 251–257.

CASTAÑEDA, I. S., SCHOUTEN, S., PÄTZOLD, J., LUCASSEN, F., KASEMANN, S., KUHLMANN, H., & SCHEFUß, E. (2016): Hydroclimate variability in the Nile River Basin during the past 28,000 years. - Earth and Planetary Science Letters, **438**, 47–56.

CHEDDADI, R., LAMB, H. F., GUIOT, J., & VAN DER KAARS, S. (1998): Holocene climatic change in

Morocco: a quantitative reconstruction from pollen data. - Climate Dynamics, **14**, 883–890.

CHEVALIER, M., & CHASE, B. M. (2015): Southeast African records reveal a coherent shift from high- to low-latitude forcing mechanisms along the east African margin across last glacial–interglacial transition. - Quaternary Science Reviews, **125**, 117–130.

COSTA, K., RUSSELL, J., KONECKY, B., & LAMB, H. (2014): Isotopic reconstruction of the African Humid Period and Congo Air Boundary migration at Lake Tana, Ethiopia. - Quaternary Science Reviews, **83**, 58–67.

DAMSTÉ, J. S. S., HOPMANS, E. C., PANCOST, R. D., SCHOUTEN, S., & GEENEVASEN, J. A. J. (2000): Newly discovered non-isoprenoid glycerol dialkyl glycerol tetraether lipids in sediments. - Chemical Communications, 1683–1684.

DE JONGE, C., HOPMANS, E. C., ZELL, C. I., KIM, J.-H., SCHOUTEN, S., & SINNINGHE DAMSTÉ, J. S. (2014): Occurrence and abundance of 6-methyl branched glycerol dialkyl glycerol tetraethers in soils: Implications for palaeoclimate reconstruction. - Geochimica et Cosmochimica Acta, **141**, 97–112.

DE JONGE, C., RADUJKOVIĆ, D., SIGURDSSON, B. D., WEEDON, J. T., JANSSENS, I., & PETERSE, F. (2019): Lipid biomarker temperature proxy responds to abrupt shift in the bacterial community composition in geothermally heated soils. - Organic Geochemistry, **137**.

DE JONGE, C., KURAMAE, E. E., RADUJKOVIĆ, D., WEEDON, J. T., JANSSENS, I. A., & PETERSE, F. (2021): The influence of soil chemistry on branched tetraether lipids in mid- and high latitude soils: Implications for brGDGT- based paleothermometry. - Geochimica et Cosmochimica Acta, **310**, 95–112.

DEARING CRAMPTON-FLOOD, E., TIERNEY, J. E., PETERSE, F., KIRKELS, F. M. S. A., & SINNINGHE DAMSTÉ, J. S. (2020): BayMBT: A Bayesian calibration model for branched glycerol dialkyl glycerol tetraethers in soils and peats. - Geochimica et Cosmochimica Acta, **268**, 142–159.

DEE, S. G., MORRILL, C., KIM, S. H., & RUSSELL, J. M. (2021): Hot Air, Hot Lakes, or Both? Exploring Mid-Holocene African Temperatures Using Proxy System Modeling. - Journal of Geophysical Research: Atmospheres, **126**, e2020JD033269.

DEMENOCAL, P., ORTIZ, J., GUILDERSON, T., ADKINS, J., SARNTHEIN, M., BAKER, L., & YARUSINSKY, M. (2000): Abrupt onset and termination of the African Humid Period: - Quaternary Science Reviews, **19**, 347–361.

EGGERMONT, H., HEIRI, O., JAMES, A., AE, R., VUILLE, M., LEEN, A., AE, A., & VERSCHUREN, D. (2010): Paleotemperature reconstruction in tropical Africa using fossil Chironomidae (Insecta: Diptera). - Journal of Paleolimnology, **43**, 413–435.

EGGERMONT, WINDAFRASH, M., VAN DAMME, M., LENS, K., & UMER M., H. (2011): Bale Moluntains Lakes : Ecosystems under pressure of global change? - Walia, **2011**, 171–180.

GARELICK, S., RUSSELL, J. M., DEE, S., VERSCHUREN, D., & OLAGO, D. O. (2021): Atmospheric controls on precipitation isotopes and hydroclimate in high-elevation regions in Eastern Africa since the Last Glacial Maximum. - Earth and Planetary Science Letters, **567**, 116984.

GARELICK, S., RUSSELL, J., RICHARDS, A., SMITH, J., KELLY, M., ANDERSON, N., JACKSON, M. S., DOUGHTY, A., NAKILEZA, B., IVORY, S., DEE, S., & MARSHALL, C. (2022): The dynamics of warming during the last deglaciation in high-elevation regions of Eastern Equatorial Africa. - Quaternary Science Reviews, **281**, 107416.

GASSE, F. (2000): Hydrological changes in the African tropics since the Last Glacial Maximum. - Quaternary Science Reviews, **19**, 189–211.

GIL-ROMERA, G., ADOLF, C., BENITO BLAS, M., BITTNER, L., JOHANSSON, M. M. U., GRADY, D. D. A., LAMB, H. H. F., LEMMA, B., FEKADU, M., GLASER, B., MEKONNEN, B., SEVILLA-CALLEJO, M., ZECH, M., ZECH, W., MIEHE, G., BENITO, B. M., BITTNER, L., JOHANSSON, M. M. U., GRADY, D. D. A., LAMB, H. H. F., LEMMA, B., FEKADU, M., GLASER, B., MEKONNEN, B., SEVILLA-CALLEJO, M., ZECH, M., ZECH, W., & MIEHE, G. (2019): Long-term fire resilience of the Ericaceous Belt, Bale Mountains, Ethiopia. - Biology Letters, **15**, 20190357.

GIL-ROMERA, G., FEKADU, M., OPGENOORTH, L., GRADY, D., LAMB, H. F., BITTNER, L., ZECH, M., & MIEHE, G. (2021): The new Garba Guracha palynological sequence: Revision and data expansion. - In S. L. Runge, J., Gosling, W.D., Lézine, A-M. (Ed.), Quaternary Vegetation Dynamics – The African Pollen Database (p. 442). - London: CRC Press.

GROOS, A. R., NIEDERHAUSER, J., WRAASE, L., HÄNSEL, F., NAUSS, T., AKÇAR, N., & VEIT, H. (2020): Implications of present ground temperatures and relict stone stripes in the Ethiopian Highlands for the palaeoclimate of the tropics. - Earth Surf. Dynam. Discuss., **2020**, 1–37.

GROOS, A., AKÇAR, N., YESILYURT, S., MIEHE, G., VOCKENHUBER, C., & VEIT, H. (2021): Nonuniform Late Pleistocene glacier fluctuations in tropical Eastern Africa. - Science Advances, **7**.

HILLMAN, J. (1988): The Bale Mountains National Park Area, Southeast Ethiopia, and Its ManagementMountain Research and Development (Vol. 8).

HOPMANS, E. C., SCHOUTEN, S., & SINNINGHE DAMSTÉ, J. S. (2016): The effect of improved chromatography on GDGT-based palaeoproxies. - Organic Geochemistry, **93**, 1–6.

HOPMANS, E. C., WEIJERS, J. W. H., SCHEFUß, E., HERFORT, L., SINNINGHE DAMSTÉ, J. S., & SCHOUTEN, S. (2004): A novel proxy for terrestrial organic matter in sediments based on branched and isoprenoid tetraether lipids. - Earth and Planetary Science Letters, **224**, 107–116.

HOVE, H., ECHEVERRIA, D., & PARRY, J.-E. (2011): Review of current and planned adaptation action: East Africa. - International Institute for Sustainable Development, Winnipeg.

HUGHES, A. C., ORR, M. C., MA, K., COSTELLO, M. J., WALLER, J., PROVOOST, P., YANG, Q., ZHU, C., & QIAO, H. (2021): Sampling biases shape our view of the natural world. - Ecography, **44**, 1259–1269.

HUGUET, C., KIM, J. H., DAMSTÉ, J. S. S., & SCHOUTEN, S. (2006): Reconstruction of sea surface temperature variations in the Arabian Sea over the last 23 kyr using organic proxies (TEX86 and $U_{37}K'$). - Paleoceanography, **21**.

HUYBERS, P. (2006): Early Pleistocene Glacial Cycles and the Integrated Summer Insolation Forcing. - Science (New York, N.Y.), **313**, 508–511.

IPCC (2021): Climate Change 2021: The Physical Science Basis. Contribution of Working Group I to the Sixth Assessment Report of the Intergovernmental Panel on Climate Change [Masson-Delmotte, V., P. Zhai, A. Pirani, S.L. Connors, C. Péan, S. Berger, N. Caud, Y. Chen,. Cambridge University Press.

IVORY, S. J., & RUSSELL, J. (2018): Lowland forest collapse and early human impacts at the end of the African Humid Period at Lake Edward, equatorial East Africa. - Quaternary Research, **89**, 7–20.

JAESCHKE, A., THIENEMANN, M., SCHEFUß, E., URBAN, J., SCHÄBITZ, F., WAGNER, B., & RETHEMEYER, J. (2020): Holocene Hydroclimate Variability and Vegetation Response in the Ethiopian Highlands (Lake Dendi). - Frontiers in Earth Science, **8**, 1–14.

JUNGINGER, A., ROLLER, S., OLAKA, L. A., & TRAUTH, M. H. (2014): The effects of solar irradiation changes on the migration of the Congo Air Boundary and water levels of paleo-Lake Suguta , Northern Kenya Rift , during the African Humid Period (15 – 5 ka BP). - Palaeogeography, Palaeoclimatology, Palaeoecology, **396**, 1–16.

KASSAMBARA, A., & MUNDT, F. (2020): factoextra: Extract and Visualize the Results of Multivariate Data Analyses. - . Retrieved from https://cran.r-project.org/package=factoextra

KIDANE, Y., STAHLMANN, R., & BEIERKUHNLEIN, C. (2012): Vegetation dynamics, and land use and land cover change in the Bale Mountains, Ethiopia. - Environmental Monitoring and Assessment, **184**, 7473–7489.

LASKAR, J., ROBUTEL, P., JOUTEL, F., GASTINEAU, M., CORREIA, A. C. M., & LEVRARD, B. (2004): A long-term numerical solution for the insolation quantities of the Earth . - A&A, **428**, 261–285. Retrieved from https://doi.org/10.1051/0004-6361:20041335

LÖFFLER, H. (1978): Limnology and paleolimnological data on the Bale Mountain Lakes. - Verth, International Verein. Limnology, **20**, 1131–1138.

LOOMIS, S. E., RUSSELL, J. M., & SINNINGHE DAMSTÉ, J. S. (2011): Distributions of branched GDGTs in soils and lake sediments from western Uganda: Implications for a lacustrine paleothermometer. - Organic Geochemistry, **42**, 739–751.

LOOMIS, S. E. S. E., RUSSELL, J. M., LADD, B., STREET-PERROTT, F. A. A., & SINNINGHE DAMSTÉ, J. S. J. S. (2012): Calibration and application of the branched GDGT temperature proxy on East African lake sediments. - Earth and Planetary Science Letters, **357**–**358**, 277–288.

LOOMIS, S. E., RUSSELL, J. M., HEUREUX, A. M., D'ANDREA, W. J., & SINNINGHE DAMSTÉ, J. S. (2014):

Seasonal variability of branched glycerol dialkyl glycerol tetraethers (brGDGTs) in a temperate lake system. - Geochimica et Cosmochimica Acta, **144**, 173–187.

LOOMIS, S. E., RUSSELL, J. M., & LAMB, H. F. (2015): Northeast African temperature variability since the Late Pleistocene. - Palaeogeography, Palaeoclimatology, Palaeoecology, **423**, 80–90.

LOOMIS, S. E., RUSSELL, J. M., VERSCHUREN, D., MORRILL, C., DE CORT, G., SINNINGHE DAMSTÉ, J. S., OLAGO, D., EGGERMONT, H., STREET-PERROTT, F. A., & KELLY, M. A. (2017): The tropical lapse rate steepened during the Last Glacial Maximum. - Science Advances, **3**.

LYON, B., & VIGAUD, N. (2017, June 22): Unraveling East Africa's Climate Paradox. - Climate Extremes.

MARSHALL, M., LAMB, H., DAVIES, S., LENG, M., BEDASO, Z., UMER, M., & BRYANT, C. (2009): Climatic change in northern Ethiopia during the past 17,000 years: A diatom and stable isotope record from Lake Ashenge. - Palaeogeography Palaeoclimatology Palaeoecology, **279**.

MARTÍNEZ-SOSA, P., TIERNEY, J. E., STEFANESCU, I. C., CRAMPTON-FLOOD, E. D., SHUMAN, B. N., & ROUTSON, C. (2021, May 6): A global Bayesian temperature calibration for lacustrine brGDGTs. - . PANGAEA.

MIEHE, S., & MIEHE, G. (1994): Ericaceous forests and heathlands in the Bale mountains of South Ethiopia : ecology and man's impact (G. Miehe & 1952-, Eds.). - Reinbek: Reinbek : Warnke.

MORRISSEY, A., & SCHOLZ, C. A. C. A. C. A. (2014): Paleohydrology of Lake Turkana and its influence on the Nile River system. - Palaeogeography, Palaeoclimatology, Palaeoecology, **403**, 88–100.

MORRISSEY, A., SCHOLZ, C. A., & RUSSELL, J. M. (2018): Late Quaternary TEX_{86} paleotemperatures from the world's largest desert lake, Lake Turkana, Kenya. - Journal of Paleolimnology, **59**, 103–117.

NEUKOM, R., BARBOZA, L. A., ERB, M. P., SHI, F., EMILE-GEAY, J., EVANS, M. N., FRANKE, J., KAUFMAN, D. S., LÜCKE, L., REHFELD, K., SCHURER, A., ZHU, F., BRÖNNIMANN, S., HAKIM, G. J., HENLEY, B. J., LJUNGQVIST, F. C., MCKAY, N., VALLER, V., VON GUNTEN, L., & CONSORTIUM, P. 2K (2019): Consistent multidecadal variability in global temperature reconstructions and simulations over the Common Era. - Nature Geoscience, **12**, 643–649.

NICHOLSON, S. E. (2017): Climate and climatic variability of rainfall over eastern Africa. - Reviews of Geophysics, **55**, 590–635.

OSMASTON, H. A., MITCHELL, W. A., & OSMASTON, J. A. N. (2005): Quaternary glaciation of the Bale Mountains, Ethiopia. - Journal of Quaternary Science, **20**, 593–606.

OSSENDORF, G., GROOS, A., BROMM, T., GIRMA TEKELEMARIAM, M., GLASER, B., LESUR, J., SCHMIDT, J., AKÇAR, N., BEKELE, T., BELDADOS, A., DEMISSEW, S., HADUSH KAHSAY, T., P NASH, B., NAUSS, T., NEGASH, A., NEMOMISSA, S., VEIT, H., VOGELSANG, R., ZERIHUN, W., & MIEHE, G. (2019): Middle

Stone Age foragers resided in high elevations of the glaciated Bale Mountains, Ethiopia. - Science, **365**, 583–587.

OTTO-BLIESNER, B. L., RUSSELL, J. M., CLARK, P. U., LIU, Z., OVERPECK, J. T., KONECKY, B., DEMENOCAL, P., NICHOLSON, S. E., HE, F., & LU, Z. (2014): Coherent changes of southeastern equatorial and northern African rainfall during the last deglaciation. - Science, **346**, 1223–1227.

PETERSE, F., VAN DER MEER, J., SCHOUTEN, S., WEIJERS, J. W. H., FIERER, N., JACKSON, R. B., KIM, J.-H., & SINNINGHE DAMSTÉ, J. S. (2012): Revised calibration of the MBT–CBT paleotemperature proxy based on branched tetraether membrane lipids in surface soils. - Geochimica et Cosmochimica Acta, **96**, 215–229.

POWERS, L. A., JOHNSON, T. C., WERNE, J. P., CASTAÑEDA, I. S., HOPMANS, E. C., SINNINGHE DAMSTÉ, J. S., & SCHOUTEN, S. (2005): Large temperature variability in the southern African tropics since the Last Glacial Maximum. - Geophysical Research Letters, **32**, 1–4.

R CORE TEAM (2021): R: A Language and Environment for Statistical Computing. - . - Vienna, Austria. Retrieved from https://www.r-project.org/

RABERG, J. H., HARNING, D. J., CRUMP, S. E., DE WET, G., BLUMM, A., KOPF, S., GEIRSDÓTTIR, Á., MILLER, G. H., & SEPÚLVEDA, J. (2021): Revised fractional abundances and warm-season temperatures substantially improve brGDGT calibrations in lake sediments. - Biogeosciences, **18**, 3579–3603.

RUSSELL, J. M., HOPMANS, E. C., LOOMIS, S. E., LIANG, J., & SINNINGHE DAMSTÉ, J. S. (2018): Distributions of 5- and 6-methyl branched glycerol dialkyl glycerol tetraethers (brGDGTs) in East African lake sediment: Effects of temperature, pH, and new lacustrine paleotemperature calibrations. - Organic Geochemistry, **117**, 56–69.

SCHOUTEN, S., FORSTER, A., PANOTO, F. E., & SINNINGHE DAMSTÉ, J. S. (2007): Towards calibration of the TEX_{86} palaeothermometer for tropical sea surface temperatures in ancient greenhouse worlds. - Organic Geochemistry, **38**, 1537–1546.

SCHREUDER, L. T., BEETS, C. J., PRINS, M. A., HATTÉ, C., & PETERSE, F. (2016): Late Pleistocene climate evolution in Southeastern Europe recorded by soil bacterial membrane lipids in Serbian loess. - Palaeogeography, Palaeoclimatology, Palaeoecology, **449**, 141–148.

SINNINGHE DAMSTÉ, J. S., RIJPSTRA, W. I. C., FOESEL, B. U., HUBER, K. J., OVERMANN, J., NAKAGAWA, S., KIM, J. J., DUNFIELD, P. F., DEDYSH, S. N., & VILLANUEVA, L. (2018): An overview of the occurrence of ether- and ester-linked iso-diabolic acid membrane lipids in microbial cultures of the Acidobacteria: Implications for brGDGT paleoproxies for temperature and pH. - Organic Geochemistry, **124**, 63–76.

THOMPSON, L. G., MOSLEY-THOMPSON, E., DAVIS, M. E., HENDERSON, K. A., BRECHER, H. H., ZAGORODNOV, V. S., MASHIOTTA, T. A., LIN, P.-N., MIKHALENKO, V. N., HARDY, D. R., & BEER, J. (2002): Kilimanjaro Ice Core Records: Evidence of Holocene Climate Change in Tropical Africa. - Science, **298**, 589–593.

TIERCELIN, J. J., GIBERT, E., UMER, M., BONNEFILLE, R., DISNAR, J. R., LÉZINE, A. M., HUREAU-MAZAUDIER, D., TRAVI, Y., KERAVIS, D., & LAMB, H. F. (2008): High-resolution sedimentary record of the last deglaciation from a high-altitude lake in Ethiopia. - Quaternary Science Reviews, **27**, 449–467.

TIERNEY, J. E., & RUSSELL, J. M. (2007): Abrupt climate change in southeast tropical Africa influenced by Indian monsoon variability and ITCZ migration. - Geophysical Research Letters, **34**.

TIERNEY, J. E., & DEMENOCAL, P. B. (2013): Abrupt Shifts in Horn of Africa Hydroclimate Since the Last Glacial Maximum. - Science, **342**, 843–846.

TIERNEY, J. E., RUSSELL, J. M., HUANG, Y., DAMSTE, J. S. S., HOPMANS, E. C., & COHEN, A. S. (2008): Northern Hemisphere Controls on Tropical Southeast African Climate During the Past 60,000 Years. - Science, **322**, 252–255.

TIERNEY, J. E., LEWIS, S. C., COOK, B. I., LEGRANDE, A. N., & SCHMIDT, G. A. (2011a): Model, proxy and isotopic perspectives on the East African Humid Period. - Earth and Planetary Science Letters, **307**, 103–112.

TIERNEY, J. E., RUSSELL, J. M., SINNINGHE DAMSTÉ, J. S., HUANG, Y., & VERSCHUREN, D. (2011b): Late Quaternary behavior of the East African monsoon and the importance of the Congo Air Boundary. - Quaternary Science Reviews, **30**, 798–807.

TIERNEY, J. E., SMERDON, J. E., ANCHUKAITIS, K. J., & SEAGER, R. (2013): Multidecadal variability in East African hydroclimate controlled by the Indian Ocean. - Nature, **493**, 389–392.

TIERNEY, J. E., PAUSATA, F. S. R., & DEMENOCAL, P. (2016): Deglacial Indian monsoon failure and North Atlantic stadials linked by Indian Ocean surface cooling. - Nature Geoscience, **9**, 46–50.

TIERNEY, J. E., PAUSATA, F. S. R., & DEMENOCAL, P. B. (2017): Rainfall regimes of the Green Sahara. - Science Advances, **3**.

TRAUTH, M. H., FOERSTER, V., JUNGINGER, A., ASRAT, A., LAMB, H. F., & SCHAEBITZ, F. (2018): Abrupt or gradual? Change point analysis of the late Pleistocene–Holocene climate record from Chew Bahir, southern Ethiopia. - Quaternary Research, **90**, 321–330.

UHLIG, S. K. (1988): Mountain Forests and the Upper Tree Limit on the Southeastern Plateau of Ethiopia. - Mountain Research and Development, **8**, 227–234.

UHLIG, S., & UHLIG, K. (1991): Studies on the Altitudinal Zonation of Forests and Alpine Plants in the Central Bale Mountains, EthiopiaMountain Research and Development (Vol. 11).

UMER, M., LAMB, H. F., BONNEFILLE, R., LÉZINE, A. M., TIERCELIN, J. J., GIBERT, E., CAZET, J. P., & WATRIN, J. (2007): Late Pleistocene and Holocene vegetation history of the Bale Mountains, Ethiopia. - Quaternary Science Reviews, **26**, 2229–2246.

VAN BREE, L. G. J., PETERSE, F., BAXTER, A. J., DE CROP, W., VAN GRINSVEN, S., VILLANUEVA, L., VERSCHUREN,

D., & SINNINGHE DAMSTÉ, J. S. (2020): Seasonal variability and sources of in situ brGDGT production in a permanently stratified African crater lake. - Biogeosciences Discuss., **2020**, 1–36.

WAGNER, B., WENNRICH, V., VIEHBERG, F., JUNGINGER, A., KOLVENBACH, A., RETHEMEYER, J., SCHAEBITZ, F., & SCHMIEDL, G. (2018): Holocene rainfall runoff in the central Ethiopian highlands and evolution of the River Nile drainage system as revealed from a sediment record from Lake Dendi. - Global and Planetary Change, **163**, 29–43.

WANG, H., LIU, W., HE, Y., ZHOU, A., ZHAO, H., LIU, H., CAO, Y., HU, J., MENG, B., JIANG, J., KOLPAKOVA, M., KRIVONOGOV, S., & LIU, Z. (2021): Salinity-controlled isomerization of lacustrine brGDGTs impacts the associated MBT5ME' terrestrial temperature index. - Geochimica et Cosmochimica Acta, **305**, 33–48.

WEBER, Y., DAMSTÉ, J. S. S., ZOPFI, J., DE JONGE, C., GILLI, A., SCHUBERT, C. J., LEPORI, F., LEHMANN, M. F., & NIEMANN, H. (2018): Redox-dependent niche differentiation provides evidence for multiple bacterial sources of glycerol tetraether lipids in lakes. - Proceedings of the National Academy of Sciences of the United States of America, **115**, 10926–10931.

WEIJERS, J. W. H., SCHEFUß, E., SCHOUTEN, S., & DAMSTÉ, J. S. S. (2007a): Coupled thermal and hydrological evolution of tropical Africa over the last deglaciation. - Science, **315**, 1701–1704.

WEIJERS, J. W. H., SCHOUTEN, S., VAN DEN DONKER, J. C., HOPMANS, E. C., & SINNINGHE DAMSTÉ, J. S. (2007b): Environmental controls on bacterial tetraether membrane lipid distribution in soils. - Geochimica et Cosmochimica Acta, **71**, 703–713.

WERDECKER, J. (1962): Eine Durchquerung des Goba-Massivs in Südäthiopien. - , **Hermann vo**, 132–144.

WILLIAMS, F. M. (2016): The Southeastern Highlands and the Ogaden. - In F. M. Williams (Ed.), (pp. 153–170). - Cham: Springer International Publishing.

WOLDU, Z., FEOLI, E., & NIGATU, L. (1989): Partitioning an elevation gradient of vegetation from southeastern Ethiopia by probabilistic methods. - Plant Ecology, **81**, 189–198.

WU, H., GUIOT, J., BREWER, S., & GUO, Z. (2007): Climatic changes in Eurasia and Africa at the last glacial maximum and mid-Holocene: reconstruction from pollen data using inverse vegetation modelling. - Climate Dynamics, **29**, 211–229.

ZENG, F., & YANG, H. (2019): Temperature changes reconstructed from branched GDGTs on the central Loess Plateau during the past 130–5 ka. - Quaternary International, **503**, 3–9.

Chapter 5

Synthesis

The high-altitude Garba Guracha sedimentary archive is situated in the Horn of Africa region, an understudied region of the world in terms of paleoclimate and environmental history. High altitude archives, especially in the Horn of Africa, are rare. The reconstruction of the catchment development and the environmental and climatic history of Garba Guracha since the last glaciation is a valuable addition to the regional and global understanding of climatic changes.

Based on the three published articles, this thesis covers the research process of the Garba Guracha sediment archive, including the development of a chronology, creating a deeper understanding of catchment processes (Chapter 2), leading to the application of innovative biomarker and isotopic analyses (Chapter 3 and 4). The synthesis aims to combine the main findings of the three research articles and discuss their implications for the reconstruction of the environmental and climatic history of the Bale Mountains and eastern Africa.

5.1 Sedimentation and chronology - What is the time frame and age-depth function of the Garba Guracha core?

Revisiting Garba Guracha in 2017, a new sediment core was retrieved in duplicates with a total depth of 1550 cm. A high resolution and robust age-depth model is the basis of working on paleo core sediments. To create a robust age and depth model, a deeper understanding of sedimentology is necessary. A common depth profile of all core sections has been developed using smear slides and XRF data. Moreover, a master core for the two duplicate cores was created using visual correlation of XRF elements (SAGNOTTI & CARICCHI, 2018).

With a common depth profile for all sections in both retrieved cores, a multi-compound dating approach was applied to gain a high resolution and robust chronology. To develop an age-depth model, the ^{210}Pb, bulk sediment, compound class-specific *n*-alkane and charcoal radiocarbon ages were combined into a Bayesian modelling framework (BLAAUW, 2010; BLAAUW ET AL., 2011).

The new retrieved Garba Guracha core covers the period from ~ 15.9 cal ka BP to modern times. The mean sedimentation rate of the entire core is ~ 0.97 mm a^{-1}, e.g. a resolution of ~ 10 years per centimeter, similar to the findings by TIERCELIN ET AL. (2008). Unfortunately, the core of TIERCELIN ET AL. (2008) and UMER ET AL. (2007) was not accessible for comparison or further research.

Comparing the results of the new sediment core to the results of the core of TIERCELIN ET AL. (2008) and UMER ET AL. (2007), overall similarities but also small-scale differences in the depth of lithological changes and chronology become evident (Fig. 5.1).

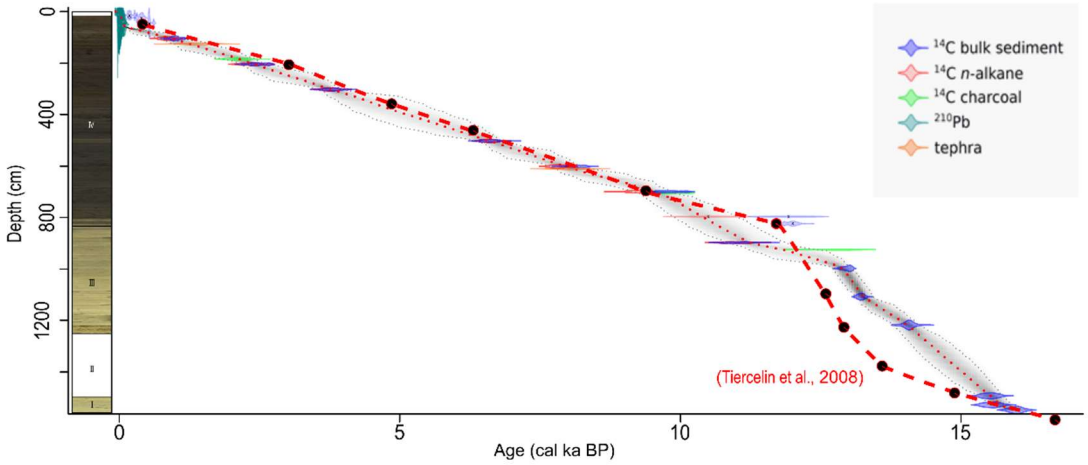

Figure 5.1: Comparison of the age-depth models of the Garba Guracha sedimentary record by TIERCELIN ET AL. (2008) (red curve, black dots are actual radiocarbon dates) and (BITTNER ET AL., 2020) (rbacon model in the background with violin plots reflecting the dates error distributions for each dating technic, the ghost plot reflects the model uncertainty). The core picture is on the left-hand side.

For the last 10 cal ka BP, the two cores are relatively similar in their age-depth function, sedimentation rate and organic-rich sedimentation. However, although the basal ages of ~ 15.9 cal ka BP and ~ 16.7 cal ka BP in the new and old core are similar, the age-depth function and sedimentology before 10 cal ka BP are different. The chronology developed by TIERCELIN ET AL. (2008) suggests a low mean sedimentation rate of 0.71 mm a^{-1} until 13.5 cal ka BP. The highest mean sedimentation rate (3.28 mm a^{-1}) of the entire core is recorded until 11.8 cal ka BP. This strongly contrasts with the reconstructed sedimentation rates in the new Garba Guracha sediment core. While the mean sedimentation rate is higher (1.64 mm a^{-1}) in the lower part of the new core, it is much lower until 11.8 cal ka BP (1.89 mm a^{-1}). In the corresponding depths (1476 - 1276 cm), a coarse sand and gravel unit, which might have been accumulated in a single event, distorts the sedimentation rate calculation. The sedimentation of coarse sand and gravel seems not as pronounced in the core of TIERCELIN ET AL. (2008) and UMER ET AL. (2007). Differences in the sedimentation rate and lithology in the same lake can be explained by lake bed geometry and the distance from the shore (SCHILLEREFF ET AL., 2014; SZMYTKIEWICZ & ZALEWSKA, 2014). Unfortunately, the exact position of the sediment core used by TIERCELIN ET AL. (2008) and UMER ET AL. (2007) is unknown. Since the calculated sedimentation rate depends primarily on the quantity, robustness and accuracy of the chronological data, the high-resolution age-depth model in the new sediment core of Garba Guracha increases the precision of reconstructed sedimentation rate changes.

The ages of the geochemically correlated Garba Guracha tephra layers were not included in the age-depth model but were used as an external age control. The ages of these tephra layers in Lake Tilo and Lake Chamo (MARTIN-JONES ET AL., 2017) are consistent with the modelled ages of the corresponding depth of GGT-1 and GGT-2 (129 and 604 cm) in the Garba Guracha age-depths model (1.2 - 1.6 and 7.8 - 8.1 cal ka BP). The tephra layers provide an independent chronological context on the age model of Garba Guracha, underlining the robustness. Additionally, despite an offset between ^{14}C bulk sediment and ^{210}Pb ages at the

top of the core, the external age control allows concluding no systematic age offset in the Garba Guracha archive.

Even though there is no systematic age offset, a discrepancy between bulk sediment ^{14}C and ^{210}Pb ages appears after ~ 1 cal ka BP. The absence of a hard water effect and the excellent agreement of ^{210}Pb and SCP lead to the hypothesis of pre-aged terrestrial organic matter accumulation due to human activity in the catchment. A stratigraphical inconsistency of ages also appears at depths 794 and 821 cm with a modelled age of 10.4 to 10.6 cal ka BP. At these depths, ^{14}C bulk sediment dating yielded stratigraphically too old ages. The inconsistency appears during times of shortly increased sedimentation rates and might be explained by old carbon inwash due to increased runoff. An *n*-alkane date at the exact same depth (794 cm) dating to 9.7 - 11.2 cal ka BP is more in line with the age-depth model. Even though the *n*-alkane age had to be excluded because it was just below the carbon mass limit, it indicates that the bulk sediment might be more strongly pre-aged than the *n*-alkane component.

Except for this period, the bulk sediment and *n*-alkane dating from the exact same centimetre did not yield any offset. In sediment cores, terrestrial *n*-alkanes and aquatic organic matter have been reported to yield different ages due to the pre-ageing of the terrestrial *n*-alkanes (DOUGLAS ET AL., 2014; GIERGA ET AL., 2016). The chemical inertness, resistance against degradation and low water solubility preserves *n*-alkanes in soils and sediments over long periods (EGLINTON & EGLINTON, 2008). However, the small Garba Guracha catchment and poorly developed soils might favour rapid sedimentation and reduce *n*-alkane pre-ageing. The overall missing ^{14}C offsets in the Garba Guracha record suggest that (i) the residence time of organic matter, especially of terrestrial *n*-alkanes in the catchment, is very short and/or (ii) the *n*-alkanes and bulk sedimentary organic matter is primarily of the same allochthonous/autochthonous origin. Moreover, the consistent compound class-specific dating of *n*-alkanes is a valuable tool for paleolimnological research.

5.2 Source identification - What is the origin of the organic material in the Garba Guracha sediment core?

The distinction of organic matter between allochthonous (terrestrial) and autochthonous (aquatic) origin is a critical issue in palaeolimnological studies (BRENNER ET AL., 1999; MEYERS, 2003) and of paramount importance for the interpretation of any further proxy analyses.
Over the entire core, a predominant autochthonous organic matter origin is supported by the following proxies:

- $\delta^{13}C$ - overall, relatively positive values (≥-22.7 ‰) and no evidence of the existence of C_4 vegetation in the Garba Guracha catchment (MEKONNEN ET AL., 2019) point to autochthonous organic matter input.
- TOC/N - overall low values with a minimum of 2.8 and a maximum of 14.9. The highest values coincide with the highest abundance of B. braunii (UMER ET AL., 2007). Compared to other algae, unusually high TOC/N ratios have been reported for *B. braunii* (LENG & MARSHALL, 2004). A cultivated *B. braunii* sample yielded a TOC/N ratio of 18 and a $\delta^{13}C$ value of -13.8 ‰. A large abundance of *B. braunii* may lead to higher TOC/N values mistakenly interpreted as an allochthonous organic matter input.
- Sugar quantification - the fucose/(arabinose+xylose) values range from 0.2 to 0.8 points to a predominant aquatic source because terrestrial plants and mosses are characterised by values < 0.1 (HEPP ET AL., 2016).

However, the source identification of *n*-alkanes in the sediments does not support an overall predominant autochthonous organic matter input. The P_{aq} proxy reveals that aquatic *n*-alkanes dominate the YD time. A mixture of aquatic and terrestrial *n*-alkanes is found in the Early and Mid-Holocene, and the Late Holocene is dominated by terrestrial *n*-alkane input. However, assigning chain lengths to terrestrial or aquatic plants of the P_{aq} ratio has been challenging in several studies. BAAS ET AL. (2000) and TARASOV ET AL. (2013) highlight the extensive production of the *n*-alkanes nC_{23} and nC_{25}, normally considered as "aquatic", by terrestrial plants (birch and *Sphagnum* species). The long chain *n*-alkanes (nC_{29}, nC_{31}, nC_{33}) are primarily produced by terrestrial vascular plants (SACHSE ET AL., 2012). A comparison of nC_{29}, nC_{31}, and nC_{33} abundances in Bale Mountain soil organic matter and Garba Guracha core sediments (Fig. 5.2) shows strong similarities indicating the predominantly terrestrial origin of these compounds in the lake sediments (Mekonnen et al., in preparation) (Table D.1 and D.2).

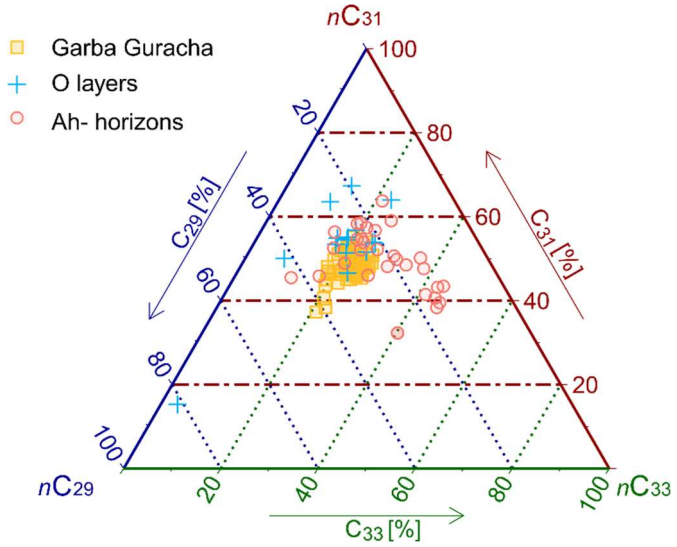

Figure 5.2: Ternary diagram illustrating the relative contributions of nC_{29}, nC_{31}, and nC_{33} in the Garba Guracha archive and catchment soil layers – O layer and Ah horizon data from LEMMA ET AL. (2019) and MEKONNEN ET AL. (2019) (Table D.1 and D.2).

5.3 Hydrology - $\delta^{18}O$ as a proxy for Garba Guracha evaporation history

The autochthonous or allochthonous origin of the sedimentary biomarkers, especially of $\delta^{18}O_{sugars}$, is crucial for interpreting the isotopic composition. $\delta^{18}O$ of plant-derived monosaccharides is modified by a biosynthetic fractionation factor (ε_{bio}) and can either reflect lake water $\delta^{18}O$ ($\delta^{18}O_{lake\ water}$) when of aquatic origin or leaf water $\delta^{18}O$ ($\delta^{18}O_{leaf\ water}$) when of terrestrial origin. The source identification has shown that the organic matter in the Garba Guracha sediments is predominantly of aquatic origin. Regarding the sugar biomarkers, a partial terrestrial contribution to the sediments cannot be entirely excluded. However, following the findings of HEPP ET AL. (2016), the terrestrial contribution of fucose can be neglected. Therefore, analysing the isotopic composition of fucose in the Garba Guracha record results in reconstructing the isotopic composition of the surrounding lake water during fucose synthesis. The isotopic composition of diatoms, a purely aquatic signal, was analysed to test this suggestion further. The results showed that

- the reconstructed $\delta^{18}O_{lake\ water}$ values of fucose and diatoms are consistent after correction for ε_{bio} (+29 ‰) (MAYR ET AL., 2015) and temperature-dependent fractionation during diatom growth (LECLERC & LABEYRIE, 1987), respectively,
- the $\delta^{18}O_{diatom}$ and $\delta^{18}O_{fucose}$ ranges of the 16 analysed samples are similar (7.9 ‰ and 7.1 ‰, respectively),
- the aquatic $\delta^{18}O_{diatom}$ and $\delta^{18}O_{fucose}$ records show identical trends in the whole record, indicating a common source water signal of $\delta^{18}O_{fucose}$ and $\delta^{18}O_{diatom}$.

Based on these findings, it can be concluded that the $\delta^{18}O_{diatom}$ record corroborates the $\delta^{18}O_{fucose}$ record to reflect primarily $\delta^{18}O_{lake\ water}$ (Fig. 5.3). The variability of $\delta^{18}O_{lake\ water}$ depends on $\delta^{18}O_{precipitation}$ and evaporative ^{18}O enrichment of lake water.

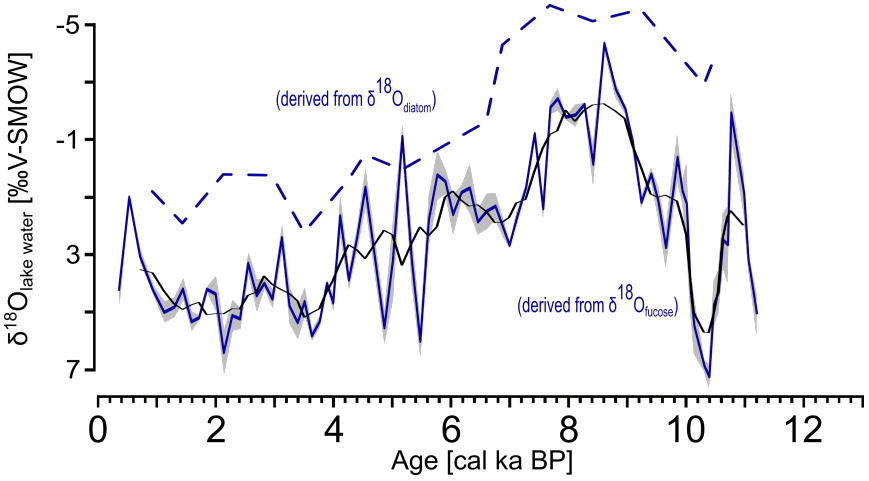

Figure 5.3: Garba Guracha $\delta^{18}O$ records – $\delta^{18}O_{lake\ water}$ derived from diatoms and fucose.

In the tropics, $\delta^{18}O_{precipitation}$ has been interpreted to represent changes in the amount of precipitation with depleted $\delta^{18}O$ values indicating high amounts of precipitation (amount effect) (DANSGAARD, 1964; ROZANSKI ET AL., 1993). However, besides the amount effect, the history of the entire moist air mass, including source region (source effect), (re)evaporative history (recycling), the air mass convection (altitude effect), and transport distance (continental effect) must be considered (SHARP, 2017). In addition, temperature (temperature effect) strongly affects $\delta^{18}O_{precipitation}$ (ROZANSKI ET AL., 1993). Temperature changes in the tropics were relatively small, especially during the Holocene, implying that the temperature effect is negligible (ROZANSKI ET AL., 1993; VUILLE ET AL., 2005). Therefore, we can assume that $\delta^{18}O_{precipitation}$ is primarily controlled by the source and amount effect in eastern Africa. Since the ^{18}O record of Garba Guracha is of aquatic origin and, in contrast to other records, reconstructs $\delta^{18}O_{lake\ water}$, not pure $\delta^{18}O_{precipitation}$, an additional strong influence of evaporative enrichment in the Garba Guracha record is suggested.

The ^{18}O enrichment of Garba Guracha lake water is evident in water samples collected from Garba Guracha during the dry season. These samples are enriched by at least ~ +5 ‰ in $\delta^{18}O$ compared to $\delta^{18}O_{precipitation}$ values measured at nearby climate stations (LEMMA ET AL., 2021). Temperatures and precipitation, among other factors, affect the intensity of the evaporative enrichment of lake water. In modern times temperatures and precipitation represent an intermediate value, surpassed in the mid-Holocene and below before 10.5 cal ka BP (Fig. 5.3 and 5.5). Therefore, it is plausible to assume that a $\delta^{18}O$ enrichment of 5 ‰ represents neither the maximum nor the minimum of the possible influence of evaporative enrichment during the last 12.5 cal ka BP. Thus, changes in evaporative enrichment could likely explain the total range of $\delta^{18}O_{lake\ water}$ of 8 ‰ in the Garba Guracha record. While the influence of $\delta^{18}O_{precipitation}$ or additional factors should not be excluded, the results emphasise the possible strong influence of evaporative enrichment. Besides temperature and precipitation,

the evaporative enrichment of lake water is mainly determined by the inflow and outflow of a water body. The most crucial control on $\delta^{18}O_{lake\ water}$ in open lake systems is $\delta^{18}O_{precipitation}$, whereas evaporative enrichment is the primary driver in closed lake systems (HORTON ET AL., 2016; LAMB ET AL., 2002; TALBOT, 1990). Currently, Garba Guracha, with a sill level at 6 m water depth, varies annually between a closed and an open lake system depending on seasonality. The $\delta^{18}O_{lake\ water}$ record of Garba Guracha likely represents changes between open and closed lake conditions and associated wet/dry phases in the past. Therefore, the $\delta^{18}O_{lake\ water}$ record is interpreted in terms of precipitation-to-evaporation ratio (P/E), with more depleted $\delta^{18}O$ values reflecting higher P/E values.

5.4 Hydrology - δ^2H – as a proxy for the Garba Guracha precipitation history

While the *n*-alkane source identification of all chain lengths is not unambiguous, long-chained n-alkanes (*n*C_{29}, *n*C_{31}, *n*C_{33}) in the Garba Guracha seem to be of terrestrial origin. The isotopic composition of terrestrial *n*-alkanes represents $\delta^2H_{leaf\ water}$ after the correction of ε_{bio} (160 ‰), affected mainly by $\delta^2H_{precipitation}$. In tropical regions, $\delta^2H_{precipitation}$ primarily reflects the amount of precipitation. High amounts of precipitation lead to more depleted $\delta^2H_{precipitation}$ values (amount effect) (DANSGAARD, 1964; SACHSE ET AL., 2012). While other influences have been discussed, such as moisture source (source effect) and air mass pathway and associated convection (continental effect and altitude effect) (COSTA ET AL., 2014; KONECKY ET AL., 2011), recent studies highlight the influence of the amount effect in modern and past times (BODÉ ET AL., 2020; GARELICK ET AL., 2021). The strong correlation between δ^2H (depleted values pointing to higher precipitation amounts) and $\delta^{18}O_{fucose}$ (depleted values pointing to higher P/E) in the Garba Guracha record supports the interpretation regarding the amount of precipitation.

The yet unpublished (manuscript in preparation) isotopic composition of the terrestrial *n*-alkanes (*n*C_{29}, *n*C_{31}, *n*C_{33}) is relatively positive prior to 11.5 cal ka BP and become more depleted until 10 cal ka BP. Followed by a stable phase with the most negative values till 7 cal ka BP. A continuous trend towards more enriched δ^2H values continues until the present time (Fig. 5.4, Table D.3).

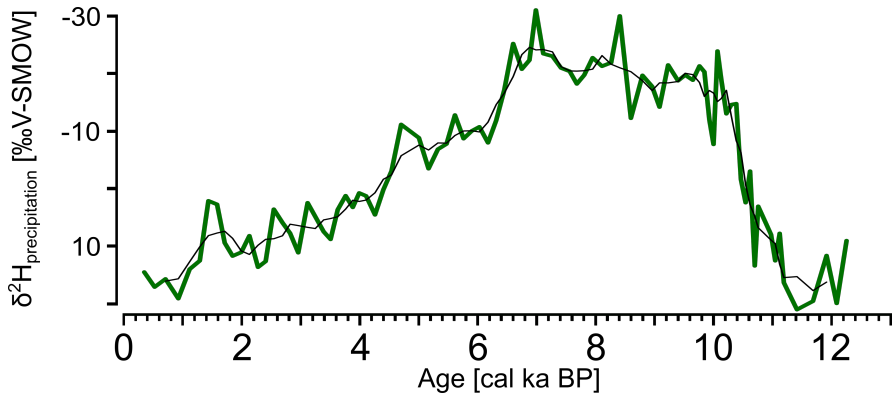

Figure 5.4: Garba Guracha δ^2H records – $\delta^2H_{precipitation}$ derived from the mean δ^2H value of *n*C_{29}, *n*C_{31}, and *n*C_{33} (Table D.3).

5.5 Temperature - brGDGTs - as a proxy for Garba Guracha MAT history

A modern calibration study is necessary to reconstruct the temperature of paleo archives using brGDGTs. A modern brGDGT calibration study of eastern African lakes has been published by RUSSELL ET AL. (2018) and the brGDGT composition of 11 Bale Mountain lakes was published by BAXTER ET AL. (2019). Comparing these datasets, it became apparent that brGDGT compositions are significantly different. In the Bale Mountain lakes, the percentage of IIIa and IIa is lower, and the IIIa' and IIa' is higher than in similar high-altitude lakes (above 3500 m) in eastern Africa. However, the combined percentage of these 5 and 6-methyl isomers is similar. The findings lead to the hypothesis that in some Bale Mountain lakes, the 6-methyl isomers (IIa' and IIIa') are formed in place of their 5-methyl equivalents (IIa and IIIa).

In addition, the isomer IIIa', which is not usually used for temperature calibrations, when summed with IIIa, improves the correlation with MAT. Therefore, the existing temperature calibration (MBT'_{5ME}) is compared to calibrations including IIIa'. The correlation coefficients of the MBT'_{5ME} ratio that includes IIIa' (r^2 = 0.93, root-mean-square error (RMSE) of 2.38 °C) are slightly better than the original MBT'_{5ME} without IIIa' (r^2 = 0.92, RMSE of 2.41 °C).

The uncommonly high abundance of brGDGTs IIIa' relative to IIIa as recorded in the Bale Mountain lake surface sediments is also evident in the Garba Guracha sediment record. The relative abundance of IIIa' is high until 10.8 cal ka BP, after which it decreases drastically. At 4.2 cal ka BP, the highest abundances of IIIa' occur. Depending on the abundance of IIIa', the MAT reconstruction results of both calibrations applied to the Garba Guracha sediment core differ. The strongest offset appears at 4.2 cal ka BP due to the abrupt high abundance of IIIa'. A sudden temperature rise is recorded by the MBT'_{5ME}, contrary to the occurring temperature drop using the MBT'_{5ME} + IIIa', which is in phase with decreasing insolation. The rise in IIIa' and, therefore, the MAT offset coincides with the 4.2 cal ka BP drought phase. In the Garba Guracha record, other proxies shift simultaneously (total organic carbon (TOC), $\delta^{13}C$, TOC/N, *Erica spp*, charcoal) (GIL-ROMERA ET AL., 2019), indicating abrupt changing catchment conditions. The decline of the *Erica* shrubland (GIL-ROMERA ET AL., 2019) could have resulted in a recorded increase in the surface lake water pH. Coinciding with these changes, the reconstructed conductivity of the lake water and the decreasing CBT' ratio supports changing lake water chemistry conditions. The abrupt change of lake water chemistry might have led to simultaneous declining proxies in the predominantly aquatic organic matter production of Garba Guracha. However, CBT' changes can also be explained by shifting bacterial communities in soils and lakes (DE JONGE ET AL., 2019; VAN BREE ET AL., 2020; WEBER ET AL., 2018). While RABERG ET AL. (2021) and WANG ET AL. (2021) proved that the brGDGT composition changes depending on lake water conductivity and salinity, respectively, DE JONGE ET AL. (2021) showed that pH-dependent community changes affect MBT'_{5ME} values in soils. Similar effects might be seen in Garba Guracha.

Therefore, changes in lake water chemistry and/or bacterial communities might be responsible for the systematical overestimation of temperatures by the MBT'_{5ME} calibration.

Due to the unique brGDGT composition of the Bale Mountains, MBT'$_{5ME}$ + IIIa' more accurately reconstructs the MAT of the Garba Guracha sediments core (Fig. 5.5).

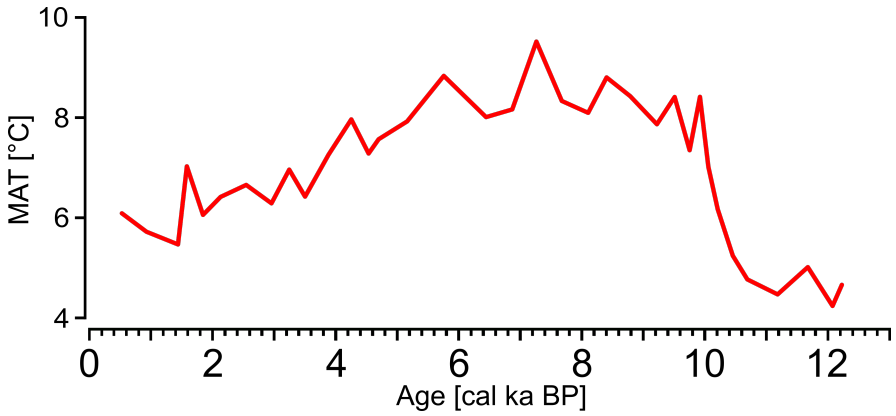

Figure 5.5: Garba Guracha MAT (°C) – MAT derived from brGDGTs using the MBT'$_{5ME}$ + IIIa'calibration.

5.6 Garba Guracha - environmental and climate reconstruction – Why and how has the climate changed?

A broad range of proxies was analysed for this thesis. Several proxies can be used to reconstruct the environmental history of the Garba Guracha catchment. The main focus, however, lies on the climatic reconstruction focusing on the isotopic composition of biomarkers (hemicellulose-derived sugar and *n*-alkanes) to reconstruct hydrological changes and the brGDGT abundances to infer temperature changes in the high-altitude Garba Guracha.

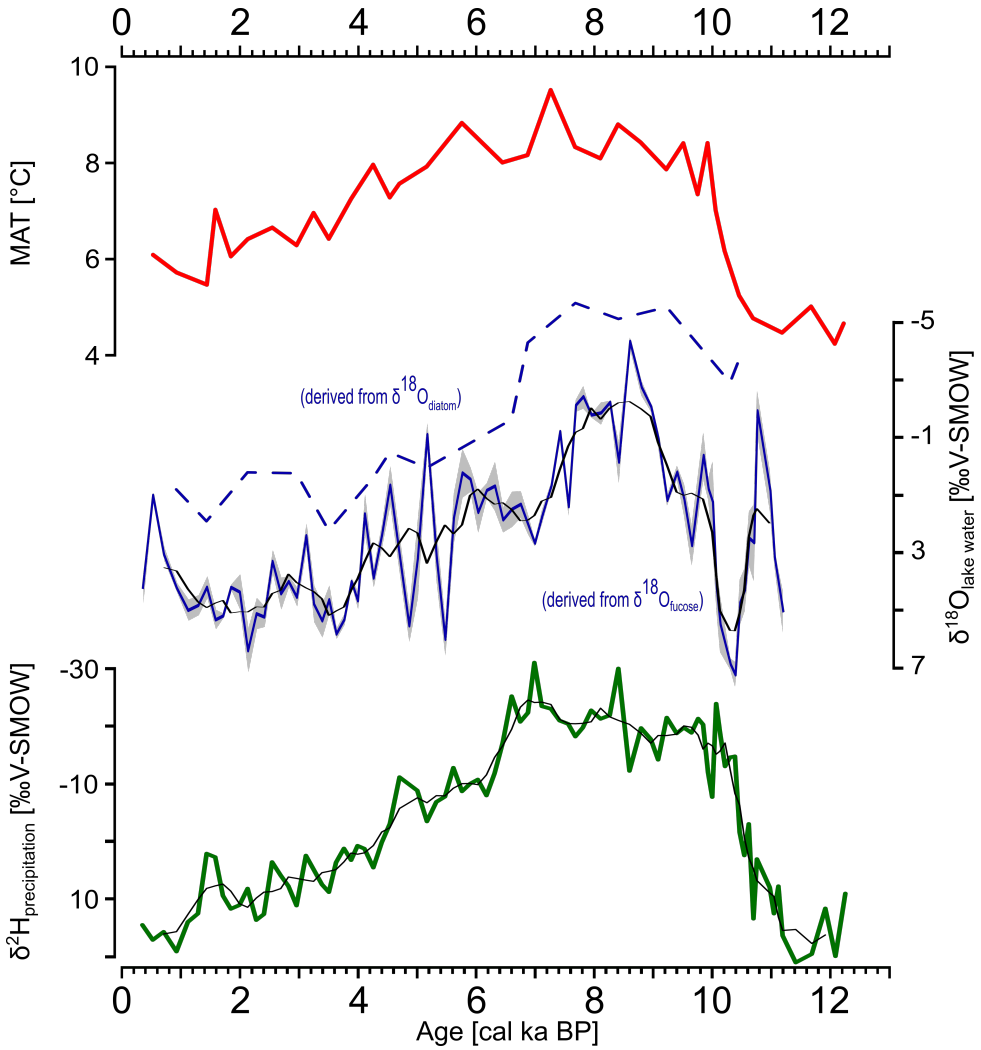

Figure 5.6: Garba Guracha climate reconstruction – (MAT (°C) (red), $\delta^{18}O_{lake\ water}$ derived from diatoms and fucose (blue) and $\delta^{2}H$ precipitation reconstruction (green).

The climate history of the Garba Guracha archive since the Late Glacial is variable and covers the deglaciation, the onset of the Holocene, the AHP and a shift to dry conditions at the termination of the AHP.

5.6.1 Deglaciation

In the Ethiopian Highlands, the timing of deglaciation is poorly constrained, and reliable glacial chronologies are rare. Minimum deglaciation ages have been inferred by basal ^{14}C ages of organic matter in afro-alpine sediment cores. In the Arsi Mountains, the first sedimentation of organic matter is dated to 11.5 cal ka BP (HAMILTON, 1982). For Garba Guracha, TIERCELIN ET AL. (2008) suggested the minimum age of deglaciation to be ~ 16.7 cal ka BP. The exposure dating in the Togona Valley (downhill from Garba Guracha) indicates a minimum age of deglaciation of ~ 16 cal ka BP (GROOS ET AL., 2021; OSSENDORF ET AL., 2019). Consistent with GROOS ET AL. (2021), the first sedimentary deposit in the 2017 Garba Guracha sediment core is dated to ~ 15.9 cal ka BP indicating glacial retreat.

The glacial retreat led to the highest values of the elements Rb, K, Ti, Fe, and Zr, representing relatively high minerogenic input. High mean sedimentation rates (1.86 mm a^{-1}) implied a fast filling glacial cirque, potentially fed by meltwater due to higher temperatures or/and precipitation. Unfortunately, it was impossible to reconstruct either temperature or precipitation indices during that time due to low amounts of organic matter in the sediments. Low amounts of organic matter (1 % TOC) originated from sparse vegetation in the catchment (GIL-ROMERA ET AL., 2019; UMER ET AL., 2007) and predominantly from aquatic algae, indicated by relatively positive $\delta^{13}C$ values (-19 ‰ to 14 ‰) and low TOC/N values of 5.

At 14 cal ka BP, rising temperatures and/or increasing precipitation might have led to a recorded increase in mean sedimentation rate of up to 2.2 mm a^{-1}, indicating further glacial recession. The sedimentation at that time was still dominated by detrital input as represented by high but decreased K, Rb, Ti, and Zr values.

5.6.2 North hemisphere forcings in the Garba Guracha catchment during the Younger Dryas period

In the Garba Guracha archive, brGDGT analyses recorded cold mean annual temperatures of < 5 °C between 12.2 - 11.2 cal ka BP. In modern times (MAT = 5.4 °C), the lake occasionally freezes slightly at night. Colder mean annual temperatures could have led to an enhanced duration of ice cover. Enhanced ice cover and dry conditions, indicated by relatively enriched $\delta^{2}H$ values (Fig. 5.6), limit the runoff and explain the dramatically decreased sedimentation rates of nearly 75 % to 0.60 mm a^{-1}. Additionally, TIERCELIN ET AL. (2008) found a change to fine-grained and laminated sediments without any signs of significant changes in lithological/geochemical characteristics. Cold temperatures and dry conditions are supported by low TOC values and decreased dominance of *Erica* heathlands (GIL-ROMERA ET AL., 2019; UMER ET AL., 2007). TIERCELIN ET AL. (2008) argue that in Garba Guracha, ice remained in the catchment until ~ 10 cal ka BP due to topographical conditions, especially the north-facing valley exposition. Remaining ice in the basin could be the reason for the recorded cold temperatures due to the inflow of cold melt water buffering the warming caused by increasing insolation (LASKAR ET AL., 2004). However, coinciding dry conditions have been reconstructed in several eastern African lakes, including Lake Albert (BEUNING ET AL., 1997), Lake Ashenge

(MARSHALL ET AL., 2009), Lake Suguta (JUNGINGER ET AL., 2014), Lake Victoria (STAGER ET AL., 2002; TALBOT & LÆRDAL, 2000), Lake Tana (MARSHALL ET AL., 2011), the Ziway-Shala basin (GILLESPIE ET AL., 1983), and the marine record of the Gulf of Aden (TIERNEY & DEMENOCAL, 2013). Due to (i) similar climatic changes in lower altitude archives, (ii) the low sedimentation rate, and (iii) the change to fine-grained and laminated sediments during the exact timing of the northern hemisphere YD (TIERCELIN ET AL., 2008) lead to the conclusion that northern hemisphere climate forcing had an impact on the Garba Guracha archive, despite possible remaining ice in the catchment.

5.6.3 Changing climatic conditions - beginning of the Holocene

While the period between 16 and 11.2 cal ka BP was mainly determined by retreating glacier/ice and was characterised by cold and dry conditions in the Garba Guracha archive, abrupt climatic and environmental changes appear around ~ 11 to 10 cal ka BP and are recorded in several proxies. Changing catchment conditions are evident in the sedimentological profile shifting from siliciclastic material to dark brown massive organic mud accompanied by changing geochemical indices like TOC and TOC/N ratio. The driving forces of this catchment transition are the increasing temperature and precipitation leading to favourable conditions for organic matter production recorded in changing vegetation around Garba Guracha (GIL-ROMERA ET AL., 2021; UMER ET AL., 2007), especially the expansion of heathlands (GIL-ROMERA ET AL., 2019). The changing environmental and climatic conditions (increased rainfall) lead to a reduction in surface water pH and lake water conductivity. The increased moisture availability in the Garba Guracha catchment started at around ~ 11.5 cal ka BP (δ^2H and $\delta^{18}O$). A minimum in P/E at 10.2 cal ka BP (Fig. 5.6), coinciding with a lake level drop in Lake Turkana (BLOSZIES ET AL., 2015; JUNGINGER ET AL., 2014), interrupts the rapid shift toward more humid conditions. The enhanced runoff led to an increased sedimentation rate (1.37 mm a^{-1}). Simultaneously with the rise in P/E at 10.5 cal ka BP, displayed by more depleted $\delta^{18}O$ values, MAT (°C) experienced an abrupt increase of ca. 3.5 °C in just ca. 600 years, from 10.5 to 9.9 cal ka BP. The strong connection between hydrology and temperature is not surprising since, in eastern Africa, both parameters are mainly controlled by rising insolation and a stronger temperature gradient enhancing the monsoonal activity.

5.6.4 The warm African Humid Period

In the Garba Guracha record, the abrupt climatic change at ~ 10 cal ka BP leads to a prolonged humid phase. High P/E ratios, supported by the reconstructed high amount of precipitation (δ^2H) and low lake water conductivity, indicate a more permanent open lake phase with more constant overflow, and less evaporative enrichment lasting until 7 cal ka BP. Several studies recorded high lake levels and stronger runoff during the AHP, indicating enhanced moisture transport into the region (BECK ET AL., 2019; FERSI ET AL., 2016; FOERSTER ET AL., 2012; JUNGINGER ET AL., 2014; LIU ET AL., 2017b; MOLOGNI ET AL., 2020; MORRISSEY & SCHOLZ, 2014; SCHNEEWEISS ET AL., 2018; TIERNEY & DEMENOCAL, 2013; TIERNEY ET AL., 2011b; WAGNER ET AL., 2018).

A coinciding thermal maximum spanned from 10 to 5.8 cal ka BP, with the highest reconstructed temperatures occurring at 7 cal ka BP. Even though similar mid-Holocene thermal optimum conditions have been recorded at several eastern African lakes, times of highest temperatures are different (Sacred Lake and Lake Tana - 7 cal ka BP; Lake Victoria - 9 cal ka BP; Lake Rutundu, Lake Malawi and Lake Tanganyika - 5 cal ka BP; Lake Turkana - 6.4 or 5 cal ka BP; Lake Mahoma – 5 to 6 cal ka BP (BERKE ET AL., 2012a; GARELICK ET AL., 2022; LOOMIS ET AL., 2017,2015,2012; POWERS ET AL., 2005; TIERNEY ET AL., 2008).

The highest temperatures in Garba Guracha coincide with local (6 °N) maximum September insolation (LASKAR ET AL., 2004). The maximum insolation might have led to the thermal optimum of several eastern African lakes during that time due to lake water restratification processes and associated epilimnetic heating (BERKE ET AL., 2012a). However, modelling studies do not support this hypothesis (DEE ET AL., 2021). In addition, the increased moisture availability and associated cloud cover leading to reduced evaporation might have affected lake water temperatures. TIERNEY ET AL. (2011) suggest that the precipitation increase during the AHP occurred mainly in June, July, and August (JJA), limiting the duration of dry periods in the area. More extended availability of effective moisture and shorter drought periods would reduce evaporation, reducing the evaporative cooling of the lake water. Less evaporation, either due to shorter drought phases or generally higher precipitation, would increase the lake water temperature and cause less positive $\delta^{18}O_{lake\ water}$ values, as recorded in the Garba Guracha record.

However, the variable temperature history of eastern Africa might also be explained partly by the limitation of archives and the lack of understanding of the complex factors influencing the brGDGT compositions. This thesis has shown that changes in conductivity and pH, among other factors, affect the local brGDGT isomer distributions limiting the precision of temperature calibrations (DE JONGE ET AL., 2021; RABERG ET AL., 2021; WANG ET AL., 2021). A deeper understanding of the driving mechanism behind brGDGT isomer abundance is necessary.

5.6.5 The termination of the African Humid Period

In the Garba Guracha archive, several proxies (TOC, TOC/N, abundance of *B. braunii*) decrease rapidly between 4.5 and 4.2 cal ka BP, indicating changing catchment conditions. The temperature decreases not abruptly but steadily after 5.8 cal ka BP coinciding with decreasing insolation (LASKAR ET AL., 2004). Despite substantial variability between 6 and 4 cal ka BP, the hydrological trend of Garba Guracha constantly changes to drier conditions. The strong variability might point to changing and unstable climatic conditions congruent with centennial variations. However, the constantly reduced amount of precipitation (δ^2H) supports the overall drying trend). Moreover, decreasing abundances of *Erica,* expansion of the dry montane forest, and charcoal indicate reduced fire activity, both starting around 5.2 cal ka BP (GIL-ROMERA ET AL., 2021). While the decline of *Erica* might explain the increased surface water pH values, the drying trend is supported by increased conductivity. The asynchronous response of individual proxies might be associated with the varying sensitivity of the proxies

to both environmental changes and individual drivers (CASTAÑEDA ET AL., 2016). It seems that climatic conditions began to change constantly, and various biological processes connected to climatic change reacted rapidly once a certain threshold was reached. The variety of interactions between the proxies makes it difficult to assign cause and effect. Even though perennial plants such as *Erica* might have declined, the seasonal organic matter input in the lake might have persisted so that any TOC decline would have been postponed decades or centuries.

In the region, a concurrent decline in lake levels was recorded at north Ethiopian lakes Ziway-Shala and Abhè at ~ 4 to 4.5 cal ka BP (GASSE, 2000; GILLESPIE ET AL., 1983; KHALIDI ET AL., 2020). More southern lakes, including Paleo-Lake Suguta, Lake Turkana, and Chew Bahir show an earlier AHP termination at ~ 5 to 5.5 cal ka BP (FOERSTER ET AL., 2012; GARCIN ET AL., 2012; JUNGINGER ET AL., 2014). Lower moisture availability and decreasing temperatures of equatorial lakes (IVORY & RUSSELL, 2018), Lake Tana (LOOMIS ET AL., 2015) and the marine Gulf of Aden record (TIERNEY ET AL., 2016) are accompanied by weak monsoonal activity in the Indian ocean records (FLEITMANN & MATTER, 2009; NAKAMURA ET AL., 2016).

5.6.6 The Late Holocene

In some records, the timing of the AHP termination coincides with a known global mega-drought at 4.2 cal ka BP (BINI ET AL., 2019). In most regions of the earth, the 4.2 cal ka BP climatic event that lasts for 200 - 300 years. By contrast, in the Garba Guracha and other African records, a climatic shift is recorded, ending the last humid conditions in north and eastern Africa.

In the Garba Guracha archive, an overall shift towards drier and warmer conditions prolonged until ~ 2 and 1.5 cal ka BP, respectively, leading to reduced organic matter production and decreasing vegetation. A slightly more humid phase is recorded in higher P/E values around ~ 3 - 2.5 cal ka BP with expanding heathland and more active fires (GIL-ROMERA ET AL., 2019), supported by similar findings in eastern Africa (GASSE & VAN CAMPO, 1994; LEZINE ET AL., 2014; MACHADO ET AL., 1998). During the last two thousand years, a slightly increasing precipitation trend concurred with an abrupt increase in the main woody communities and enhanced fire activities around Garba Guracha (GIL-ROMERA ET AL., 2021). However, human influence favouring both woody encroachment and fire activity can not be discarded. Pollen data and archaeological findings show increased human activity in the Bale Mountains over the last 3 cal ka BP (manuscript in preparation) (GIL-ROMERA ET AL., 2022). In this period, straightforward interpretations of climatic change are difficult. However, a shift towards higher P/E at 0.5 cal ka BP might point to the Little Ice Age (GROVE, 2004), which is poorly understood and studied in the African continent (NASH ET AL., 2016).

5.7 Garba Guracha – Climatic implications and driving mechanisms

5.7.1 Comparison of high and low altitudes in eastern Africa

The amplitude of temperature change over the last 13 ka at Garba Guracha is relatively high (~ 6 °C) and similar to other high-altitude sites (Lake Mahoma and Lake Rutundu) (GARELICK ET AL., 2022; LOOMIS ET AL., 2017) (Fig. 5.7). The lowest amplitudes are recorded in low altitude, equatorial archives (Lake Victoria and Lake Tanganyika) (BERKE ET AL., 2012b; TIERNEY ET AL., 2008), whereas higher temperature amplitudes are recorded in the low altitude Lake Tana record, located at slightly higher latitude (LOOMIS ET AL., 2015). The latitudinal position of Garba Guracha is also slightly higher compared to other temperature records in eastern Africa. This, additionally to the high-altitude of Garba Guracha, might explain some of the highest temperature amplitude during the Holocene. Similar enhanced high-altitude warming has been reported for past temperature changes at the Last Glacial Maximum in eastern Africa (GARELICK ET AL., 2022; LOOMIS ET AL., 2017) due to changes in the temperature lapse rate. Warming in high-altitude regions is driven by (i) a higher sensitivity to insolation forcing (OHMURA, 2012), (ii) a reduced cooling effect of aerosols and solar dimming (ZENG ET AL., 2015), and (iii) a higher reduction of the vertical temperature gradient, due to increased latent heat release above the condensation level (HELD & SODEN, 2006).

The amplitude of $\delta^2H_{leaf\ water}$ changes over the last 13 cal ka BP at Garba Guracha is relatively high (~ 50 ‰) and similar to other high-altitude sites. Except for Lake Tana (COSTA ET AL., 2014), altitude and the amplitude of $\delta^2H_{leaf\ water}$ correlate in eastern African lake records. In contrast, absolute δ^2H values of African lakes are not correlated with altitude. Such a trend could be explained by (i) the rising water storage capacity in warmer air masses, (ii) higher wind speeds due to increased land-ocean pressure gradients (NCHABA ET AL., 2017), (iii) enhanced orographic convection, all leading to relatively stronger amount of precipitation changes in higher altitudes. However, the influences on δ^2H are complex, and since total δ^2H values of eastern African lakes do not correlate with altitude, other effects (such as source-, amount-, continental-, temperature-, seasonality effect, and evapo-transpirative enrichment (SHARP, 2017)) might have a more substantial and spatially different pronounced impact on the isotopic composition. The altitude effect is constant in the Holocene, whereas effects like the source and amount effect vary with changing atmospheric circulation patterns.

Due to the relatively new and innovative $\delta^{18}O_{fucose}$ approach, similar records, especially in the same time period, do not yet exist in northern and eastern Africa. However, the interpretation regarding open (overflowing/high) and closed (low) lake conditions is supported by several reconstructed lake level records of varying altitudes in eastern Africa with similar hydrological shifts (GARCIN ET AL., 2012; GASSE & STREET, 1978; GASSE, 2000; GILLESPIE ET AL., 1983; JUNGINGER ET AL., 2014). However, comparing different proxies in regards to altitude, latitude, and longitude is impossible.

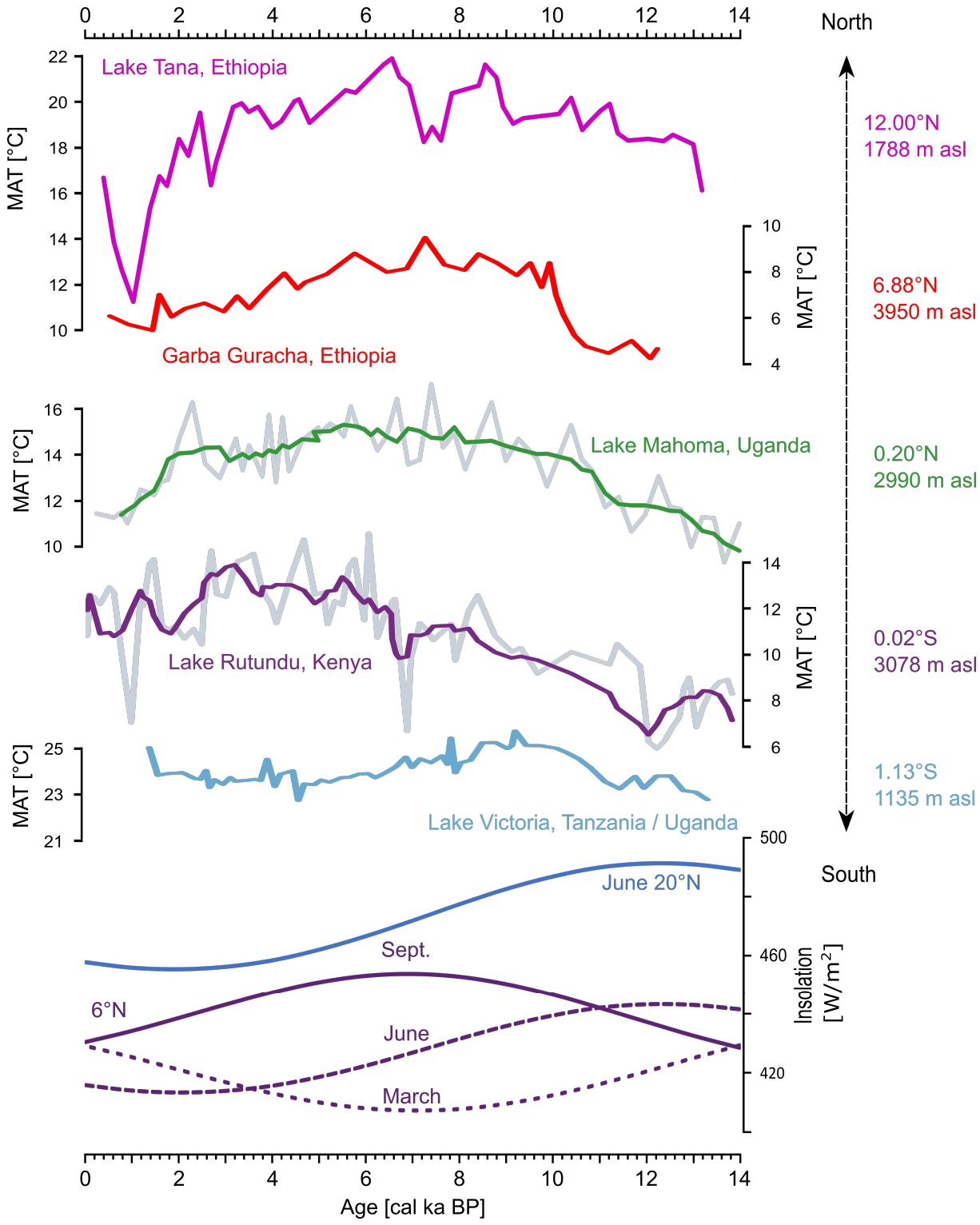

Figure 5.7: Comparison of records. MAT: Lake Tana (LOOMIS ET AL., 2015); Garba Guracha; Lake Mahoma (GARELICK ET AL., 2022); Lake Rutundu (LOOMIS ET AL., 2017); Lake Victoria (BERKE ET AL., 2012a); and insolation 6 °N and June 20 °N (LASKAR ET AL., 2004).

While the hydrological changes between high and low altitudes in eastern Africa do not allow an unambiguous interpretation, high altitudes have been affected by relatively higher temperature changes than low altitudes, further depending on their latitudinal position.

5.7.2 Atmospheric circulation

The atmospheric circulation in eastern and northeastern Africa is very complex, and the precipitation distribution is spatially very different (LEVIN ET AL., 2009; NICHOLSON, 2017; VISTE & SORTEBERG, 2013). In modern times the rainfall pattern in Ethiopia is bimodal, associated with the convergence of northeast and southwest winds due to the northern and southern location of the ITCZ between June and September and between October and March, respectively (TIERCELIN ET AL., 2008). Additionally, contributions from Congo Basin Air masses have been found at Lake Tana (COSTA ET AL., 2014), and for Ethiopia in general, except in the southwestern part (LEVIN ET AL., 2009; VISTE & SORTEBERG, 2013). However, a modern study suggests no contributions from the Congo Basin to Ethiopia (1980 - 2018) (STOJANOVIC ET AL., 2022).

In the case of the Bale Mountains, MIEHE & MIEHE (1994) and UHLIG (1988) suggest the Indian Ocean monsoon and the Equatorial Westerlies as moisture sources. However, a recent back-trajectory study for the Bale Mountains (LEMMA ET AL., 2020) supports the findings of LEVIN ET AL. (2009), finding air mass contributions principally from the Indian Ocean, the Mediterranean and the Red Sea. However, even though the air mass contributions in Ethiopia are still highly debated, a recent study by FINNEY ET AL. (2020) suggests that even low air mass contributions of westerly winds are responsibly for disproportionately high precipitation in eastern Africa. Even if there is only minor or no air mass contribution from the Congo Basin in Ethiopia today, this may have been different in the past due to changing atmospheric circulation patterns.

The Garba Guracha record, like most eastern African records, is marked by three major climatic shifts associated with different atmospheric circulation patterns, cold and dry conditions during the YD (see Section 5.6.2), humid and warm conditions during the AHP (see Section 5.6.4), and dry conditions after the AHP termination (see Section 5.6.6).

During the north-hemisphere YD, a weakening of the North Atlantic Deep Water formation linked to increased freshwater input, the ITCZ was forced south of the equator due to an interhemispheric thermal gradient (BROCCOLI ET AL., 2006; CHIANG & BITZ, 2005; NICHOLSON, 1982). The southern displacement of the ITCZ led to (i) a weakened ISM system, (ii) anomalous northeastern winds (DEMENOCAL & RIND, 1993), (iii) a weakening of the Somali Jet (CAMBERLIN, 1997), and (iv) sea surface temperature anomalies (TIERNEY ET AL., 2015). Consequently, the Indian Ocean region, especially northeastern and eastern Africa, experienced dry conditions with reduced precipitation and low lake stands (CASTAÑEDA ET AL., 2016; STREET-PERROTT & PERROTT, 1990).

An abrupt change in hydroclimate at the termination of the YD was driven by a major reorganization of monsoonal circulation, likely due to a rapid re-establishment of the Atlantic Meridional Overturning Circulation (MCMANUS ET AL., 2004; TALBOT ET AL., 2007; WELDEAB ET AL., 2014). The monsoonal intensity of the West African Monsoon (WAM) and the ISM increased due to a stronger thermal land-ocean gradient driven by rising north hemisphere insolation, forcing the tropical rain belt northwards (NICHOLSON, 2017; PAUSATA ET AL., 2020; PIAO ET AL., 2020). The atmospheric circulation reorganization led to enhanced humidity during the AHP in eastern Africa (CASTAÑEDA ET AL., 2016; JUNGINGER ET AL., 2014). However, the records show

spatial and temporal differences and the exact reasons for this are still not fully understood. It has been argued that due to the strengthening of the WAM and the ISM, the CAB has shifted to the East, leading to the input of Atlantic moisture into the area (COSTA ET AL., 2014; JUNGINGER ET AL., 2014). Additionally to the rather east-west character of CAB changes, meridional processes like the mean annual position of the ITCZ, driven by precessional insolation changes, might be dominant factors for the temporal and spatial distribution of moisture (GASSE, 2000; KUTZBACH & OTTO-BLIESNER, 1982; VERSCHUREN ET AL., 2009). The termination of the AHP is differently pronounced across northern and eastern Africa and has been described as rapid (COLLINS ET AL., 2017), as synchronous and abrupt (TIERNEY & DEMENOCAL, 2013), or asynchronous and gradual (COSTA ET AL., 2014; FOERSTER ET AL., 2012; VAN DER LUBBE ET AL., 2017).

Further understanding of the temporal and special diverse thermal and hydrological history of eastern Africa and the driving atmospheric circulation changes is precluded by the limited, sparse and patchy paleoclimate records. The new results of the high-altitude Garba Guracha, situated further East than most of the eastern African records, helps further to disentangle the atmospheric circulation influences in eastern Africa.

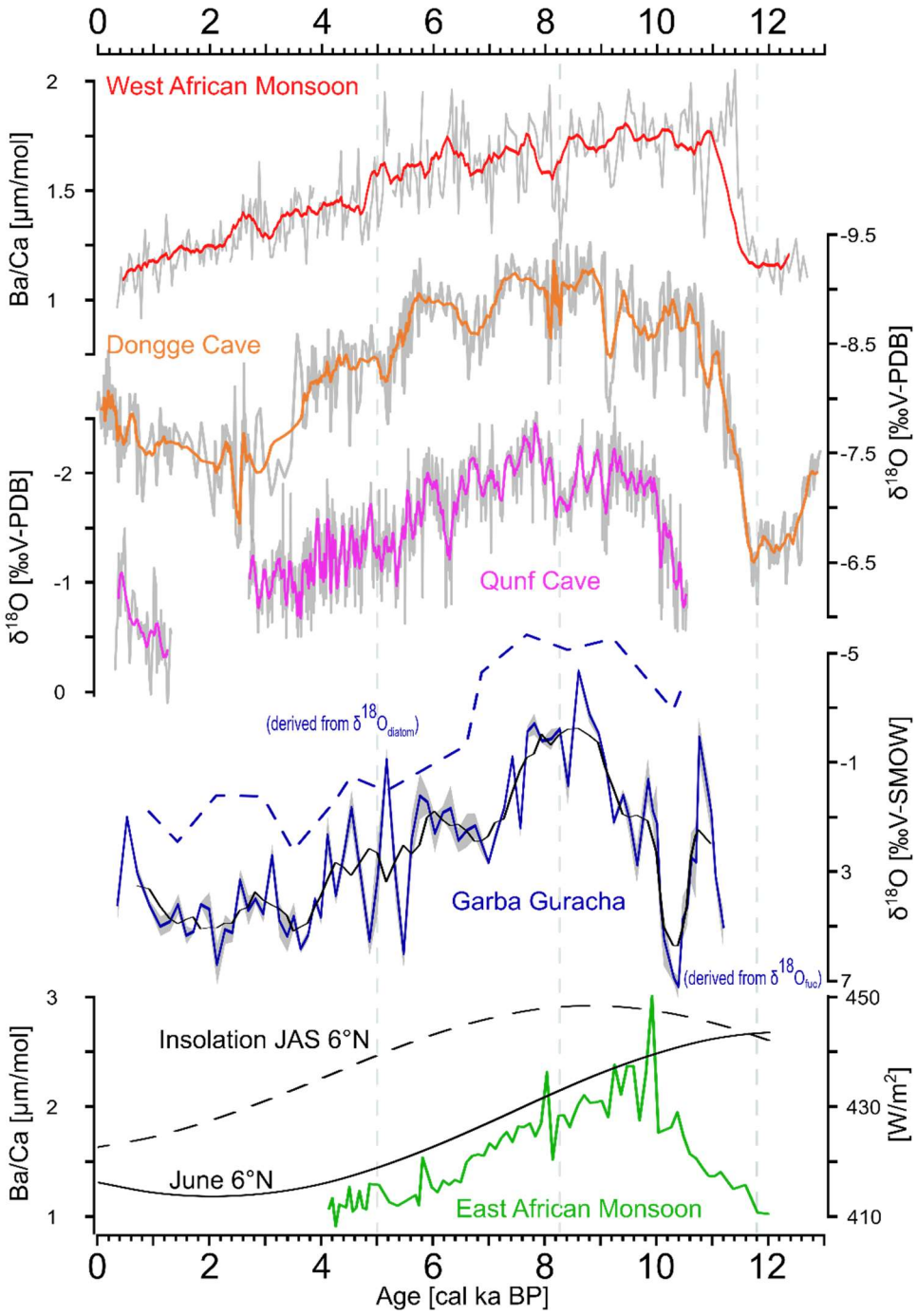

Figure 5.78: Comparison of $\delta^{18}O$ and Ba/Ca records - West African Monsoon (WELDEAB ET AL., 2007), Dongge Cave (DYKOSKI ET AL., 2005), Qunf Cave (FLEITMANN ET AL., 2003), Garba Guracha, East African Monsoon (WELDEAB ET AL., 2014).

Overall, the stable isotope climate proxies ($\delta^{2}H$ and $\delta^{18}O$) at Garba Guracha have strong similarities to both regional and northern hemisphere records (Fig. 5.8 and 5.9). The $\delta^{18}O$ of Garba Guracha coincides with the $\delta^{18}O$ speleothem records of Dongge Cave in China (DYKOSKI ET AL., 2005) and Qunf Cave in Oman (FLEITMANN ET AL., 2007), indicating similar driving mechanisms in low and high northern latitudes. While a close connection of monsoonal records in the northern hemisphere is not surprising, the similar trends and several coinciding minima and maxima (for example: 8.2 cal ka BP, 3.6 cal ka BP and 0.5 cal ka BP) of Qunf Cave and Garba Guracha $\delta^{18}O$ indicate a regional connection between the EAM and western ISM

region. Moreover, at ~ 6.5 cal ka BP a pronounced two-phased minimum in the $\delta^{18}O$ of Qunf Cave (Fig. 5.8) (FLEITMANN ET AL., 2007) coincides with two organic poor sediment layers accompanied by only one minimum in $\delta^{18}O$ due to the smoothed character of the Garba Guracha sampling.

The Qunf Cave and Dongge Cave are interpreted to represent monsoon intensity and associated precipitation amounts (DYKOSKI ET AL., 2005; FLEITMANN ET AL., 2007). Compared to the onset of the WAM (WELDEAB ET AL., 2007) and the ISM activity recorded in the Dongge Cave, the reconstructed enhanced monsoonal activity of Qunf Cave and the precipitation increase at Garba Guracha are delayed by ~ 1200 years. A postulated influence of the eastwards moving CAB might explain the delayed changes at the Garba Guracha site but is not able to explain the delayed increased precipitation at the Qunf Cave. In contrast, an enhanced EAM activity after ~ 10.5 cal ka BP coincides with the decreasing $\delta^{18}O$ values in Qunf Cave and Garba Guracha (Fig. 5.8). A strengthening of the EAM might be supported by the eastern African local JAS insolation maxima (LASKAR ET AL., 2004) and an increased local land-ocean temperature gradient. These findings suggest similar driving mechanisms, possibly the EAM, for Garba Guracha and Qunf Cave. However, high-resolution $\delta^{18}O$ records in the area are rare.

Far more studies have been conducted, reconstructing paleohydrological changes using $\delta^{2}H$. The $\delta^{2}H$ record of Garba Guracha (manuscript in preparation) is coherent with several $\delta^{2}H$ records of eastern and equatorial Africa (BERKE ET AL., 2012b; COSTA ET AL., 2014; GARELICK ET AL., 2021; JAESCHKE ET AL., 2020; TIERNEY & DEMENOCAL, 2013). In eastern Africa, $\delta^{2}H$ records north of 9 °S coincide with the north hemisphere (20 °N) summer insolation intensity, whereas $\delta^{2}H$ records south of 9 °S concur with southern summer insolation intensity (BARKER & GASSE, 2003) (Fig. 5.9). The number of $\delta^{2}H$ records continues to increase, as does the understanding of the large-scale changes in climate and atmospheric circulation at the onset and termination of the AHP. Moreover, spatial differences across eastern Africa become more evident (GARELICK ET AL., 2021; JAESCHKE ET AL., 2020). In the last 14 cal ka BP, the most northern record Lake Tana (COSTA ET AL., 2014) experienced the earliest shift towards humid conditions, followed by Lake Challa (TIERNEY ET AL., 2011b) and Lake Tanganyika (TIERNEY ET AL., 2010). The intermediate located Lake Dendi (JAESCHKE ET AL., 2020), Garba Guracha and Lake Rutundu (GARELICK ET AL., 2021), all above 2800 m a. s. l., experienced delayed shifts towards humid conditions (Fig. 5.9). These findings might indicate a delayed or buffered high altitude response to changing climatic conditions. However, Lake Victoria (1135 m a. s. l.), located in lower altitudes as Lake Tana (1788 m a. s. l.), also records delayed climatic changes. Lake Victoria (1.13 °S), though, is situated at a latitude similar to Lake Rutundu (0.02 °S). The different timings of climate change, recorded in the $\delta^{2}H$ lake records, rather concur with the latitudinal position than altitude, pointing to meridional processes as driving mechanisms.

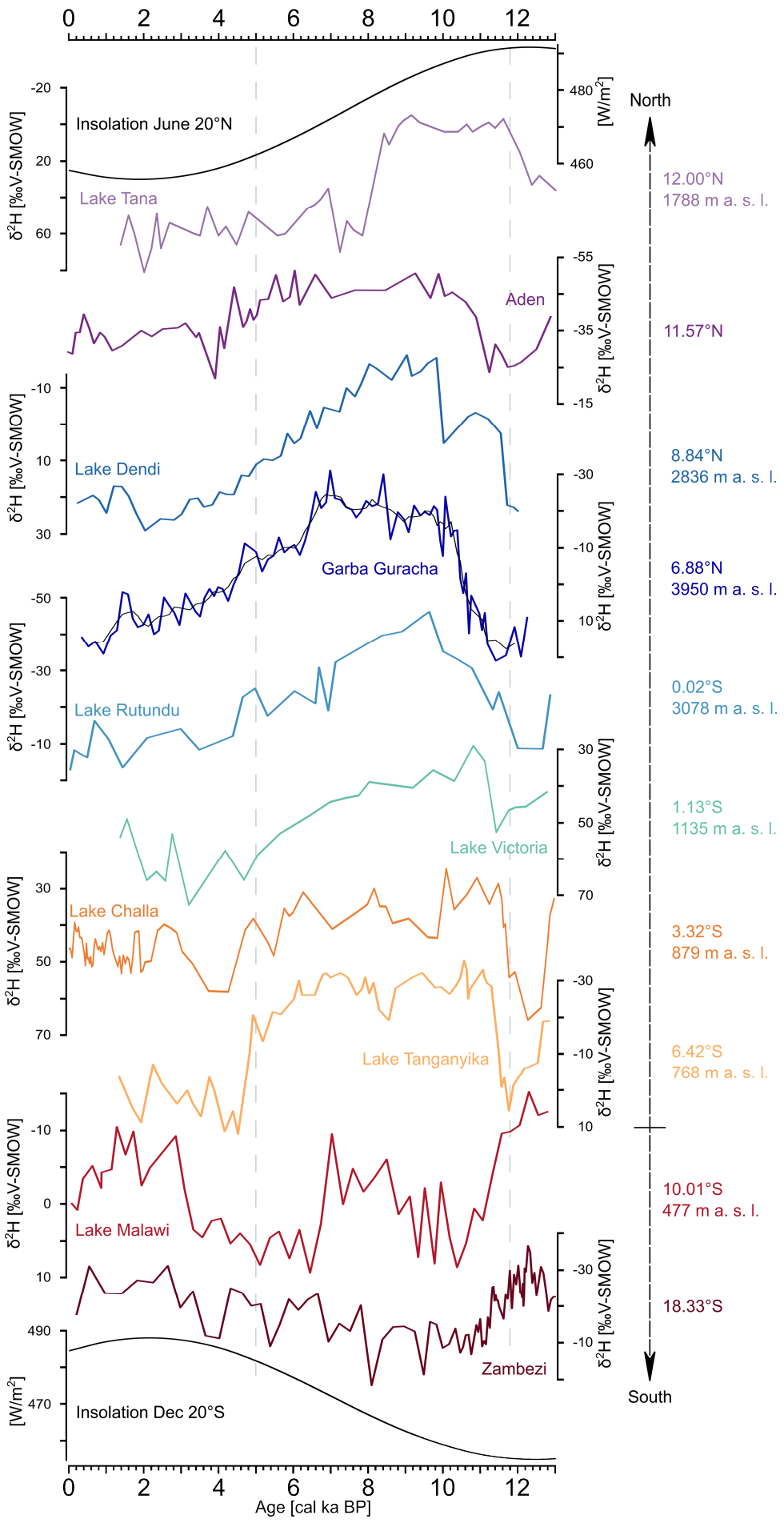
Insolation June 20°N
Lake Tana
Aden
Lake Dendi
Garba Guracha
Lake Rutundu
Lake Victoria
Lake Challa
Lake Tanganyika
Lake Malawi
Zambezi
Insolation Dec 20°S
δ²H [‰V-SMOW]
[W/m²]
Age [cal ka BP]
North
South
12.00°N
1788 m a. s. l.
11.57°N
8.84°N
2836 m a. s. l.
6.88°N
3950 m a. s. l.
0.02°S
3078 m a. s. l.
1.13°S
1135 m a. s. l.
3.32°S
879 m a. s. l.
6.42°S
768 m a. s. l.
10.01°S
477 m a. s. l.
18.33°S

Figure 5.79: Comparison of δ^2H_{wax} records in eastern Africa - insolation June 20 °N (LASKAR ET AL., 2004), Lake Tana (COSTA ET AL., 2014), Gulf of Aden (TIERNEY & DEMENOCAL, 2013), Lake Dendi (JAESCHKE ET AL., 2020), Garba Guracha, Lake Rutundu (GARELICK ET AL., 2021), Lake Victoria (BERKE ET AL., 2012a), Lake Challa (TIERNEY ET AL., 2011b), Lake Tanganyika (TIERNEY ET AL., 2010), Lake Malawi (KONECKY ET AL., 2011), Zambezi (SCHEFUß ET AL., 2011), and insolation June 20 °S (LASKAR ET AL., 2004).

There is no evidence for an extensive east-west driven change at Lake Tanganyika, Lake Rutundu, Lake Dendi, Garba Guracha and the Gulf of Aden. During the AHP, all these records have similar ranges in δ^2H of ~ 40 to 50 ‰ and no clear east-west pattern in timing, amplitude, or total values, which the different altitudes of the archives can not explain. This is supported by modifying a figure of COSTA ET AL. (2014) by adding new data from Lake Dendi (JAESCHKE ET AL., 2020), Lake Rutundu (GARELICK ET AL., 2021), and Garba Guracha (Fig. 5.10). The interpretation of COSTA ET AL. (2014) concerning the CAB movement (dotted lines) does not agree with the new δ^2H data. A clear east-west pattern of climatic change over the last 14 cal ka BP is not evident. The CAB movement might not have been the dominant driving mechanism, at least not at all times. However, to be able to compare the data, COSTA ET AL. (2014) used a mean δ^2H value of the last 5000 years to normalise the data and account for constant δ^2H effects (e.g. altitude effect). Due to the underlying assumption that the δ^2H records were affected by similar and constant isotope effects during the last 5000 years, the results must be carefully interpreted.

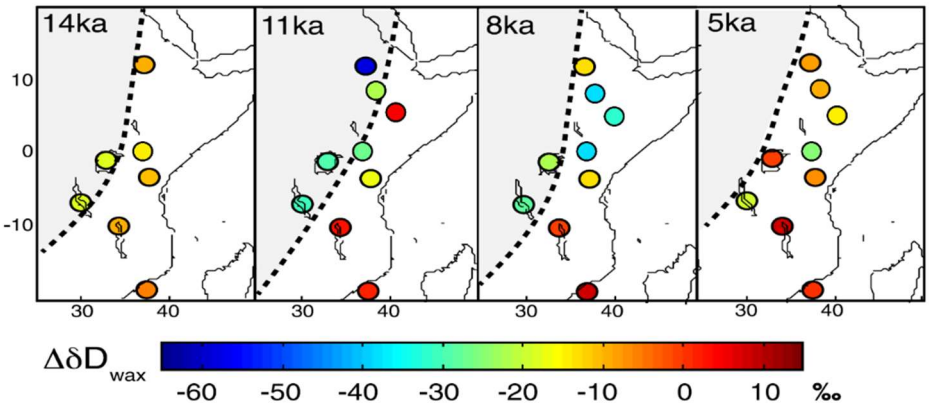

Figure 5.710: Comparison of δ^2H records in eastern Africa in time slices (after COSTA ET AL., 2014; Fig. 9) – data from Lake Tana (LOOMIS ET AL., 2015), Victoria (BERKE ET AL., 2012a), Challa (TIERNEY ET AL., 2010), Tanganyika (TIERNEY ET AL., 2008), Malawi (KONECKY ET AL., 2011), and Zambezi Fan (SCHEFUß ET AL., 2011) - data added for Lake Dendi (JAESCHKE ET AL., 2020), Lake Rutundu (GARELICK ET AL., 2021), and Garba Guracha. The amplitude is quantified as $\Delta\delta D_{wax}$ ($\delta D_{wax} = \delta^2H_{leaf\,wax}$), calculated from δ^2H of the indicated time (t) and the δ^2H average of the last 5000 years (Late Holocene (LH)) ($\Delta\delta D_{wax} = \delta D^{t}_{wax} - \delta D^{LH}_{wax}$). CAB position (dotted line).

The intensity and timing of the AHP termination seem to depend on the latitude, similar to the beginning of the AHP. While all eastern African δ^2H records between 8.5 °N and 1.13 °S (Lake Dendi, Lake Garba Guracha, Lake Rutundu and Lake Victoria) show a gradual termination of the AHP, records situated more northern (Lake Tana) or southern (Lake Challa and Lake Tangyianika) show relatively more abrupt terminations (Fig. 5.10). These findings point to a meridional atmospheric process, not an East-West pattern. The abrupt shift in δ^2H recorded in Lake Tana, interpreted as a rapid westward retreat of the CAB at the termination

of the AHP (COSTA ET AL., 2014), is not evident in Garba Guracha, Lake Rutundu or Lake Dendi (GARELICK ET AL., 2021; LOOMIS ET AL., 2017). One would expect a similar influence on the other archives due to the retreat of Congo air masses and their associated depleted δ^2H values.

With the available climate reconstructions, a predominantly meridional influence on the climatic changes since the last deglaciation becomes apparent, locally modulated by the various effects and drivers like altitude, the CAB movement and regional climatic forcings. For instance, the southern Lakes Challa and Tanganyika might have been fed by short rains during autumn (Oct-Nov) due to sea surface temperature anomalies in the Western Indian Ocean (KUHNERT ET AL., 2014). Lake Victoria and other extensive lake systems create their own mesoclimate strongly modulating regional moisture availability (NICHOLSON ET AL., 2021). Moreover, an enhanced vegetation cover and a changed vegetation composition at the end of the AHP, spatially different across eastern Africa, might explain some variation in the climate records due to vegetation and climatic feedback (SPRACKLEN ET AL., 2018). Vegetation, especially forests, impacts the $\delta^{18}O$ and δ^2H values due to moisture recycling (AMPUERO ET AL., 2020). Additionally, uncertainties for the reconstructed δ^2H and $\delta^{18}O$ records arise due to the unknown source of the compounds (*n*-alkanes, fatty acids and monosaccharides) and their age structure. Except for the Garba Guracha record, compound-specific *n*-alkane dating has, to my knowledge, not been applied to any of the eastern African δ^2H records.

5.8 References

AMPUERO, A., STRÍKIS, N. M., APAÉSTEGUI, J., VUILLE, M., NOVELLO, V. F., ESPINOZA, J. C., CRUZ, F. W., VONHOF, H., MAYTA, V. C., & MARTINS, V. T. S. (2020): The forest effects on the isotopic composition of rainfall in the northwestern Amazon Basin. - Journal of Geophysical Research: Atmospheres, **125**, e2019JD031445.

BAAS, M., PANCOST, R., VAN GEEL, B., & SINNINGHE DAMSTÉ, J. S. (2000): A comparative study of lipids in Sphagnum species. - Organic Geochemistry, **31**, 535–541.

BARKER, P., & GASSE, F. (2003): New evidence for a reduced water balance in East Africa during the Last Glacial Maximum: implication for model-data comparison. - Quaternary Science Reviews, **22**, 823–837.

BAXTER, A. J., HOPMANS, E. C., RUSSELL, J. M., & SINNINGHE DAMSTÉ, J. S. (2019): Bacterial GMGTs in East African lake sediments: Their potential as palaeotemperature indicators. - Geochimica et Cosmochimica Acta, **259**, 155–169.

BECK, C. C., FEIBEL, C. S., WRIGHT, J. D., & MORTLOCK, R. A. (2019): Onset of the African Humid Period by 13.9 kyr BP at Kabua Gorge, Turkana Basin, Kenya. - Holocene, **29**, 1011–1019.

BERKE, M. A., JOHNSON, T. C., WERNE, J. P., GRICE, K., SCHOUTEN, S., & SINNINGHE DAMSTÉ, J. S. (2012a): Molecular records of climate variability and vegetation response since the Late Pleistocene in the Lake Victoria basin, East Africa. - Quaternary Science Reviews, **55**, 59–74.

BERKE, M. A., JOHNSON, T. C., WERNE, J. P., SCHOUTEN, S., & SINNINGHE DAMSTÉ, J. S. (2012b): A mid-Holocene thermal maximum at the end of the African Humid Period. - Earth and Planetary Science Letters, **351**–**352**, 95–104.

BEUNING, K. R. M., TALBOT, M. R., & KELTS, K. (1997): A revised 30,000-year paleoclimatic and paleohydrologic history of Lake Albert, East Africa. - Palaeogeography, Palaeoclimatology, Palaeoecology, **136**, 259–279.

BINI, M., ZANCHETTA, G., PERŞOIU, A., CARTIER, R., CATALÀ, A., CACHO, I., DEAN, J. R., DI RITA, F., DRYSDALE, R. N., FINNÈ, M., ISOLA, I., JALALI, B., LIRER, F., MAGRI, D., MASI, A., MARKS, L., MERCURI, A. M., PEYRON, O., SADORI, L., SICRE, M.-A., WELC, F., ZIELHOFER, C., & BRISSET, E. (2019): The 4.2 ka BP Event in the Mediterranean region: an overview. - Clim. Past, **15**, 555–577.

BITTNER, L., BLIEDTNER, M., GRADY, D., GIL-ROMERA, G., MARTIN-JONES, C., LEMMA, B., MEKONNEN, B., LAMB, H. F., YANG, H., GLASER, B., SZIDAT, S., SALAZAR, G., ROSE, N. L., OPGENOORTH, L., MIEHE, G., ZECH, W., & ZECH, M. (2020): Revisiting afro-alpine Lake Garba Guracha in the Bale Mountains of Ethiopia: rationale, chronology, geochemistry, and paleoenvironmental implications. - Journal of Paleolimnology.

BLAAUW, M. (2010): Methods and code for 'classical' age-modelling of radiocarbon sequences. - Quaternary Geochronology, **5**, 512–518.

BLAAUW, M., CHRISTENY, J. A., & CHRISTEN, J. A. (2011): Flexible paleoclimate age-depth models using an autoregressive gamma process. - Bayesian Analysis, **6**, 457–474.

BLOSZIES, C., FORMAN, S. L., & WRIGHT, D. K. (2015): Water level history for Lake Turkana, Kenya in the past 15,000 years and a variable transition from the African Humid Period to Holocene aridity. - Global and Planetary Change, **132**, 64–76.

BODÉ, S., DE WISPELAERE, L., HEMP, A., VERSCHUREN, D., & BOECKX, P. (2020): Water-isotope ecohydrology of Mount Kilimanjaro. - Ecohydrology, **13**, e2171.

BRENNER, M., WHITMORE, T. J., CURTIS, J. H., HODELL, D. A., & SCHELSKE, C. L. (1999): Stable isotope (δ13C and δ^{15}N) signatures of sedimented organic matter as indicators of historic lake trophic state. - Journal of Paleolimnology, **22**, 205–221.

BROCCOLI, A. J., DAHL, K. A., & STOUFFER, R. J. (2006): Response of the ITCZ to Northern Hemisphere cooling. - Geophysical Research Letters, **33**.

CAMBERLIN, P. (1997): Rainfall Anomalies in the Source Region of the Nile and Their Connection with the Indian Summer Monsoon. - Journal of Climate, **10**, 1380–1392.

CASTAÑEDA, I. S., SCHOUTEN, S., PÄTZOLD, J., LUCASSEN, F., KASEMANN, S., KUHLMANN, H., & SCHEFUß, E. (2016): Hydroclimate variability in the Nile River Basin during the past 28,000 years. - Earth and Planetary Science Letters, **438**, 47–56.

CHIANG, J. C. H., & BITZ, C. M. (2005): Influence of high latitude ice cover on the marine Intertropical Convergence Zone. - Climate Dynamics, **25**, 477–496.

COLLINS, J. A., PRANGE, M., CALEY, T., GIMENO, L., BECKMANN, B., MULITZA, S., SKONIECZNY, C., ROCHE, D., & SCHEFUß, E. (2017): Rapid termination of the African Humid Period triggered by northern high-latitude cooling. - Nature Communications, **8**.

COSTA, K., RUSSELL, J., KONECKY, B., & LAMB, H. (2014): Isotopic reconstruction of the African Humid Period and Congo Air Boundary migration at Lake Tana, Ethiopia. - Quaternary Science Reviews, **83**, 58–67.

DANSGAARD, W. (1964): Stable isotopes in precipitation. - Tellus, **16**, 436–468.

DE JONGE, C., RADUJKOVIĆ, D., SIGURDSSON, B. D., WEEDON, J. T., JANSSENS, I., & PETERSE, F. (2019): Lipid biomarker temperature proxy responds to abrupt shift in the bacterial community composition in geothermally heated soils. - Organic Geochemistry, **137**.

DE JONGE, C., KURAMAE, E. E., RADUJKOVIĆ, D., WEEDON, J. T., JANSSENS, I. A., & PETERSE, F. (2021): The influence of soil chemistry on branched tetraether lipids in mid- and high latitude soils: Implications for brGDGT- based paleothermometry. - Geochimica et Cosmochimica Acta, **310**, 95–112.

DEE, S. G., MORRILL, C., KIM, S. H., & RUSSELL, J. M. (2021): Hot Air, Hot Lakes, or Both? Exploring Mid-Holocene African Temperatures Using Proxy System Modeling. - Journal of Geophysical Research: Atmospheres, **126**, e2020JD033269.

DEMENOCAL, P. B., & RIND, D. (1993): Sensitivity of Asian and African climate to variations in seasonal insolation, glacial ice cover, sea surface temperature, and Asian orography. - Journal of Geophysical Research, **98**, 7265–7287.

DOUGLAS, P. M. J. J., PAGANI, M., EGLINTON, T. I., BRENNER, M., HODELL, D. A., CURTIS, J. H., MA, K. F., & BRECKENRIDGE, A. (2014): Pre-aged plant waxes in tropical lake sediments and their influence on the chronology of molecular paleoclimate proxy records. - Geochimica et Cosmochimica Acta, **141**, 346–364.

DYKOSKI, C. A., EDWARDS, R. L., CHENG, H., YUAN, D., CAI, Y., ZHANG, M., LIN, Y., QING, J., AN, Z., & REVENAUGH, J. (2005): A high-resolution, absolute-dated Holocene and deglacial Asian monsoon record from Dongge Cave, China. - Earth and Planetary Science Letters, **233**, 71–86.

EGLINTON, T. I., & EGLINTON, G. (2008): Molecular proxies for paleoclimatology. - Earth and Planetary Science Letters, **275**, 1–16.

FERSI, W., LÉZINE, A.-M., & BASSINOT, F. (2016): Hydro-climate changes over southwestern Arabia and the Horn of Africa during the last glacial–interglacial transition: A pollen record from the Gulf of Aden. - Review of Palaeobotany and Palynology, **233**, 176–185.

FINNEY, D. L., MARSHAM, J. H., WALKER, D. P., BIRCH, C. E., WOODHAMS, B. J., JACKSON, L. S., & HARDY, S. (2020): The effect of westerlies on East African rainfall and the associated role of tropical cyclones and the Madden–Julian Oscillation. - Quarterly Journal of the Royal Meteorological Society, **146**, 647–664.

FLEITMANN, D., BURNS, S. J., NEFF, U., MANGINI, A., & MATTER, A. (2003): Changing moisture sources over the last 330,000 years in Northern Oman from fluid-inclusion evidence in speleothems. - Quaternary Research, **60**, 223–232.

FLEITMANN, D., BURNS, S. J., MANGINI, A., MUDELSEE, M., KRAMERS, J., VILLA, I., NEFF, U., AL-SUBBARY, A. A., BUETTNER, A., HIPPLER, D., & MATTER, A. (2007): Holocene ITCZ and Indian monsoon dynamics recorded in stalagmites from Oman and Yemen (Socotra). - Quaternary Science Reviews, **26**, 170–188.

FLEITMANN, D., & MATTER, A. (2009): The speleothem record of climate variability in Southern Arabia. - Comptes Rendus - Geoscience, **341**, 633–642.

FOERSTER, V., JUNGINGER, A., LANGKAMP, O., GEBRU, T., ASRAT, A., UMER, M., LAMB, H. F., WENNRICH, V., RETHEMEYER, J., NOWACZYK, N., TRAUTH, M. H., & SCHAEBITZ, F. (2012): Climatic change recorded in the sediments of the Chew Bahir basin, southern Ethiopia, during the last 45,000 years. - Quaternary International, **274**, 25–37.

GARCIN, Y., MELNICK, D., STRECKER, M. R. M. R., OLAGO, D., & TIERCELIN, J.-J. J.-J. (2012): East African mid-Holocene wet–dry transition recorded in palaeo-shorelines of Lake Turkana, northern Kenya Rift. - Earth and Planetary Science Letters, **331**–**332**, 322–334.

GARELICK, S., RUSSELL, J. M., DEE, S., VERSCHUREN, D., & OLAGO, D. O. (2021): Atmospheric controls on precipitation isotopes and hydroclimate in high-elevation regions in Eastern Africa since the Last Glacial Maximum. - Earth and Planetary Science Letters, **567**, 116984.

GARELICK, S., RUSSELL, J., RICHARDS, A., SMITH, J., KELLY, M., ANDERSON, N., JACKSON, M. S., DOUGHTY, A., NAKILEZA, B., IVORY, S., DEE, S., & MARSHALL, C. (2022): The dynamics of warming during the last deglaciation in high-elevation regions of Eastern Equatorial Africa. - Quaternary Science Reviews, **281**, 107416.

GASSE, F. (2000): Hydrological changes in the African tropics since the Last Glacial Maximum. - Quaternary Science Reviews, **19**, 189–211.

GASSE, E., & STREET, F. A. (1978): Late Quaternary Lake-level fluctuations and environments of the northern Rift valley and Afar region (Ethiopia and Djibouti). - Palaeogeography, Palaeoclimatology, Palaeoecology, **24**, 279–325.

GASSE, F., & VAN CAMPO, E. (1994): Abrupt post-glacial climate events in West Asia and North Africa monsoon domains. - Earth and Planetary Science Letters, **126**, 435–456.

GIERGA, M., HAJDAS, I., VAN RADEN, U. J., GILLI, A., WACKER, L., STURM, M., BERNASCONI, S. M., & SMITTENBERG, R. H. (2016): Long-stored soil carbon released by prehistoric land use: Evidence from compound-specific radiocarbon analysis on Soppensee lake sediments. - Quaternary Science Reviews, **144**, 123–131.

GIL-ROMERA, G., ADOLF, C., BENITO BLAS, M., BITTNER, L., JOHANSSON, M. M. U., GRADY, D. D. A., LAMB, H. H. F., LEMMA, B., FEKADU, M., GLASER, B., MEKONNEN, B., SEVILLA-CALLEJO, M., ZECH, M., ZECH, W., MIEHE, G. (2019): Long-term fire resilience of the Ericaceous Belt, Bale Mountains,

Ethiopia. - Biology Letters, **15**, 20190357.

GIL-ROMERA, G., FEKADU, M., OPGENOORTH, L., GRADY, D., LAMB, H. F., BITTNER, L., ZECH, M., & MIEHE, G. (2021): The new Garba Guracha palynological sequence: Revision and data expansion. - In S. L. Runge, J., Gosling, W.D., Lézine, A-M. (Ed.), Quaternary Vegetation Dynamics – The African Pollen Database (p. 442). - London: CRC Press.

GIL-ROMERA, G., BITTNER, L., GRADY, D. A., EPP, L. S., OSSENDORF, G., ZECH, M., OPGENOORTH, L., MIEHE, G., & LAMB, H. F. (2022): The highest altitude paleoecological record of early pastoralism in Africa. - EGU General Assembly 2021.

GILLESPIE, R., STREET-PERROTT, F. A., & SWITSUR, R. (1983): Post-glacial arid episodes in Ethiopia have implications for climate prediction. - Nature, **306**, 680–683.

GROOS, A., AKÇAR, N., YESILYURT, S., MIEHE, G., VOCKENHUBER, C., & VEIT, H. (2021): Nonuniform Late Pleistocene glacier fluctuations in tropical Eastern Africa. - Science Advances, **7**.

GROVE, J. M. (2004): Little Ice Ages (2nd ed.). - London: Routledge.

HAMILTON, A. C. (1982): Environmental History of East Africa: A Study of the Quaternary. - London, New York: Academic Press. Retrieved from https://search.lib.virginia.edu/catalog/u137562

HELD, I. M., & SODEN, B. J. (2006): Robust Responses of the Hydrological Cycle to Global Warming. - Journal of Climate, **19**, 5686–5699.

HEPP, J., RABUS, M., ANHÄUSER, T., BROMM, T., LAFORSCH, C., SIROCKO, F., GLASER, B., & ZECH, M. (2016): A sugar biomarker proxy for assessing terrestrial versus aquatic sedimentary input. - Organic Geochemistry, **98**, 98–104.

HORTON, T. W., DEFLIESE, W. F., TRIPATI, A. K., & OZE, C. (2016): Evaporation induced 18O and 13C enrichment in lake systems: A global perspective on hydrologic balance effects. - Quaternary Science Reviews, **131**, 365–379.

IVORY, S. J., & RUSSELL, J. (2018): Lowland forest collapse and early human impacts at the end of the African Humid Period at Lake Edward, equatorial East Africa. - Quaternary Research, **89**, 7–20.

JAESCHKE, A., THIENEMANN, M., SCHEFUß, E., URBAN, J., SCHÄBITZ, F., WAGNER, B., & RETHEMEYER, J. (2020): Holocene Hydroclimate Variability and Vegetation Response in the Ethiopian Highlands (Lake Dendi). - Frontiers in Earth Science, **8**, 1–14.

JUNGINGER, A., ROLLER, S., OLAKA, L. A., & TRAUTH, M. H. (2014): The effects of solar irradiation changes on the migration of the Congo Air Boundary and water levels of paleo-Lake Suguta , Northern Kenya Rift , during the African Humid Period (15 – 5 ka BP). - Palaeogeography, Palaeoclimatology, Palaeoecology, **396**, 1–16.

KHALIDI, L., MOLOGNI, C., MÉNARD, C., COUDERT, L., GABRIELE, M., DAVTIAN, G., CAULIEZ, J., LESUR, J., BRUXELLES, L., CHESNAUX, L., REDAE, B. E., HAINSWORTH, E., DOUBRE, C., REVEL, M., SCHUSTER, M.,

& ZAZZO, A. (2020): 9000 years of human lakeside adaptation in the Ethiopian Afar: Fisher-foragers and the first pastoralists in the Lake Abhe basin during the African Humid Period. - Quaternary Science Reviews, **243**, 106459.

KONECKY, B. L., RUSSELL, J. M., JOHNSON, T. C., BROWN, E. T., BERKE, M. A., WERNE, J. P., & HUANG, Y. (2011): Atmospheric circulation patterns during late Pleistocene climate changes at Lake Malawi, Africa. - Earth and Planetary Science Letters, **312**, 318–326.

KUHNERT, H., KUHLMANN, H., MOHTADI, M., MEGGERS, H., BAUMANN, K., & PÄTZOLD, J. (2014): Holocene tropical western Indian Ocean sea surface temperatures in covariation with climatic changes in the Indonesian region. - , 423–437.

KUTZBACH, J. E., & OTTO-BLIESNER, B. L. (1982): The Sensitivity of the African-Asian Monsoonal Climate to Orbital Parameter Changes for 9000 Years B.P. in a Low-Resolution General Circulation Model. - Journal of Atmospheric Sciences, **39**, 1177–1188.

LAMB, H. F., KEBEDE, S., LENG, M. J., RICKETTS, D., TELFORD, R. J., & UMER, M. (2002): Origin and Isotopic Composition of Aragonite Laminae in an Ethiopian Crater Lake. - In The East African Great Lakes: Limnology, Palaeolimnology and Biodiversity (pp. 487–508).

LASKAR, J., ROBUTEL, P., JOUTEL, F., GASTINEAU, M., CORREIA, A. C. M., & LEVRARD, B. (2004): A long-term numerical solution for the insolation quantities of the Earth . - A&A, **428**, 261–285. Retrieved from https://doi.org/10.1051/0004-6361:20041335

LECLERC, A. J., & LABEYRIE, L. (1987): Temperature dependence of the oxygen isotopic fractionation between diatom silica and water. - Earth and Planetary Science Letters, **84**, 69–74.

LEMMA, B., MEKONNEN, B., GLASER, B., ZECH, W., NEMOMISSA, S., BEKELE, T., BITTNER, L., & ZECH, M. (2019): Chemotaxonomic patterns of vegetation and soils along altitudinal transects of the Bale Mountains, Ethiopia, and implications for paleovegetation reconstructions – Part II: lignin-derived phenols and leaf-wax-derived n-alkanes. - E&G Quaternary Sci. J., **68**, 189–200.

LEMMA, B., KEBEDE GURMESSA, S., NEMOMISSA, S., OTTE, I., GLASER, B., & ZECH, M. (2020): Spatial and temporal ^{2}H and ^{18}O isotope variation of contemporary precipitation in the Bale Mountains, Ethiopia. - Isotopes in Environmental and Health Studies, **56**, 122–135.

LEMMA, B., BITTNER, L., GLASER, B., KEBEDE, S., NEMOMISSA, S., ZECH, W., & ZECH, M. (2021): $\delta^{2}H_{n\text{-alkane}}$ and $\delta^{18}O_{sugar}$ biomarker proxies from leaves and topsoils of the Bale Mountains, Ethiopia, and implications for paleoclimate reconstructions. - Biogeochemistry.

LENG, M. J., & MARSHALL, J. D. (2004): Palaeoclimate interpretation of stable isotope data from lake sediment archives. - Quaternary Science Reviews, **23**, 811–831.

LEVIN, N. E., ZIPSER, E. J., & CEDING, T. E. (2009): Isotopic composition of waters from Ethiopia and Kenya: Insights into moisture sources for eastern Africa. - Journal of Geophysical Research Atmospheres, **114**, 1–13.

LEZINE, A.-M., BASSINOT, F., PETERSCHMITT, J. Y. J.-Y., LÉZINE, A. M., BASSINOT, F., & PETERSCHMITT, J. Y. J.-Y. (2014): Orbitally-induced changes of the Atlantic and Indian monsoons over the past 20,000 years: New insights based on the comparison of continental and marine records. - Bulletin de La Societe Geologique de France, **185**, 3–12.

LIU, X., RENDLE-BÜHRING, R., KUHLMANN, H., & LI, A. (2017): Two phases of the Holocene East African Humid Period: Inferred from a high-resolution geochemical record off Tanzania. - Earth and Planetary Science Letters, **460**, 123–134.

LOOMIS, S. E. S. E., RUSSELL, J. M., LADD, B., STREET-PERROTT, F. A. A., & SINNINGHE DAMSTÉ, J. S. J. S. (2012): Calibration and application of the branched GDGT temperature proxy on East African lake sediments. - Earth and Planetary Science Letters, **357**–**358**, 277–288.

LOOMIS, S. E., RUSSELL, J. M., & LAMB, H. F. (2015): Northeast African temperature variability since the Late Pleistocene. - Palaeogeography, Palaeoclimatology, Palaeoecology, **423**, 80–90.

LOOMIS, S. E., RUSSELL, J. M., VERSCHUREN, D., MORRILL, C., DE CORT, G., SINNINGHE DAMSTÉ, J. S., OLAGO, D., EGGERMONT, H., STREET-PERROTT, F. A., & KELLY, M. A. (2017): The tropical lapse rate steepened during the Last Glacial Maximum. - Science Advances, **3**.

MACHADO, M. J., PÉREZ-GONZÁLEZ, A., & BENITO, G. (1998): Paleoenvironmental Changes during the Last 4000 yr in the Tigray, Northern Ethiopia. - Quaternary Research, **49**, 312–321.

MARSHALL, M., LAMB, H., DAVIES, S., LENG, M., BEDASO, Z., UMER, M., & BRYANT, C. (2009): Climatic change in northern Ethiopia during the past 17,000 years: A diatom and stable isotope record from Lake Ashenge. - Palaeogeography Palaeoclimatology Palaeoecology, **279**.

MARSHALL, M. H. M. H., LAMB, H. F. H. F., HUWS, D., DAVIES, S. J. S. J., BATES, R., BLOEMENDAL, J., BOYLE, J., LENG, M. J. M. J., UMER, M., & BRYANT, C. (2011): Late Pleistocene and Holocene drought events at Lake Tana, the source of the Blue Nile. - Global and Planetary Change, **78**, 147–161.

MARTIN-JONES, C. M., LANE, C. S., PEARCE, N. J. G., SMITH, V. C., LAMB, H. F., SCHAEBITZ, F., VIEHBERG, F., BROWN, M. C., FRANK, U., & ASRAT, A. (2017): Recurrent explosive eruptions from a high-risk Main Ethiopian Rift volcano throughout the Holocene. - Geology, **45**, 1127–1130. Retrieved from http://dx.doi.org/10.1130/G39594.1

MAYR, C., LAPRIDA, C., LÜCKE, A., MARTÍN, R. S., MASSAFERRO, J., RAMÓN-MERCAU, J., & WISSEL, H. (2015): Oxygen isotope ratios of chironomids, aquatic macrophytes and ostracods for lake-water isotopic reconstructions – Results of a calibration study in Patagonia. - Journal of Hydrology, **529**, 600–607.

MCMANUS, J. F., FRANCOIS, R., GHERARDL, J.-M., KELGWIN, L., & DROWN-LEGER, S. (2004): Collapse and rapid resumption of Atlantic meridional circulation linked to deglacial climate changes. - Nature, **428**, 834–837.

MEKONNEN, B., ZECH, W., GLASER, B., LEMMA, B., BROMM, T., NEMOMISSA, S., BEKELE, T., & ZECH, M. (2019): Chemotaxonomic patterns of vegetation and soils along altitudinal transects of

the Bale Mountains, Ethiopia, and implications for paleovegetation reconstructions – Part 1: stable isotopes and sugar biomarkers. - E&G Quaternary Sci. J., **68**, 177–188.

MEYERS, P. A. (2003): Applications of organic geochemistry to paleolimnological reconstructions: a summary of examples from the Laurentian Great Lakes. - Organic Geochemistry, **34**, 261–289.

MIEHE, S., & MIEHE, G. (1994): Ericaceous forests and heathlands in the Bale mountains of South Ethiopia : ecology and man's impact (G. Miehe & 1952-, Eds.). - Reinbek: Reinbek : Warnke.

MOLOGNI, C., REVEL, M., BLANCHET, C., BOSCH, D., DEVELLE, A.-L., ORANGE, F., LUC, B., KHALIDI, L., DUCASSOU, E., & MIGEON, S. (2020): Frequency of exceptional Nile flood events as an indicator of Holocene hydro-climatic changes in the Ethiopian Highlands. - Quaternary Science Reviews, **247**.

MORRISSEY, A., & SCHOLZ, C. A. C. A. C. A. C. A. (2014): Paleohydrology of Lake Turkana and its influence on the Nile River system. - Palaeogeography, Palaeoclimatology, Palaeoecology, **403**, 88–100.

NAKAMURA, A., YOKOYAMA, Y., MAEMOKU, H., YAGI, H., OKAMURA, M., MATSUOKA, H., MIYAKE, N., OSADA, T., ADHIKARI, D. P., DANGOL, V., IKEHARA, M., MIYAIRI, Y., & MATSUZAKI, H. (2016): Weak monsoon event at 4.2 ka recorded in sediment from Lake Rara, Himalayas. - Quaternary International, **397**, 349–359.

NASH, D. J., DE CORT, G., CHASE, B. M., VERSCHUREN, D., NICHOLSON, S. E., SHANAHAN, T. M., ASRAT, A., LÉZINE, A.-M., & GRAB, S. W. (2016): African hydroclimatic variability during the last 2000 years. - Quaternary Science Reviews, **154**, 1–22.

NCHABA, T., MPHOLO, M., & LENNARD, C. (2017): Long-term austral summer wind speed trends over southern Africa. - International Journal of Climatology, **37**, 2850–2862.

NICHOLSON, S. E. (1982): Pleistocene and Holocene climates in Africa. - Nature, **296**, 779.

NICHOLSON, S. E. (2017): Climate and climatic variability of rainfall over eastern Africa. - Reviews of Geophysics, **55**, 590–635.

NICHOLSON, S. E., KLOTTER, D., & HARTMAN, A. T. (2021): Lake-Effect Rains over Lake Victoria and Their Association with Mesoscale Convective Systems. - Journal of Hydrometeorology, **22**, 1353–1368.

OHMURA, A. (2012): Enhanced temperature variability in high-altitude climate change. - Theoretical and Applied Climatology, **110**, 499–508.

OSSENDORF, G., GROOS, A., BROMM, T., GIRMA TEKELEMARIAM, M., GLASER, B., LESUR, J., SCHMIDT, J., AKÇAR, N., BEKELE, T., BELDADOS, A., DEMISSEW, S., HADUSH KAHSAY, T., P NASH, B., NAUSS, T., NEGASH, A., NEMOMISSA, S., VEIT, H., VOGELSANG, R., ZERIHUN, W., & MIEHE, G. (2019): Middle Stone Age foragers resided in high elevations of the glaciated Bale Mountains, Ethiopia. -

Science, **365**, 583–587.

PAUSATA, F. S. R., GAETANI, M., MESSORI, G., BERG, A., MAIA DE SOUZA, D., SAGE, R. F., & DEMENOCAL, P. B. (2020): The Greening of the Sahara: Past Changes and Future Implications. - One Earth, **2**, 235–250.

PIAO, J., CHEN, W., WANG, L., PAUSATA, F. S. R., & ZHANG, Q. (2020): Northward extension of the East Asian summer monsoon during the mid-Holocene. - Global and Planetary Change, **184**, 103046.

POWERS, L. A., JOHNSON, T. C., WERNE, J. P., CASTAÑEDA, I. S., HOPMANS, E. C., SINNINGHE DAMSTÉ, J. S., & SCHOUTEN, S. (2005): Large temperature variability in the southern African tropics since the Last Glacial Maximum. - Geophysical Research Letters, **32**, 1–4.

RABERG, J. H., HARNING, D. J., CRUMP, S. E., DE WET, G., BLUMM, A., KOPF, S., GEIRSDÓTTIR, Á., MILLER, G. H., & SEPÚLVEDA, J. (2021): Revised fractional abundances and warm-season temperatures substantially improve brGDGT calibrations in lake sediments. - Biogeosciences, **18**, 3579–3603.

ROZANSKI, K., ARAGUÁS-ARAGUÁS, L., & GONFIANTINI, R. (1993): Isotopic Patterns in Modern Global Precipitation. - Climate Change in Continental Isotopic Records.

RUSSELL, J. M., HOPMANS, E. C., LOOMIS, S. E., LIANG, J., & SINNINGHE DAMSTÉ, J. S. (2018): Distributions of 5- and 6-methyl branched glycerol dialkyl glycerol tetraethers (brGDGTs) in East African lake sediment: Effects of temperature, pH, and new lacustrine paleotemperature calibrations. - Organic Geochemistry, **117**, 56–69.

SACHSE, D., BILLAULT, I., BOWEN, G. J., CHIKARAISHI, Y., DAWSON, T. E., FEAKINS, S. J., FREEMAN, K. H., MAGILL, C. R., MCINERNEY, F. A., VAN DER MEER, M. T. J., POLISSAR, P., ROBINS, R. J., SACHS, J. P., SCHMIDT, H.-L., SESSIONS, A. L., WHITE, J. W. C., WEST, J. B., & KAHMEN, A. (2012): Molecular Paleohydrology: Interpreting the Hydrogen-Isotopic Composition of Lipid Biomarkers from Photosynthesizing Organisms. - Annual Review of Earth and Planetary Sciences, **40**, 221–249.

SAGNOTTI, L., & CARICCHI, C. (2018): StratFit: An Excel Workbook for correlation of multiple stratigraphic trendsAnnals of Geophysics (Vol. 61).

SCHEFUß, E., KUHLMANN, H., MOLLENHAUER, G., PRANGE, M., & PÄTZOLD, J. (2011): Forcing of wet phases in southeast Africa over the past 17,000 years. - Nature, **480**, 509–512.

SCHILLEREFF, D. N., CHIVERRELL, R. C., MACDONALD, N., & HOOKE, J. M. (2014): Flood stratigraphies in lake sediments: A review. - Earth-Science Reviews, **135**, 17–37.

SCHNEEWEISS, J., BECKER, F., MOLODIN, V. I., & PARZINGER, H. (2018): ScienceDirect Radiocarbon chronology of occupation of the site Chicha and Bayesian statistics for the assessment of a discontinuous transition from Late Bronze to Early Iron Age (West Siberia). - Russian Geology and Geophysics, **59**, 635–651.

SHARP, Z. (2017): Principles of Stable Isotope Geochemistry, 2nd Edition.

SIROCKO, F., DIETRICH, S., VERES, D., GROOTES, P. M., SCHABER-MOHR, K., SEELOS, K., NADEAU, M.-J., KROMER, B., ROTHACKER, L., RÖHNER, M., KRBETSCHEK, M., APPLEBY, P., HAMBACH, U., ROLF, C., SUDO, M., & GRIM, S. (2013): Multi-proxy dating of Holocene maar lakes and Pleistocene dry maar sediments in the Eifel, Germany. - Quaternary Science Reviews, **62**, 56–76.

SPRACKLEN, D. V, BAKER, J. C. A., GARCIA-CARRERAS, L., & MARSHAM, J. H. (2018): The effects of tropical vegetation on rainfall. - Annual Review of Environment and Resources, **43**, 193–218.

STAGER, J. C., MAYEWSKI, P. A., & MEEKER, L. D. (2002): Cooling cycles, Heinrich event 1, and the desiccation of Lake Victoria. - Palaeogeography, Palaeoclimatology, Palaeoecology, **183**, 169–178.

STOJANOVIC, M., MULUALEM, G. M., SORÍ, R., VÁZQUEZ, M., NIETO, R., & GIMENO, L. (2022): Precipitation Moisture Sources of Ethiopian River Basins and Their Role During Drought Conditions . - Frontiers in Earth Science.

STREET-PERROTT, F. A., & PERROTT, R. A. (1990): Abrupt climate fluctuations in the tropics: the influence of Atlantic Ocean circulation. - Nature, **343**, 607–612.

SZMYTKIEWICZ, A., & ZALEWSKA, T. (2014): Sediment deposition and accumulation rates determined by sediment trap and ^{210}Pb isotope methods in the Outer Puck Bay (Baltic Sea). - Oceanologia, **56**, 85–106.

TALBOT, M. R. (1990): A review of the palaeohydrological interpretation of carbon and oxygen isotopic ratios in primary lacustrine carbonates. - Chemical Geology: Isotope Geoscience Section, **80**, 261–279.

TALBOT, M. R., & LÆRDAL, T. (2000): The Late Pleistocene - Holocene palaeolimnology of Lake Victoria, East Africa, based upon elemental and isotopic analyses of sedimentary organic matter. - Journal of Paleolimnology, **23**, 141–164.

TALBOT, M. R., FILIPPI, M. L., JENSEN, N. B., & TIERCELIN, J.-J. (2007): An abrupt change in the African monsoon at the end of the Younger Dryas. - Geochemistry, Geophysics, Geosystems, **8**, n/a-n/a.

TARASOV, P. E., MÜLLER, S., ZECH, M., ANDREEVA, D., DIEKMANN, B., & LEIPE, C. (2013): Last glacial vegetation reconstructions in the extreme-continental eastern Asia: Potentials of pollen and n-alkane biomarker analyses. - Quaternary International, **s 290–291**, 253–263.

TIERCELIN, J. J., GIBERT, E., UMER, M., BONNEFILLE, R., DISNAR, J. R., LÉZINE, A. M., HUREAU-MAZAUDIER, D., TRAVI, Y., KERAVIS, D., & LAMB, H. F. (2008): High-resolution sedimentary record of the last deglaciation from a high-altitude lake in Ethiopia. - Quaternary Science Reviews, **27**, 449–467.

TIERNEY, J. E., RUSSELL, J. M., HUANG, Y., DAMSTE, J. S. S., HOPMANS, E. C., & COHEN, A. S. (2008):

Northern Hemisphere Controls on Tropical Southeast African Climate During the Past 60,000 Years. - Science, **322**, 252–255.

TIERNEY, J. E., RUSSELL, J. M., EGGERMONT, H., HOPMANS, E. C., VERSCHUREN, D., & SINNINGHE DAMSTÉ, J. S. (2010): Environmental controls on branched tetraether lipid distributions in tropical East African lake sediments. - Geochimica et Cosmochimica Acta, **74**, 4902–4918.

TIERNEY, J. E., LEWIS, S. C., COOK, B. I., LEGRANDE, A. N., & SCHMIDT, G. A. (2011a): Model, proxy and isotopic perspectives on the East African Humid Period. - Earth and Planetary Science Letters, **307**, 103–112.

TIERNEY, J. E., RUSSELL, J. M., SINNINGHE DAMSTÉ, J. S., HUANG, Y., & VERSCHUREN, D. (2011b): Late Quaternary behavior of the East African monsoon and the importance of the Congo Air Boundary. - Quaternary Science Reviews, **30**, 798–807.

TIERNEY, J. E., & DEMENOCAL, P. B. (2013): Abrupt Shifts in Horn of Africa Hydroclimate Since the Last Glacial Maximum. - Science, **342**, 843–846.

TIERNEY, J. E., ABRAM, N. J., ANCHUKAITIS, K. J., EVANS, M. N., GIRY, C., KILBOURNE, K. H., SAENGER, C. P., WU, H. C., & ZINKE, J. (2015): Tropical sea surface temperatures for the past four centuries reconstructed from coral archives. - Paleoceanography, **30**, 226–252.

TIERNEY, J. E., PAUSATA, F. S. R., & DEMENOCAL, P. (2016): Deglacial Indian monsoon failure and North Atlantic stadials linked by Indian Ocean surface cooling. - Nature Geoscience, **9**, 46–50.

UHLIG, S. K. (1988): Mountain Forests and the Upper Tree Limit on the Southeastern Plateau of Ethiopia. - Mountain Research and Development, **8**, 227–234.

UMER, M., LAMB, H. F., BONNEFILLE, R., LÉZINE, A. M., TIERCELIN, J. J., GIBERT, E., CAZET, J. P., & WATRIN, J. (2007): Late Pleistocene and Holocene vegetation history of the Bale Mountains, Ethiopia. - Quaternary Science Reviews, **26**, 2229–2246.

VAN BREE, L. G. J., PETERSE, F., BAXTER, A. J., DE CROP, W., VAN GRINSVEN, S., VILLANUEVA, L., VERSCHUREN, D., & SINNINGHE DAMSTÉ, J. S. (2020): Seasonal variability and sources of in situ brGDGT production in a permanently stratified African crater lake. - Biogeosciences Discuss., **2020**, 1–36.

VAN DER LUBBE, H. J. L., KRAUSE-NEHRING, J., JUNGINGER, A., GARCIN, Y., JOORDENS, J. C. A., DAVIES, G. R., BECK, C., FEIBEL, C. S., JOHNSON, T. C., & VONHOF, H. B. (2017): Gradual or abrupt? Changes in water source of Lake Turkana (Kenya) during the African Humid Period inferred from Sr isotope ratios. - Quaternary Science Reviews, **174**, 1–12.

VERSCHUREN, D., SINNINGHE DAMSTÉ, J. S., MOERNAUT, J., KRISTEN, I., BLAAUW, M., FAGOT, M., & HAUG, G. H. (2009): Half-precessional dynamics of monsoon rainfall near the East African Equator. - Nature, **462**, 637–641.

VISTE, E., & SORTEBERG, A. (2013): Moisture transport into the Ethiopian highlands. -

International Journal of Climatology, **33**, 249–263.

VUILLE, M., WERNER, M., BRADLEY, R. S., & KEIMIG, F. (2005): Stable isotopes in precipitation in the Asian monsoon region. - Journal of Geophysical Research: Atmospheres, **110**.

WAGNER, B., WENNRICH, V., VIEHBERG, F., JUNGINGER, A., KOLVENBACH, A., RETHEMEYER, J., SCHAEBITZ, F., & SCHMIEDL, G. (2018): Holocene rainfall runoff in the central Ethiopian highlands and evolution of the River Nile drainage system as revealed from a sediment record from Lake Dendi. - Global and Planetary Change, **163**, 29–43.

WANG, H., LIU, W., HE, Y., ZHOU, A., ZHAO, H., LIU, H., CAO, Y., HU, J., MENG, B., JIANG, J., KOLPAKOVA, M., KRIVONOGOV, S., & LIU, Z. (2021): Salinity-controlled isomerization of lacustrine brGDGTs impacts the associated MBT5ME' terrestrial temperature index. - Geochimica et Cosmochimica Acta, **305**, 33–48.

WEBER, Y., DAMSTÉ, J. S. S., ZOPFI, J., DE JONGE, C., GILLI, A., SCHUBERT, C. J., LEPORI, F., LEHMANN, M. F., & NIEMANN, H. (2018): Redox-dependent niche differentiation provides evidence for multiple bacterial sources of glycerol tetraether lipids in lakes. - Proceedings of the National Academy of Sciences of the United States of America, **115**, 10926–10931.

WELDEAB, S., SCHNEIDER, R. R., & MÜLLER, P. (2007): Comparison of Mg/Ca- and alkenone-based sea surface temperature estimates in the fresh water–influenced Gulf of Guinea, eastern equatorial Atlantic. - Geochemistry, Geophysics, Geosystems, **8**.

WELDEAB, S., MENKE, V., & SCHMIEDL, G. (2014): The pace of East African monsoon evolution during the Holocene. - Geophysical Research Letters, **41**, 1724–1731.

ZENG, Z., CHEN, A., CIAIS, P., LI, Y., LI, L. Z. X., VAUTARD, R., ZHOU, L., YANG, H., HUANG, M., & PIAO, S. (2015): Regional air pollution brightening reverses the greenhouse gases induced warming-elevation relationship. - Geophysical Research Letters, **42**, 4563–4572.

Chapter 6

Conclusions and Outlook

The Garba Guracha cirque lake in the Bale Mountains, Ethiopia, is a valuable sediment archive for paleolimnological research in a relatively undisturbed high-altitude setting. With the first applied biomarker analyses to a high-altitude lake archive in the Bale Mountains and the Horn of Africa, this thesis provides the first insights into the regional climate history. The thesis not only advances the understanding of climatic changes in the Horn of Africa, an understudied region of the world but also contributes to the methodological development of isotopic research of biomarkers, especially of hemicellulose-derived sugars. Based on the main findings discussed in the synthesis, several conclusions can be inferred:

- The Garba Guracha record, with a high resolution of 10 years per cm and a variety of applied dating technics and materials, yields one of the most robust and high-resolution chronologies of eastern Africa. The consistent external age control using the dated tephra layers not only contributes to the robustness but also validates the non-existence of a constant ^{14}C age offset. The relatively innovative compound class-specific *n*-alkane dating showed overall no age offsets. The supposed pre-aging of the terrestrial *n*-alkanes is negligible due to the short residence times in the small catchment or the possible aquatic origin of some *n*-alkanes. In small catchment areas, the innovative *n*-alkane dating is a valuable tool in paleolimnological research.

- High altitude Garba Guracha and its relatively small catchment preserved an undisturbed archive recording the progression from a glacier dominated to a cirque lake catchment. The minimum age of deglaciation inferred from the bottom-most age of the retrieved sediment core is ~ 15.9 cal ka BP. Prevailing siliciclastic-rich sedimentation during the glacial retreat is replaced around ~ 11 cal ka BP by increasing accumulation of organic matter, recording a shift towards favourable growth conditions in the Holocene.

- The shift towards increased organic matter production at ~ 11 cal ka BP divides the Garba Guracha sediments into organic-poor lower and organic-rich upper parts. The organic matter in the Garba Guracha archive is predominantly of aquatic origin. Apart from *n*-alkanes, high lake productivity is indicated by (i) relatively low TOC/N values, (ii) the relatively high fucose/(arabinose+xylose) ratios, and (iii) relatively positive $\delta^{13}C$ values in combination with no evidence for C_4 vegetation.

- The measurements of the isotopic composition of fucose and the purely aquatic derived diatom revealed consistent results, identical trends and similar ranges in reconstructed $\delta^{18}O_{lake\ water}$. This not only underlines the predominant aquatic origin of fucose. Furthermore, it highlights the value of sugar biomarkers as a proxy in paleolimnological research. Therefore, $\delta^{18}O$ inferred from the predominantly aquatic-derived sugar biomarker fucose is a valuable tool for reconstructing the lake water isotopic composition in paleolimnological studies.

- The cirque lake Garba Guracha has no large tributaries and is mainly fed by rainfall. Alternating between open and closed phases, the isotopic composition of the lake water is determined by evaporative enrichment and the precipitation signal. Overflow into the adjacent valley reduces the evaporative enrichment. Due to varying open and closed lake conditions in the past, the lake water isotopic composition of Garba Guracha can be interpreted as P/E. Primarily open lake conditions began at ~ 10 cal ka BP and lasted until 7 cal ka BP. At ca. 7 cal ka BP, a continuous shift towards drier conditions began, indicating a change towards a predominantly closed lake system. Small minima, representing phases of lower P/E, occurred at 10.8 cal ka BP, 10.2 cal ka BP, 3.5 cal ka BP, and 0.5 cal ka BP. Despite differences in apparent intensity, reconstructed dry and wet phases are broadly coincident with Rift Valley records, indicating similar climate controls.

- The brGDGT composition in Garba Guracha sediments is affected by several influences, aside from the mean annual temperature, like water chemistry and the bacterial community. Due to unique brGDGT compositions, a new temperature calibration, including a 6-methyl isomer, was developed, performing slightly better than the MBT'_{5ME} calibration. The results of this new calibration clearly show that the local (6 °N) and the northern hemisphere insolation variability in millennial time scales mainly drive MAT. On shorter time scales, MAT was affected by glacier and permafrost melting during deglaciation and the regional atmospheric circulation. These additional mechanisms partly explain the asynchronicity between the Garba Guracha MAT record in the high altitude afro-alpine region of the Horn of Africa and other eastern African lake records. Moreover, high-altitude lake archives are more affected relatively by temperature changes and record a higher temperature amplitude since the last deglaciation than low-altitude records in the region.

- The cirque lake Garba Guracha contains information about environmental changes since the deglaciation of the catchment. The minimum age of deglaciation (15.9 cal ka BP) is in good agreement with exposure dating of the down valley glacial features. The glacial retreat from the north-facing valley likely did not happen rapidly but continuously over a more extended period, and ice remained in the catchment. The Garba Guracha archive is sensitive to northern hemisphere climatic drivers recorded in reduced sedimentation rate and cold temperatures during the YD times. The period before 11.2 cal ka BP was mainly determined by glacial/ice retreat and was characterised by cold and dry conditions. Around ~ 11 cal ka BP sudden climatic and environmental changes are recorded in several proxies. MAT increased by ca. 3.5 °C in just ca. 600 years, and rising precipitation led to a prolonged humid and warm phase in the Early and Mid-Holocene. The humid phase latest until ~ 7 cal ka BP, when moisture availability began to decrease constantly, followed by MAT at ~ 6 cal ka BP coinciding with decreasing insolation (6 °N Sept). Even though climatic conditions (MAT

and $\delta^{18}O$) constantly decreased, other proxies (TOC, TOC/N, abundance of *B.braunii*) dropped rapidly at 4.5 cal ka BP, indicating a substantial change in the catchment environment. During the last 4 thousand years, MAT and P/E were on low to intermediate values.

- The Garba Guracha paleoclimate research has enhanced the understanding of climatic changes in the region. Overall, the $\delta^{18}O$ changes of Garba Guracha and Dongge cave highlight the connection between high and low latitude climatic changes in the northern hemisphere. Moreover, similarities between Qunf cave and Garba Guracha prove the connection of EAM and ISM regions and question the influence of the CAB and associated Atlantic moisture in the Bale Mountains. The meridional pattern in the $\delta^{2}H$ records of eastern Africa highlights the influence of the ITCZ and the associated tropical rain belt. Therefore, the Bale Mountains were under the influence of cold northeastern winds after the deglaciation and driven by insolation changes, the EAM strengthened, and precipitation was enhanced at the Holocene onset by meridional processes. The resulting humid phase lasted until 7 cal ka BP and then gradually transitioned to drier conditions, likely driven by a reorganization of the atmospheric circulation pattern due to decreasing northern summer and increasing southern summer insolation.

The thesis reconstructed the environmental and paleoclimatic history of Garba Guracha, enhancing the knowledge about paleoclimatic changes in the Horn of Africa. The results of this thesis highlight the potential of biomarker and stable isotope analysis for paleoclimate research. By applying innovative methods and analyses (*n*-alkane dating, $\delta^{18}O_{fucose}$) and comparing them with well-established methods, these proxies have proven to be valuable paleoclimatic tools and, in the case of $\delta^{18}O_{fucose}$, an excellent sensor of climatic changes.

The results of this thesis have answered several questions, but an equal number of questions have arisen, and further research ideas have emerged:

- Has the Little Ice Age affected the climate of the Garba Guracha catchment and influenced local pastoralism?
- What is the reason for the poor organic sedimentation at 6.5 ka?
- Is there a connection between volcanic eruptions and the local climate?
- How exactly did the northern hemisphere YD event influence the climate of the Bale Mountains?

Due to the low resolution of ~ 100 years per sample (10 cm mixed sediment) in the current climatic records, a higher resolution is necessary to investigate interesting time periods in more detail and to compare the results to archaeological and pollen data. The Garba Guracha record yields a high resolution of up to 10 years per centimeter.

- How is the age structure of climatic proxies (e.g. brGDGTs, sugar molecules) compared to the bulk sediment?

The first application of compound-class-specific *n*-alkane dating in the Horn of Africa, perhaps in eastern Africa, has shown the potential of compound-class-specific *n*-alkane dating. This thesis has not found an offset between ^{14}C bulk sediment and compound-class-specific *n*-alkane dating in the small Garba Guracha catchment. However, this might differ in larger catchments with longer residence times in soils and sediments, creating an age offset between aquatic and terrestrial compounds. Further research and the application of compound-specific dating of climatic proxies (e.g. *n*-alkanes, sugars) are necessary to overcome chronological uncertainties. Furthermore, a suitable dating method for sugar molecules and brGDGTs has yet to be developed.

- How different was the climate change of the last 13 cal ka BP pronounced across the Bale Mountains, especially concerning altitude and aspects?

During the field trips in 2017 and 2018, several sediment cores were taken in the Bale Mountains. With the same set of paleoclimatic methods applied to these cores, it might be possible to (i) calculate a paleo lapse rate of temperature changes with altitude, (ii) explore paleo air mass sources, and (iii) evaluate differences between the high and low altitude in the Bale Mountains.

Garba Guracha is one of the best studied and dated high-altitude archives in eastern Africa. Further research and publications (in preparation or planned) will enhance the understanding of climatic changes in the Bale Mountains and beyond.

Appendix A

Supplements to Chapter 2

Supplementary Data

Table A.1: Chronology BAL-GGU17-AB. Uncertainties of ^{14}C ages refer to 68% probabilities (1σ), whereas ranges of calendar ages represent 95% probabilities (2σ). ^{14}C ages were calibarated with IntCal13.

Lab. Name	Dating lab code	IPE-CSIC/ UH code	Dating method	Depth [cm]	^{14}C age [BP]	Uncertainty [yr]	Calendar ages [cal BP]
ECRC-UCL	BAL0	BAL0	^{210}Pb-^{137}Cs	0		1	-67
	BAL1.5	BAL1.5		1.5		2	-64
	BAL4.5	BAL4.5		4.5		2	-47
	BAL6.5	BAL6.5		6		3	-26
	BAL7.5	BAL7.5		7		5	-13
	BAL8.5	BAL8.5		8		5	-10
	BAL9.5	BAL9.5		9		5	-8
	BAL10.5	BAL10.5		10		5	-6
	BAL12.5	BAL12.5		12		5	-1
	BAL14.5	BAL14.5		14		5	4
	BAL16.5	BAL16.5		16		6	8
	BAL18.5	BAL18.5		18		6	13
	BAL20.5	BAL20.5		20		6	17
	BAL22.5	BAL22.5		22		7	21
	BAL24.5	BAL24.5		24		7	26
	BAL26.5	BAL26.5		26		8	31
	BAL28.5	BAL28.5		28		9	34
	BAL31.5	BAL31.5		31		10	40
	BAL34.5	BAL34.5		34		11	46
	BAL38.5	BAL38.5		38		13	56
	BAL42.5	BAL42.5		42		14	68
	BAL46.5	BAL46.5		46		15	78
	BAL51.5	BAL51.5		51		18	94
LARA Bern	BE-7931.1.1	GG1B1	^{14}C-Bulk Sediment	105	935	118	662-1081
	BE-8273.1.1	GG1B1A	^{14}C-n-alkane	105	1076	79	892-1180
	BE-8282.1.1	2L15.16	^{14}C-Charcoal	185	2124	129	1779-2366
	BE-7930.1.1	GG1B2	^{14}C-Bulk Sediment	205	2323	111	2110-2722
	BE-8272.1.1	GG1B2A	^{14}C-n-alkane	205	2399	101	2302-2743
	BE-8271.1.1	GG1B3A	^{14}C-n-alkane	303	3476	89	3556-3979
	BE-7929.1.1	GG1B3	^{14}C-Bulk Sediment	303	3517	111	3555-4091
	BE-8270.1.1	GG1B5A	^{14}C-n-alkane	503	5789	109	6391-6804
	BE-7928.1.1	GG1B5	^{14}C-Bulk Sediment	503	5794	135	6305-6903
	BE-8269.1.1	GG1B6A	^{14}C-n-alkane	602	6967	123	7589-8003
	BE-7927.1.1	GG1B6	^{14}C-Bulk Sediment	602	7320	144	7922-8404
	BE-8268.1.1	GG1B7A	^{14}C-n-alkane	700	8267	137	8973-9535
	BE-7926.1.1	GG1B7	^{14}C-Bulk Sediment	700	8753	156	9516-10201
	BE-8279.1.1	7L35.36	^{14}C-Charcoal	705	8753	162	9496-10206

	BE-7925.1.1*	GG1B8	^{14}C-Bulk Sediment	794	10214	203	11267-12531
	BE-8267.1.1*	GG1B8A	^{14}C-n-alkane	794	9301	273	9740-11235
	BE-8266.1.1	GG1B9A	^{14}C-n-alkane	898	9650	155	10545-11368
	BE-7924.1.1	GG1B9	^{14}C-Bulk Sediment	898	9706	175	10563-11640
	BE-8276.1.1	9L55.56	^{14}C-Charcoal	925	10925	364	11823-13567
Direct AMS	D-AMS 033974*	GG1B015	^{14}C Bulk Sediment	15	180	23	140-289
	D-AMS 033975*	GG1B025		25	310	23	304-456
	D-AMS 033976*	GG1B045		45	524	26	510-624
	D-AMS 033977*	GG1B8C		821	10243	46	11773-12140
	D-AMS 029493	GG1B10		998	11110	48	12828- 13082
	D-AMS 029494	GG1B11		1108	11377	50	13102- 13313
	D-AMS 029495	GG1B12		1218	12181	51	13906-14230
	D-AMS 027899	GG1B15		1493	12977	53	15291-15740
	D-AMS 029496	GG1B15b		1528	12997	57	15304-15772
	D-AMS 029497	GG1B15c		1548	13294	59	15772-16193

- Not considered for the age depth model

Table A.2: ^{210}Pb concentrations in core BAL-GGU17-1A-1L taken from Lake Garba Guracha, Ethiopia.

Depth	Dry Mass	^{210}Pb						Cum Unsupported ^{210}Pb	
		Total		Supported		Unsupp			
cm	g cm^{-2}	Bq Kg^{-1}	±	Bq Kg^{-1}	±	Bq Kg^{-1}	±	Bq m^{-2}	±
1.5	0.0661	1293.51	26.68	35.51	3.12	1258	26.86	855	44.6
4.5	0.4389	1008.99	31.88	36.56	4.04	972.43	32.13	4989.7	228.4
6.5	0.7642	709.4	29.51	34.71	4.45	674.69	29.84	7639.3	285.4
7.5	0.9188	665.94	29.15	26.44	3.94	639.5	29.42	8654.9	295.5
8.5	1.0774	537.72	27.79	34.6	4.2	503.12	28.11	9556.7	302.5
9.5	1.2495	377.38	15.46	41.52	2.92	335.86	15.73	10269	307.6
10.5	1.4216	373.38	26.47	33.25	4.18	340.13	26.8	10850.7	310.8
12.5	1.8091	291.27	15.35	42.58	2.84	248.69	15.61	11982.3	325.3
14.5	2.184	210.3	14.48	38.03	2.98	172.27	14.78	12762.6	332.8
16.5	2.5007	173.6	13.65	41.31	2.9	132.29	13.95	13242.1	337.2
18.5	2.8881	105.53	12.48	31.15	2.71	74.38	12.77	13631.7	341.5
20.5	3.3863	98.8	8.5	32.29	1.85	66.51	8.7	13982.3	346.4
22.5	3.8918	91.72	10.6	31.87	2.54	59.85	10.9	14301.4	349.9
24.5	4.3597	87.72	9.94	39.39	2.56	48.33	10.26	14553.5	353.9
26.5	4.7295	65.03	7.72	32.82	2.35	32.21	8.07	14700.4	356.1
28.5	5.017	83.85	8.88	39.53	2.24	44.32	9.16	14809.5	357
31.5	5.5316	59.6	9.1	33.97	2.15	25.63	9.35	14985.1	359.6
34.5	6.0403	72.58	6.75	39.99	1.71	32.59	6.96	15132.5	362.5
38.5	6.742	54.55	10.91	38.02	2.64	16.53	11.22	15298.5	366.7
42.5	7.4532	61.55	8.65	40.91	2.29	20.64	8.95	15430.2	374.5
46.5	8.1826	42.22	5.05	34.6	1.35	7.62	5.23	15525.5	379.2
51.5	9.1197	40.76	5.73	35.4	1.54	5.36	5.93	15600.3	382.3

Table A.3: Artificial fallout radionuclide concentrations in core BAL-GGU17-1A-1L.

Depth	Cs-137		Am-241	
cm	Bq Kg^{-1}	±	Bq Kg^{-1}	±
1.5	50.26	2.46	0	0
4.5	89.11	4.22	0	0
6.5	113.64	4.86	0	0
7.5	140.75	5.08	2.82	1.7
8.5	102.63	4.67	0	0
9.5	42.19	2.16	0	0
10.5	38.21	3.22	0	0
12.5	21.79	1.86	0	0
14.5	21.3	1.87	0	0
16.5	11.01	1.37	0	0
18.5	8.5	1.36	0	0
20.5	8.87	0.92	0	0
22.5	9.52	1.34	0	0
24.5	7.28	1.24	0	0
26.5	3.75	1.21	0	0
28.5	4.49	1	0	0
31.5	2.68	0.99	0	0
34.5	3.41	0.71	0	0
38.5	3.01	1.14	0	0
42.5	0	0	0	0
46.5	0	0	0	0
51.5	0	0	0	0

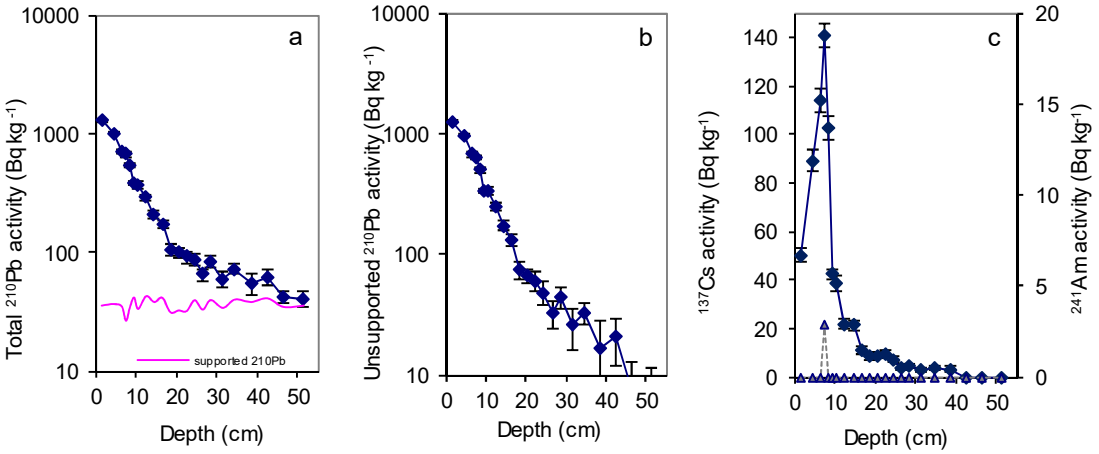

Figure A.1: Fallout radionuclide concentrations in core BAL-GGU17-1A-1L taken from Lake Garba Guracha, Ethiopia, showing (a) total ^{210}Pb, (b) unsupported ^{210}Pb, and (c) ^{137}Cs and ^{241}Am concentrations versus depth.

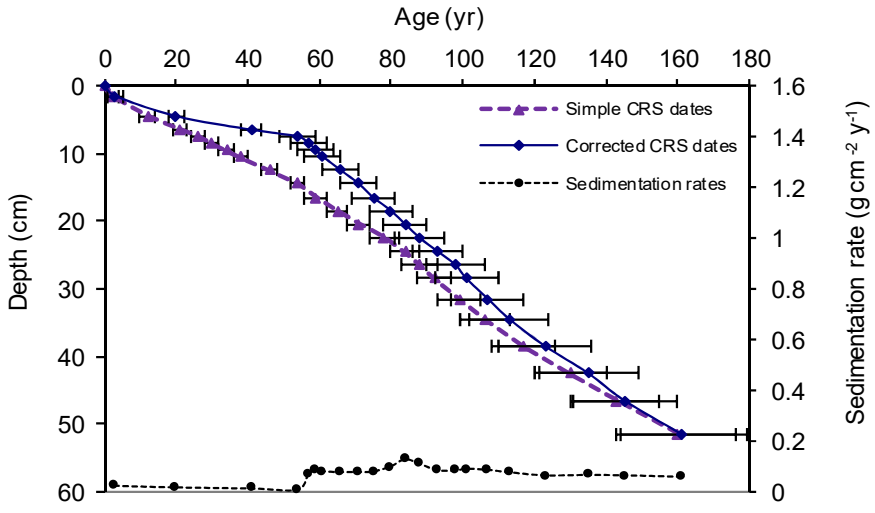

Figure A.2: Radiometric chronology of core BAL-GGU17-1A-1L taken from Lake Garba Guracha, Ethiopia, showing the CRS model ^{210}Pb dates and sedimentation rates.

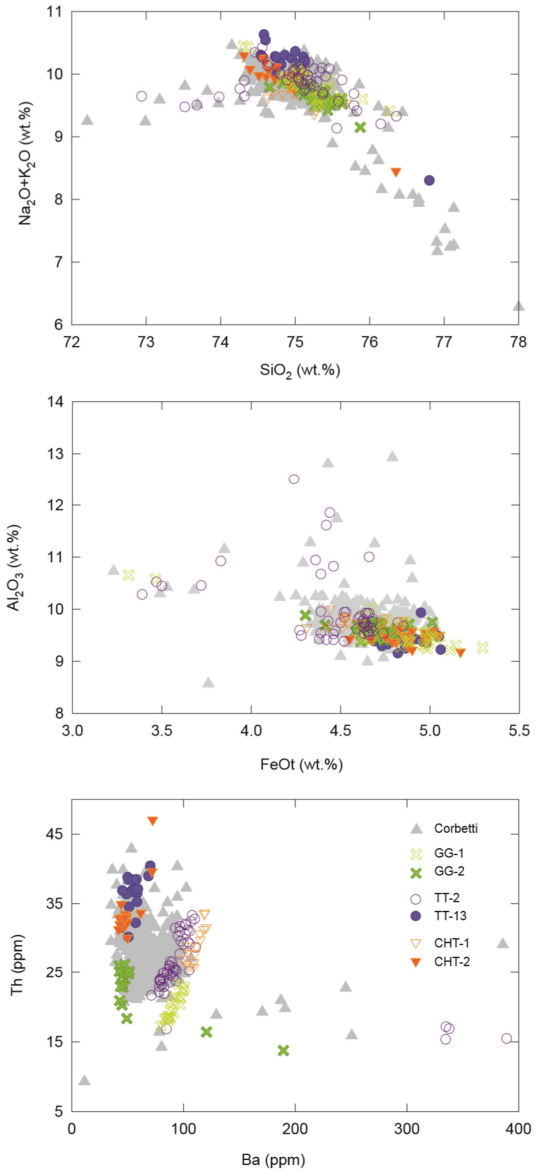

Figure A.3: Bi-plots showing the concentrations of major and trace elements in glass shards within the Garba Gurache tephras. The compositions of rocks erupted from the Corbetti is shown in grey for comparison, alongside the composition tephra deposits from two of its largest Holocene eruptions, found at lakes Tilo and Chamo in the central Main Ethiopian Rift. Concentrations of Ba and Th clearly differentiate the tephras. The similarity in Ba/Th ratios suggests that GG-1 correlates to the Tilo tephra TT-2 and CHT-1 at Chamo, whilst GG-2 correlates to TT-13 and CHT-2.

Appendix B

Supplements to Chapter 3

Supplementary Data

Table B.1: Measured $\delta^{18}O_{diatom}$ values in the Garba Guracha sediment core: calculated contamination (c_{cont}), $\delta^{18}O$ values corrected for contamination ($\delta^{18}O_{Al2O3corr}$), and standard deviation SD ($\delta^{18}O$ s.d. N).

Sample ID	Depth [cm]	Age [cal. BP]	Al_2O_3	SiO_2	$\delta^{18}O$	$\delta^{18}O$ [‰]	$\delta^{18}O$	$\delta^{18}O$ mean [‰]	$\delta^{18}O$ s.d. S	$\delta^{18}O$ s.d. N	C_{cont}	$\delta^{18}O_{Al_2O_{3corr}}$ [‰]	$\Delta^{18}O_{corr}$ [‰]
BAL-01	105	931	0.91	98.46	41.59	41.54		41.57	0.04	0.03	5.51%	43.39	-1.82
BAL-02	135	1442	1.89	96.89	40.77	40.40		40.58	0.26	0.18	11.43%	44.49	-3.91
BAL-03	185	2136	0.95	98.74	40.38	41.41	40.98	40.93	0.51	0.42	5.76%	42.80	-1.87
BAL-04	245	2962	1.16	98.58	40.41	40.81	40.48	40.57	0.21	0.17	6.97%	42.83	-2.27
BAL-05	283	3508	1.01	97.88	43.05	42.37		42.71	0.48	0.34	6.10%	44.81	-2.10
BAL-06	343	4259	0.60	98.59	42.11	41.51		41.81	0.42	0.30	3.61%	42.99	-1.18
BAL-07	363	4540	0.79	99.04	40.83	40.35		40.59	0.34	0.24	4.79%	42.11	-1.52
BAL-08	403	5167	0.72	99.13	41.23			41.23			4.35%	42.64	-1.41
BAL-09	503	6601	1.51	98.07	38.22	38.16		38.19	0.04	0.03	9.08%	40.97	-2.78
BAL-10	523	6875	0.63	98.68	37.29	37.19		37.24	0.07	0.05	3.80%	38.31	-1.06
BAL-11	582	7680	0.38	99.29	36.48	36.18		36.33	0.21	0.15	2.30%	36.94	-0.61
BAL-12	632	8407	0.66	98.71	36.39	35.63	36.42	36.40	0.02	0.01	4.01%	37.49	-1.09
BAL-13	680	9225	0.62	98.95	35.90	36.27		36.09	0.26	0.19	3.72%	37.08	-0.99
BAL-14	720	9757	1.53	96.43	35.97	35.60		35.79	0.26	0.18	9.24%	38.38	-2.59
BAL-15	784	10296	2.28	95.74	35.61	35.70		35.66	0.06	0.04	13.74%	39.69	-4.03
BAL-16	804	10457	0.97	98.51	37.03	37.33		37.18	0.21	0.15	5.86%	38.85	-1.67
			EDX	*EDX*	*single measurements*			*statistics*			*final corrected values*		

Heavy fraction (>2.5g/cm³) (for Contamination Correction)			Al_2O_3	SiO_2	$\delta^{18}O$
BAL-01	105	931	16.05	70.55	10.38
BAL-05	283	3508	16.04	67.82	10.18
BAL-09	503	6601	17.61	66.53	10.41
			mean: 16.57	68.30	10.32
			0.1657		
				for % cont	

Table B.2: Measured $\delta^{18}O_{fuc}$ values in the Garba Guracha sediment core: $\delta^{18}O_{fuc}$ ($\delta^{18}O_{fuc}$) and standard error mean SEM (SEM).

Sample ID	Depth min [cm]	Depth max [cm]	Depth mean [cm]	Age [cal. Yr. BP]	$\delta^{18}O_{fuc}$ [‰]	SEM [‰]
26169	70	79	75	356	33.25	0.50
26170	80	89	85	531	30.02	0.02
26171	90	99	95	715	32.06	0.23
26172	100	109	105	931	33.21	0.16
26173	110	119	115	1124	33.98	0.36
26174	120	129	125	1296	33.81	0.34
26175	130	139	135	1442	33.19	0.37
26176	140	149	145	1588	34.31	0.33
26177	150	159	155	1716	34.17	0.07
26178	160	169	165	1850	33.19	0.10
26179	170	179	175	1997	33.35	0.60
26180	180	189	185	2136	35.37	0.76
26181	190	199	195	2280	34.10	0.54
26182	200	209	205	2411	34.21	0.35
26183	210	219	215	2550	32.30	0.38
26184	220	229	225	2694	33.41	0.55
26185	230	239	235	2824	32.99	0.18
26186	240	249	245	2962	33.53	0.32
26187	250	259	255	3121	31.42	0.42
26188	260	267	264	3251	33.77	0.62
26189	268	277	273	3391	34.34	0.58
26190	278	287	283	3508	33.62	0.48
26191	288	297	293	3631	34.80	0.18
26192	298	307	303	3764	34.30	0.19
26193	308	317	313	3887	32.99	0.10
26194	318	327	323	3993	33.65	0.29
26195	328	337	333	4111	30.66	0.68
26196	338	347	343	4259	32.87	0.32
26197	348	357	353	4402	31.38	0.40
26198	358	367	363	4540	29.68	0.66
26302	378	387	383	4862	34.51	0.56
26303	388	397	393	5006	32.20	1.36
26304	398	407	403	5167	27.94	0.41
26305	408	417	413	5326	32.17	0.87
26306	418	427	423	5472	34.98	0.57
26307	428	437	433	5616	30.80	0.85
26308	438	447	443	5761	29.25	0.84
26309	448	457	453	5897	29.47	0.42
26310	458	467	463	6028	30.61	0.69
26199	468	477	473	6174	29.85	0.26
26200	478	487	483	6311	29.71	0.84
26201	488	497	493	6449	30.87	0.43
26202	498	507	503	6601	30.50	0.61
26203	508	517	513	6748	30.33	0.45
26204	518	527	523	6875	31.04	0.33
26205	528	537	533	6987	31.67	0.10
26206	538	547	543	7109	30.75	0.23
26207	548	557	553	7267	29.68	0.13
26208	558	566	562	7413	27.83	0.11
26209	567	576	572	7557	30.41	0.30
26210	577	586	582	7680	26.92	0.21
26211	587	596	592	7806	26.63	0.39
26212	597	606	602	7945	27.26	0.06
26213	607	616	612	8107	27.19	0.38
26214	617	626	622	8258	26.82	0.07
26215	627	636	632	8407	28.88	0.71
26216	637	646	642	8595	24.73	0.17
26217	647	656	652	8791	26.31	0.26
26218	657	664	661	8952	26.98	0.14

26219	665	674	670	9077	28.09	0.27
26220	675	684	680	9225	30.20	0.17
26221	685	694	690	9392	29.23	0.23
26222	695	704	700	9512	30.16	0.54
26223	705	714	710	9642	31.75	0.68
26225	725	734	730	9838	28.65	0.81
26226	735	744	740	9923	29.81	0.37
26227	745	754	750	9995	30.25	1.40
26228	755	758	757	10060	33.21	0.75
26229	759	768	764	10124	34.47	0.96
26231	779	788	784	10296	35.85	0.19
26232	789	798	794	10377	36.20	0.42
26233	799	808	804	10457	33.71	0.79
26234	809	818	814	10537	33.28	0.74
26235	819	828	824	10613	31.50	0.93
26236	829	838	834	10693	31.65	1.32
26237	839	842	841	10749	27.12	0.71
26238	863	872	868	10967	29.87	0.68
26239	873	882	878	11040	32.15	0.24
26241	893	902	898	11186	34.05	0.71

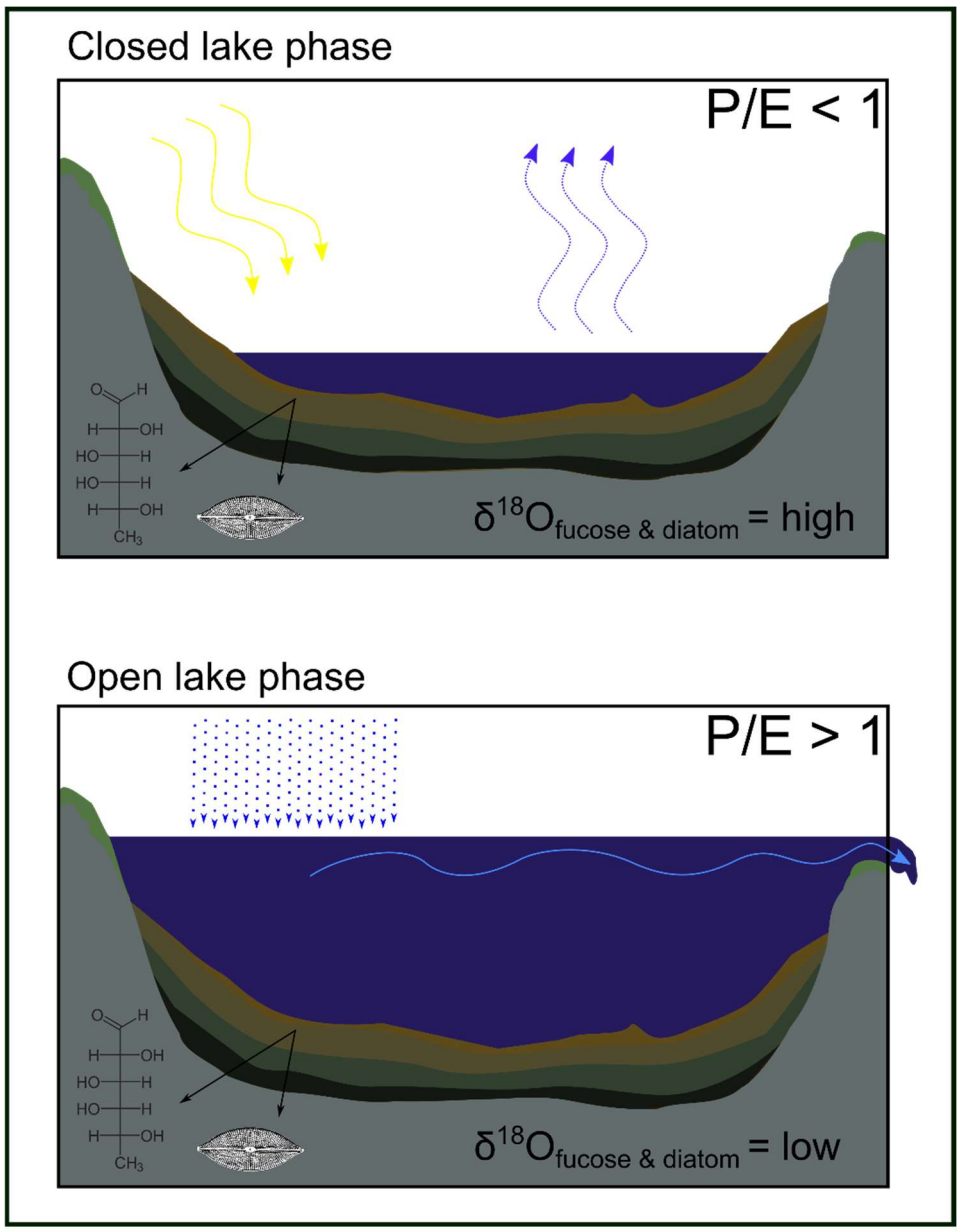

Figure B.1: A schematic figure of evaporative enrichment of lake water in open and closed lake systems.

Figure B.2: Scanning Electron Microscope picture of the diatom sample 26186 (245 cm depth).

Appendix C

Supplements to Chapter 4

Supplementary Data

Table C.1: Bale Mountain lakes - Environmental data (BAXTER ET AL., 2019)

Lake	Country	Latitude	Longitude	Elevation (m asl)	Depth (m)	MAT (°C)	T_{Mean} (°C)	pH_{Mean}
Central	ETH	6.854	39.881	4121	0.6	4.2	9.6	8
Crane	ETH	6.855	39.893	4047	0.3	4.6	10.7	9.4
Dimtu	ETH	6.830	39.859	4092	0.2	4.3	8.2	8.8
Garba Guracha	ETH	6.880	39.871	3917	5.6	5.4	12.1	7.6
Hara Laki	ETH	6.836	39.846	4099	0.4	4.3	9.0	8.7
Hara Lucas (L4)	ETH	6.858	39.884	4101	0.3	4.3	4.9	7.2
Haro Lakota 1	ETH	6.883	39.891	4031	0.4	4.7	11.5	7.1
Haro Lakota 2	ETH	6.884	39.892	4029	0.6	4.7	11.9	7.3
Koromi	ETH	6.893	39.908	3948	0.5	5.2	9.8	7.8
Kuware	ETH	6.840	39.869	4141	0.5	4.0	9.3	8
Togona	ETH	6.885	39.895	3998	0.5	4.9	10.0	7.3

Table 6.0.1 Table C.2: Bale Mountain lakes – Fractional abundance of brGDGT

	branched Glycerol Dialkyl Glycerol Tetraethers (brGDGTs)														
Lake	**Ia**	**Ib**	**Ic**	**IIa**	**IIb**	**IIc**	**IIa'**	**IIb'**	**IIc'**	**IIIa**	**IIIb**	**IIIc**	**IIIa'**	**IIIb'**	**IIIc'**
Central	0.0911	0.0223	0.0036	0.1912	0.0548	0.0071	0.1921	0.0077	0.0004	0.2057	0.0063	0.0015	0.2148	0.0911	0.0223
Crane	0.1141	0.0750	0.0216	0.2535	0.1322	0.0221	0.0632	0.0095	0.0012	0.2270	0.0104	0.0025	0.0644	0.1141	0.0750
Dimtu	0.0940	0.0133	0.0020	0.1899	0.0200	0.0024	0.2083	0.0075	0.0003	0.2376	0.0023	0.0004	0.2209	0.0940	0.0133
Garba Gurach	0.0931	0.0198	0.0044	0.1480	0.0591	0.0046	0.1526	0.0359	0.0020	0.2202	0.0066	0.0007	0.2434	0.0931	0.0198
Hara Laki	0.1611	0.0279	0.0053	0.2735	0.0443	0.0091	0.1479	0.0067	0.0001	0.2124	0.0037	0.0013	0.1052	0.1611	0.0279
Hara Lucas (L4)	0.1049	0.0426	0.0138	0.2520	0.1247	0.0164	0.0718	0.0090	0.0005	0.2632	0.0113	0.0018	0.0865	0.1049	0.0426
Haro Lakota 1	0.1449	0.0222	0.0084	0.2139	0.0304	0.0057	0.2055	0.0066	0.0001	0.1761	0.0035	0.0008	0.1798	0.1449	0.0222
Haro Lakota 2	0.1271	0.0457	0.0114	0.2865	0.0979	0.0122	0.0693	0.0064	0.0004	0.2659	0.0077	0.0008	0.0675	0.1271	0.0457
Koromi	0.1235	0.0548	0.0169	0.2702	0.1121	0.0178	0.0666	0.0088	0.0008	0.2489	0.0081	0.0012	0.0686	0.1235	0.0548
Kuware	0.0737	0.0212	0.0037	0.0468	0.0362	0.0047	0.2021	0.0366	0.0012	0.0817	0.0070	0.0017	0.4743	0.0737	0.0212
Togona	0.1293	0.0336	0.0062	0.2875	0.0914	0.0089	0.0698	0.0072	0.0000	0.2864	0.0074	0.0007	0.0713	0.1293	0.0336

Table C.3: Bale Mountain soil samples – Fractional abundance of brGDGT

			branched Glycerol Dialkyl Glycerol Tetraethers (brGDGTs)														
Sample ID	**Latitude**	**Longitude**	**Ia**	**Ib**	**Ic**	**IIa**	**IIb**	**IIc**	**IIa'**	**IIb'**	**IIc'**	**IIIa**	**IIIb**	**IIIc**	**IIIa'**	**IIIb'**	**IIIc'**
23441	6 °52′41″	39 °52′02″	0.32	0.03	0.01	0.37	0.01	0.00	0.11	0.01	0.00	0.11	0.00	0.00	0.02	0.00	0.00
23442	6 °52′43″	39 °52′02″	0.23	0.01	0.01	0.34	0.01	0.00	0.15	0.01	0.00	0.17	0.00	0.00	0.06	0.00	0.00
23447	6 °51′58″	39 °52′05″	0.17	0.00	0.00	0.34	0.00	0.00	0.19	0.00	0.00	0.14	0.00	0.08	0.08	0.01	0.00
23451	6 °52′38″	39 °51′58″	0.28	0.00	0.00	0.42	0.00	0.00	0.04	0.00	0.00	0.22	0.00	0.00	0.01	0.00	0.00
23452	6 °52′42″	39 °52′03″	0.11	0.02	0.01	0.12	0.01	0.00	0.23	0.04	0.00	0.09	0.00	0.02	0.33	0.02	0.00
23453	6 °52′40″	39 °52′05″	0.23	0.02	0.01	0.27	0.01	0.00	0.17	0.01	0.00	0.19	0.00	0.01	0.08	0.00	0.00
23481	6 °43′17″	39 °44′11″	0.21	0.08	0.01	0.09	0.03	0.00	0.29	0.08	0.00	0.04	0.01	0.01	0.15	0.00	0.00
23482	6 °46′42″	39 °44′39″	0.25	0.02	0.00	0.34	0.01	0.00	0.14	0.02	0.00	0.13	0.00	0.01	0.07	0.00	0.00
23485	6 °49′31″	39 °49′08″	0.07	0.03	0.01	0.07	0.03	0.01	0.21	0.06	0.00	0.14	0.00	0.01	0.33	0.01	0.01
23486	6 °48′22″	39 °47′50″	0.18	0.07	0.01	0.26	0.05	0.01	0.09	0.01	0.00	0.23	0.00	0.00	0.09	0.00	0.00
23487	6 °46′36″	39 °44′43″	0.33	0.03	0.01	0.31	0.02	0.00	0.14	0.01	0.00	0.11	0.00	0.00	0.04	0.00	0.00

Table C.4: Garba Guracha sediment core – Fractional abundance of brGDGT

	branched Glycerol Dialkyl Glycerol Tetraethers (brGDGTs)																
Age (cal yrs BP)	**Ia**	**Ib**	**Ic**	**IIa**	**IIb**	**IIc**	**IIa'**	**IIb'**	**IIc'**	**IIIa**	**IIIb**	**IIIc**	**IIIa'**	**IIIb'**	**IIIc'**	**BIT**	**CBT'**
531	0.122	0.037	0.010	0.155	0.071	0.011	0.142	0.038	0.002	0.198	0.012	0.002	0.195	0.006	0.001	1.00	-0.08
931	0.120	0.032	0.009	0.178	0.077	0.010	0.147	0.027	0.001	0.171	0.012	0.002	0.206	0.007	0.001	0.99	-0.07
1442	0.120	0.028	0.008	0.178	0.070	0.009	0.141	0.029	0.001	0.199	0.010	0.002	0.197	0.007	0.001	0.99	-0.11
1588	0.144	0.033	0.007	0.175	0.063	0.009	0.171	0.031	0.001	0.175	0.008	0.002	0.173	0.005	0.001	0.99	-0.10
1850	0.137	0.029	0.007	0.190	0.059	0.007	0.139	0.019	0.001	0.196	0.007	0.002	0.202	0.003	0.001	0.99	-0.15
2136	0.136	0.027	0.007	0.165	0.054	0.007	0.166	0.037	0.003	0.155	0.008	0.001	0.223	0.008	0.001	0.99	-0.01
2550	0.126	0.032	0.011	0.153	0.051	0.008	0.187	0.047	0.004	0.142	0.007	0.001	0.222	0.008	0.001	0.99	0.06
2962	0.127	0.023	0.010	0.157	0.048	0.008	0.194	0.044	0.004	0.145	0.007	0.001	0.223	0.008	0.001	0.99	0.05
3251	0.144	0.026	0.011	0.177	0.046	0.008	0.177	0.035	0.002	0.134	0.008	0.001	0.222	0.008	0.001	0.99	-0.00
3508	0.135	0.026	0.011	0.188	0.055	0.010	0.166	0.034	0.002	0.141	0.008	0.001	0.215	0.008	0.001	0.99	-0.02
3887	0.156	0.028	0.011	0.206	0.051	0.011	0.160	0.025	0.001	0.129	0.008	0.001	0.207	0.006	0.001	1.00	-0.08
4259	0.166	0.026	0.010	0.178	0.039	0.021	0.181	0.027	0.009	0.131	0.006	0.001	0.197	0.005	0.001	1.00	-0.04
4540	0.161	0.029	0.009	0.212	0.072	0.009	0.134	0.029	0.002	0.194	0.010	0.002	0.131	0.005	0.001	1.00	-0.26
4702	0.167	0.031	0.009	0.226	0.078	0.009	0.124	0.032	0.003	0.209	0.011	0.002	0.094	0.006	0.000	1.00	-0.35
5167	0.189	0.026	0.005	0.240	0.078	0.006	0.118	0.023	0.000	0.203	0.013	0.001	0.093	0.005	0.000	1.00	-0.41
5761	0.199	0.035	0.008	0.238	0.086	0.010	0.121	0.019	0.001	0.193	0.012	0.002	0.074	0.005	0.001	1.00	-0.44
6449	0.171	0.029	0.025	0.201	0.069	0.011	0.105	0.019	0.001	0.247	0.011	0.002	0.098	0.010	0.001	1.00	-0.38
6875	0.193	0.033	0.009	0.248	0.084	0.011	0.092	0.014	0.001	0.225	0.014	0.002	0.071	0.003	0.001	1.00	-0.54
7267	0.209	0.035	0.009	0.207	0.082	0.012	0.130	0.025	0.001	0.205	0.009	0.002	0.068	0.005	0.001	1.00	-0.42
7680	0.177	0.043	0.018	0.223	0.103	0.018	0.086	0.021	0.001	0.202	0.015	0.002	0.085	0.005	0.001	1.00	-0.44
8107	0.179	0.038	0.017	0.265	0.082	0.015	0.080	0.021	0.002	0.205	0.014	0.002	0.075	0.005	0.001	1.00	-0.51
8407	0.194	0.039	0.013	0.254	0.076	0.014	0.098	0.019	0.002	0.199	0.010	0.002	0.072	0.006	0.001	1.00	-0.49
8791	0.178	0.035	0.014	0.240	0.073	0.012	0.118	0.034	0.004	0.180	0.009	0.002	0.089	0.011	0.001	1.00	-0.34
9225	0.157	0.050	0.024	0.235	0.117	0.022	0.074	0.016	0.002	0.208	0.015	0.003	0.073	0.005	0.001	1.00	-0.49
9512	0.163	0.052	0.024	0.229	0.117	0.023	0.088	0.021	0.001	0.199	0.013	0.002	0.061	0.006	0.001	1.00	-0.47
9757	0.138	0.052	0.026	0.205	0.122	0.024	0.083	0.022	0.002	0.245	0.011	0.003	0.063	0.004	0.001	1.00	-0.47
9923	0.156	0.052	0.027	0.206	0.128	0.026	0.100	0.019	0.001	0.191	0.017	0.003	0.068	0.005	0.001	1.00	-0.40
10060	0.138	0.041	0.022	0.194	0.106	0.019	0.092	0.036	0.005	0.256	0.010	0.002	0.072	0.006	0.001	0.99	-0.40
10212	0.130	0.041	0.017	0.224	0.096	0.015	0.086	0.013	0.001	0.280	0.013	0.002	0.078	0.005	0.001	1.00	-0.50
10457	0.107	0.034	0.015	0.180	0.071	0.010	0.122	0.025	0.003	0.293	0.011	0.003	0.120	0.006	0.001	0.99	-0.30
10693	0.114	0.025	0.011	0.183	0.058	0.009	0.108	0.009	0.000	0.307	0.012	0.003	0.156	0.003	0.000	0.98	-0.32
11186	0.103	0.027	0.013	0.172	0.057	0.011	0.100	0.012	0.001	0.324	0.010	0.004	0.155	0.009	0.001	0.88	-0.31
11678	0.112	0.029	0.014	0.174	0.060	0.013	0.106	0.011	0.000	0.281	0.013	0.005	0.172	0.009	0.000	0.88	-0.26
12078	0.098	0.026	0.013	0.160	0.055	0.011	0.104	0.012	0.001	0.302	0.011	0.005	0.193	0.009	0.001	0.86	-0.23
12229	0.103	0.028	0.014	0.181	0.054	0.011	0.107	0.015	0.000	0.289	0.011	0.005	0.172	0.008	0.001	0.88	-0.26

Table C.5: Garba Guracha sediment core – Calibrations and temperature reconstruction

	Ratio values			Recontsructed MAT (°C)		
Age (cal yrs BP)	**MBT'_{5ME}**	**MBT'_{5ME} + IIIa'**	**Ia/(Ia+IIa+IIIa+IIIa')**	**MAT= -1.8299 + 33.304 x MBT'_{5ME}**	**MAT= -1.4734 + 35.777 x MBT'_{5ME} + IIIa'**	**MAT= -0.773 + 35.646 x Ia/(Ia+IIa+IIIa+IIIa')**
531	0.28	0.21	0.18	7.47	6.07	5.32
931	0.27	0.20	0.18	7.16	5.71	5.16
1442	0.26	0.19	0.17	6.69	5.45	4.99
1588	0.30	0.24	0.22	8.31	7.01	6.55
1850	0.28	0.21	0.19	7.42	6.04	5.58
2136	0.31	0.22	0.20	8.46	6.40	5.97
2550	0.32	0.23	0.20	8.93	6.64	5.82
2962	0.31	0.22	0.20	8.48	6.27	5.79
3251	0.33	0.24	0.21	9.19	6.94	6.41
3508	0.30	0.22	0.20	8.31	6.40	5.91
3887	0.33	0.24	0.22	9.12	7.24	6.79
4259	0.35	0.26	0.25	9.95	7.94	7.67
4540	0.29	0.24	0.23	7.86	7.26	7.08
4702	0.28	0.25	0.24	7.65	7.55	7.41
5167	0.29	0.26	0.26	7.98	7.90	8.14
5761	0.31	0.29	0.28	8.66	8.81	8.95
6449	0.30	0.26	0.24	8.13	7.99	7.34
6875	0.29	0.27	0.26	7.91	8.14	8.19
7267	0.33	0.31	0.30	9.29	9.49	9.72
7680	0.30	0.27	0.26	8.26	8.31	8.05
8107	0.29	0.27	0.25	7.89	8.07	7.66
8407	0.31	0.29	0.27	8.58	8.78	8.47
8791	0.31	0.28	0.26	8.48	8.40	8.08
9225	0.28	0.26	0.23	7.62	7.84	7.16
9512	0.30	0.28	0.25	8.04	8.39	7.74
9757	0.27	0.25	0.21	7.00	7.33	6.38
9923	0.30	0.28	0.25	8.15	8.39	7.80
10060	0.26	0.24	0.21	6.79	7.00	6.28
10212	0.23	0.21	0.18	5.96	6.15	5.33
10457	0.22	0.19	0.15	5.46	5.23	4.26
10693	0.21	0.17	0.15	5.25	4.76	4.15
11186	0.20	0.17	0.14	4.91	4.46	3.67
11678	0.23	0.18	0.15	5.72	5.00	4.20
12078	0.21	0.16	0.13	5.02	4.23	3.45
12229	0.21	0.17	0.14	5.31	4.65	3.74

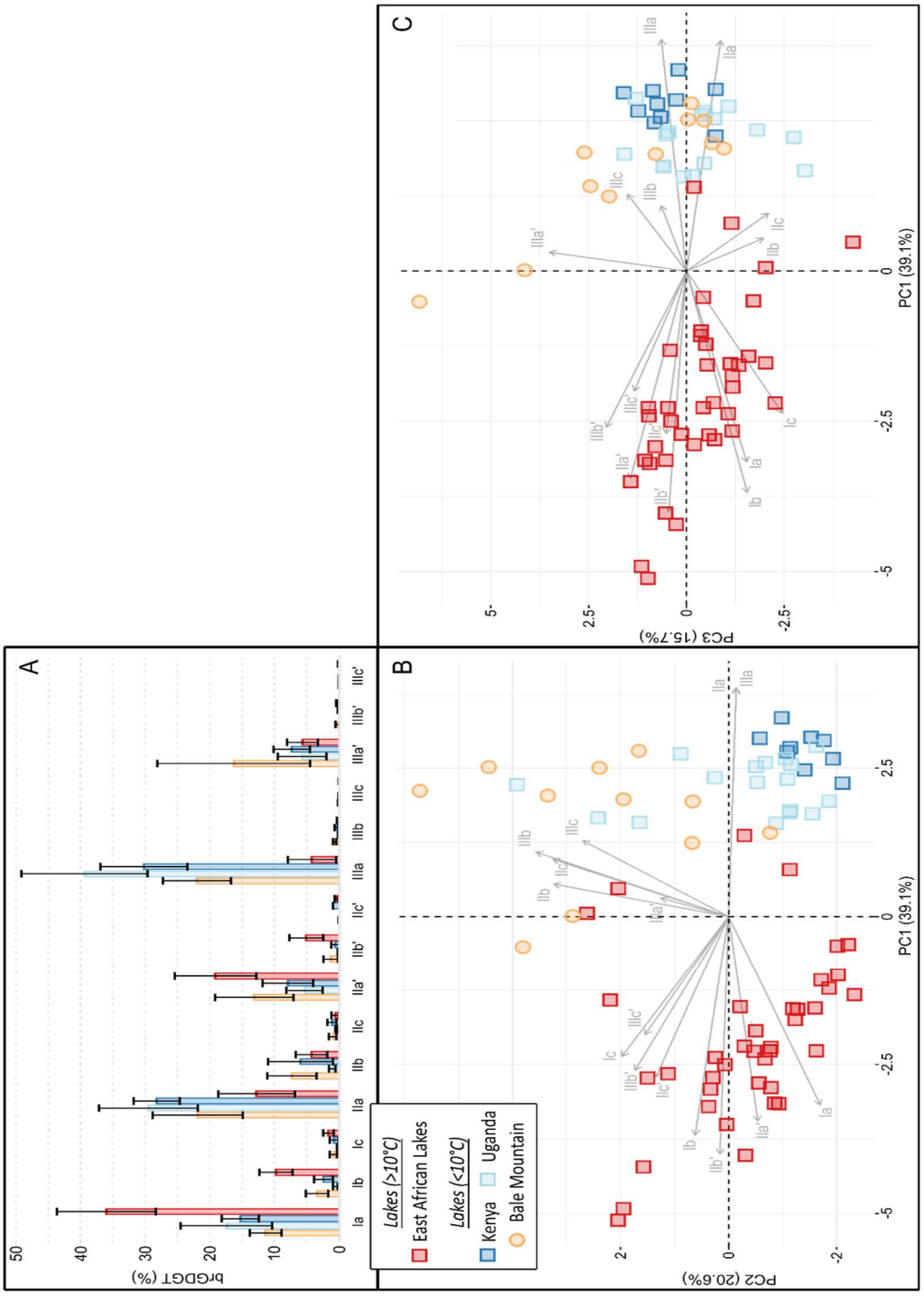

Figure C.1: A) Barplot of average brGDGT percentages in East African lake surface sediments (BAXTER ET AL., 2019; RUSSELL ET AL., 2018), with standard deviation plotted as error flags and PCA of brGDGTs of Eastern African lakes – B) PCA with all brGDGT isomers PC1 vs PC2 and C) PC1 vs PC3; data from RUSSELL ET AL. (2018) and BAXTER ET AL. (2019) - lakes >10 °C (red) and lakes <10 °C (Bale Mountain - orange, Kenya - blue and Uganda - light blue).

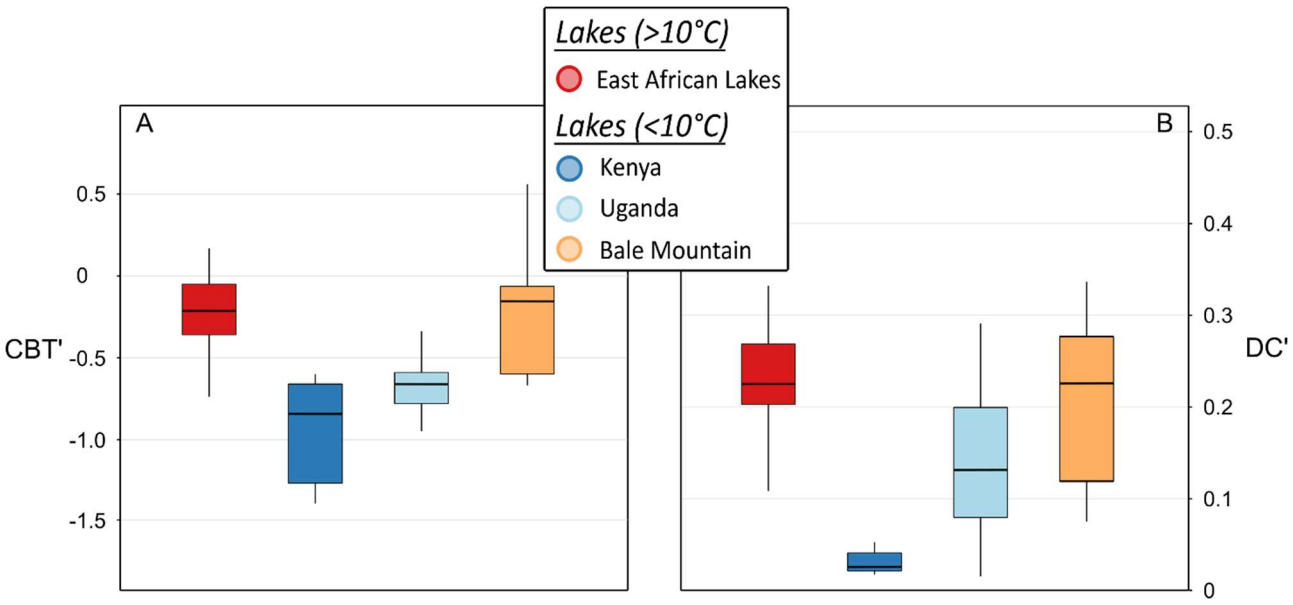

Figure C.2: A) Boxplot of CBT' in East African lake surface sediments (BAXTER ET AL., 2019; RUSSELL ET AL., 2018); B) Boxplot of the degree of cyclization (DC') in East African lake surface sediments - data from RUSSELL ET AL. (2018) and BAXTER ET AL. (2019) - lakes >10 °C (red) and lakes <10 °C (Bale Mountain - orange, Kenya - blue and Uganda - light blue).

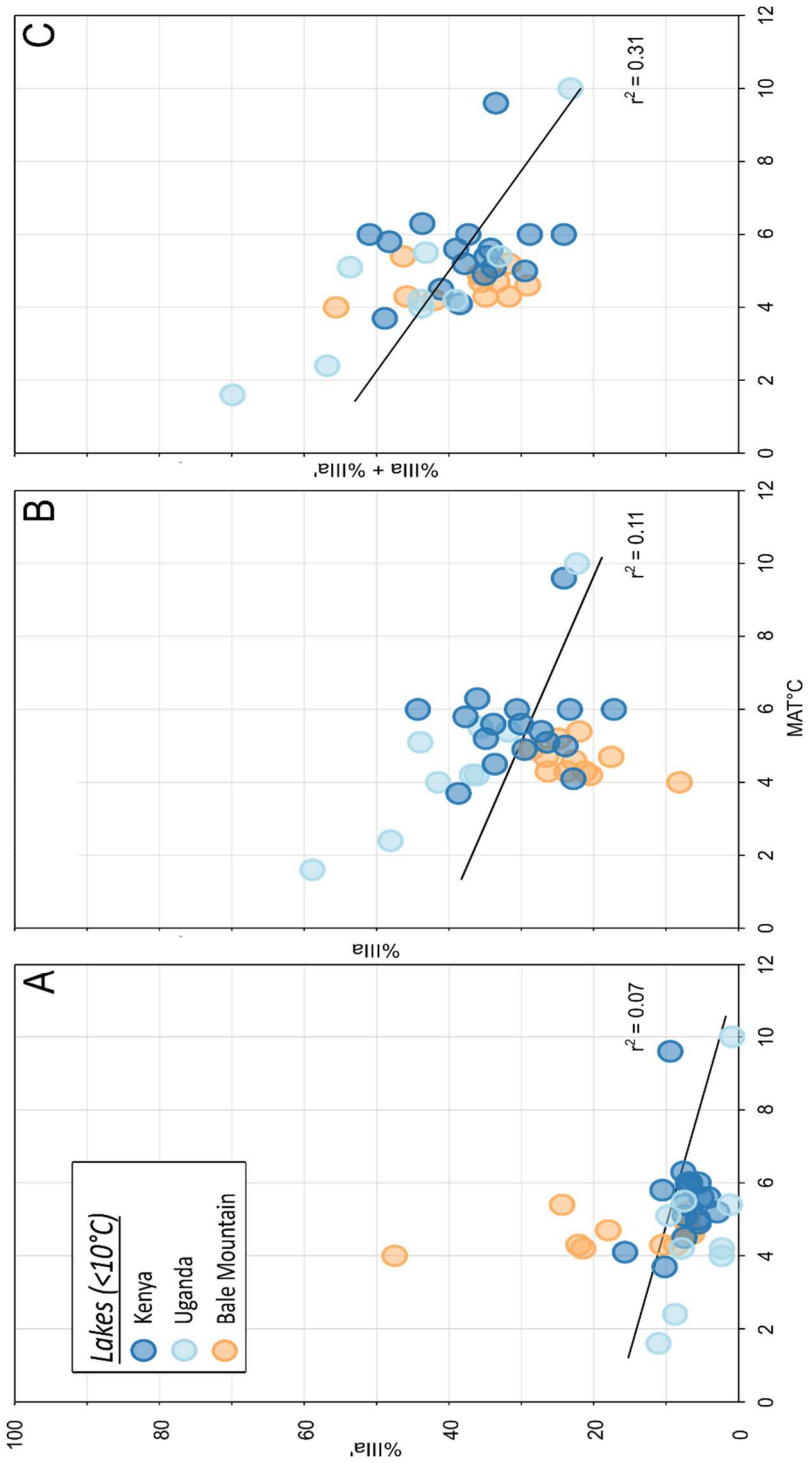

Figure C3: (A) Linear correlation between IIIa' and MAT (r^2 = 0.07), (B) between IIIa and MAT (r^2 = 0.11) and (C) IIIa + IIIa' to MAT (r^2 = 0.31) - data from RUSSELL ET AL. (2018) and BAXTER ET AL. (2019) - (Bale Mountain - orange, Kenya - blue and Uganda - light blue)

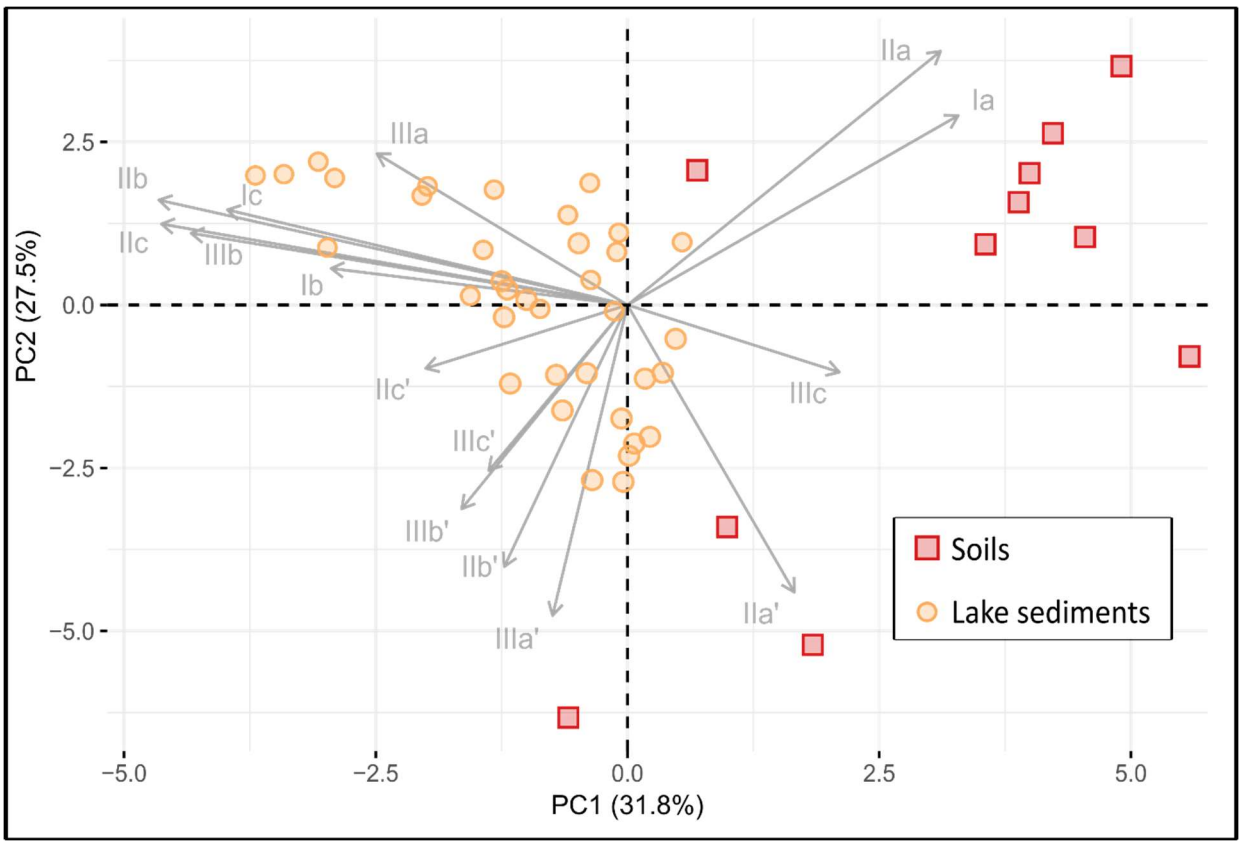

Figure C.4: PCA of Bale Mountain soils (red) and Garba Guracha lake sediments (orange).

Appendix D

Supplements to Chapter 5

Supplementary Data

Table D.1: n-Alkane abundances in percent of plants, and soil horizons in the Bale Mountains from MEKONNEN ET AL. (2019) and LEMMA ET AL. (2019).

Lab Code	Sample	Sample Type	Altitude [m a. s. l.]	C_{29} [%]	C_{31} [%]	C_{33} [%]
23497	*Erica arborea*	**Plant**	3226	17.36	32.05	14.95
23498	*Erica arborea*	**Plant**	3230	18.54	31.26	18.02
23496	*Erica arborea*	**Plant**	3670	21.45	36.70	10.95
23499	*Erica arborea*	**Plant**	3850	14.60	31.06	11.93
23519	*Erica arborea*	**Plant**	4210	25.87	40.94	12.47
23469	*Erica trimera*	**Plant**	3530	18.24	45.83	17.47
23468	*Erica trimera*	**Plant**	3870	31.89	43.35	12.35
23477	*Erica trimera*	**Plant**	3950	23.56	34.51	13.41
23467	*Erica trimera*	**Plant**	3960	24.08	33.57	9.80
23478	*Erica trimera*	**Plant**	3970	32.30	40.11	10.63
23473	*Poaceae/grass*	**Plant**	3870	9.10	34.80	24.85
23474	*Poaceae/grass*	**Plant**	3920	27.95	54.72	5.56
23470	*Poaceae/grass*	**Plant**	3922	34.78	45.60	6.81
23475	*Poaceae/grass*	**Plant**	3960	9.60	57.21	19.46
23465	*Poaceae/grass*	**Plant**	4070	9.94	51.36	25.78
23500	Poaceae/grass	**Plant**	4400	14.17	51.89	18.12
23454	*Kniphofia foliosa*	**Plant**	3930	28.82	2.36	0.31
23466	*Alchemilla spp.*	**Plant**	3870	19.76	60.85	12.65
23462	*Alchemilla spp.*	**Plant**	3945	4.13	27.52	52.86
23463	*Alchemilla spp.*	**Plant**	3947	17.34	58.92	15.12
23476	*Alchemilla spp.*	**Plant**	3947	17.82	56.25	16.27
23471	*Alchemilla spp.*	**Plant**	4100	5.31	16.15	45.70
23502	*Helichrysum splendidum*	**Plant**	3955	25.15	52.73	9.72
23501	*Helichrysum splendidum*	**Plant**	4400	27.25	49.38	8.56
23464	*Lobelia rhynchopetalum*	**Plant**	3922	38.49	36.03	4.58
23493	*Of/Erica arborea*	**Organic layer**	3226	18.67	39.69	18.61
23489	*Of/Erica arborea*	**Organic layer**	3230	18.73	28.50	13.95
23495	*Of/Erica arborea*	**Organic layer**	3670	20.24	48.19	16.51
23492	*Of/Erica arborea*	**Organic layer**	3850	22.05	46.22	15.65
23488	*Of/Erica arborea*	**Organic layer**	4210	25.41	45.81	14.63
23491	*Of/Erica trimera*	**Organic layer**	3530	17.84	44.28	19.98
23460	*Of/Erica trimera*	**Organic layer**	3870	23.69	42.68	16.68
23461	*Of/Erica trimera*	**Organic layer**	3950	22.91	46.73	16.11
23459	*Of/Erica trimera*	**Organic layer**	3960	22.67	43.61	13.15
23457	*Of/Erica trimera*	**Organic layer**	3970	17.93	44.95	20.84
23456	*Of/Poaceae/grass*	**Organic layer**	3920	33.52	40.01	6.47
23455	*Of/Poaceae/grass*	**Organic layer**	3922	16.38	56.83	11.25
23472	*Of/Kniphofia foliosa*	**Organic layer**	3930	31.74	5.96	1.34
23458	*Of/Alchemilla spp.*	**Organic layer**	3947	12.01	59.41	21.48
23494	*Of/Helichrysum splendidum*	**Organic layer**	4400	22.41	55.36	9.39
23487	Ah/Erica arborea	**Ah**	3226	18.53	38.29	16.77
23482	Ah/Erica arborea	**Ah**	3230	20.15	34.74	20.64
23479	Ah/Erica arborea	**Ah**	3670	19.01	48.73	15.86
23480	Ah/Erica arborea	**Ah**	3850	9.91	22.88	9.08
23484	Ah/Erica arborea	**Ah**	4210	14.74	42.08	17.37
23503	Ah/Erica arborea	**Ah**	4210	19.84	39.39	10.70
23483	Ah/Erica trimera	**Ah**	3530	17.05	38.83	16.22
23449	Ah/Erica trimera	**Ah**	3870	9.10	33.03	23.75
23445	Ah/Erica trimera	**Ah**	3950	16.95	29.24	9.45
23442	Ah/Erica trimera	**Ah**	3960	14.27	38.03	12.75
23451	Ah/Erica trimera	**Ah**	3970	19.65	43.59	16.57
23448	Ah/Poaceae/grass	**Ah**	3870	9.22	30.51	24.35
23444	Ah/Poaceae/grass	**Ah**	3922	14.79	15.72	4.06
23441	Ah/Poaceae/grass	**Ah**	3960	4.39	16.85	7.30
23446	Ah/Poaceae/grass	**Ah**	4070	2.58	6.73	7.26
23443	Ah/Poaceae/grass	**Ah**	4134	12.48	20.32	8.74
23452	Ah/Kniphofia foliosa	**Ah**	3930	19.05	23.73	8.97
23453	Ah/Alchemilla spp.	**Ah**	3947	12.49	53.49	17.95
23447	Ah/Alchemilla spp.	**Ah**	4100	10.72	27.87	31.99
23450	Ah/Alchemilla spp.	**Ah**	4100	10.71	25.93	25.92
23486	Ah/Helichrysum splendidum	**Ah**	3955	15.22	40.48	24.25
23485	Ah/Helichrysum splendidum	**Ah**	4400	16.78	45.41	16.92

Table D.2: Measured n-alkane abundance in percent of nC_{29}, nC_{31},and nC_{33}, in the Garba Guracha sediment core.

Lab Code	Depth [cm]	C_{29} [%]	C_{31} [%]	C_{33} [%]
26169	75	10.86	19.17	8.35
26170	85	7.84	17.07	8.72
26171	95	8.68	15.49	7.44
26172	105	8.83	16.36	7.84
26173	115	7.13	12.48	6.42
26174	125	4.99	9.67	5.19
26175	135	11.98	12.58	6.50
26176	145	15.56	13.92	7.82
26177	155	14.02	13.65	7.98
26178	165	9.18	13.46	7.21
26179	175	7.37	12.23	6.90
26180	185	9.52	13.79	6.51
26181	195	10.44	16.74	7.61
26182	205	11.74	18.74	10.85
26183	215	11.89	19.02	10.13
26184	225	13.55	19.43	10.09
26185	235	10.79	18.00	9.58
26186	245	8.91	16.56	9.16
26187	255	7.59	15.22	8.30
26188	263	8.25	16.35	8.59
26189	273	10.99	16.48	8.24
26190	283	12.01	20.38	10.81
26191	293	10.90	16.87	7.81
26192	303	16.68	29.29	14.73
26193	313	11.40	18.24	9.65
26194	323	12.67	19.12	8.59
26195	333	10.63	17.10	7.69
26196	343	7.45	12.73	5.41
26197	353	12.12	19.72	9.89
26198	363	10.00	17.78	9.08
26301	373	15.47	26.83	13.58
26302	383	18.52	30.72	15.25
26303	393	14.15	22.80	10.21
26304	403	15.42	27.34	14.65
26305	413	12.21	23.10	12.71
26306	423	11.66	20.84	11.20
26307	433	18.55	34.84	18.01
26308	443	18.05	32.95	16.08
26309	453	16.61	31.52	15.20
26310	463	16.72	27.09	12.71
26199	473	16.36	30.18	13.48
26200	483	16.16	25.92	12.95
26201	493	10.70	17.95	8.44
26202	503	8.81	15.95	8.42
26203	513	15.64	27.64	12.77
26204	523	13.37	26.03	12.53
26205	533	18.52	31.26	16.51
26206	543	15.24	27.55	12.50
26207	553	13.35	25.79	11.60
26208	562	12.93	22.92	9.84
26209	572	14.74	24.19	11.41
26210	582	14.48	22.89	10.28
26211	592	18.17	23.84	11.87
26212	602	10.07	15.66	7.66
26213	612	14.14	22.29	11.06
26214	622	16.31	26.21	12.42
26215	632	16.26	25.61	12.34
26216	642	13.96	25.89	11.94
26217	652	13.10	22.34	10.48
26218	661	13.87	20.05	9.40
26219	670	13.25	18.62	7.85
26220	680	9.25	17.71	8.26
26221	690	9.41	15.38	7.39
26222	700	8.81	14.87	6.92
26223	710	10.59	15.86	7.89
26224	720	10.32	16.37	8.07

26225	730	9.62	15.73	7.43
26226	740	12.47	19.31	9.43
26227	750	11.88	18.56	10.13
26228	757	9.63	12.12	5.22
26229	764	8.35	11.15	4.59
26230	774	6.73	8.02	3.61
26231	784	8.47	11.58	4.59
26232	794	10.12	14.30	5.34
26233	804	3.47	6.55	3.04
26234	814	2.10	4.87	2.06
26235	824	4.17	6.52	2.42
26236	834	3.33	6.04	2.34
26237	841	1.76	3.85	1.38
26238	868	3.21	5.40	1.97
26239	878	2.35	4.66	1.74
26240	888	1.86	3.36	1.26
26241	898	2.35	4.17	1.50
26242	908	2.03	4.00	1.43
26243	918	2.11	3.98	1.63
26244	928	2.77	4.95	1.93
26245	938	1.99	3.83	1.46
26246	948	2.06	3.68	1.48

Table D.3: Measured δ^2H of nC_{29}, nC_{31},and nC_{33}, in the Garba Guracha sediment core.

Sample ID	Depth [cm]	Age [cal years BP]	δ^2H_{nC29} [‰]	δ^2H_{nC31} [‰]	δ^2H_{nC33} [‰]	δ^2H_{nC29} [‰]	δ^2H_{nC31} [‰]	δ^2H_{nC33} [‰]	Mean (*n*C29, *n*C31, *n*C33) [‰]	Mean SD [‰]
26169	75	356	-132.34	-147.17	-157.01	27.66	12.83	2.99	14.49	3.05
26170	85	531	-125.81	-147.79	-145.40	34.19	12.21	14.60	20.33	7.54
26171	95	715	-134.59	-144.40	-153.73	25.41	15.60	6.27	15.76	4.74
26172	105	931	-130.86	-142.04	-147.54	29.14	17.96	12.46	19.85	4.61
26173	115	1124	-132.52	-149.26	-149.83	27.48	10.74	10.17	16.13	1.68
26174	125	1296	-131.32	-150.55	-154.49	28.68	9.45	5.51	14.55	5.90
26175	135	1442	-139.41	-161.40	-165.90	20.59	-1.40	-5.90	4.43	5.61
26176	145	1588	-141.90	-160.39	-163.43	18.10	-0.39	-3.43	4.76	3.83
26177	155	1716	-138.81	-153.22	-154.47	21.19	6.78	5.53	11.17	2.37
26178	165	1850	-135.86	-150.24	-154.94	24.14	9.76	5.06	12.99	1.83
26179	175	1997	-139.19	-152.01	-149.49	20.81	7.99	10.51	13.10	2.25
26180	185	2136	-141.80	-155.17	-151.83	18.20	4.83	8.17	10.40	1.04
26181	195	2280	-137.05	-147.53	-152.19	22.95	12.47	7.81	14.41	3.78
26182	205	2411	-139.78	-147.98	-153.15	20.22	12.02	6.85	13.03	3.46
26183	215	2550	-143.72	-157.11	-167.12	16.28	2.89	-7.12	4.01	3.31
26184	225	2694	-146.48	-154.75	-159.87	13.52	5.25	0.13	6.30	6.77
26185	235	2824	-147.14	-153.29	-154.28	12.86	6.71	5.72	8.43	2.64
26186	245	2962	-138.33	-151.87	-150.49	21.67	8.13	9.51	13.10	4.77
26187	255	3121	-140.65	-160.54	-165.55	19.35	-0.54	-5.55	4.42	4.49
26188	264	3251	-145.41	-157.85	-156.94	14.59	2.15	3.06	6.60	2.40
26189	273	3391	-147.20	-153.72	-154.36	12.80	6.28	5.64	8.24	1.61
26190	283	3508	-145.83	-152.12	-153.89	14.17	7.88	6.11	9.39	2.37
26191	293	3631	-146.85	-158.12	-160.65	13.15	1.88	-0.65	4.80	2.05
26192	303	3764	-148.92	-160.87	-162.36	11.08	-0.87	-2.36	2.62	2.59
26193	313	3887	-150.83	-157.21	-161.50	9.17	2.79	-1.50	3.49	4.51
26194	323	3993	-144.47	-162.11	-165.57	15.53	-2.11	-5.57	2.61	3.75
26195	333	4111	-148.70	-160.67	-163.00	11.30	-0.67	-3.00	2.54	2.42
26196	343	4259	-147.94	-156.20	-160.92	12.06	3.80	-0.92	4.98	2.67
26197	353	4402	-143.84	-164.23	-162.80	16.16	-4.23	-2.80	3.04	5.46
26198	363	4540	-153.32	-166.73	-161.89	6.68	-6.73	-1.89	-0.65	2.95
26301	373	4702	-157.23	-173.17	-179.28	2.77	-13.17	-19.28	-9.89	9.64
26303	393	5006	-163.10	-169.92	-171.48	-3.10	-9.92	-11.48	-8.16	6.77
26304	403	5167	-151.24	-162.21	-179.63	8.76	-2.21	-19.63	-4.36	3.04
26305	413	5326	-163.81	-165.83	-173.10	-3.81	-5.83	-13.10	-7.58	4.67
26306	423	5472	-163.61	-168.50	-170.02	-3.61	-8.50	-10.02	-7.37	3.78
26307	433	5616	-166.48	-174.12	-175.40	-6.48	-14.12	-15.40	-12.00	4.10
26308	443	5761	-163.02	-170.26	-169.95	-3.02	-10.26	-9.95	-7.74	3.03
26309	453	5897	-160.99	-170.15	-178.90	-0.99	-10.15	-18.90	-10.01	4.03
26310	463	6028	-159.85	-172.08	-177.86	0.15	-12.08	-17.86	-9.93	3.94
26199	473	6174	-156.84	-168.95	-176.32	3.16	-8.95	-16.32	-7.37	5.31
26200	483	6311	-154.61	-174.00	-182.81	5.39	-14.00	-22.81	-10.47	

26201	493	6449	-159.78	-181.33	-182.28	0.22	-21.33	-22.28	-14.46	4.74
26202	503	6601	-179.79	-186.12	-188.22	-19.79	-26.12	-28.22	-24.71	4.05
26203	513	6748	-176.47	-180.71	-185.58	-16.47	-20.71	-25.58	-20.92	3.63
26204	523	6875	-172.30	-183.14	-190.17	-12.30	-23.14	-30.17	-21.87	3.24
26205	533	6987	-179.61	-192.89	-197.30	-19.61	-32.89	-37.30	-29.93	1.51
26206	543	7109	-172.99	-186.19	-186.07	-12.99	-26.19	-26.07	-21.75	2.72
26207	553	7267	-172.29	-184.31	-190.15	-12.29	-24.31	-30.15	-22.25	3.84
26208	562	7413	-165.00	-183.08	-190.93	-5.00	-23.08	-30.93	-19.67	2.06
26209	572	7557	-166.08	-183.88	-184.58	-6.08	-23.88	-24.58	-18.18	6.04
26210	582	7680	-161.79	-183.41	-179.34	-1.79	-23.41	-19.34	-14.84	7.58
26211	592	7806	-157.70	-186.18	-182.81	2.30	-26.18	-22.81	-15.56	6.68
26212	602	7945	-166.91	-186.90	-186.41	-6.91	-26.90	-26.41	-20.07	2.93
26213	612	8107	-160.20	-188.49	-181.04	-0.20	-28.49	-21.04	-16.58	2.24
26214	622	8258	-170.58	-184.09	-186.89	-10.58	-24.09	-26.89	-20.52	5.27
26215	632	8407	-183.70	-193.20	-187.10	-23.70	-33.20	-27.10	-28.00	11.54
26216	642	8595	-164.56	-174.61	-172.95	-4.56	-14.61	-12.95	-10.71	5.12
26217	652	8791	-169.99	-180.80	-186.29	-9.99	-20.80	-26.29	-19.03	5.71
26218	661	8952	-163.11	-181.47	-181.50	-3.11	-21.47	-21.50	-15.36	5.10
26219	670	9077	-155.02	-179.00	-179.07	4.98	-19.00	-19.07	-11.03	4.57
26220	680	9225	-177.91	-181.22	-186.22	-17.91	-21.22	-26.22	-21.78	5.24
26221	690	9392	-171.26	-179.31	-184.79	-11.26	-19.31	-24.79	-18.45	5.04
26222	700	9512	-179.18	-178.49	-184.43	-19.18	-18.49	-24.43	-20.70	3.45
26223	710	9642	-171.05	-179.04	-186.45	-11.05	-19.04	-26.45	-18.85	6.84
26224	720	9757	-178.28	-181.67	-183.61	-18.28	-21.67	-23.61	-21.19	2.60
26225	730	9838	-195.55	-175.26	-180.49	-35.55	-15.26	-20.49	-23.77	
26226	740	9923		-169.83	-178.69		-9.83	-18.69	-14.26	9.17
26227	750	9995		-166.18	-172.36		-6.18	-12.36	-9.27	4.44
26228	757	10060		-182.79	-187.55		-22.79	-27.55	-25.17	9.42
26229	764	10124	-180.44	-179.26	-177.42	-20.44	-19.26	-17.42	-19.04	3.96
26230	774	10212		-175.50	-165.76		-15.50	-5.76	-10.63	8.34
26231	784	10296		-178.80	-162.18		-18.80	-2.18	-10.49	5.67
26232	794	10377		-179.45	-160.90		-19.45	-0.90	-10.17	10.07
26233	804	10457	-162.60	-162.36	-158.53	-2.60	-2.36	1.47	-1.17	8.81
26234	814	10537	-145.24	-161.84	-157.27	14.76	-1.84	2.73	5.22	2.37
26235	824	10613	-172.58	-160.32	-161.83	-12.58	-0.32	-1.83	-4.91	9.05
26236	834	10693	-141.73	-145.79	-153.94	18.27	14.21	6.06	12.85	5.68
26237	841	10749	-145.48	-159.75	-159.97	14.52	0.25	0.03	4.93	4.47
26238	868	10967	-141.79	-154.09	-156.00	18.21	5.91	4.00	9.37	2.49
26239	878	11040	-128.23	-152.56	-151.55	31.77	7.44	8.45	15.89	3.80
26240	888	11113	-138.87	-154.46	-158.96	21.13	5.54	1.04	9.23	5.59
26241	898	11186	-122.52	-148.48	-150.28	37.48	11.52	9.72	19.58	3.92
26242	908	11408	-122.31	-140.69	-150.46	37.69	19.31	9.54	22.18	4.54
26243	918	11678	-122.64	-142.47	-152.12	37.36	17.53	7.88	20.92	3.73
26244	928	11907	-123.96	-153.30	-158.01	36.04	6.70	1.99	14.91	4.46
26245	938	12078	-121.16	-141.31	-155.26	38.84	18.69	4.74	20.75	4.64
26246	948	12246	-135.53	-157.10	-147.95	24.47	2.90	12.05	13.14	2.48